The University Of Sheffield.

Age-related changes affect human astrocyte function and have important implications for the function of SOD1 and its role in amyotrophic lateral sclerosis (ALS)

Noemi Gatto

A thesis submitted in partial fulfilment of the requirements for the degree of Doctor of Philosophy

The University of Sheffield
Faculty of Medicine, Dentistry and Health
Department of Neuroscience
Sheffield Institute for Translational Neuroscience (SITraN)

June 2020

Preface

This thesis follows the publication thesis format. In fact, chapter 3 comprises a manuscript, which is submitted for publication and currently under revision in the peer-reviewed journal: Aging Cell. I, Noemi Gatto, am the first and primary author of the manuscript, and contributed (80%) to the experimental planning, execution, and preparation of the research data for publication.

In this thesis, Chapter 1 is dedicated to giving a general introduction to amyotrophic lateral sclerosis (ALS), the mechanisms involved in this devastating disease and their involvement in ageing. Successively, Chapter 2 summarises the material and methods used in chapters 3 and 4. The first results chapter, Chapter 3, presents the results demonstrating that the cell model used in this study is able to retain ageing features from the human fibroblast donors without inserting any age-causing genetic manipulation. In fact, I have shown here that directly derived astrocytes from young and old donor skin fibroblasts diverge in a number of age-related signatures, including oxidative stress response and nucleocytoplasmic shuttling impairment. These cellular functions are particularly relevant when modelling ALS and its disease mechanisms. In fact, in chapter 4, I focused on investigating the role of SOD1, a key protein involved in the antioxidant response, and its link with nucleocytoplasmic transport in ALS patient derived astrocytes.
Finally, Chapter 5 includes an overall discussion of both results chapters and how they are linked together.

Abstract

ALS is a fatal neurodegenerative disorder, partly understood through studies on the first gene associated with familial ALS (fALS), *SOD1.* Several pieces of evidence indicate that misfolded wild-type SOD1 may also play a role in the pathophysiology of sporadic ALS (sALS), through different processes, such as misfolding, aggregation and prion-like pathogenic behaviour. Moreover, there is evidence indicating that SOD1 could function as a transcription factor.

The main risk factor for ALS is ageing; ageing and neurodegeneration share several pathways. Remarkably, it has been demonstrated that glial cells change their gene expression dramatically during physiological brain ageing. Thus, it is important to have these cells suitable for disease modelling, especially in neurodegenerative diseases like ALS, in which astrocytes actively contribute to motor neuron death.

In my study, directly derived astrocytes from young and old donor fibroblasts preserve ageing signatures, representing a valuable model to study astrocytic function. To study the effect of wild-type SOD1 in fALS and sALS, induced astrocytes from control and patient fibroblasts were also generated. Staining for misfolded SOD1 showed nuclear aggregation of the protein in sALS astrocytes. This poses a question on the role of SOD1 in this cellular compartment. The nuclear presence of SOD1 in patient astrocytes was confirmed via cell fractionation, indicating that SOD1 might indeed act as a transcription factor or a co-activator. Furthermore, exportin-1 (XPO1) is able to shuttle misfolded SOD1 to the cytoplasm as a defence mechanism against toxicity. My data show that the expression levels of this protein naturally decrease with age. Its levels further decrease in sALS patients compared to controls, consistent with the finding of accumulation of misfolded SOD1 in the nucleus. I confirmed the interaction between XPO1-SOD1 through a proximity ligation assay. Moreover, a decrease in the interaction between XPO1 and misfolded SOD1 was detected in sALS and C9orf72 ALS cases, in agreement with the higher levels of nuclear SOD1 observed in these ALS patient subgroups.

Acknowledgements

First, I would like to thank my primary supervisor Dr. Laura Ferraiuolo and my secondary supervisor Prof. Dame Pamela Shaw for giving me the opportunity to undertake this doctoral work and for their support over the last 3 and a half years. I am very grateful to Laura for her guidance, positivity and mentoring. She really helped me to grow as a scientist by being really inspirational for me. It was an honour being part of her team. I would also like to thank Pam for her remarkable help and great advice during my PhD.

Further, I would like to thank everyone in the Ferry lab, my second family, Matt, Cleide, Sophie, Nora, Monika, Chloe, Andre, Allan, Lai Mei, Simon, Jannigje and Marco for their help and support. All great scientists and incredible people, I have been very lucky to have you as colleagues. I am thankful to everyone in SITraN, my second home in Sheffield, where I met real friends. In particular, a big thank you to Camilla, Aurélie, Erica, Simeon, Ruby, Daniela, Ale and Francesca for supporting me during my PhD journey.

Huge thanks also to my dearest friends in Italy, my “grannies” Federica, Giulia, Alice, Valentina, Chiara and Marta, always there for me, although separated by 1500 km.

Next, I would like to acknowledge my big and wonderful family, Mum and Dad, my sisters Carmen and Barbara, my brothers-in-law Tony and Ale, my nephews Davide and Mattia and my nieces Alice and Alessia. Nothing would be possible without them and their help and constant support. I hope I have made you proud of me!

Lastly, special thanks to my boyfriend Tiziano, for being by my side during the last and most stressful year of my PhD. Thank you for being there for me.

Thank you very much to everyone (forgive me if I forgot to mention you) it has been an incredible experience. If I got this far, it is thanks to you all.

“I am among those who think that science has great beauty. A scientist in his laboratory is not only a technician: he is also a child placed before natural phenomena which impress him like a fairy tale. We should not allow it to be believed that all scientific progress can be reduced to mechanisms, machines, gearings, even though such machinery also has its beauty.

Neither do I believe that the spirit of adventure runs any risk of disappearing in our world. If I see anything vital around me, it is precisely that spirit of adventure, which seems indestructible and is akin to curiosity”

(Marie Curie 1867 – 1934)

Table of Contents

List of Tables

List of Figures

List of Abbreviations

AALS	Appel ALS rating scale
AD	Alzheimer's disease
ALS	Amyotrophic lateral sclerosis
ALSFRS-R	Revised ALS Functional Rating scale
ATP	Adenosine triphosphate
BBB	Blood brain barrier
BDNF	Brain derived neurotrophic factor
BMAA	β-Methylamino-l-alanine,
C9orf72	Chromosome 9 open reading frame 72
CD106	Cluster of differentiation 106
CD11	Alpha component of various integrins
CD68	Cluster of Differentiation 68
CNS	Central nervous system
CSF	Cerebrospinal fluid
DNA	DeoxyriboNucleic Acid
DPRs	Dipeptide repeat proteins
EAAT2	Excitatory amino acid transporter 2
EAE	Experimental autoimmune encephalomyelitis
ECT	Electron transport chain
ER	Endoplasmic reticulum
ERAD	ER-associated protein degradation
fALS	Familial Amyotrophic Lateral Sclerosis
FDA	Food and drugs administration
FTD	Fronto Temporal Dementia
FUS	Fused In Sarcoma
GFAP	Glial fibrillary acidic protein
GTPase	Nucleotide guanosine triphosphate (GTP) hydrolysis
H_2O_2	Hydrogen peroxide
hnRNP-H	Heterogeneous nuclear ribonucleoprotein H
iAstrocytes	induced astrocytes
IFN-γ	Interferon gamma
IGF-1	Insulin-like growth factor 1
IL-10	Interleukin 10
IL-1β	Interleukin 1 beta
IL-4	Interleukin 4
iNPC	induced neural progenitor cell
IPSCs	Induced pluripotent stem cells
kDa	kiloDalton
MAPK	Mitogen-activated protein kinase
MN	Motor neuron
MND	Motor neuron disease

mRNA	messanger ribonucleic acid
mSOD1	mutated SOD1
NADPH	Reduced form of nicotinamide adenine dinucleotide phosphate
NES	Nuclear export signal
Nf	Neurofilament
NfH	Heavy chain neurofilament
NFkB	Nuclear factor kappa-light-chain-enhancer of activated B cells
NfL	Light chain neurofilament
NfκB	Nuclear factor kappa B
NGF	Nerve growth factor
NLS	Nuclear localisation signal
NMJ	Neuromuscular junction
NO	Nitric oxide
Nox2	NADPH oxidase 2
Nrf2	Nuclear factor erythroid 2-related factor 2
NTR	Nuclear transport receptor
NuPC	Nuclear pore complex
Nups	Nucleoporins
p62	Ubiquitin-binding protein p62
p75	NGFR, Nerve growth factor receptor
PBS	Phosphate-buffered saline
PD	Parkinson's Disease
PLA	Proximity ligation assay
PM	Post-mortem
qPCR	Quantitative polymerase chain reaction
Rac1	Rac Family Small GTPase 1
RAN	Repeat-associated non-ATG
RBP	RNA binding protein
RNA	Ribonucleic acid
RNS	Reactive nitrogen species
ROS	Reactive oxygen species
sALS	Sporadic amyotrophic lateral sclerosis
SDS	Sodium dodecyl sulfate
shRNA	short hairpin RNA
SOD1	Superoxide dismutase 1
TARDBP	Transactive response (TAR) DNA-binding protein
TDP-43	TAR DNA-binding protein 43
Tg	transgenic
TNFα	Tumor necrosis factor alpha
UPS	Ubiquitin-proteasome system
WT	Wild type
XPO1	Exportin-1

1. Introduction

1.1 Amyotrophic lateral sclerosis (ALS)

ALS is the most common adult-onset motor neuron (MN) disorder. Motor neuron diseases (MNDs) are a heterogeneous group of neurological disorders that share the predominant loss of motor neurons. ALS accounts for approximately 85-90% of the total cases of MNDs and is characterised by loss of both upper and lower MN (Rowland and Shneider, 2001). In the United States and Canada, the disease is commonly called Lou Gehrig's Disease, after the name of the famous baseball player who developed this disease (Lou Gehrig 1903-1941).

The pathology is responsible for the loss of skeletal muscle innervation that leads to muscular atrophy and paralysis. ALS is a fatal disorder where death is usually caused by respiratory failure due to denervation of respiratory muscles within 3-5 years from diagnosis (Chiò *et al.*, 2009; Andersen and Al-Chalabi, 2011).

The vast majority of ALS cases (about 90%) are sporadic (sALS) with no family history of the disease, while in 5-10% of cases, the pathology is familial (fALS) and it is caused by specific inherited mutations (Kiernan *et al.*, 2011). Remarkably, familial and sporadic ALS are for the most part clinically indistinguishable.

ALS is a rare disease with an average incidence (number of new cases/year) of 1.5-2.7 per 100,000 inhabitants and an average prevalence (proportion of individuals in a population having the disease) which varies from 2.7 to 7.4 per 100,000 (Beghi *et al.*, 2011; Silani *et al.*, 2011; Chiò *et al.*, 2013). However, its impact is greater, because it has been calculated that the life-time risk of ALS is 1 in 400 for women and 1 in 350 for men (Kiernan *et al.*, 2011). The incidence of ALS is the same worldwide, except for some Western Pacific areas where it peaks 50-100 times higher than elsewhere (Steele and McGeer, 2008). In fact, there are high incidence foci in the Kii peninsula of Japan and the Western Pacific island of Guam. The increased incidence of ALS in these areas has been associated with environmental causes, particularly the ingestion of a neurotoxic non protein aminoacid, β-N-methyl-amino-l-alanine (BMAA). BMAA is in cycad seeds and is produced by cyanobacteria. Furthermore, it is present in brain and spinal cord tissues from sporadic ALS and Alzheimer's disease (AD) patients, but the precise involvement of BMAA in the disease is not totally understood (Vyas and

Weiss, 2009). This endemic form of ALS is associated with Parkinson's disease and dementia and is considered as a distinct disease compared to pure ALS.

Apart from age (section 1.5), no risk factor has been consistently associated with ALS. However, physical trauma and sports activities have been investigated: a higher risk of developing ALS was found in Italian professional soccer players (Belli and Vanacore, 2005; Chiò *et al.*, 2005), in American football players (Lehman *et al.*, 2012) and in military personnel (Beghi and Morrison, 2005). It is hypothesised that in addition to physical stress, performance-enhancing drugs, and fertilizers used in playgrounds could have an important role (Al-Chalabi and Leigh, 2005; Harwood *et al.*, 2016). Moreover, a hypothesis suggests that prenatal exposure to testosterone may play a role in the development of the disease (Wicks, 2012); however, the data produced so far are not conclusive.

ALS is heterogeneous in age and site of onset, as well as prognosis. Such diversity may depend on genetic and hormonal influences as well as environmental risk factors. ALS mainly strikes in adulthood, with a mean age of onset between 55 and 65 years and a median onset of 64 years of age (Silani *et al.*, 2011), but there are also rare cases of early onset characterised by a different disease course. Patients with an onset prior to 41 years show a survival rate three times higher than patients with onset after 60 years (Eisen *et al.*, 1993). Clinical manifestations of the disease are indicative of degeneration and subsequent death of the motor neurons at all levels (upper and lower). The loss of these motor neurons leads to severe muscle atrophy defined as denervation atrophy. Early symptoms depend on the body region first affected by the disease. The onset is “bulbar” (25% of patients) in the case of speech and swallowing muscles being initially affected. When symptoms begin in the arms or legs (upper and/or lower extremities), it is referred to as *“*limb onset*”* ALS (75% of patients) (Kiernan *et al.*, 2011). The degeneration of upper or lower MN leads to different symptoms in bulbar or limb onset patients. Limb onset disease is normally associated with weakness, lack of coordination and spasticity determined by upper MN alterations, while the loss of lower MN induces muscle wasting and fasciculation. In bulbar onset cases, the spastic dysarthria is attributed to upper MN degeneration, while dysphagia, atrophy of the tongue and fasciculation result from the loss of lower MN in the cranial nuclei of the brainstem.

Two rating scales are used in clinical practice for assessing ALS disease progression: the revised ALS Functional Rating scale (ALSFRS-R) and the Appel ALS rating scale

(AALS) (Cudkowicz, Qureshi and Shefner, 2004).The most frequently used is ALSFRS-R.

To date, there is no effective drug treatment for ALS. Riluzole and Edaravone are the only drugs approved by the US Food and Drugs Administration (FDA), providing modest benefits only in some patients (Petrov *et al.*, 2017; Sawada, 2017). Riluzole may reduce the loss of MN (Kalra *et al.*, 1998) and extend lifespan by about 3-6 months (Miller, Mitchell and Moore, 2012). Its mechanism of action remains obscure since it has many different targets. Among its effects are inhibition of voltage-gated Na^+ currents at the pre-synaptic terminal; inhibition of glutamatergic transmission both at presynaptic and postsynaptic levels; interaction with other types of ion channels (Ca^{2+} and K^+) and increased production of brain derived neurotrophic factor (BDNF) (Bellingham, 2011). Edaravone is an intravenous drug approved in May 2017 after a Phase 3 clinical trial in Japan, that showed its ability to slow decline in the daily ALSFRS, potentially by reducing oxidative stress (Hardiman and van den Berg, 2017). More than 500 compounds with potential neuroprotective effects have been studied, which include: anti-oxidants, anti-excitotoxic agents, inhibitors of apoptosis, anti-inflammatory agents, neurotrophins, chelators of metal ions and modulators of ion channels. Unfortunately several drugs, which showed some benefits in animal models of ALS, did not show efficacy in human clinical trials (Carrì, Grignaschi and Bendotti, 2006). Various reasons can account for this lack of translation: the non-physiological levels of mutant protein overexpressed by the mouse model, the genetic and phenotypic heterogeneity of patients, the difficulty in establishing patient-relevant pharmacokinetic parameters in order to replicate the same biological activity in humans, the different disease time points at which the treatment was started, and the limitations of the mutant SOD1 model in reproducing the heterogeneity of the various ALS forms (Carrì, Grignaschi and Bendotti, 2006; Benatar, 2007; Oliveira and Pereira, 2009).

Furthermore, approximately 5% of patients with ALS fulfil the consensus criteria for definite or probable fronto-temporal dementia (FTD) (Kiernan *et al.*, 2011) and up to 50% may have some evidence of altered fronto-temporal function on detailed neuropsychological testing. Recent genetic discoveries, which have linked mutations in chromosome 9 open reading frame 72 (*C9ORF72*) and TAR DNA binding protein 43 (*TARDBP*) to both ALS and FTD, have highlighted how these two pathologies belong to the same disease spectrum.

This further adds to the complexity of ALS and translation from animal models to patients.

1.1.1 ALS genetics

ALS is considered a multifactorial disease due to the interplay between genetic and environmental factors. Most ALS cases (about 90%) are sporadic (sALS) with no family history of the disease, while in 5-10%, the pathology is familial (fALS) and it is caused by specific inherited mutations (Kiernan *et al.*, 2011). FALS is characterized in most cases by an autosomal dominant transmission with age dependent penetrance (Al Sultan *et al.*, 2016), but recessive and X-linked forms have also been described (Chen *et al.*, 2013). The clinical phenotype of fALS and sALS is usually indistinguishable, but fALS is usually characterized by an earlier age at onset compared to sALS. Moreover, familial patients show an equal male/female ratio and in general a longer disease duration; whereas sALS is commoner in males, with a male/female ratio of 1.5/1 (Manjaly *et al.*, 2010; Ticozzi *et al.*, 2011).

1.1.1.1 Familial ALS (fALS)

Each new gene (Table 1.1) that is linked to ALS aetiology provides important information on the involvement of specific pathogenic mechanisms, consequently attracting a lot of interest in the identification of new gene mutations.

Molecular genetic techniques, such as genome-wide association studies and next-generation sequencing, have contributed to the understanding of the genetic causes of fALS with approximately 60-70% of cases accounted for by variants in known ALS-linked genes (Renton, Chiò and Traynor, 2014; Zou *et al.*, 2017). The most frequent pathogenic variants are present in *SOD1* (~20% fALS)*, C9ORF72* (~40% fALS)*, FUS* (~4% fALS) and *TARDBP* (~5% fALS) (Boylan, 2015; Al Sultan *et al.*, 2016). Given the central role of SOD1 in my thesis, the function of this protein in ALS is going to be described in section 1.3. C9orf72 genetic mutations were first observed in 2011 in patients with FTD, and subsequently in ALS patients (DeJesus-Hernandez *et al.*, 2011; Renton *et al.*, 2011). This represents the most common inherited cause of ALS in European populations, approximately 34-40% of fALS cases (Zou *et al.*, 2017). TDP-43 was identified by histological studies as a main component of cytosolic inclusions in FTD and ALS patients (Arai *et al.*, 2006; Neumann *et al.*, 2006) and it is now considered a pathological hallmark of ALS, being present in the majority of ALS

patients including cases without mutations in *TARDBP* (Giordana *et al.*, 2010; Schipper *et al.*, 2016; Takeuchi *et al.*, 2016). To date, around 50 variants in *TARDBP* have been described in ALS (Lattante, Rouleau and Kabashi, 2013). Notably, dominant mutations were identified as a primary cause of ALS (Kabashi *et al.*, 2008; Sreedharan *et al.*, 2008; Yokoseki *et al.*, 2008). FUS pathogenic variants were identified in 2009, in a subset of ALS patients (Kwiatkowski *et al.*, 2009; Vance *et al.*, 2009). Interestingly, mutations in *FUS* often lead to an early onset form of ALS (Hübers *et al.*, 2015; Gromicho *et al.*, 2017; Zou *et al.*, 2017). More details on aberrant pathogenic variants and their disease related mechanisms will be discussed in the following sections of this thesis.

The genes associated with ALS can be linked into functional groups: such as RNA metabolism, protein quality control system (including autophagy, molecular chaperones and proteases) and endosomal trafficking. These main pathways have been found to be dysregulated not only in patients carrying specific mutations, but also in samples from sALS patients.

Table 1.1 *Altered pathways and genetic determinants identified so far in ALS and respective subtypes of ALS*

Autosomal dominant (AD); Autosomal recessive (AR), X-linked (XD)

Pathway	ALS type	Gene (protein)	Inheritance	Reference
Oxidative stress	ALS1	*SOD1* (Superoxide dismutase 1)	AD or AR	(Rosen *et al.*, 1993)
RNA metabolism	ALS4	*SETX* (Senataxin)	AD	(Suraweera *et al.*, 2007)
	ALS6	*FUS* (RNA-binding protein FUS)	AD or AR	(Kwiatkowski *et al.*, 2009; Vance *et al.*, 2009)
	ALS9	*ANG* (Angiogenin)	AD	(Greenway *et al.*, 2006)

	ALS10	*TARDBP* (TAR DNA-binding protein 43)	AD	(Rutherford *et al.*, 2008; Sreedharan *et al.*, 2008; Kabashi *et al.*, 2009)
	ALS13	*ATX2* (Ataxin 2)	AD	(Elden *et al.*, 2010)
	ALS20	*HNRNPA1* (Heterogeneous nuclear ribonucleoprotein A1)	AD	(Kim *et al.*, 2013)
	ALS21	*MATR3* (Matrin 3)	AD	(Johnson, Pioro, *et al.*, 2014)
RNA metabolism and autophagy	ALS-FTD1	*C9orf72* (Guanine nucleotide exchange chromosome 9 open reading frame 72)	AD	(DeJesus-Hernandez *et al.*, 2011; Renton *et al.*, 2011)
Membrane receptor/transporter	ALS5	*SPG11* (Spatacsin)	AR	(Daoud *et al.*, 2012)
Endosomal trafficking/ Endoplasmic reticulum stress	ALS2	*ALS2* (Alsin)	AR	(Hadano *et al.*, 2010)
	ALS11	*FIG4* (Polyphosphoinositide phosphatase)	AD	(Chow *et al.*, 2009)
	ALS17	*CHMP2B* (Charged multivesicular body protein 2B)	AD	(Cox *et al.*, 2010)

	ALS8	*VAPB* (Vesicle-associated membrane protein-associated protein B/C)	AD	(Nishimura *et al.*, 2004; Gkogkas *et al.*, 2008; Chen *et al.*, 2010)
Autophagy/ Ubiquitin-proteasome system	ALS12	*OPTN* (Optineurin)	AD or AR	(Maruyama *et al.*, 2010)
	ALS14	*VCP* (Valosin-containing protein)	AD	(Johnson *et al.*, 2010)
	ALS-FTD3	*SQSTM1* (Sequestosome 1)	AD	(Fecto *et al.*, 2011)
	ALS-FTD4	*TBK1* (Serine/threonine-protein kinase TBK1)	Unknown	(Freischmidt *et al.*, 2015)
	ALS15	*UBQLN2* (Ubiquilin-2)	XD	(Deng *et al.*, 2011)
	ALS16	*SIGMAR1* (Sigma non-opioid intracellular receptor 1)	AD	(Luty *et al.*, 2010; Al-Saif, Al-Mohanna and Bohlega, 2011)
Cytoskeleton	ALS18	*PFN1* (Profilin 1)	AD	(Wu *et al.*, 2012)
	ALS22	*TUBA4A* (Tubulin α4A)	AD	(Smith *et al.*, 2014)
Mitochondrial maintenance	ALS-FTD2	*CHCHD10* (Coiled-coil-helix-coiled-coil-	AD	(Johnson, Glynn, *et al.*, 2014)

		helix domain-containing 10)		
Neuronal development	ALS19	*ERBB4* (Receptor tyrosine-protein kinase erbB 4)	AD	(Takahashi *et al.*, 2013)
Unknown	ALS3	Unknown	AD	(Hand *et al.*, 2002)
	ALS7	Unknown	AD	(Sapp *et al.*, 2003)

1.1.1.2 Sporadic ALS (sALS)

Although the aetiology of sALS is largely unknown, genetic factors contribute to its pathogenesis. In some sALS cases gene changes highlighted in Table 1.1 can be found. Mutations in the genes listed in Table 1.2 can lead to ALS interacting with other genetic or environmental risk factors (Schymick, Talbot and Traynor, 2007) however, sALS cases bearing particular genetic variants represent only a small proportion of the sALS cases (20%). The reason may be attributable to an inheritance complex pattern of low penetrance; a high level of heterogeneity and/or the existence of other predisposing factors.

Table 1.2 *Susceptibility genes for sporadic ALS (sALS)*

Gene	Protein	Function	Association to ALS	References
VEGF	Vascular endothelial growth factor	Vascular permeability, neuronal growth and repair	Two haplotypes in VEGF promoter	(Lambrechts *et al.*, 2003)
NFH	Neurofilament heavy subunit	Provides a supporting network for neuronal axons	Deletions in C-terminal and insertions	(Figlewicz *et al.*, 1994; Tomkins *et al.*, 1998; Al-

			in KSP domain	Chalabi *et al.*, 1999)
PRPH	Peripherin	Neuronal intermediate filament involved in axonal growth	Missense mutation and frameshift deletion, presence in motoneuronal inclusions	(Gros-Louis *et al.*, 2004; Leung *et al.*, 2006)
SMN1/2	Survival motoneuron	Neuronal proteins involved in RNA processing	Alterations in copy number	(Corcia *et al.*, 2002; Veldink *et al.*, 2005; Lee *et al.*, 2012)
ATXN2	PolyQ protein mutated in spinocerebellar ataxia type 2	CAG repeated expansions	Potent modifier of TDP-43 toxicity	(Elden *et al.*, 2010)
PON	Paraoxonase	Serum enzyme involved in detoxification of organophosphate and neurotoxins	PON1 and PON2 polymorphism	(Ticozzi *et al.*, 2010)
ApoE ε4	Apolipoprotein E (APOE)	Involved in lipoprotein metabolism	Apo ε4 carriers	(Praline *et al.*, 2011)
GLE1	GLE1 RNA export mediator	Involved in RNA export	Two deleterious mutations	(Kaneb *et al.*, 2015)

1.1.2 Pathogenic mechanisms

ALS is a multifactorial disease, with involvement of several cell types and pathogenic mechanisms (Ferraiuolo *et al.*, 2011). Although *in vivo* (Yamanaka *et al.*, 2008; Hooten *et al.*, 2015) and *ex vivo* (Ferraiuolo *et al.*, 2007; Nardo *et al.*, 2013) studies have indicated that not all pathways and cell types are involved in disease pathology at once, the exact sequence of events involved in disease onset, progression and end stages is yet to be unravelled. Nevertheless, it is clear that the interplay between various factors and cell types plays an important role in the presentation of disease symptoms and progressive degeneration of MN (Figure 1.1). In the following sections, I will give a brief overview of the main pathways associated with the pathophysiology of ALS emerging from *in vitro* and *in vivo* studies.

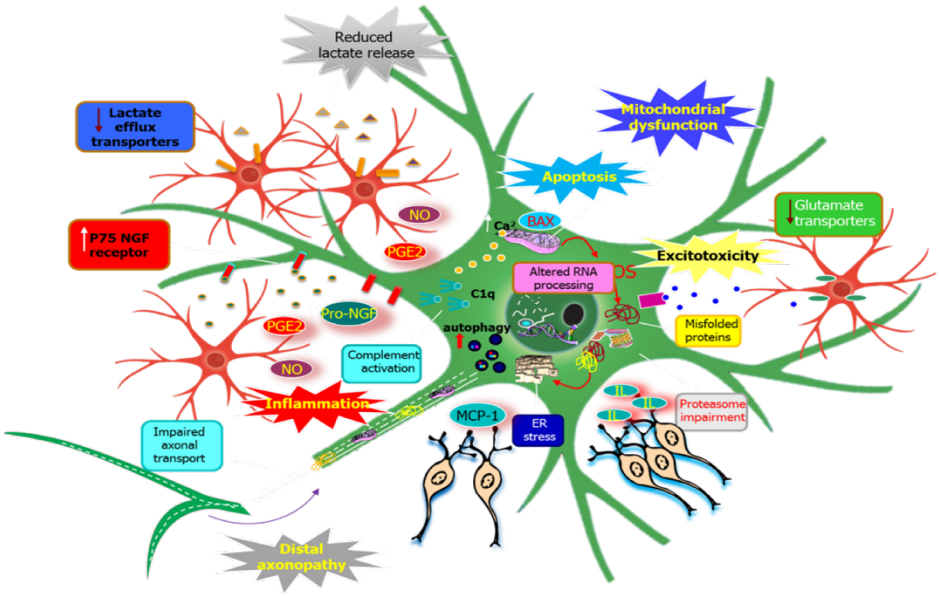

(Ferraiuolo et al. 2011 Nature Reviews Neurology)

Figure 1.1 *Molecular mechanisms of motor neuron injury in ALS*

Several cell types and mechanisms are involved in ALS. Astrocytes contribute to motor neuron injury through different pathways: release of inflammatory mediators, reduced expression and activity of the glutamate reuptake transporter excitatory amino acid transporter 2 (EAAT2); reduced lactate release; and activation of pro-NGF–p75 receptor signaling, while microglia activate an inflammatory response. Transcriptional dysregulation and altered RNA processing may occur in motor neuron themselves, that together with overproduction of reactive oxygen species (ROS) contributes to aberrant protein folding. This can lead to the formation of aggregates and subsequently to proteasome impairment and ER stress. Eventually autophagy and apoptotic pathways are activated. The activation of apoptosis is also determined by mitochondrial impairment and dysregulation of calcium homeostasis. Axonal transport is also impaired which may contribute to an energy deficit in the distal axon.

ER, endoplasmic reticulum; IL, interleukin; MCP-1, monocyte chemoattractant protein 1; NGF, nerve growth factor; NO, nitric oxide; PGE2, prostaglandin E2.

1.1.2.1 Oxidative stress

One of the first pathways investigated in ALS was oxidative stress, due to the identification of ALS-causing mutations in SOD1, an anti-oxidant enzyme, in 1993 (Rosen *et al.*, 1993). ROS are produced by aerobic metabolism and they can potentially damage cells by oxidizing many biomolecules, such as DNA, proteins and lipids. It is well known that prevention of the activation of this deleterious pathway involves antioxidant agents in the removal of these reactive species. Biochemical markers of oxidative stress are present in *post-mortem* tissues from patients affected by several neurological diseases, including ALS (Islam, 2017). Oxidative stress results from an imbalance between the production of oxidant species, such as reactive oxygen (ROS), nitrogen (RNS) species and hydrogen peroxide (H_2O_2) and the cellular antioxidant mechanisms that remove them, including the SOD1 enzyme. An increase of oxidative damage markers has been reported in both sALS and fALS patients (Shibata *et al.*, 2001; Nardo *et al.*, 2009; Lopez-Gonzalez *et al.*, 2016) as well as in mouse models of the disease (Casoni *et al.*, 2005; Nardo *et al.*, 2009). Oxidative damage has been observed not only in neurons, but also in glial cells in *post-mortem* tissues from ALS patients (Shibata and Kobayashi, 2008). Indeed, a recent study reported induced pluripotent stem cells (iPSC) derived astrocytes carrying *C9orf72* mutations to be toxic to MN through soluble factors, downregulating the secretion of various antioxidant proteins (Birger *et al.*, 2019). Moreover, in a mouse study, conditioned medium derived from astrocytes expressing mutated *SOD1* or *TARDBP* has been shown to induce rapid oxidative stress and extensive spinal MN death within few days (Rojas *et al.*, 2014). This evidence suggests that the oxidative stress pathway may play a role in multiple disease genotypes. Indeed, oxidative stress may lead to loss of MN through several mechanisms, including mitochondrial damage, deleterious post-translational changes to proteins, cytoskeleton alterations, glial activation and release of pro-inflammatory cytokines and DNA/RNA oxidation (Banati *et al.*, 1993; Crow *et al.*, 2002; Rao, Yin and Weiss, 2003; Barber and Shaw, 2010).

1.1.2.2 Dysregulation of proteostasis

Protein misfolding is also one of the hallmarks of ALS. This process occurs physiologically in the cell, however, it is ameliorated through several mechanisms, such as the action of molecular chaperones, the ER-associated protein degradation (ERAD) and the ubiquitin-proteasome system (UPS). These and other mechanisms

work synergistically with each other and the impairment of one of these pathways may lead to protein accumulation. Extra and intracellular proteinaceous inclusions containing misfolded and abnormal ubiquitinated proteins are features of both sALS and fALS (Migheli et al., 1990; Kato, 1999) and they are also observed in the spinal cord of SOD1 G93A mice (Stieber, Gonatas and Gonatas, 2000; Cheroni et al., 2005, 2009). Inclusions contain different proteins, such as SOD1, ubiquitin, chaperones (Watanabe et al., 2001), TDP-43 (Sanelli et al., 2007), dorfin (a ubiquitin ligase) (Hishikawa et al., 2003), neurofilaments and p38-MAPK (Bendotti et al., 2004). Alterations of the ubiquitin-proteasome system and insufficient levels of chaperone proteins in the ER contribute to protein aggregation (Cheroni et al., 2009) and protein aggregates may exert toxic effects by sequestering important key cellular elements.
In this regard, in 2006, TDP-43 was identified as a key component of the insoluble and ubiquitinated inclusions in the brains of ALS and FTD patients (Arai *et al.*, 2006; Neumann *et al.*, 2006). Strikingly, aggregation of TDP-43 is present in ~97% of the ALS cases and ~45% of all FTD cases (Ling, Polymenidou and Cleveland, 2013; Tan *et al.*, 2017). However, it is still controversial whether TDP-43 pathology occurs in SOD1-ALS (Arai *et al.*, 2006; Mackenzie *et al.*, 2007; Robertson *et al.*, 2007; Turner *et al.*, 2008; Shan, Vocadlo and Krieger, 2009; Mackenzie, Rademakers and Neumann, 2010). Several studies in SOD1 mice reported there is no redistribution of TDP-43 (Robertson et al., 2007; Turner et al., 2008), and only a few studies have reported a low number of SOD1-related fALS cases displaying TDP-43 cytoplasmic inclusions (Neumann *et al.*, 2006; Tan *et al.*, 2007). This evidence has led to the conclusion that patients with SOD1 mutations do not have the typical TDP-43 proteinopathy which characterises most cases of ALS. Patients carrying SOD1 mutations, in fact, display SOD1 cytoplasmic inclusions the pathological impact of which will be reviewed in more detail in section 1.3.2.2.

1.1.2.3 Excitotoxicity

Another pathway associated with ALS is excitotoxicity, caused by glutamate accumulation at the synapse. Glutamate is the main excitatory neurotransmitter in the central nervous system (CNS), through activation of ionotropic and metabotropic postsynaptic receptors. The excitatory signal terminates when glutamate is removed from the synaptic cleft by transporters, such as the excitatory amino acid transporter 2 (EAAT2, SLC1A2 or GLT1). Excessive levels of synaptic glutamate cause

glutamate-induced excitotoxicity. Support for this toxic mechanism in ALS has been provided by human and animal studies (Trotti *et al.*, 1999; Boillée, Vande Velde and Cleveland, 2006). In fact, increased glutamate levels in cerebrospinal fluid (CSF) were reported in ALS patients (Rothstein *et al.*, 1991; Shaw *et al.*, 1995) and reduced expression and activity of the astrocyte excitatory amino acid transporter 2 (EAAT2) were detected in *post-mortem* motor cortex and spinal cord of ALS patients (Lin *et al.*, 1998). In a transgenic SOD1 mouse model increased glutamate release from nerve terminals in mutant SOD1 mice was observed (Trotti *et al.*, 1999; Milanese *et al.*, 2011). Glutamate-mediated excitotoxicity leads to a cascade of cellular events and pathway dysregulation well characterised in ALS, including abnormal calcium influx in MN, Ca^{2+} overload of mitochondria and alteration of ER storage ability, activation of protein kinases, phospholipases and nitric oxide synthase and free radical production. Further supporting a pathogenic role of glutamate in ALS is the neuroprotective action of the anti-glutamate agent Riluzole (Miller *et al.*, 2002).

1.1.2.4 Mitochondrial dysfunction

Mitochondrial dysfunction is also considered a potential pathogenetic factor involved in the aetiology of ALS. Mitochondria are important organelles playing a key role in the production of cellular energy as adenosine triphosphate (ATP), but they are involved in other essential functions such as regulation of calcium homeostasis, steroid metabolism and apoptosis regulation. Morphological and functional defects in mitochondria were found in both human MN from ALS patients (Sasaki, Horie and Iwata, 2007) and ALS cell and animal models (Hong et al., 2012; Magrané et al., 2014). In particular, in mice overexpressing mutant SOD1, it has been consistently found that mitochondria are less elongated and more spherical in MN (Higgins, Jung and Xu, 2003; De vos et al., 2007; Vande Velde et al., 2011). Moreover, mutant SOD1 was found to be associated with mitochondria. In fact, SOD1 aggregates have been found in the intermembrane space of mitochondria in MN of various mouse models and in ALS patients (Higgins, Jung and Xu, 2003). Misfolded SOD1 protein aggregates impair mitochondrial function by firstly damaging the mitochondrial membrane and secondly, leading to the loss of mitochondrial membrane potential, swelling of the organelle and excess superoxide production (Pasinelli *et al.*, 2004; Pickles *et al.*, 2013, 2016). Another ALS-associated protein, TDP-43 has been shown to interact with mitochondria (Wang *et al.*, 2016). Mutant TDP-43 accumulation occurs in

mitochondria, possibly mediated by internal mitochondrial targeting sequences in TDP-43 (Wang *et al.*, 2016). In this organelle, TDP-43 may directly affect the regulation of mRNA coding for proteins involved in mitochondrial physiology, altering the mitochondria dynamics (Wang *et al.*, 2013). Mitochondria produce ATP via oxidative phosphorylation, an essential substrate for cellular metabolism. Alteration in energy homeostasis and ATP deficits have been observed in skeletal muscle biopsies from ALS patients. Evidence confirmed a reduction in the activity of respiratory chain complexes I, II, III and IV in *post-mortem* spinal cord of sALS patients (Borthwick et al., 1999; Wiedemann et al., 2002), this is linked with defective energy metabolism (Pasinelli and Brown, 2006). Mutant SOD1 also affects the electron transport chain (ECT) (Vijayvergiya et al., 2005; Ferri et al., 2006), leading to a decreased production of ATP (Mattiazzi et al., 2002; Knott et al., 2008). Impaired mitochondrial respiration and ATP production have also been seen in models of non-SOD1 related familial ALS (Duan et al., 2009; Hong et al., 2012; Wang et al., 2013). Furthermore, mitochondria in MN are responsible for buffering cytosolic calcium levels. Calcium represents one of the main intracellular messaging systems, regulating synaptic transmission, neuronal development and metabolic pathways. It has been reported that mutant SOD1 affects calcium homeostasis and in general, intracellular calcium homeostasis is altered in ALS patients, with lower calcium buffering ability being a significant risk factor for MN damage (Alexianu *et al.*, 2000; Beers *et al.*, 2001; Jaiswal, 2013). Lastly, several studies confirmed the disruption of axonal transport of mitochondria in ALS patients (Borthwick *et al.*, 1999; Mórotz *et al.*, 2012). Indeed, axonal transport impairment alters the degradation and recycling processes of damaged mitochondria, leading to higher levels of disrupted mitochondria at the distal axon, with alterations in both anterograde and retrograde transport of mitochondria (De vos *et al.*, 2007; Magrané and Manfredi, 2009; Shi *et al.*, 2010). Conclusively, all these studies show that mitochondrial dysfunction is a critical feature of the pathophysiology in ALS. However, it is not clear whether mitochondrial dysfunction is a primary event or whether it occurs secondary to other cellular processes that lead to neuronal injury.

1.1.2.5 Axonal and cytoskeletal dysfunction

The transport of molecules and organelles in neurons is highly organized to be able to reach the axon terminus that might be located one metre away from the cell body in the case of motor neurons. Neurofilaments (Nf) are specific intermediate filaments of

neuronal cells that allow the transport of proteins synthesized in the cell body and directed towards the neuromuscular junction (NMJ) (anterograde transport) or substances, such as trophic factors, directed toward the cell body (retrograde transport). Nf accumulation in cell bodies and proximal axons of MN have been described in sALS and fALS patients (Hirano *et al.*, 1984). Remarkably, cytoskeletal disorganization and inhibition of axonal transport due to the presence of SOD1 aggregates was also found in SOD1 transgenic mice (Borchelt *et al.*, 1998; Ligon *et al.*, 2005). Furthermore, increased Nf levels are found in the CSF of ALS patients (Tortelli et al., 2012) and Nf accumulation in degenerating axons and an altered axonal transport are present in fALS mice (Ligon et al., 2005; Perlson et al., 2009; King et al., 2012). Importantly, it has been shown that Nf heavy (NfH) and light (NfL) chain levels reflect neuronal injury and therefore can represent a valuable biomarker in ALS. In particular, in CSF the phosphorylated form of NfH level seems to be the most accurate diagnostic marker for ALS, while both phosphorylated and non-phosphorylated Nf in serum or plasma could predict survival and disease progression (Poesen and Van Damme, 2019). Overexpression of NfH provokes MN axonal defects with Nf inclusions in mice, which can be rescued by NfL overexpression (Meier *et al.*, 1999), thus suggesting that an imbalance in the stoichiometry of Nf subunits may be important. Consistent with this hypothesis, decreasing NfL levels and overexpression of NfH levels in the SOD1 mouse model of ALS, increased the survival of these animals (Couillard-Després *et al.*, 1998; Williamson *et al.*, 1998). In this mouse model, MN degeneration is generally accompanied by a progressive increase in blood Nf levels, correlating with treatment responses (Boylan *et al.*, 2009; Lu *et al.*, 2012). A defect in axonal transport is one of the earliest events seen in ALS, though it still unclear if this is causative for disease.

1.1.2.6 Aberrant RNA metabolism

The identification of ALS-causing mutations in two RNA binding proteins: TDP-43 and FUS/TLS has led to hypothesis that alterations in the RNA processing pathway may represent an important pathogenic mechanism in ALS (Blitterswijk and Landers, 2010). The specific role of these two proteins is not fully understood, but both are multifunctional proteins that are involved in different steps of gene expression/regulation including RNA splicing, transcription, translation and RNA transport. TDP-43 is a ubiquitous protein that contains two RNA-binding protein

domains, nuclear import and export signals and a glycine-rich domain (Lagier-Tourenne, Polymenidou and Cleveland, 2010). Normally TDP-43 functions as a shuttle between the cytoplasm and nucleus (Ayala *et al.*, 2008; Lagier-Tourenne, Polymenidou and Cleveland, 2010). Fused in sarcoma (*FUS*) mutations as a cause of ALS were discovered shortly after the identification of *TARDBP* (Kwiatkowski *et al.*, 2009; Vance *et al.*, 2009). Similar to TDP-43, FUS/TLS is mainly nuclear but binds RNAs and shuttles between the nucleus and cytoplasm (Zinszner *et al.*, 1997).
The hypothesis was put forward that ALS-causing mutations in *TARDBP* and *FUS* lead to a toxic gain of function when their respective products form cytoplasmic aggregates (Lagier-Tourenne, Polymenidou and Cleveland, 2010). Moreover, TDP-43 and FUS/TLS have been associated with stress granules, which are protein-RNA complexes that reversibly form under stress (Bosco *et al.*, 2010; Liu-Yesucevitz *et al.*, 2010; Sama *et al.*, 2013; Walker *et al.*, 2013). In ALS pathology, stress granules act as hubs that may facilitate toxic protein aggregation (Chen and Cohen, 2019; Baradaran-Heravi, Van Broeckhoven and van der Zee, 2020). The other complementary, non-exclusive hypothesis, is that TDP-43 and FUS aggregates lead to a loss of function, as consequence of their nuclear depletion, this causes loss of correct splicing in the nucleus, aberrant transcripts and loss of normal shuttling between nucleus and cytoplasm (Ishigaki and Sobue, 2018; Prasad *et al.*, 2019).

The noncoding GGGGCC (G4C2) hexanucleotide repeat located in the first intron of *C9orf72* has gained importance in ALS research. The repeat expansion counts for a significant percentage, around 40% of fALS, and around 25% of familial FTD cases (DeJesus-Hernandez et al., 2011; Renton et al., 2011; Majounie et al., 2012). Moreover, it has been found that around 7% of apparently sALS cases in European populations carry mutations in *C9orf72*. Three competing but non-exclusive disease mechanisms have been proposed: loss of function of the C9orf72 protein, toxic gain of function from C9orf72 repeat RNA foci or from dipeptide repeat proteins (DPRs), poly-GA, poly-GP, poly-GR, poly-PA and poly-PR, produced by repeat-associated non-ATG (RAN) translation (Ash *et al.*, 2013; Gendron *et al.*, 2013; Mori, Arzberger, *et al.*, 2013; Mori, Weng, *et al.*, 2013; Zu *et al.*, 2013). The reduction of C9orf72 protein level may cause inhibition of endosomal trafficking and the perturbation of endocytosis, leading to autophagy (Farg *et al.*, 2014; Waite *et al.*, 2014; Nassif, Woehlbier and Manque, 2017). Alterations in protein homeostasis are reviewed in

section 1.1.2.2. However, C9orf72 conditional knockout in mice does not cause motor neuron degeneration or motor deficits, indicating that a loss of C9orf72 function by itself was not sufficient to cause motor neuron disease (Koppers *et al.*, 2015). Moreover, it has been reported that haploinsufficiency for C9orf72 activity contributes to neurodegeneration in C9orf72 ALS patients, this may be explained by the accumulation of glutamate receptors, causing excitotoxicity and impaired clearance of misfolded proteins and neurotoxic DPRs (Shi *et al.*, 2018). This suggests a synergism between gain and loss of functions in C9orf72 ALS.

Like the other repeat expansion diseases, RNA binding proteins (RBPs) can be sequestered by RNA foci, leading to downstream consequences. For example, the interaction with heterogeneous nuclear ribonucleoprotein hnRNP-H and multiple RNA transcripts, lead to important dysregulation of RNA processing (Lee et al., 2013). Additionally, this G4C2 expansion mutation can be transcribed in both sense and anti-sense directions, generating DPRs identified in the p62-positive aggregates in the CNS of C9orf72-ALS patients (Gendron *et al.*, 2013; Mann *et al.*, 2013; Zu *et al.*, 2013). The exact role of DPRs and RNA foci toxicity in C9orf72-associated pathophysiology remains controversial, but it is becoming clear that they have detrimental effects on nucleolar function and RNA metabolism (Barker *et al.*, 2017).

1.2 Non cell autonomous effects

ALS is a "non cell autonomous" disease with evidence that other cells, such as astrocytes, oligodendrocytes, peripheral glial cells (i.e. Schwann cells) and cells of the immune system (macrophages, T lymphocytes), have an important role in the neurodegenerative process. Microglia and astrocyte activation and infiltrating T cells and dendritic cells have been extensively documented in *post-mortem* CNS tissues of ALS patients (Troost *et al.*, 1989; Troost, van den Oord and Jong, 1990; Kawamata *et al.*, 1992; Henkel *et al.*, 2004). In addition, a substantial loss of interneurons has been reported in the spinal cord (Stephens *et al.*, 2006), indicating that motor neurons are not the only neuronal population affected in this area of the CNS. Moreover, at the peripheral level, skeletal muscles are dramatically affected even at the earliest stage of the disease and undergo massive atrophy and several additional alterations (Léger *et al.*, 2006; Yin *et al.*, 2012). However, the involvement of the skeletal muscle in ALS is still controversial, as, despite early alterations, several studies suggest that these changes are only a secondary effect resulting from denervation (Miller *et al.*, 2006;

Dobrowolny *et al.*, 2008). In particular, the use of a deletable mutant gene to reduce mutant SOD1 from muscle did not provide any benefit in slowing disease onset or progression (Miller *et al.*, 2006). Of relevance in this context, genetic studies focusing on expression or repression of mutant SOD1 in selected cell types have helped us understand the role and interplay between different non-neuronal cells. For example, gene mutations leading to human fALS, cause ALS-like disease in animal models only if expressed both in neurons and glial cells. Attempts to generate disease from selective mutant SOD1 expression only in MN failed. Furthermore, the silencing of mutant SOD1 only in MN induced a moderate effect on onset (delay of 20%) without interfering with the progression of the disease (Boillée *et al.*, 2006), while silencing of mutant SOD1 selectively in glial cells affected disease progression without altering onset (Yamanaka *et al.*, 2008).

In vitro studies have clearly demonstrated that human astrocytes (Haidet-Phillips *et al.*, 2011; Meyer *et al.*, 2014; Re *et al.*, 2014) and oligodendrocytes (Ferraiuolo *et al.*, 2016) from fALS and sALS cases, as well as primary murine microglia (Frakes *et al.*, 2014) not only are active players in disease progression in the presence of an injured neuron, but they can in fact actively induce death of healthy motor neurons. To date, how the non-neuronal cells induce toxicity remains incompletely understood. However, several hypotheses involving metabolic support, inflammation and glutamate toxicity, have been put forward. Due to the focus of this thesis, I will mainly concentrate on the contribution of astrocytes and microglia to the disease rather than other non-neuronal cells.

1.2.1 Astrocytes

Astrocytes are a large group of glial cells, necessary for homeostasis, defence and regeneration of the CNS (Burda and Sofroniew, 2014). The loss of neuroprotective functions and the gain of a neurotoxic function are two possible roles that astrocytes can assume in the pathophysiology of ALS. Astrocytes of spinal and cortical areas that show motor neuron degeneration, exhibit a selective loss or dysfunction of glutamate transporters, suggesting a contribution of glutamate-mediated excitotoxicity in neuronal death (Maragakis and Rothstein, 2006; Rattray and Bendotti, 2006). Indeed, one of the first pieces of evidence of glial dysfunction in human patients and in animal models of ALS came from observation of marked decrease in the expression of EAAT2 (called GLUT-1 in rodents) in the motor cortex and spinal cord, in mouse models as

well as in both familial and sporadic ALS patients (Rothstein, Martin and Kuncl, 1992; Bruijn *et al.*, 1997). Molecular knockdown of this astroglial protein also induced MN degeneration and paralysis (Rothstein *et al.*, 1996). In this regard, β-lactam antibiotics have been identified as potential therapeutic molecules and they can stimulate the expression of glutamate transporters in astrocytes, thereby increasing the absorption and reducing the neurotoxic action of glutamate in animal models of ALS and ischaemia (Rothstein, Martin and Kuncl, 1992; Rothstein *et al.*, 2005). Remarkably, it has been shown that transplantation of healthy astrocytes has neuroprotective effects in murine models of ALS, suggesting that this may represent a potential therapeutic strategy (Lepore *et al.*, 2008). On the other hand, however, it can be observed that astrocytes may have a neurotoxic effects in ALS. It has been shown, in fact, that the expression of mutant SOD1 (mSOD1) exclusively in astrocyte cells accelerates the progression of the pathology (Yamanaka *et al.*, 2008) through the production of soluble molecules that have a toxic effect on motor neurons, but not on the interneurons of the spinal cord. The molecular mechanisms of toxicity are not entirely clear (Nagai *et al.*, 2007; Di Giorgio *et al.*, 2008). It has also been demonstrated that transplantation of glial precursors expressing mSOD1 into the spinal cord of wild-type mice, is able to induce the degeneration of motor neurons and activate the surrounding microglia (Papadeas *et al.*, 2011). Astrocyte characteristics change in the presence of mSOD1 and, as mentioned before, they contribute to motor neuron degeneration (Ferraiuolo *et al.*, 2011). Noticeably, decreased metabolic support from lactate release and activation of the p75 receptor signalling pathway appear to be important players in astrocyte toxicity. Removal of the astrocyte toxicity could be obtained by increasing lactate provision to motor neurons, reducing NGF levels, or blocking the p75 receptor (Ferraiuolo *et al.*, 2011; Madji Hounoum *et al.*, 2017). When astrocytes encounter any biological risk in their immediate proximity, they become reactive and increase the expression of some astrocyte markers, such as the glial fibrillary acidic protein (GFAP), in a process termed astrogliosis. Astrogliosis has been detected both in human and rodent ALS models (Schiffer *et al.*, 1996; Levine *et al.*, 1999). Interestingly, downregulation or knockout of the master regulator of inflammation, NfκB, in astrocytes resulted in no significant beneficial effect in the mouse model of ALS (Crosio *et al.*, 2011) or in *in vitro* assays (Frakes *et al.*, 2014). On the contrary, both *in vivo* and *in vitro* studies have shown that inhibition of NfκB in microglia results in significant improvement in survival and delay in disease progression (Frakes *et al.*,

2014). These results suggest that the timing and the inflammatory response of different cell types has a great impact on ALS disease progression and proposed anti-inflammatory therapies will have to be carefully aimed in terms of timing.

1.2.2 Microglia

Microglia release a full range of pro-inflammatory versus anti-inflammatory cytokines and chemokines when encountering any potential hazard. They will react through the release of pro-inflammatory factors, e.g. interleukin 1beta (IL-1β), tumour necrosis factor alpha (TNFα), nitric oxide (NO) and interferon gamma (IFN-γ), which remove and/or confine biological risks. This phenotype is also called “classically activated” or M1. An alternative phenotype release anti-inflammatory factors, e.g. insulin growth factor 1 (IGF-1), interleukin 4 (IL-4) and IL-10, which repair and mediate recovery and is termed “alternatively activated” or M2 (Philips and Rothstein, 2014). Both pro and anti-inflammatory processes mediated by microglia are influenced by an intricate crosstalk with astrocytes as well as T-lymphocytes. Microglia do not solely express either M1 or M2 phenotypes. They can release several combinations of cytokines and chemokines according to the environment they are exposed to and their interplay with other cells. Thus, microglia may present different phenotypes at different time points and locations in the CNS. Microglial reaction is characterized by the upregulation of several markers that are used to identify these cells such as CD11b and Iba1 in addition to CD86, NO synthase and CD106 (Philips and Rothstein, 2014). Activation and proliferation of microglia were detected in the primary motor cortex, motor nuclei of the brainstem, corticospinal tract and the ventral horns in the spinal cord of ALS patients (Ince *et al.*, 1996). Moreover, in animal models, an enhancement in microglial reactivity is detected in the ventral horn of the spinal cord that follows closely the denervation of the neuromuscular junction, one of the first pathological signs of MN degeneration (Alexianu, Kozovska and Appel, 2001; Saxena, Cabuy and Caroni, 2009). Strikingly, deleting mSOD1 in microglia has a protective effect in the SOD1 G93A mouse model, resulting in a slowing of disease progression and reduced motor neuron degeneration (Beers *et al.*, 2006; Boillée *et al.*, 2006). The elimination of proliferating microglia, expressing mSOD1 did not however have any impact (Gowing *et al.*, 2008). This observation suggests that there may be a subpopulation of microglia, which exert a protective effect for motor neurons. Therefore, a positive effect

could be achieved through the selective depletion of neurotoxic microglia.

In the CNS, myeloid cells of haematopoietic origin inhabit the perivascular spaces and, in terms of damage or inflammation, may penetrate the CNS parenchyma, which perform the function of macrophages. To date, there are no markers able to distinguish the microglia derived by macrophage infiltration (Durafourt *et al.*, 2012; Shechter and Schwartz, 2013), but it is known that both are present in the sites of inflammation, as demonstrated in EAE models (Taupin *et al.*, 1997; Ajami *et al.*, 2011). Different studies have revealed the existence of different types of microglia, which reflect this model i.e. the polarization of peripheral macrophages (Gordon, 2003). It is hypothesized that, in ALS, polarized M2 microglia, active in the early stages of the disease, exert protective effects; while in the later stages, possibly induced by the accumulation of misfolded and aggregated mSOD1 and other toxic insults, this will cause a change in bias towards microglia with a cytotoxic M1 phenotype (Henkel *et al.*, 2009; Appel, Beers and Henkel, 2010; Beers *et al.*, 2011).

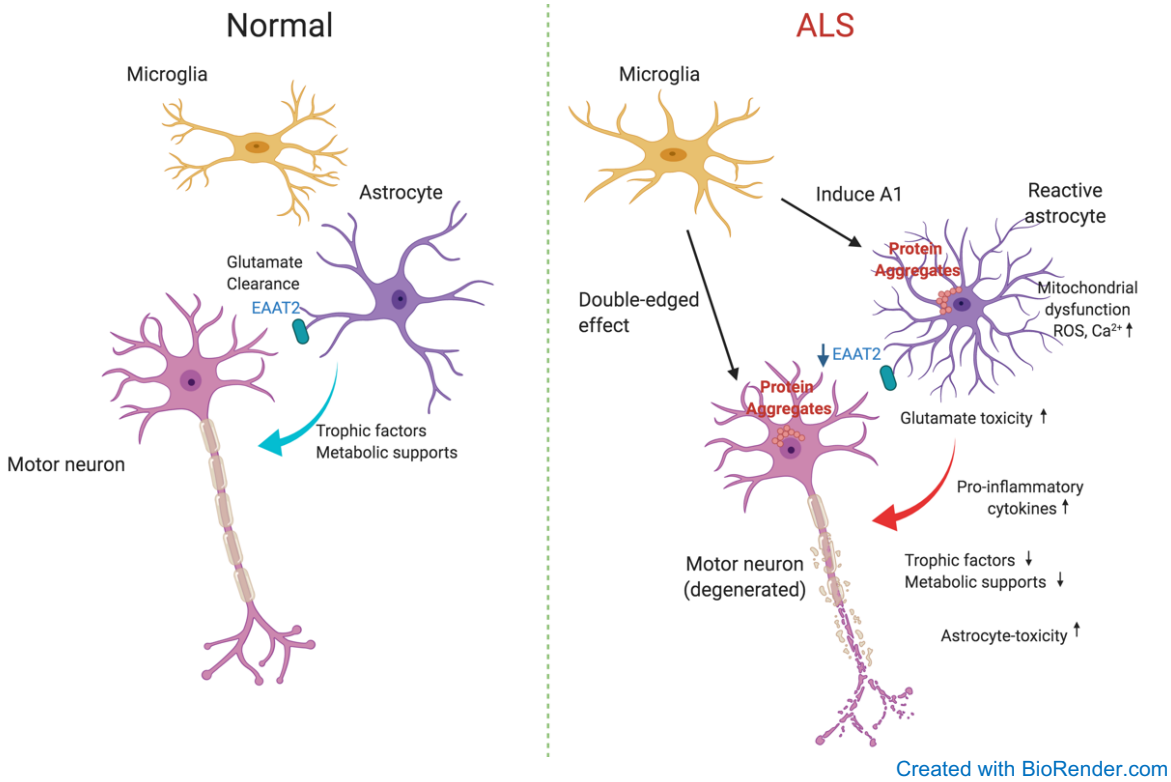

Figure 1.2 *The roles of astrocytes and microglia in ALS*

Astrocytes and microglia contribute to ALS through several mechanisms. Microglia has a dual role, the anti-inflammatory (M1) and pro-inflammatory (M2) phenotype. The activated microglia induces the A1 phenotype in astrocytes, that become reactive, producing more pro-inflammatory molecules and leading to neuroinflammation. Moreover, reactive astrocytes express more GFAP. Dysregulation of glutamate transporters in astrocytes leads to glutamate accumulation and results in excitotoxicity. Protein aggregates, such as mSOD1, accumulate also in glial cells, leading to neurodegeneration.

1.3 SOD1 and its role in ALS

1.3.1 SOD1 function and conformation of the wild-type (WT) protein

SOD1 mutations are the best characterized genetic link to ALS, since they were first identified in 1993 (Rosen *et al.*, 1993). *SOD1* mutations constitute 20% of fALS cases (Bruijn, Miller and Cleveland, 2004), equivalent to 1-2% of the total ALS cases (Chiò *et al.*, 2008; Kwon *et al.*, 2012). More than 170 different mutations have been identified in SOD1 (http://alsod.iop.kcl.ac.uk). Various forms of mutant SOD1 have been widely used for the generation of transgenic animal models, which reliably mimic the human disease phenotype.

The ALS1 locus is on the long arm of chromosome 21 (Siddique *et al.*, 1991). The gene has a length of 9.3kb and consists of 5 exons and 4 introns. Its protein product is copper-zinc superoxide dismutase 1 (Cu/Zn SOD1), a ubiquitous homodimeric enzyme of 32 kDa, consisting of 153 amino acids. It is predominantly localized in the cytosol, but is also present in the mitochondrial intermembrane space (Lindenau *et al.*, 2000; Okado-Matsumoto and Fridovich, 2002), in the nucleus, lysosomes and peroxisomes (Chang *et al.*, 1988). SOD1, which represents about 1% of total cytosolic proteins, is very abundant in CNS cells, particularly in motor neurons (Pardo *et al.*, 1995). Each monomer is formed by β sheet motifs and contains two important functional loops, referred to as the electrostatic loop and metal-binding loop (residues 49-84) that surround the region dedicated to the bond with metals (Tainer *et al.*, 1982). The metal-binding loop contains residues capable of Cu^{2+} and Zn^{2+} binding, while the electrostatic loop confers stability to the protein. They contribute in the determination of the conformation stability, a network of hydrogen bonds, welding the structure around metal ions (Strange *et al.*, 2003). Copper is required for SOD1 enzymatic activity, while zinc probably has a role in maintaining the stability of the protein structure (Antonyuk *et al.*, 2005). Human SOD1 contains four cysteine residues and two of them (Cys57 and Cys146) form a disulphide bridge (S-S). The maturation of the protein requires several steps, including copper insertion, zinc insertion, the formation of disulphide bridges and dimerization. The structural characteristics of SOD1 give it a high stability even under denaturing conditions, while the reduction of S-S bond weakens the bond between subunits and favours its aggregation (Furukawa and O'Halloran, 2005). The protein belongs to a dismutase family and plays an oxido-reductant activity that catalyses the transfer of electrons from a reductant molecule (donor) to an oxidizing molecule (acceptor). Therefore, it plays an important

antioxidant action: it is able to transform oxygen free radicals, highly toxic for the cell, into less reactive intermediates. The SOD1 protein converts the superoxide anion (O^{2-}) into oxygen and hydrogen peroxide (H_2O_2), which is subsequently transformed into water by glutathione peroxidase and catalase. Catalysis is mediated, in two asymmetric steps, with the copper atom being alternately reduced and oxidized by superoxide (Cleveland and Liu, 2000).

1.3.2 Potential mechanisms for SOD1 dysfunction in ALS

1.3.2.1 Mutations and their effect on wild-type function

To date, more than 170 different mutations have been identified in the 5 exons of SOD1 that give rise to ALS (http://alsod.iop.kcl.ac.uk). Most mutations are missense and they cause the substitution of a single amino acid in the protein, while deletions and nonsense mutations, which lead to a truncated form of the protein, are rare. In addition, 8 silent and 9 intronic mutations have been identified in SOD1 and, presumably, are not pathogenic (Al-Chalabi *et al.*, 2012). The traditionally used numbering of the amino acids in SOD1 omits the start codon, whilst the modern numbering includes an additional codon. In general, pathogenic SOD1 mutations are inherited in an autosomal dominant fashion and individuals with two copies of the mutated gene display an anticipation of symptom onset (Boylan, 2015).

An exception is represented by anomalous mutations, like D90A (first methionine excluded with the traditional numbering, p.D91A with the modern numbering). The D90A mutation is the most common mutation in Europe, accounting for 50% of all ALS cases in Sweden and Finland; it has a distinctive pattern of inheritance that shows both recessive and autosomal dominant patterns in different populations, with differences in the clinical phenotype, such as site of onset and disease progression (Andersen *et al.*, 1996; Al-Chalabi, 1998).

Mutations in SOD1 are located in all the regions of the primary structure and in all the functional domains of the protein. The mutated forms are differentiated by their various characteristics, such as the catalytic activity, charge, or the metal affinity. Two groups of mutants were identified: mutant forms which do not display changes in metal binding affinity (e.g. SOD1 G93A); and metal binding site mutated forms which, consequently, have a decreased affinity for copper and zinc ions (e.g. SOD1 G85R). Generally, the mutations may cause changes in the protein maturation steps and also, in metal

interaction. This leads to an unstable enzyme (Lindberg, Tibell and Oliveberg, 2002), characterized by abnormal folding with abnormal domain interactions not present in the native structure. These interactions can also be created with other proteins (heat shock proteins, the electron cascade proteins, etc.), making them unable to perform their functions, and inducing the formation of aggregates (Wang, Popko and Roos, 2011). Some forms of mutant SOD1 are more sensitive to temperature variations (Hayward *et al.*, 2002) and to the disulphide bond reduction than the native form (Lindberg, Tibell and Oliveberg, 2002). The disulphide bond reduction and the loss of metals from the active site induce the dissociation of two subunits and the balance shifting from the dimeric to the monomeric form (Lindberg *et al.*, 2004).

One of the hypotheses initially formulated to explain the mechanism by which mutant SOD1 causes ALS assumed loss of normal enzyme catalytic activity (loss of function hypothesis) (Deng *et al.*, 1993). This hypothesis was supported mainly by the accumulation of free radicals in the cerebrospinal fluid of ALS patients. Several studies have shown an overall SOD1 activity reduction in SOD1 fALS patients, as measured in red blood cells, fibroblasts and lymphoblastoid cells (Saccon *et al.*, 2013). Remarkably, indirect evidence suggests that SOD1 aggregation and misfolding reduces dismutase activity (Eun *et al.*, 2009; Graffmo *et al.*, 2013). Interestingly, in 2007, Sau and colleagues tested the hypothesis that the reduced solubility of mutant G93A-SOD1 may reduce the nuclear protection normally exerted by this enzyme, which is necessary to block ROS-induced DNA damage. They showed that an altered cytoplasmic versus nuclear distribution of mutant SOD1 compared with wtSOD1 may lead to increased nuclear DNA damage after oxidative stress insult (Sau *et al.*, 2007). However, a large body of evidence has indicated that motor neuron injury is caused by acquisition of new toxic functions by the mutated enzyme (gain of function hypothesis) (Watanabe *et al.*, 2001; L. Wang *et al.*, 2008). Transgenic mice overexpressing the mutated human SOD1, for example, develop a motor neuron disease similar to ALS, despite the presence of the corresponding wild-type murine enzyme (Gurney *et al.*, 1994). In these models, the levels of dismutase activities are comparable, if not increased compared to those of non-transgenic mice. On the other hand, mice deficient in murine SOD1 gene do not show motor neuron degeneration (Shefner *et al.*, 1999), thus confirming that loss of function is not responsible for the pathologic phenotype. It has to be noted, however, that mice totally lacking SOD1 develop a form of peripheral neuropathy and are more sensitive to motor neuron stress

compared to wild-type mice (Kondo *et al.*, 1997; Shefner *et al.*, 1999). Moreover, mice overexpressing wild-type SOD1 (wtSOD1) develop a modest neurodegenerative insult (Dal Canto and Gurney, 1994), indicating that overexpression *per se* might contribute to the overall disease phenotype.

1.3.2.2 Oxidative stress, SOD1 Misfolding and Aggregation

Generally, SOD1 behaves as an antioxidant enzyme by detoxifying superoxide (O_2^-) free radicals (Hayashi, Homma and Ichijo, 2016). Oxidative damage by mutated SOD1 is mainly attributed to a gain of toxicity through ROS up-regulation rather than to a loss of function. ROS are produced via numerous mechanisms, including NADPH oxidase activity. In glia, NADPH oxidase 2 (Nox2) makes a complex with a GTPase Rac1, which in its GTP-bound activated state stimulates the production of ROS by Nox2. It has been reported that mutant SOD1 binds strongly to Rac1, which keeps Rac1 in its active state and leads to the persistent activation of Nox2 together with the overproduction of O_2^-(Harraz *et al.*, 2008). Furthermore, the mitochondrial respiratory chain physiologically generates ROS and there are studies showing that the mutated form of SOD1 induces dysfunction of mitochondria. This evidence suggests that mutant SOD1 causes an increase in the production of ROS via modifications in electron transport chain complex activity or an excess of Ca^{2+} influx (Li *et al.*, 2010; Tadic *et al.*, 2014). In ALS, mitochondrial dysfunction has been demonstrated to contribute to disease, but it is not clear precisely when this occurs during the disease course. It is well known that mitochondria have several roles, including maintenance of the distal axonal. It also has been discovered that free radicals are accumulated in the intermembrane space of mitochondria that usually contained the lowest SOD1 levels; this is followed by a slow gradual neuropathy (De vos *et al.*, 2007). It is suggested that mitochondrial damage through higher levels of ROS in the intermembrane space may have an important consequence on distal axons of motor neurons. Recent studies in SOD1 G93A mice have shown an increase of markers of oxidative stress at the time of symptom onset. Moreover, it is reported that cellular respiration, intracellular ATP and mitochondrial elements (Cox, cytochrome c, complex I, enzyme activity) are decreased for the entire life of the affected mice (Irvin, Kim and Mitchell, 2015; Kaur, McKeown and Rashid, 2016).

The protein misfolding mechanisms underlying the development of ALS are poorly understood. Oxidative damage is usually involved in the misfolding of SOD1 mutants

that cause fALS (Rakhit *et al.*, 2002, 2004; Kerman *et al.*, 2010) and accumulations of oxidized proteins appear during cell ageing (Brandes *et al.*, 2013). In fact, the dismutase activity that produces H_2O_2 may make SOD1 more vulnerable to oxidative post-translational modifications (Valentine, Doucette and Zittin Potter, 2005). Interestingly, a study of ALS screening found a novel SOD1 mutation, c.352C>G (L117V), in two Syrian ALS families, that live in Europe. Synofzik et al., demonstrated that the structural stabilities of the pathogenic L117V mutant and wild-type SOD1 in denaturing conditions are similar. They have not reported differences in the content of misfolded SOD1 between extracts of fibroblasts from an L117V patient and from controls, using an ELISA specific for misfolded SOD1. Conversely, they found high levels of misfolded SOD1 in fibroblasts from ALS patients with seven other mutations in the Cu/Zn superoxide dismutase gene. Mutations in SOD1 resulting in a totally stable protein are linked with low disease penetrance and may be found in cases of sALS. Wild-type human SOD1 is relatively stable, and has been found to be within the stability range of ALS-inducing SOD1 variants, supporting the hypothesis that wild-type SOD1 could be more generally involved in ALS pathogenesis through misfolding (Synofzik *et al.*, 2012).

In the past 10 years, several studies suggested that SOD1 could be pathogenic in both fALS and sALS, through either hereditary or non-hereditary modifications. Misfolded SOD1, in fact, has been found also in patients without SOD1 mutations (Bosco *et al.*, 2010; Ayers *et al.*, 2016; Paré *et al.*, 2018; Forsberg *et al.*, 2019). A further link between wild-type SOD1 and ALS is provided by experiments showing that decreasing SOD1 levels in astrocytes derived from sALS patients inhibits astrocyte-mediated toxicity towards motor neurons (Haidet-Phillips *et al.*, 2011). This suggests that wild-type SOD1 may acquire toxic features analogous to fALS-linked mutated SOD1 through post-translational alterations. Consistently, an experiment undertaken by Guareschi et al., utilising patient lymphoblasts, demonstrated that wild-type SOD1 is altered post-translationally in sALS and is oxidized in a subgroup of patients with bulbar onset. Through other analysis of oxidized carbonyl compounds on immunoprecipitated SOD1, the group has identified a form of oxidized SOD1 that is similar to mutated SOD1 in its characteristics including mitochondria dysfunction and the development of a toxic complex with Bcl-2 (Guareschi *et al.*, 2012). Using a conformation-specific antibody that detects misfolded SOD1 (C4F6), it was observed that oxidized wild-type SOD1 and mutant SOD1 share a conformational epitope that

is not present in normal wild-type SOD1. In a subset of human sALS cases, motor neurons in the lumbosacral spinal cord were C4F6 immunoreactive, suggesting the presence of an aberrant wild-type SOD1 species (Bosco *et al.*, 2010). Different studies have described the mutation-induced conformational changes of SOD1 as the cause of SOD1 toxicity. MS785 (mutant SOD1-specific antibody clone 785), a conformation-specific antibody has shown that most SOD1 mutants share a common conformational property. Mutated SOD1 contains a N-terminal short region, that stimulates ER stress, by affecting an ER protein, Derlin-1 (Fujisawa *et al.*, 2012). Moreover, mutated SOD1 has an increased tendency to expose its hydrophobic faces in comparison to wild-type SOD1, and that the variable hydrophobicity within mutated SOD1 associates with its aggregation tendency (Münch and Bertolotti, 2010). More recently, a study using an immunoprecipitation assay and sandwich ELISA confirmed the presence of misfolded SOD1 in the cerebrospinal fluid (CSF) from patients with sALS as well as several other neurodegenerative disorders, suggesting that the misfolding of wild-type SOD1 in CSF is a common pathological process in ALS cases, even in the absence of SOD1 mutations (Tokuda *et al.*, 2019). Consistently, other studies have reported abnormal changes in SOD1 in Alzheimer's Disease (AD) and Parkinson's disease (PD) (Choi *et al.*, 2005; Trist *et al.*, 2017).

Various experiments have shown that SOD1 aggregation reduces dismutase activity. The analysis of liver and muscle samples from transgenic mice, overexpressing wild-type SOD1, revealed that aggregation was absent, while there was an increase of SOD1 protein levels and SOD1 activity (Graffmo *et al.*, 2013). An increase in the SOD1 protein was also found in the spinal cord and brain but, in these tissues, SOD1 aggregation was marked and there was no increase in SOD1 activity. This suggests a strong relation between aggregation of the protein and overall decreased activity (Graffmo *et al.*, 2013). An *in vitro* study of human neuroglioma cells co-expressing G93A SOD1 and amyloid-β, suggested that aggregate formation decreased SOD1 activity (Eun *et al.*, 2009). It is thought that aggregate accumulation of altered SOD1 plays a role in disturbing cellular functions by damaging mitochondria, protein folding and proteasome function (Boillée, Vande Velde and Cleveland, 2006). SOD1 aggregates are present not only in neurons, but also in the neighbouring glial cells (Tobisawa *et al.*, 2003). Misfolded SOD1 within microglial cells and astrocytes can exacerbate neuroinflammation and this produces an amplified release of toxic factors (Boillée, Vande Velde and Cleveland, 2006). SOD1 protein inclusions have been

found in patients with SOD1 mutations and in SOD1 transgenic mice (Gurney *et al.*, 1994; Watanabe *et al.*, 2001; Forsberg *et al.*, 2010). Moreover, misfolded SOD1 aggregation was detected in the nuclei of glial cells in ALS patients carrying or lacking *SOD1* mutations (Forsberg *et al.*, 2011) and recently, a study revealed misfolded SOD1 inclusions in motor neurons from patients with mutations in *C9orf72* and other ALS/FTD-associated genes (Forsberg *et al.*, 2019). Therefore, there is a body of evidence suggesting that the soluble form of SOD1 confers toxicity in the context of SOD1-mediated ALS. Supporting this idea, it has been demonstrated that the level of solubility of mutated SOD1 correlates with toxicity and that reduced aggregation of SOD1 in transgenic mice does not improve the disease course (Brotherton, Li and Glass, 2013; Parone *et al.*, 2013). On the other hand, other studies have shown that the aggregation tendency correlates with the disease severity (Q. Wang *et al.*, 2008; Prudencio *et al.*, 2009).

In conclusion, the presence of misfolded SOD1 inclusions found in ALS patients carrying SOD1 mutations as well as in sporadic and familial ALS patients lacking such mutations, suggests that misfolded SOD1 is involved in the pathogenesis of ALS; whereas, its presence in astrocytes, microglia and oligodendrocytes supports the idea of a pathological interplay between neurons and glial cells.

1.3.2.3 Prion-like hypothesis and spreading mediated by extracellular vesicles

It has been demonstrated that human SOD1 has prion-like characteristics that can activate its aggregation (Grad *et al.*, 2011). Several studies suggest that a harmful property of SOD1 includes its prion-like propagation. This theory is explained by two properties of SOD1, one is cell-to-cell transmission and the other is the seeded aggregation. As an initial event underlying intercellular transmission, both mutant and wtSOD1 aggregates can be released from damaged cells (Grad *et al.*, 2014). Mutated SOD1 can be also released through a principal secretory pathway which is controlled by chromogranin-A (CgA) and chromogranin-B (CgB), components of neurosecretory vesicles (Urushitani *et al.*, 2006). Furthermore, oxidized wtSOD1 interacts with chromogranin-B (CgB) (Ezzi, Urushitani and Julien, 2007). Extracellular mutant or wild-type SOD1 aggregates are then absorbed by other cells via micropinocytosis (Münch, O'Brien and Bertolotti, 2011; Sundaramoorthy *et al.*, 2013). Both mutant and wild-type SOD1 aggregates are shown to seed the aggregation of wtSOD1 *in vitro* (Grad and Cashman, 2014; Grad *et al.*, 2014). There is other evidence which reports

that spinal cord homogenates from SOD1 G93A transgenic mice transformed the recombinant SOD1 G93A protein (self-seeding) and wtSOD1 protein (cross-seeding) into fibrillar species (Chia *et al.*, 2010). Indeed, a recent study demonstrated this prion-like propagation in transgenic mouse models of ALS (Ayers *et al.*, 2014). In this experiment, Ayers and colleagues, injected directly spinal cord homogenates from paralyzed SOD1 G93A transgenic mice, into the spinal cord of neonatal SOD1 G85R-SOD1:YFP (G85R-SOD1 mutant protein fused to the yellow fluorescent protein (YFP)), transgenic mice that expressed low levels of mutant SOD1 protein but did not manifest disease symptoms. Some of the SOD1 G85ReYFP transgenic mice that were inoculated with the spinal cord homogenate from SOD1 G93A transgenic mice developed the disease, indicating that ALS transmission is a strain-like property and that there is a factor able to induce the aggregation of SOD1.

Pathogenic disease-causing proteins could also propagate by extracellular vesicles (EVs). EVs mediate the secretion of a variety of macromolecular cargo, including miRNAs, lipids, mRNAs and proteins (Pant, Hilton and Burczynski, 2012; C. C. Y. Li *et al.*, 2013; Raposo and Stoorvogel, 2013), transmit their cargo from cell to cell and interact with neighbouring cells (Valadi *et al.*, 2007; Pegtel *et al.*, 2010; Colombo, Raposo and Théry, 2014). Recent evidence has shown that EVs from brains and spinal cords of the SOD1-G93A ALS mouse model, as well as from human SOD1 fALS patient spinal cord, contained abundant misfolded and non native disulfide-cross-linked aggregated SOD1. These findings suggest that CNS-derived EVs from an ALS animal model contain pathogenic disease-causing proteins and indicate that astrocytes and neurons produce these EVs (Silverman *et al.*, 2019). Therefore, in conclusion, exploring the molecular mechanism of prion-like and EVs propagation may provide insights to develop novel therapeutic strategies for ALS.

1.3.2.4 A newly discovered function: SOD1 as a transcriptional regulator

Ataxia telangiectasia mutated (ATM) is a human kinase that behaves like an oxidative sensor, directly activated by H_2O_2 (Guo, Deshpande and Paull, 2010). A study has demonstrated that there is a relationship between SOD1 and Mec1, a yeast homologue of ATM (Carter *et al.*, 2005), and this MEC1 pathway is dependent on SOD1. Several studies on the role of Mec1 found that inactivation of the temperature-sensitive Mec1-1 allele nullifies the ability of ROS to induce SOD1 nuclear localisation. Moreover, through yeast proteomic mass spectrometry, it has been demonstrated that

SOD1 forms a potential protein complex with Dun1 kinase (Ho *et al.*, 2002) that is a Mec1 effector (Zhou and Elledge, 1993; Zhao and Rothstein, 2002). SOD1 is bound to Dun1 and their interaction is increased by oxidative stress, whilst the deletion of Dun1 stops ROS-induction of SOD1 nuclear localisation. Since Dun1 is a kinase, it is thought that SOD1 is regulated through Dun1-mediated phosphorylation, thus leading to its nuclear localisation. Furthermore, it has been shown that nuclear SOD1 controls the expression of a group of oxidative response genes (Tsang *et al.*, 2014). If H_2O_2 levels increase, SOD1 associates with the promoters of the target antioxidant genes, that SOD1 controls at the transcriptional level. Experiments in yeast have confirmed that oxidative stress promotes SOD1 nuclear translocation. These suggest that SOD1 responds to oxidative stress and is probably regulated by endogenous ROS (Tsang *et al.*, 2014). Tsang et al., in fact, measured the level of genomic DNA damage through Comet assay in different yeast strains after inducing oxidative stress and showed that nuclear SOD1 plays a critical role against oxidative DNA damage caused by environmental and endogenous ROS. Moreover, COMET assay was previously utilized to test SOD1 toxicity in the nuclei of NSC34 cells (Sau *et al.*, 2007).

Following from the evidence of SOD1 as a transcription factor or potentially as a transcription regulator, SOD1 nuclear localisation has been reported in the literature. In fact, in 1992 Crapo et al. described SOD1 primarily as a cytosolic protein in human cells and tissues; but, using different antibodies, they could also detect a small percentage of SOD1 in the nucleus (Crapo et al., 1992). This nuclear localisation had previously been reported also in rat hepatocytes (Chang *et al.*, 1988).
In 2012, Gertz et al., confirmed the nuclear localisation of human SOD1 (hSOD) in transgenic (tg) mice expressing mutated forms of hSOD1. In particular, they used tg mice expressing hSOD1-G93A, hSOD1-G37R, and hSOD1-wild-type to investigate a new subcellular pathology involving mutant hSOD1. Moreover, they reported the disruption of the nuclear architecture, looking at the survival motor neuron protein (SMN) complex. SMN was in fact disrupted in motor neuron nuclei prior to disease onset in hSOD1-G93A and -G37R mice; whilst age-matched hSOD1-wild-type mice did not show SMN disruption despite the presence of SOD1 in the nucleus. Their data suggest new mechanisms involving hSOD1 accumulation in the cell nucleus and mutant hSOD1-specific disruption of the SMN complex in ALS mouse models and a

potential overlap of pathogenic mechanisms with spinal muscular atrophy (Gertz, Wong and Martin, 2012).

The nuclear presence of SOD1 described above poses the questions of how it gains access to the nucleus and its subcellular function in this location. Bidirectional movement of small proteins occurs via passive diffusion through the nuclear pore complex, whilst proteins larger than ~40 kDa normally require specific transportation (Terry, Shows and Wente, 2007). In rat hepatocytes, nuclear SOD1 can be depleted by dialysis. The size of the native SOD1 dimer is 32 kDa, and it should therefore be able to move freely between the nucleus and the cytosol, through nuclear pores (Chang *et al.*, 1988). Its function could be to catalyse the dismutation of superoxide radicals produced by nuclear membrane cytochromes P450 and b5 and NADPH oxidase (Chang *et al.*, 1988; Li and Shah, 2002). Interestingly, SOD1 is essential for viability in DT40 cells, and it has been reported that nuclear SOD1 functions as a guardian of the genome by mitigating the accumulation of DNA lesions formed directly or indirectly by superoxide generated in or near the nucleus (Inoue *et al.*, 2010). Of great relevance in this context, another study showed that mutant Gly93 → Ala (G93A) SOD1 is present in the nucleus of human neuroblastoma cells in association with DNA. In this study, the cells were transfected to achieve low-level expression of either wild-type or G93A fALS mutant SOD1. Their findings indicate that the G93A SOD1 association with DNA could induce DNA damage and activate apoptosis by inducing p53. This toxic activity of mutant SOD1 in the nucleus may have a critical role in the complex interplay of pathways associated with motor neuron death in ALS (Barbosa et al., 2010).

In addition, also the misfolded form of SOD1 was detected in the nucleus of motoneurons and glial cells in spinal cord tissue from ALS patients, considering the nucleus as a potential site of SOD1 toxicity (Forsberg *et al.*, 2011).

More recently, a report has shown that misfolded SOD1 and wtSOD1 expose a normally buried nuclear export signal (NES)-like sequence. NES-like sequence exposure is only a feature of ALS-linked SOD1 mutants and misfolded wtSOD1. The nuclear export carrier protein is XPO1 (Chromosomal Maintenance 1, CRM1 or Exportin 1), which recognizes this NES-like sequence and exports misfolded SOD1 to the cytoplasm. This indicates that SOD1 mutants are removed from the nucleus by XPO1 likely as a defence mechanism against toxicity of nuclear misfolded SOD1 (Zhong *et al.*, 2017).

1.4 Ageing as a risk factor for ALS: common pathways involved in ageing and ALS

Ageing is a major risk factor for neurodegenerative diseases (Khan, Singer and Vaughan, 2017), in particular for the development of ALS (Alonso *et al.*, 2009). In fact, a number of ALS/FTD causing genes are involved in ageing pathways. Autophagy, inflammation, nuclear cytoplasmic transport and splicing of RNA are common dysregulated pathways in both ageing and ALS, thus this overlap could explain why ageing is the main risk factor for this disease (Niccoli, Partridge and Isaacs, 2017). Interestingly, several studies have proposed ALS as a multi-step process (Al-Chalabi *et al.*, 2014), thus ageing may facilitate some aspects of its development (Niccoli, Partridge and Isaacs, 2017).

1.4.1 Protein degradation and autophagy

The maintenance of the proteome involves a complex network of molecular chaperones and protein degradation pathways. Chaperones promote the folding of proteins or refolding of misfolded protein. Newly folded proteins are directed to the endoplasmic-reticulum (ER)-Golgi pathway for post-translational modification and secretion. Proteins non-correctly folded are recognized by ER-associated degradation (ERAD), targeted for ubiquitin-proteasome system (UPS) degradation or autophagy. Autophagy is normally classified into three types: microautophagy, macroautophagy and chaperone-mediated autophagy (CMA). All of these processes involve lysosomal degradation but they have different mechanisms. Microautophagy is the direct invagination of small parts at the lysosome surface, followed by vesicle degradation in the lysosomal lumen and release of breakdown products into the cytoplasm. Macroautophagy, generally referred as autophagy, involves multiple proteins coordinating vesicle formation through different steps, followed by fusion with lysosomes to form the so-called autolysosomes. CMA is a selective and direct elimination system for a particular group of soluble cytosolic proteins containing the pentapeptide KFERQ as recognition sequence. These are targeted to lysosomes and directly translocated across the lysosome membrane for degradation, without the formation of additional vesicles.

It is been reported that the ability to maintain a stable and functional proteome declines with age, thus, as consequence, misfolded and damaged proteins accumulate,

impairing cell function and tissue homeostasis (López-Otín *et al.*, 2013). ALS, like other neurodegenerative disorders that are age-related diseases, is characterized by the presence of misfolded protein aggregation, suggesting that the protein quality control is affected. In fact, several mutated proteins associated with ALS, are involved in protein degradation pathways (see Table 1.1) and can also be found as aggregates. In particular, ageing might contribute to genetic mutations that dysregulate these pathways. For example, it has been reported that partial loss of function of *TBK1*, a major genetic cause for ALS/FTD, leads to age-dependent neurodegeneration. TBK1 is an endogenous inhibitor of RIPK1, a mediator of neuroinflammation and apoptosis. TAK1 is another endogenous RIPK1 inhibitor and decreases in expression in ageing human brains. In 2018, a study showed that the embryonic lethality of *Tbk1*−/− mice is dependent on RIPK1 kinase activity. Moreover, in *Tbk1*+/− mice, the reduced myeloid TAK1 expression induces all the key hallmarks of ALS/FTD, which are rescued by inhibition of RIPK1 (Xu *et al.*, 2018). Therefore ageing enables RIPK1 activation by decreasing TAK1 expression, which cooperates with genetic risk factors to promote the onset of ALS/FTD.

1.4.2 Nucleocytoplasmic transport and RNA metabolism

A key-player in the nucleocytoplasmic transport, powered by a RanGTP-gradient (Schmidt and Görlich, 2016), is the nuclear pore complex (NuPC), that regulates the communication between the nuclear and the cytoplasm compartments. The NuPC is a defined structure of evolutionary conserved proteins, called nucleoporins (Nups). Nups are vulnerable to age-related damage and, importantly, ALS-causing mutations have been identified in these proteins. For example, loss-of-function mutations in *GLE1* lead to defects in mRNA export (Nousiainen *et al.*, 2008; Kaneb *et al.*, 2015). Proteins are imported or exported through the NuPC via nuclear transport receptors (NTRs), members of the karyopherin β family, known as importins and exportins (Cautain *et al.*, 2015; Soniat and Chook, 2015). The NTRs are characterized by a conserved Ran-GTP-binding motif at the N-terminal, while at the C-terminal they vary and are involved in substrate recognition (Görlich *et al.*, 1997). Impaired nucleocytoplasmic shuttling has recently emerged as mechanism contributing to ALS pathology and other neurodegenerative diseases, as well as being present in physiological ageing (Kim and Taylor, 2017). The main pathological hallmark in neurodegenerative diseases is the aggregation of protein that forms cytoplasmic

inclusions. In most cases of ALS, both sporadic and familial, the nuclear protein TDP-43 (Ayala *et al.*, 2008) is depleted from the nucleus and accumulates in the cytoplasm (Neumann *et al.*, 2006), where it can interfere with nucleocytoplasmic transport of protein and RNA (Woerner *et al.*, 2016). Several studies also reported impaired nucleocytoplasmic transport as consequence of several ALS mutations, such as mutations in the nuclear localisation signals (NLSs) of FUS and hnRNPA1 (Dormann *et al.*, 2010; Gal *et al.*, 2011; Q. Liu *et al.*, 2016). Furthermore, evidence of dysregulation in this mechanism has been observed in C9Orf72 ALS/FTD cases (Freibaum *et al.*, 2015; Jovičić *et al.*, 2015; Zhang *et al.*, 2015; Boeynaems *et al.*, 2016; Shi *et al.*, 2017). Thus, in conclusion, ageing could have impact on disease. The disruption of NuPC and changes in expression of transport factors could potentially accelerate the mis-localisation process, with subsequent accumulation of aggregated proteins.

1.4.3 Neuroinflammation

Neuroinflammation has also a role in ALS pathophysiology. Neuroinflammation associated with neuronal loss is characterised by activation of microglia and astrocytes, production of pro-inflammatory cytokines and infiltration of T lymphocytes (Endo, Komine and Yamanaka, 2016). Multiple studies have confirmed the activation of microglia in ALS (Turner et al., 2004; Corcia et al., 2012). As mentioned in section 1.2.2, when microglia encounter any potential hazard, they release a full range of pro-inflammatory versus anti-inflammatory cytokines and chemokines. This may induce the neurotoxic activation of astrocytes that could contribute to the death of neurons and oligodendrocytes (Liddelow et al., 2017). Astrocytes, as described in section 1.2.1, are responsible for homeostasis, defence and regeneration of the CNS (Burda and Sofroniew, 2014). Therefore, a body of evidence (section 1.2) indicates that inflammation is a crucial mechanism for neuronal injury and ALS progression. Nevertheless, also the human ageing brain displays elevated inflammatory markers (Janowitz et al., 2019). Thus, the imbalance between anti-inflammatory and pro-inflammatory cytokines in ageing increases the risk for neurodegenerative diseases.

1.5 Modelling ALS

In order to investigate the disease mechanisms that lead to MN degeneration, several models have been created. The development of animal models represented a crucial

point in ALS research. Different model systems have contributed to the knowledge of ALS disease mechanisms. Small *in vivo* models, such as *C.elegans, drosophila* and zebrafish are widely used for genetic screening; while rodent models should mimic the disease more closely and are used to investigate pathogenic mechanisms and for proof of concept therapeutic studies (Van Damme, Robberecht and Van Den Bosch, 2017). Moreover, through the use of animal models it is possible to follow the pathology, monitoring the pathogenetic events, from pre-symptomatic stages to the end stages, and to study the early mechanisms that trigger the development of the disease. Numerous *SOD1* and other genetic mutation mouse models have been created since 1994, to better understand the mechanisms involved in the pathogenesis of ALS, and with the aim of producing reliable animal models that mimic the clinical phenotype of ALS (Van Damme, Robberecht and Van Den Bosch, 2017). Indeed, SOD1 models have been invaluable to understand some of the disease mechanisms, but the translation of findings from model systems to the clinic has been unsuccessful so far (Mitsumoto, Brooks and Silani, 2014). Despite the differences in the number of copies of the transgene, in the expressed protein levels, in the dismutase activity and in some neuropathological features, all the introduced mutations cause, in the same way, degeneration and death of motor neurons, leading to progressive muscle atrophy and paralysis, typical ALS symptoms. Moreover, these animals display the same histopathological features associated with ALS in humans, such as the presence of aggregates containing SOD1 and ubiquitin in degenerating motor neurons, astrogliosis and microgliosis. The differences in the onset and progression of the pathology observed between the different mutations, but also in the context of a single mutation, may depend not only on the different number of copies of the transgene (Alexander *et al.*, 2004), but also on gender and the genetic strain of the mouse. This suggests an important effect of the background and other genetic factors in the development of the disease (Heiman-Patterson *et al.*, 2005; Mancuso *et al.*, 2012; Nardo *et al.*, 2013). Also, TDP-43, FUS and C9orf72 models were created but they only partially recapitulate the disease phenotype and the disease hallmarks observed in *post-mortem* tissues. Finally, the rodent mouse models only represent a small portion of familial cases.

A powerful tool for ALS modelling is represented by induced pluripotent stem cells (iPSCs). This implies generating models from patient-derived stem cells, thus having the most important advantage that they remove the need to overexpress transgenes

containing pathogenic ALS gene mutations. This type of *in vitro* model has greatly contributed to the understanding of ALS pathogenic mechanisms, although it does display some limitations. First of all, iPSCs present clonal variability; this in ALS research was shown in a study using iPSC lines of ALS patients, carrying a *TARDBP* mutation. Differentiated motor neurons of individual clones from the same patient showed variations in TDP-43 expression, aggregate formation and oxidative stress induced cell death (Egawa *et al.*, 2012). Secondly, another important limitation relating to the induction of pluripotency in adult fibroblasts is that this reverts cellular age to an embryonic status (Lapasset et al., 2011; Patterson et al., 2012), which is retained even after conversion into neurons, thus erasing ageing-associated signatures (Miller *et al.*, 2013). To circumvent this limitation, recent studies have shown that neurons directly reprogrammed from fibroblasts without the use of pluripotency factors, retain ageing signatures compared to iPSCs-derived neurons (Mertens et al., 2015; Huh et al., 2016; Tang et al., 2017; Victor et al., 2018).

1.5.1 Cell Reprogramming

The discovery of reprogramming fibroblasts into induced pluripotent stem cells (iPSCs) (Takahashi *et al.*, 2007) allowed to model *in vitro* not only fALS, but also sALS, the majority of ALS cases. In 2008, the reprogramming of human fibroblasts to a pluripotent state, using transcription factors led to the first ALS-patient iPSCs, that were then successfully differentiated in motor neurons (Dimos *et al.*, 2008). Since then, many different techniques have been used to produce iPSC lines via genetic reprogramming of several somatic cells types, including keratinocytes and adipocytes (Aasen *et al.*, 2008; Taura *et al.*, 2009). Moreover, the production of induced neural progenitor cells (iNPCs) (Meyer *et al.*, 2014) and motor neurons (Son *et al.*, 2011) was possible through direct conversion technology. Originally, the transcription factors were introduced by lentiviral or retroviral constructs, leading to the random integration of the transgene into the target genome, which can alter the expression of endogenous genes. Recently, less invasive approaches have been developed, such as non-integrating viral vectors, like plasmids, adenoviruses, microRNA (miRNA) and Sendai virus (Myszczynska and Ferraiuolo, 2016).

Using iPSCs has allowed to ALS research to investigate disease mechanisms not only linked to mutations in the familial cases. Since iPSCs recapitulate various aspects of disease pathophysiology, such as the aggregation and/or mis-localisation of proteins

(Matus, Medinas and Hetz, 2014) it was also possible to produce many results from sporadic ALS patients-derived cells to better characterise pathways that contribute to disease (Table 1.3). Furthermore, ALS iPSCs represent a valuable tool to design novel therapeutic strategies, such as targeting the degradation of sense and antisense C9orf72 RNA foci (Lagier-Tourenne *et al.*, 2013; Sareen *et al.*, 2013), and also to perform compound screening (Egawa *et al.*, 2012).

Table 1.3 *Pathways that contribute to ALS, identified with iPSC studies*

iPSC-derived cell subtype	Functional phenotype identified	References
Motor neurons	Mutant TDP-43 induces selective cell-specific vulnerability	(Bilican *et al.*, 2012)
Motor neurons	Mutant SOD1 induces neurofilament disorganization	(Chen *et al.*, 2014)
Neurons	C9orf72 disrupts nucleocytoplasmic transport	(Zhang *et al.*, 2015)
Motor neurons	Changes in excitability	(Kiskinis *et al.*, 2014)
Oligodendrocytes	Involvement in MN death through a SOD1-dependent mechanism	(Ferraiuolo *et al.*, 2016)
Astrocytes	Non-cell autonomous toxicity to MN	(Meyer *et al.*, 2014)

1.6 Hypothesis and aims

Ageing is considered a key primary risk factor for ALS. Moreover, ageing is linked to several pathways, altered in ALS, such as protein misfolding and mis-localisation, and changes in nucleocytoplasmic transport. This led to the hypothesis of this doctorate work, investigating whether:

1. Ageing has impact in our directly reprogrammed iNPC-derived astrocytes (Meyer *et al.*, 2014) modelling neurodegenerative disease;

2. SOD1 nuclear presence affects the nucleocytoplasmic transport in the context of fALS and sALS astrocytes.

A set of aims was established creating the basis of this thesis:

1. To determine the ability of our model to retain ageing features and to understand the astrocytic contribution to human health and disease in the human CNS, examining pathways involved in neurodegeneration, i.e. oxidative stress response, inflammatory response and nucleocytoplasmic transport changes;

2. To investigate the localization of wild-type and misfolded SOD1 in astrocytes from ALS patients and its link with the alteration of nucleocytoplasmic transport, focusing on the interaction with XPO1.

2. Material and Methods

2.1 Materials

All cell culture reagents and chemicals were purchased as described as follow:

2.1.1 Cell culture media and reagents

- iNPC medium
  - ✓ B27-Supplement (Gibco Life technologies)
  - ✓ DMEM/F-12 (1:1) (1X) + GlutaMAX (Gibco Life technologies)
  - ✓ N2-Supplement (Gibco Life technologies)
  - ✓ bFGF (Peprotech)
- Hu Plasma Fibronectin (Millipore)
- StemPro® Accutase (Gibco Life technologies)
- iAstrocyte medium
  - ✓ Dulbecco's Modified Eagle's Medium (DMEM) (Sigma)
  - ✓ Foetal Bovine Serum (FBS) (Life Science Products)
  - ✓ N2-Supplement (Gibco Life technologies)
  - ✓ Penicillin/Streptomycin (Lonza BioWhittaker)
- Formaldehyde (Fischer Scientific)
- Triton™ X-100 (AppliChem)
- DEPC (BioChemica)
- Hoechst 33342, Trihydrochloride, Trihydrate (Life Technologies)
- Phosphostop (PS) (Roche)
- Proteinase Inhibitor Cocktail (PIC) (Roche)
- ProtoGel 30% (w/v) Acrylamide: 0.8% (w/v) Bis-Acrylamide Stock Solution (GeneFlow)
- Ammonium persulphate (APS) (Sigma)

- Tetramethylethylenediamine (TEMED) (Sigma)
- Bradford protein assay dye reagent (Bio-Rad Laboratories)
- PMSF (Phenylmethanesulfanyl)
- Pre-stained protein ladder (GeneFlow)
- Dried Skimmed Milk (Marvel)
- Bovine Serum Albumin (BSA) (Fisher Scientific)
- EZ-ECL kit (Geneflow)
- RNAeasy Mini kit (Qiagen)
- High Capacity cDNA Reverse Transcription Kit (Applied Biosystems)
- 2x SYBR Green/Rox PCR Master Mix (Bimike.com)
- CellROX® Reagent (Life Technologies)
- Duolink® In Situ Orange Starter Kit Mouse/Rabbit (Sigma-Aldric)

All tissue culture (TC) plastics were purchased from Greiner-Bio, Fisher Scientific and Thermo Scientific.

2.1.2 Solutions

Table 2.1 *Solutions used in the study*

Solution	*Components*
PBS 1X	137mM NaCl, 2.68mM KCl, 10.14mM Na_2HPO_4 (anhydrous), 1.76mM KH_2PO_4 (anhydrous) made up to volume with deionised water
DEPC treated PBS	0.2% v/v of diethyl pyrocarbonate (DEPC) in PBS solution autoclaved
DEPC treated water	0.2% v/v of diethyl pyrocarbonate (DEPC) in water autoclaved
IP lysis buffer	150mM NaCl, 50mM HEPES, 1mM EDTA, 1mM DTT, 0.5% (v/v) Triton™ X-100, 20µL/mL PIC, pH 8.0

IP T/N Lysis Buffer	150mM NaCl, 50mM HEPES, 1mM EDTA, 1mM DTT, 1% (v/v) Triton™ X-100, 1% Sodium deoxycholate, 20µL/mL PIC, pH 8.0
Hypotonic Lysis Buffer	10mM HEPES, 1.5mM MgCl2, 10mM KCl, 0.5mM DTT, 20µL/mL PIC
Resolving buffer	1.5 M Trizma®, 13.9 mM SDS, pH 8.8, filtered
Stacking buffer	0.5 M Trizma®, 13.9 mM SDS, pH 6.8, filtered
4x Laemmli buffer	228mM Tris-HCl, 38% (v/v) glycerol, 277mM SDS, 0.038% (w/v) bromophenol blue, 5% (v/v) β-mercaptoethanol pH 6.8
Running buffer	25mM Tris, 3.5mM SDS, 20mM glycine
Transfer buffer	47.9mM Tris, 38.6mM glycine, 1.38mM SDS
Tris Buffered Saline, with Tween® 20 (TBST)	20mM Tris, 137mM NaCl, 0.2% (v/v) Tween® 20, pH 7.6
Oxidised RNA pull down Lysis Buffer	DEPC PBS, 0.1% Triton, PIC (20 µL/mL), DNase (1 µL/mL), RiboSafe RNase Inhibitor (1 µL/mL, Bioline)
Binding buffer	20mM Tris-HCl, 1M NaCl, 1% SDS, 0.2mM EDTA up to 400mL of DEPC water
Total RNA pull down Lysis Buffer	50mM Tris-HCl pH7.5, 100mM NaCl, 2mM $MgCl_2$, 1mM EDTA pH8, 0.5% Igepal C9-630 (NP40), 0.5% Na-deoxycholate in DEPC water, 20µL PIC/mL and 1µL/mL RNase Inhibitor
Elution buffer	10mM Tris, pH7.5, 1mM EDTA up to 200mL DEPC water
Ponceau	0.1% (w/v) Ponceau S (Sigma), 5% (v/v) acetic acid in dH2O
Blocking Buffer Immunostaining	5% horse serum (Dako), 0.05% Triton in PBS

2.1.3 Cell culture

2.1.3.1 Induced neural progenitor cells (iNPCs)

Human skin fibroblast samples were obtained from different sources (Table 2.2). Prof. Pamela Shaw (PJS) and Dr Daniel Blackburn (DB) provided the fibroblast samples

from the University of Sheffield (Study number STH16573, Research Committee reference 12/YH/0330 and MODEL-AD research study number STH19080 Research and Ethics Committee number: 16/YH/0155 respectively). Prof Stephen J. Kolb (SJK) provided the fibroblast samples from the ALS/MND Clinic, Department of Neurology, The Ohio State University (OSU), Wexner Medical Center, Columbus, OH (Ethics number 04304AR). Five fibroblast lines (including underaged donors) were purchased from the biorepository Coriell under material transfer agreement (MTA). Informed consent was obtained from all subjects before sample collection.

Table 2.2 *Summary of the information on the astrocytes and fibroblast lines used in this study*

ID	Cell line	Biobank	Phenotype	Age at biopsy collection	Gender
Y1	GM08680	Coriell Institute	Non-ALS control	5 months	Male
Y2	GM00498	Coriell Institute	Non-ALS control	3 years	Male
Y3	GM03813	Coriell Institute	Non-ALS control	3 years	Male
CTR_1 (O3)	155	PJS	Non-ALS control	42 years	Male
CTR_2 (O2)	3050	PJS	Non-ALS control	55 years	Male
CTR_3 (O1)	MAD14	DB	Non-ALS control	56 years	Male
CTR_4	AG08620	Coriell	Non-ALS control	64 years	Female
sALS_1	PAT009	SJK	sALS	61 years	Female
sALS_2	PAT12	SJK	sALS	29 years	Male
sALS_3	PAT17	SJK	sALS	47 years	Male
C9_1	PAT78	PJS	C9Orf72	66 years	Male
C9_2	PAT183	PJS	C9Orf72	50 years	Male
C9_3	PAT201	PJS	C9Orf72	66 years	Female

SOD1_1	PAT100	SJK	SOD1 (A4V)	Not known	Female
SOD1_2	PAT102	SJK	SOD1 (A4V)	Not known	Female
SOD1_3	PATND	Coriell	SOD1 (D90A)	56 years	Male

2.1.4 Primers

All primers were ordered from Sigma-Aldrich®.

Table 2.3 *Primer sequences used for qPCR*

(Fw=forward, Rv=Reverse)

Primer	**Sequence (5'-3')**
B-Actin_Fw	TCCCCCAACTTGAGATGTATGAAG
B-Actin_Rv	AACTGGTCTCAAGTCAGTGTACAGG
RLP13A_Fw	CAAGCGGATGAACACCAACC
RLP13A_Rv	TTTTGTGGGGCAGCATACCT
U1_Fw	CCATGATCACGAAGGTGGTT
U1_Rv	ATGCAGTCGAGTTTCCCACA
GAPDH_Fw	CAACTTTGGTATCGTGGAAGGAC
GAPDH_Rv	ACAGTCTTCTGGATGGCAGTG
TERF2_Fw	TTATTCGAGAAAAGAACTTGGCCC
TERF2_Rv	TGAGGAGGTAGGGCTCGG
RANBP17_Fw	CACTTCGATGCAGAGAGGCTA
RANBP17_Rv	CACTGGTTCCGACAGTCTTC
LAMA3_Fw	TGTTTAAACTGCAGCCTCCCA
LAMA3_Rv	ACACATTTCAAGTTCCCGGC

2.1.5 Antibodies

2.1.5.1 Primary antibodies

Table 2.4 *Primary antibodies used in the study (ICC=immunocytochemistry, WB=western blot, PLA=Proximity Ligation Assay, IP=immunoprecipitation)*

Primary antibody	**Species**	**Assays**	**Working Dilution**	**Supplier**
Nestin	Mouse	ICC	1:1,000	Abcam, ab18102
Pax6	Rabbit	ICC	1:1,000	Abcam, ab5790
CD44	Rabbit	ICC	1:200	Abcam, ab157107
GFAP	Rabbit	ICC	1:1,000	Dako, Z0334
Vimentin	Chicken	ICC	1:1,000	Millipore, ab5733
8-Hydroxyguanosine	Mouse	Oxidised RNA pull-down	2µl/sample	Abcam, ab62623
SOD1	Rabbit	ICC WB	1:500 1:1,000	Cell Signalling, 2770
SOD1	Mouse	PLA	1:500	R&D, MAB3418
Misfolded SOD1 (B8H10)	Mouse	ICC IP	1:100 -	Medimabs, MM-0070-P
TDP-43 (C-terminal)	Rabbit	ICC WB	1:100 1:1,000	Proteintech, 12892-1-AP
p62	Mouse	ICC, PLA WB	1:200 1:1,000	BD Biosciences, 610833
LC3	Rabbit	PLA	1:1,000	Novus Biologicals, 2220

SSRP1	Mouse	WB	1:500	Abcam, ab26212
β-actin	Mouse	WB	1:10,000	Abcam, ab6276
β-tubulin	Chicken	WB	1:1,000	Millipore, ab9354
NRF2	Rabbit	WB	1:1,000	Abcam, ab31163
GAPDH	Rabbit	WB	1:1,000	Cell Signalling, 21185
XPO1/CRM1	Rabbit	WB	1:2,000	Abcam, ab180144
XPO1/CRM1	Rabbit	PLA	1:1,000	Cell signalling, 46249
IPO5	Rabbit	WB	1:1,000	Abcam, ab88695
RANBP17	Rabbit	WB	1:2,000	Abcam, ab168842
Histone H3 (tri methyl K9)	Rabbit	ICC	1:800	Abcam, ab8898
Lamin A/C	Mouse	ICC	1:800	Abcam, ab40567

2.1.5.2 Secondary antibodies

Table 2.5 *Secondary antibodies used in the study (ICC=immunocytochemistry, WB=western blot)*

Secondary antibody	Source	Assay	Dilution used
Alexa Fluor 586 donkey α-mouse IgG(H+L)	Invitrogen,ThermoFisher A10037	ICC	1:1,000
Alexa Fluor 586 goat α-rabbit IgG(H+L)	Invitrogen,ThermoFisher A11011	ICC	1:1,000

Alexa Fluor 488 goat α-rabbit IgG(H+L)	Invitrogen,ThermoFisher A11008	ICC	1:1,000
Alexa Fluor 488 goat α-chicken IgG(H+L)	Invitrogen,ThermoFisher A11039	ICC	1:1,000
α-Rabbit IgG (H+L), HRP Conjugate	Promega W401B	WB	1:5,000
α-mouse IgG (H+L), HRP Conjugate	Promega W402B	WB	1:5,000
α-chicken IgGY (H+L), HRP Conjugate	Invitrogen,ThermoFisher A16054	WB	1:5,000

2.2 Methods

2.2.1 Direct Reprogramming of Skin Fibroblasts to iNPCs

Direct conversion was conducted as described previously in Meyer et al., 2014. Fibroblasts were seeded in a well of a six-well plate (Greiner-Bio) and treated with retroviral vectors for OCT3, Sox2 and KLF4 (Meyer *et al.*, 2014). The medium was switched to NPC conversion medium, consisting of DMEM/F12, 1% N2, 1% B27, EGF (40ng/ml) and FGF (20 ng/mL). After 2-4 days the cells changed shape to look smaller and rounded. These were collected or lifted using accutase and, depending on the density and their growth rate, they were expanded in multiple wells of a six-well plate or a 10cm dish (Thermo Scientific) coated with human fibronectin (5 µg/mL). The cells were stained for Nestin and PAX6 to establish that iNPC conversion was successful. Staining was repeated every 5 passages to confirm retention of neural progenitor characteristics. The efficiency of the conversion ranged between 98%-100%. The reprogramming and quality control work were performed by Dr Laura Ferraiuolo, Dr Simon Bell and Mr Allan Shaw. iNPC maintenance was carried out by myself, Miss Monika Myszczynska and Mr Allan Shaw.

2.2.2 Differentiation of iNPCs into iAstrocytes

To induce astrocyte differentiation, about 500,000 iNPCs were plated in medium made up of DMEM, 10% Fetal Bovine Serum (FBS), 1% Penicillin-Streptomycin, 0.2% N2-supplement in a 10-cm dish coated with human fibronectin (2.5 µg/mL). Astrocytes were allowed to differentiate for 7 days with a medium change at day 3-4 (Figure 2.1). These cells were stained with typical cell biomarkers, including vimentin, CD44, S100b, GFAP and EAAT2 by at least one lab member every month.

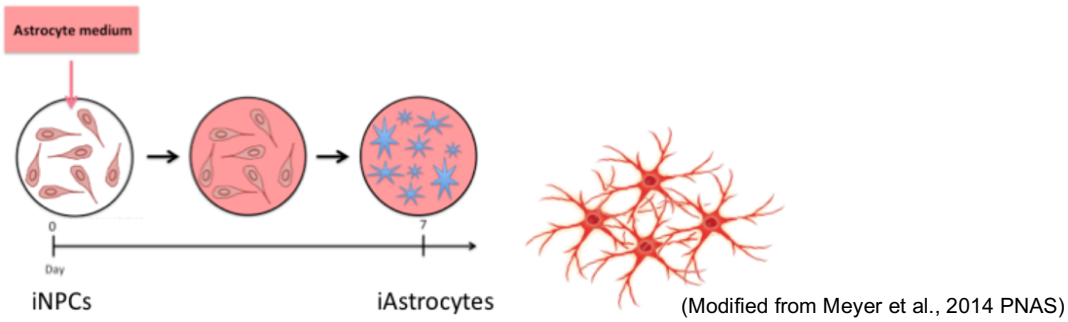

(Modified from Meyer et al., 2014 PNAS)

Figure 2.1 *Schematic depicting the iAstrocyte differentiation protocol.*

2.2.3 Treatment for stress response assessment and cell collection

Serum starvation experiments were carried out by washing the cells with PBS twice and changing the culture medium to fresh media without FBS at day 6.

On day 7 iAstrocytes were washed twice with PBS to remove residual medium and harvested by cell scraping. The cell pellets were stored at -80°C until processed for RNA or protein extraction.

2.2.4 SOD1 knock-down treatment

SOD1 knock-down treatment was achieved by using a commercially available adenovirus expressing a short hairpin RNA (shRNA) against SOD1 (Ad-h-SOD1-shRNA, cat# 1859, Vector Biolabs). The cells were transduced 24h post-seeding (MOI, Multiplicity of infection=5-7).

2.2.5 Microarray analysis

Microarray analysis of human fetal astrocytes (purchased from Sciencell), *post-mortem* (PM) astrocytes laser-captured from brain samples and iAstrocytes (iA) reprogrammed from fibroblast donors was performed at SITraN, University of Sheffield, at different time points and for different studies (Table 2.6). Fetal astrocytes were run on GeneChip™ Human Gene 2.0 ST Array; while *post-mortem* astrocytes and iAstrocytes were run on GeneChip™ Human Genome U133 Plus 2.0 Array. The U133 arrays have their probe sets located at the 3'UTR of the gene, whilst the 1.0 ST arrays have probe sets across the entire transcript.

Table 2.6 *Summary of the information on microarray data*

ID	Origin	Age	Gender	GEO accession number
Fetal_1	Sciencell	-	M/F	10.15131/shef.data.12162282
Fetal_2	Sciencell	-	M/F	10.15131/shef.data.12162282
Fetal_3	Sciencell	-	M/F	10.15131/shef.data.12162282
PM_1	Laser-captured from brain	72 years	F	GSE83670
PM_2	Laser-captured from brain	75 years	M	GSE83670

PM_3	Laser-captured from brain	78 years	F	GSE83670
PM_4	Laser-captured from brain	78 years	F	GSE83670
Old iA_1	Direct reprogramming from skin fibroblasts	55 years	F	GSE87385
Old iA_2	Direct reprogramming from skin fibroblasts	69 years	F	GSE87385
Old iA_3	Direct reprogramming from skin fibroblasts	47 years	M	GSE87385
Young iA_1	Direct reprogramming from skin fibroblasts	3 years	F	10.15131/shef.data.12162282
Young iA_2	Direct reprogramming from skin fibroblasts	8 years	F	10.15131/shef.data.12162282
Young iA_3	Direct reprogramming from skin fibroblasts	5 months	M	10.15131/shef.data.12162282

All the included data were already available and had in place relevant ethical approval. The quality of array data CEL files was assessed using the Affymetrix Expression Console software. Normalisation: all the transcripts were normalised against beta-tubulin, and harmonisation across Chip files was obtained using the Robust Multi-Array (RMA) algorithm. Differential gene expression between samples was determined using Qlucore Omics Explorer after normalisation. The software was used also for Principal Component Analysis (PCA) and hierarchical clustering. To access the functions of genes found in the meta-analysis, the Database for Annotation, Visualization and Integrated Discovery (DAVID, https://david.ncifcrf.gov/) and

IMPaLA: Integrated Molecular Pathway Level Analysis (http://impala.molgen.mpg.de/) software tools were used. The website Human Genomic Resources (HAGR, http://genomics.senescence.info/) was used to identify ageing-related genes.

2.2.6 qPCR primer design

Genomic DNA sequences were imported using Ensembl.org (www.ensemble.org), and primers were designed using the online tool Primer-BLAST (https://www.ncbi.nlm.nih.gov/tools /primer-blast/). Each primer pair (Table 2.3) was diluted in water to a 100μM stock.

2.2.7 RNA Isolation and quantitative polymerase chain reaction (qPCR)

RNA was extracted using the RNAeasy Mini kit from the astrocyte pellet as per manufacturer's instructions. Total RNA was reverse-transcribed with a High Capacity cDNA Reverse Kit according to the manufacturer's instructions.

2.2.7.1 Reverse transcription

A master mix from the High Capacity cDNA Reverse Transcription Kit was prepared using the components described in the table below:

Table 2.7 *Components of the master mix*

Component	**Volume**
10 x RT Buffer	2.0 μl
25 x dNTP Mix (100mM)	0.8 μl
10 x RT Random Primers	2.0 μl
MultiScribe™ Reverse Transcriptase	1.0 μl
Nuclease-free H_2O	3.2 μl
Total per Reaction	**10.0 μl**

The master mix was mixed on ice before adding 10 μl to each 0.2 reaction tube. 10 μl of RNA sample (12.5 ng/μl per well) was added to each tube and mixed. The tubes were spun briefly and placed in the DNA Engine PTC-200 thermocycler (MJ Research) with a heated lid at 80°C, running the following program:

Table 2.8 *qPCR cycle programme*

Temperature	Time
25°C	10 min
37°C	120 min
85°C	5 min
4°C	-

Samples were used immediately or stored at -20°C and were loaded at a concentration of 12.5 ng/µl per well. qPCR was performed using 2x SYBR Green/Rox PCR Master Mix and forward and reverse primers (5µM), to a total volume of 20µL.

Table 2.9 Components of the PCR Master Mix

Component	Volume
SYBR green	10 µl
Forward primer	1 µl
Reverse primer	1 µl
dH_2O	7 µl
cDNA Template	1 µl
Total per Reaction	19 µl

The reaction was run on a Stratagene MX300P machine, using the programme in Table 2.10. At the end, a dissociation curve was created to ensure amplification of a single product and absence of primer dimers.

Table 2.10 *qPCR programme*

Step	Temperature	Time	Cycles
Initial Denaturation	95°C	10 min	1
Denaturation	95°C	30 secs	40
Annealing	60°C	60 secs	
Extension	95°C	60 secs	1
Final extension	55°C	30 secs	
	95°C	30 secs	

GAPDH was tested against other housekeeping genes, i.e. beta-actin, RLP13A and U1. GAPDH showed the most consistent and stable expression across samples of different ages as well as between fibroblasts and astrocytes. Hence, GAPDH was amplified on each plate to normalize expression levels of target genes between different samples using the ΔΔCt calculation (ABI) and to assess assay reproducibility.

2.2.8 Seeding iAstrocytes

At day 5/6, a 96 well tissue culture treated black plate (Griener Bio-One) was coated with fibronectin diluted 1:400 in PBS. iAstrocytes were first washed with PBS before incubating with accutase for 5 minutes at 37°C. The accutase was neutralised in an appropriate volume of iAstrocyte medium and cells were collected in a 15ml falcon and centrifuged at 200g for 4 minutes. The obtained pellet was resuspended in an appropriate volume of medium and the cells were counted using a 0.100 mm Burker hemocyctometer (Marienfeld). The cells were seeded at the desired density (usually 6,000/well for staining) and were left for 24 hours to adhere.

2.2.9 Oxidative-stress assay

7,000 iAstrocytes were plated per well in 96-well plates at day 5 of differentiation in complete astrocyte medium. On day 6, medium was replaced either with complete or with serum-free astrocyte medium for 12 hours. After 12h, medium was replaced in all conditions with complete astrocyte medium and CellROX baseline measurements were collected, using the Opera Phenix Imaging System (Perkin Elmer). A time-course experiment was also performed, in which CellROX measurements were collected every 2 hours for 6 hours. CellROX® Reagent (Life Technologies) was used at a final concentration of 2.5 µM as per manufacturer's instructions and incubated with cells for 30 minutes at 37°C. CellROX® Reagent was then removed, cells were washed three times with PBS before imaging.

2.2.10 Immunocytochemistry

Cells were plated in 96-well plates (Griener Bio-One) and fixed 24h after seeding with 4% paraformaldehyde (PFA) for 10 min and washed 3 times with PBS before the blocking solution consisting of PBS with 5% horse serum, 0.05% Triton X-100, was

applied for 1 h. All primary antibodies were diluted in blocking solution and their dilution and provider are listed in Table 2.4. Incubation of the primary antibody was performed overnight at 4°C. The next day, cells were washed 3 times in PBS before the secondary antibody (Table 2.5) in blocking solution was applied for 1 h at room temperature. Hoechst reagent diluted 1:6,000 was added for 5 minutes to visualise the nucleus. Cells were then washed twice with PBS and imaged using the Opera Phenix high-content imager (Perkin Elmer).

2.2.11 Columbus Analysis

Columbus Software was used in the image analysis setting to measure different parameters including nuclei numbers, nuclear size (µm2) (mean per well), CellROX intensity/cell area, Lamin A/C distribution, H3K9me3 intensity and SOD1-XPO1 interaction. CellROX, Lamin and H3K9me3 quantifications were carried out by Dr Ferraiuolo and Mr Shaw. In iAstrocytes stained for PLA the number of nuclei were identified and segmented using the Hoechst nuclear stain. Nuclear PLA foci were identified using the built-in spot analysis script using Hoechst-created masks and factoring in relative focus intensity as well as a splitting coefficient for accurate focus discrimination.

2.2.12 Western Blotting

2.2.12.1 Protein extraction

Medium was removed and the plate was washed twice with PBS. The cells were scraped using a cell scraper (VWR®), collected in a 1.5 Eppendorf tube and spun at 16,000g for 1 minute to obtain the pellet, which was stored at -80°C until use. PhosSTOP was added to the IP lysis buffer if specific phosphorylated protein isoforms were probed for by immunoblotting. 20-60 µl of IP lysis buffer were added per pellet, depending on the sizes, and then they were left for 15 mins on ice. The lysate was then centrifuged at 17,000g for 5 mins at 4°C. The lysate supernatant was reserved whilst the pellet of debris was discarded.

2.2.12.2 Bradford Assay

Bradford assay was used to quantify the protein concentration of cell lysates. Firstly, the protein assay dye reagent concentrate (Bio-Rad) was diluted in dH_2O in a 1:4 ratio to make a working concentration of Bradford reagent. 1µL of cell lysate was added to

1mL Bradford reagent, and mixed. The Bradford reagent and protein sample was loaded into a polystyrene cuvette with 1cm path length, and the optical density shift at A595nm (OD595nm) of the sample relative to a blank control was measured using a WPA S1200 Diode Array Spectrophotometer (Biochrom®). The concentration of the protein lysate was then calculated and converted to µg/mL using the Beer-Lambert law (OD595nm = εcl; where ε = 1/15, and l = 1cm).

2.2.12.3 SDS-Polyacrylamide Gel Preparation

The separation of proteins was carried out on the basis of the molecular weight by a polyacrylamide gel under denaturing conditions. Resolving gels of the required acrylamide % (w/v) (Table 2.11) were prepared by mixing reagents described in Table 2.12. Spacer plates with 1.0 mm integrated spacers (Bio-Rad) and short plates (Bio-Rad) were assembled on the Mini-PROTEAN® Tetra Cell Casting Stand and clamps (Bio-Rad) with gaskets (Bio-Rad). Gels were poured into glass plates, and a layer of isopropanol was placed on top of the gels. The gels were left for at least 15 minutes to set and the isopropanol was removed. 5% stacking gels were prepared by mixing reagents described in Table 2.12, and then poured onto the set resolving gels in the glass plates. 1.0 mm 15-well Mini-PROTEAN® Combs (Bio-Rad) were then inserted into the stacking gels, and left for at least 15 minutes to set.

Table 2.11 *Appropriate gel percentage based on protein size*

Protein size (kDa)	**Gel Percentage (%)**
12-45 kDa	15%
10-70 kDa	12%
15-100 kDa	10%

Table 2.12 *Composition of 5% Stacking gels, 10%, 12% and 15% Resolving gels*

	5% Stacking gel	**10% Resolving gel**	**12% Resolving gel**	**15% Resolving gel**

dH_2O	5.8 mL	4.2 mL	3.5 mL	2.5 mL
30 % (w/v) Acrylamide	1.7 mL	3.3 mL	4.0 mL	5.0 mL
Resolving buffer	-	2.5 mL	2.5 mL	2.5 mL
Stacking buffer	2.5 mL	-	-	-
10 % (w/v) APS	50 µL	50 µL	50 µL	50 µL
TEMED	20 µL	20 µL	20 µL	10 µL

2.2.12.4 Polyacrylamide Gel Electrophoresis

Cell lysates were mixed with 4X Laemmli buffer (See Table 2.1) and boiled for 5 minutes at 95°C to denature the proteins. 12% or 15% SDS-Polyacrylamide gels were loaded into a Mini-PROTEAN® Tetra Vertical Electrophoresis Cell (Bio-Rad), and the apparatus was filled with running buffer (see Table 2.1). Typically, 20µg of denatured protein was loaded per well onto the SDS-polyacrylamide gels. 2µL pre-stained protein ladder (BLUeye, Geneflow) was loaded as a molecular weight marker in one well per gel. Gel electrophoresis was performed at 50V for 30mins, then 150V for approximately 1.3h until the dye front reached the bottom of the gel.

2.2.12.5 Transfer on nitrocellulose membrane

Gels were then removed from the electrophoresis cell, and assembled with transfer buffer (see Table 2.1)-saturated Whatman paper, and transfer buffer-saturated nitrocellulose membrane in a semi-dry transfer apparatus (Biometra) (Figure 2.2). Electrophoretic transfer of the proteins from the gels to the membranes was performed at 0.15A/gel transferred for 1h. Membranes were then stained with Ponceau stain 0.1% (w/v) Ponceau S, 5% (v/v) acetic acid, and trimmed.

Figure 2.2 *Semi-dry transfer apparatus and gel/membrane setup*

2.2.12.6 Immunoblotting

For general immunoblotting, membranes were blocked in 5% (w/v) milk/Tris buffered saline, with Tween® 20 (TBST) for 1h at room temperature on a roller. The membranes were incubated with primary antibody (Table 2.4) in 5% milk (w/v)/TBST over-night at 4°C on a roller.

The following day membranes were washed 3 times in TBST for 15 minutes at room temperature. The membranes were then incubated with secondary antibody (Table 2.5) conjugated to horseradish peroxidase (HRP) in 5% milk/TBST for 1h at room temperature on a roller. The membranes were then washed 3 times in TBST for 15 minutes at room temperature and were then incubated with ECL for 1 minute and imaged using a G:BOX (Syngene).

2.2.12.7 Quantification of protein levels

Quantification of proteins was performed by densitometric analysis of bands obtained by immunoblotting using GeneTools (Syngene) image analysis software. The semi-quantitative assay was obtained by correlating the densitometric value of the band obtained for the protein of interest to the value of a normaliser, employing a housekeeping gene like β-actin. Statistical analyses were made using Prism software (GraphPad).

2.2.13 Nuclear and Cytoplasmic Fractionation

Cell fractionation was used to assess the presence of SOD1 in the nucleus of iAstrocytes.

Total fraction One 10cm plate was used for the total fraction. The medium was removed, and the cells washed once with PBS. The cells were then lysed with 250µL of IP T/N Lysis Buffer (See Table 2.1), scraped, collected in a tube and left 10 minutes on ice. After this incubation, the lysates were spun down at 13,300rpm, for 4 minutes, at 4˚C and the supernatant was collected in a fresh tube as total fraction.

Cytoplasmic Fraction Two plates were used for the nuclear and cytoplasmic fraction. After one wash with PBS, 1mL of accutase was added and the plates were incubated at 37°C for 2 minutes. Accutase was neutralised with media and the cells were collected in a tube and spun at 200g for 4 minutes. The media were removed and the pellet was washed twice with PBS and then left to dry. 400µL of hypotonic lysis buffer

(See Table 2.1) was added to the pellet, re-suspending it with a cut tip, to avoid shearing cells. At this point the lysate was passed through a 19g needle 10 times, left for 10 minutes on ice and then, spun down at 4,000rpm for 3 minutes at 4°C to separate the nuclear fraction from the cytoplasmic. The supernatant was transferred to a fresh tube, and spun again at 6,000rpm for 8 minutes at 4°C. The supernatant was collected into a new tube and spun down at 13,300rpm for 1 minute at, 4°C. The final supernatant was the cytoplasmic fraction.

Nuclear Fraction To the pellet (from the cytoplasmic fraction) 250µL of IP lysis buffer with 60µL of PMSF were added. At this point the lysate was passed through a 25g needle 10 times and then left for 30 minutes on ice. It was spun at 13,300rpm for 4 minutes at 4°C. The supernatant was the nuclear fraction. Bradford assay and Western Blot were performed as described in section 2.1.12. Equal loading was done on the basis of protein content estimated separately in the cytoplasmic and in the nuclear fraction.

2.2.14 Pull-down

2.2.14.1 Oxidised RNA

30µL of Protein G Sepharose beads (GE Healthcare) were taken as a slurry for each sample/condition, using a 1ml pipette tip cut at the bottom to enlarge the point. The beads were washed once with DEPC PBS and then diluted in 1ml DEPC PBS, centrifuged for 1 minute at 500g, then the supernatant was removed. 1mL 2% BSA in DEPC PBS was added and the tubes were left rotating at 4°C for 1 hour to block the beads. The tubes containing the beads were spun down at 500g for 1 minute at 4°C. 1mL of DEPC PBS with 0.5% Triton was added. 2 µL of antibody, 8hydroxyguanosine was added to each tube, and then they were left rotating at 4°C overnight. The following day, on ice, the media were removed from cells that were washed once with DEPC PBS. 1mL of DEPC PBS was added to the 10cm dish and UV-crosslinked with 300mJ/cm^2. The cells were scraped and transferred to a pre-chilled 1.5mL tube. The lysate was passed through a 19G needle 10 times and left on ice for a further 10minutes. Subsequently the preparation was centrifuged for 10min, 17,000g at 4°C and the supernatant was transferred to a new tube, and the protein concentration was measured through a Bradford assay, as previously described. The sample was diluted

to 2mg/mL. The beads were centrifuged for 1min at 500g and the supernatant was removed. The same volume of lysate was added to the beads and the 1:1(v:v) of PBS plus 1M NaCl was added. The samples were incubated rotating at 4°C overnight.
The tubes were centrifuged for 1 minute at 500g and the supernatant was removed. The pellet was washed once with PBS+1M NaCl+0.1% Triton and twice with Lysis buffer (PBS + 0.5% Triton). The supernatant was removed and 50µL of elution buffer and 1µL of RNase A (10mg/ml) were added. The tubes were vortexed slowly and then incubated at 37°C for 30 minutes, flicking them every 5 minutes. After this incubation they were centrifuged for 1min at 17,000g. The supernatant containing RNA-bound proteins was collected. On SDS-PAGE the input and eluted protein (output) were processed as described before in the western blot analysis section 2.1.12.

2.2.14.2 PolyA RNA precipitation

For this assay 4 dishes per cell line were used. The medium was removed from cells, which were washed with DEPC PBS. Half samples were treated with UV to crosslink proteins and RNA, while half were not crosslinked as a negative control.
For the “no UV” samples: PBS was removed, 500µL of lysis buffer was added, and then, the cells were scraped and transferred into pre-labelled tubes.
For UV samples: PBS was removed, 1mL of DEPC PBS was added to cover the cells. The plates were placed on ice without lids and UV crosslinked at 0.3 J/cm_2 (3,000x100 µL/cm_2). The PBS was removed and 500µL lysis buffer was added. The cells were scraped and transferred to pre-labelled tubes. All of the samples were incubated on ice for 5 minutes and then spun for 10 minutes at maximum speed at 4°C. While spinning, 50µL of magnetic oligo(dt) beads (New England BioLab) per treatment were taken and were placed on a magnet for 2 minutes. The supernatant was removed. The beads were washed with 200µL lysis buffer. The beads were returned to the magnet and the lysis buffer was removed. The beads were re-suspended in 200µL lysis buffer and stored on ice. The cleared lysates were transferred to fresh tubes and quantified using the Bradford assay. Samples were normalised to the lowest one, not exceeding 4mg protein/mL extract. The beads were placed on the magnet and the lysis buffer was removed. The beads were mixed with the samples and an equal volume of 2x binding buffer was added. The samples were incubated at room temperature, rotating at 10rpm, for 90 minutes. Supernatant was removed from the beads using the magnet. The beads were washed 5 times with 500µL 1x binding buffer (diluted with DEPC

water) and re-suspended in 50µL elution buffer plus 1µL PIC and 1µL RNase A. The samples were incubated at 37°C for 30 minutes, gently agitating the beads every 5 minutes. On SDS-PAGE inputs and eluted protein (output) were loaded and processed as described before in western blot analysis section 2.1.12.

2.2.15 Misfolded SOD1 and WT SOD1 Immunoprecipitation

30µL of protein G sepharose beads (GE Healthcare) were taken as a slurry for each sample, cutting the tip. The beads were washed twice with 1ml of IP lysis buffer, centrifuged for 2 minutes at 2,000G, then the supernatant was removed. 1mL 0.5% BSA in IP lysis buffer was added and the tubes were left rotating at 4°C for at least 1 hour to block the beads. The tubes containing the beads were spun down at 500g for 1 minute at 4°C. Lysis buffer was discarded. 1µL of antibody (misfolded SOD1 or WT SOD1) was added to each tube, and then they were left rotating at 4°C overnight. The following day, on ice, the media were removed from cells, that were washed once with PBS. The cells were scraped and transferred to a pre-chilled 1.5mL tube. The lysate was passed through a 19G needle 10 times and left on ice for a further 15 minutes. Subsequently the preparation was centrifuged for 10min at 17,000g and 4°C the supernatant was transferred to a new tube, and the protein concentration was measured by a Bradford assay. The sample was diluted to 2mg/mL. The beads were centrifuged for 1min at 500g and the supernatant was removed. The same volume of lysate was added to the beads. The samples were incubated by rotating at 4°C overnight. The tubes were centrifuged for 1minute at 500g and the supernatant was removed. The beads were washed 5 times with IP lysis buffer. The samples were eluted in 2x Laemmli buffer, sonicated for 10s on ice using the Soniprep 150 (MSE) for 10 seconds at 25% amp and boiled 5 minutes at 95°C. SDS-PAGE inputs and eluted protein (output) were loaded and processed as described in section 2.1.12.

2.2.16 Proximity Ligation Assay (PLA)

The proximity ligation assay (PLA) was performed in the 96 well plate using Duolink® In Situ Orange Starter Kit Mouse/Rabbit (Sigma-Aldric); 7,000-10,000 cells were plated per well. Firstly, the medium was removed from the wells and the cells were gently washed with PBS. The cells were fixed with 4% formaldehyde in PBS. After fixing, the cells were washed twice with PBS and permeabilised with 0.5% Triton in PBS for 10 mins at room temperature (RT). The cells were then washed twice with

PBS. Secondly, droplets of PLA blocking buffer (from the PLA kit) were placed to cover the wells. The plate was incubated for 30 mins at 37°C. During the blocking step, the primary antibodies were prepared and diluted in PBS.

The primary antibodies were incubated overnight at 4°C. The following day the PLA secondary probes (from the PLA kit) were prepared. After the primary antibody incubation, cells were washed twice with PLA wash buffer A (from the PLA kit). 40-50 µl of PLA secondary probes were added onto each well and the secondary antibodies were incubated for 1 hour at 37°C. During this incubation, the PLA ligation reagents (from the PLA kit) were prepared. After the secondary PLA probe incubation, the cells were washed twice with PLA wash buffer A. 40-50 µl of the ligation mix was placed onto each well and incubated for 30 mins at 37°C. The PLA amplification reagents (from the PLA kit) were prepared. After the PLA ligation incubation, the cells were washed twice with PLA wash buffer A. The amplification mix was incubated for 100 mins at 37°C. After the PLA amplification incubation, cells were washed twice in 0.01X wash buffer B (from the PLA kit). Hoechst reagent was diluted 1:10,000 in wash buffer B and incubated for 5 minutes at RT. Lastly, cells were washed twice with 0.01X wash buffer B to remove Hoechst from the cells. At this point, the plate was ready to be scanned with the Opera Phenix high content imaging system.

2.2.17 Statistical Analysis

All experiments were performed at least in triplicate. Data were analysed using GraphPad Prism Software (V8.4.2): one-way ANOVA with Tukey's multiple comparisons post-test or, two-way ANOVA with Tukey's multiple comparisons post-test. t test was used to compare old donor samples to the young donor samples for qPCR and western blot and for control sample to specific patient subgroups for western blot.

3. Results

Characterisation of the ageing phenotype in directly reprogrammed astrocytes and the impact of these findings when modelling neurodegenerative diseases

3.1 Preface

Astrocytes are the most abundant group of glial cells, necessary for homeostasis, defence and regeneration of the CNS. It has been reported that ageing affects glial cells to a greater extent than neurons in the human brain (Soreq *et al.*, 2017). Ageing, in fact, provokes a reduction in the ability of glial cells, in particular astrocytes, to maintain a balanced and healthy CNS homeostasis. Astrocytes have preserved some of their roles across species, but their reaction to insults and their role in neuronal support make mammalian astrocytes unique. In addition, human astrocytes have evolved to develop a unique response to inflammatory stimuli and a finely tuned cross-talk with neurons (Verkhratsky and Nedergaard, 2016). Thus, it is important to have a model of human astrocytes suitable for ageing and disease modelling, especially in relation to neurodegenerative disorders, in which non-cell autonomous mechanisms are involved.

In my PhD project, I focused on ALS, where it is well known that astrocytes contribute to disease pathophysiology and ageing represents a major risk factor. This led to addressing the first aims of my PhD thesis:

1. To determine the ability of the direct reprogramming protocol used in my laboratory to retain phenotypic age-related properties of donor fibroblasts in the induced astrocytes derived from the reprogramming.

2. To determine the functional properties of induced astrocytes derived from donors at different ages, based on known age and disease-related functional changes, i.e. oxidative stress response, inflammatory response and nucleocytoplasmic transport changes.

This first results chapter of my thesis addressing these aims is composed of the research article submitted for publication and currently under revision in the journal “Aging Cell”.

Directly converted astrocytes retain the ageing features of the donor fibroblasts and elucidate the astrocytic contribution to human CNS health and disease

Noemi Gatto[1], Cleide Dos Santos Souza[1], Simon M. Bell[1], Allan C. Shaw[1], Monika A. Myszczynska[1], Samantha Powers[2], Kathrin Meyer[2], Paul R. Heath[1], Lydia M. Castelli[1], Evangelia Karyka[1], Heather Mortiboys[1], Mimoun Azzouz[1], Guillaume M. Hautbergue[1], Nóra M. Márkus[1], Pamela J. Shaw[1], and Laura Ferraiuolo[1].*

[1]Sheffield Institute for Translational Neuroscience (SITraN), University of Sheffield, Sheffield S10 2HQ, UK

[2]The Research institute, Nationwide Children's Hospital, Columbus, Ohio 43205, USA

*Corresponding author and Lead Contact: l.ferraiuolo@sheffield.ac.uk

Abstract

Astrocytes are highly specialised cells, responsible for CNS homeostasis and neuronal activity. Lack of human *in vitro* systems able to recapitulate the functional changes affecting astrocytes during ageing represents a major limitation to studying mechanisms and potential therapies aiming to preserve neuronal health. Here we show that induced astrocytes from fibroblast donors in their childhood or adulthood display age-related transcriptional differences and functionally diverge across a spectrum of age-associated features, such as altered nuclear compartmentalization, nucleocytoplasmic shuttling properties, oxidative stress response and DNA damage response. Remarkably, we also show an age-related differential response of iAstrocytes in their ability to support neurons in co-culture upon exposure to pro-inflammatory stimuli. These results show that iAstrocytes are a renewable, readily available resource of human glia that retain the age-related features of the donor fibroblasts, making them a unique and valuable model to interrogate human astrocyte function over time in human CNS health and disease.

Keywords: direct reprogramming, astrocytes, ageing, neurodegeneration, *in vitro* model, nucleocytoplasmic transport, neuron-astrocyte crosstalk, neuroinflammation, oxidative stress, nuclear abnormalities.

Introduction

Ageing is considered the primary risk factor for many devastating pathologies, including neurodegenerative diseases, which primarily affect neurons. There is robust evidence, however, for non-cell autonomous mechanisms in which neurodegeneration is influenced or even driven by glial cells (Lobsiger and Cleveland, 2007; Meyer *et al.*, 2014; Lee *et al.*, 2016; Chai and Kohyama, 2019; di Domenico *et al.*, 2019).

Astrocytes, the most abundant non-neuronal cell population in the central nervous system (CNS), are known to guide brain development (Verkhratsky and Nedergaard, 2016) and to play a crucial role in CNS homeostasis and repair (Parpura *et al.*, 2012). Moreover, studies interrogating the gene expression profile of rodent and humans neurons, astrocytes and microglia have found that astrocytes, more than neurons, dramatically change their gene expression pattern with age (Soreq *et al.*, 2017). This indicates that they might be significant drivers of the ageing process and preservation of their physiological functions over time will clearly support neuronal health.

Changes in glial functions, such as reduced redox homeostasis and increased pro-inflammatory responses, are hallmarks of the ageing brain (Lynch *et al.*, 2010; Bellaver *et al.*, 2017; Matias, Morgado and Gomes, 2019). Consistently, *in vitro* studies comparing primary astrocytes from young and old rodents have shown changes in the expression of the nuclear factor erythroid-derived 2-like 2 (Nrf2) (Duan *et al.*, 2009; Lewis *et al.*, 2015) and nuclear factor kappa B (NFκB) (Tilstra *et al.*, 2011; Osorio *et al.*, 2016), master regulators of the antioxidant and inflammatory responses respectively. A decrease in the effectiveness of the antioxidant response in the ageing brain leads to accumulation of oxidised nucleic acids, proteins and lipids (Gemma *et al.*, 2007), while increased NFκB activity exacerbates the production of pro-inflammatory cytokines (Lynch, 2010; Rea *et al.*, 2018). Both processes are known to participate in neurodegeneration and are therefore considered appealing therapeutic targets.

The lack of human *in vitro* models that recapitulate the functional changes affecting astrocytes throughout ageing represents a major limitation for studying relevant mechanisms and potential therapies aiming to preserve brain health, as well as targeting age-related neurodegenerative disorders. Studies using astrocytes isolated from *post-mortem* (PM) human samples (Blasko *et al.*, 2000; Re *et al.*, 2014) have shed light on important disease mechanisms, but the availability of these cells is

limited and their function might be altered by factors related to *post-mortem* collection, hence the need for widely available, reproducible human *in vitro* models that retain age-related biochemical alterations.

So far, somatic cell reprogramming is the most commonly used methodology (Takahashi *et al.*, 2007) to address the challenges of modelling human neurodegenerative diseases. The induction of pluripotency factors in adult fibroblasts, however, reverts cellular age to an embryonic status (Lapasset *et al.*, 2011; Patterson *et al.*, 2012), which is retained even after conversion into neurons, erasing ageing-associated signatures (Miller *et al.*, 2013). To circumvent this limitation, recent studies have shown that neurons directly reprogrammed from fibroblasts without the use of pluripotency factors, retain ageing signatures compared to induced pluripotent stem cells (iPSC)-derived neurons (Mertens *et al.*, 2015; Huh *et al.*, 2016; Tang *et al.*, 2017; Victor *et al.*, 2018). Direct conversion preserves ageing features in neurons; however, no study has yet achieved this goal in astrocytes. Most available protocols for derivation of human astrocytes utilise iPSCs, are time consuming and have low conversion efficiency (Almad and Maragakis, 2018). Although recent methodologies have made human astrocyte production from iPSCs faster (Canals *et al.*, 2018; Tchieu *et al.*, 2019), the field is still lacking an *in vitro* human astrocyte system able to retain the ageing characteristics of the donor.

In 2014, we described the first human-derived astrocytes differentiated from tripotent induced neural progenitor cells (iNPCs) directly converted from adult fibroblasts (Meyer *et al.*, 2014). This protocol is fast and highly efficient and does not involve clonal expansion, thus greatly reducing the variability associated with iPSCs (Ortmann and Vallier, 2017; Mertens *et al.*, 2018). Induced NPCs can be expanded and stored for several passages and are an immediate source of neurons (Webster *et al.*, 2016), oligodendrocytes (Ferraiuolo *et al.*, 2016) and astrocytes. Induced astrocytes (iAstrocytes) can be obtained from iNPCs in only 7 days and have been utilised to study childhood (Boczonadi *et al.*, 2018) and adult-onset neurodegenerative disorders, including amyotrophic lateral sclerosis (ALS) (Meyer *et al.*, 2014; Hautbergue *et al.*, 2017; Varcianna *et al.*, 2019).

The ability of this protocol to retain ageing features at transcriptional and functional level has not been interrogated previously.

In the present study we assess the ability of this direct conversion methodology to retain the ageing features of the donor's fibroblasts. Comparing the gene expression profiles of iAstrocytes derived from donors in childhood or adulthood with transcriptomic data from adult *post-mortem* (PM) and fetal astrocytes revealed that iAstrocytes reproduce transcriptional age-related features. We then showed how iAstrocytes from the two different age groups diverge in relation to a spectrum of age-associated features, such as accumulation of DNA damage, altered nuclear compartmentalization, oxidative stress and nucleocytoplasmic shuttling defects. Furthermore, we showed an age-related differential response of iAstrocytes in their ability to support neurons in co-culture upon stimulation with the inflammatory cytokine interleukin-1 beta (IL-1β).

In conclusion, our results show that age-related features are retained in iAstrocytes reprogrammed from donor fibroblasts, thus making this model a reliable and accessible tool to interrogate human astrocyte function over the life course in health and disease.

Results

Efficient differentiation of iAstrocytes from young and old donor fibroblasts

To determine whether astrocytes derived from induced neuronal progenitor cells (iNPCs) directly converted from fibroblasts (Meyer *et al.*, 2014) retain the ageing features of the donor, we set out to directly reprogramme fibroblasts from individuals belonging to two distinct age groups. Fibroblast samples from three donors ranging in age from 42 to 56 years and three donors ranging in age from 5 months to 3 years (Table S1) were directly reprogrammed to iNPCs (Figure 1A), which stained positive for the neural progenitor markers Pax6 and Nestin (Figure 1B). Passage matched old and young donor-derived iNPCs were then differentiated into iAstrocytes in 7 days as previously described (Meyer *et al.*, 2014). iAstrocytes from both young and old donors expressed typical astrocytic markers, including glial fibrillary acidic protein (GFAP), vimentin (VIM), CD44, as well as the glutamate transporter EAAT2, a marker of mature astrocytes. The cells derived from young and old donors have similar confluency rate, despite the difference in their size (Figure 1C). This protocol is highly efficient, yielding >98% cells positive for the above markers (Figure S1).

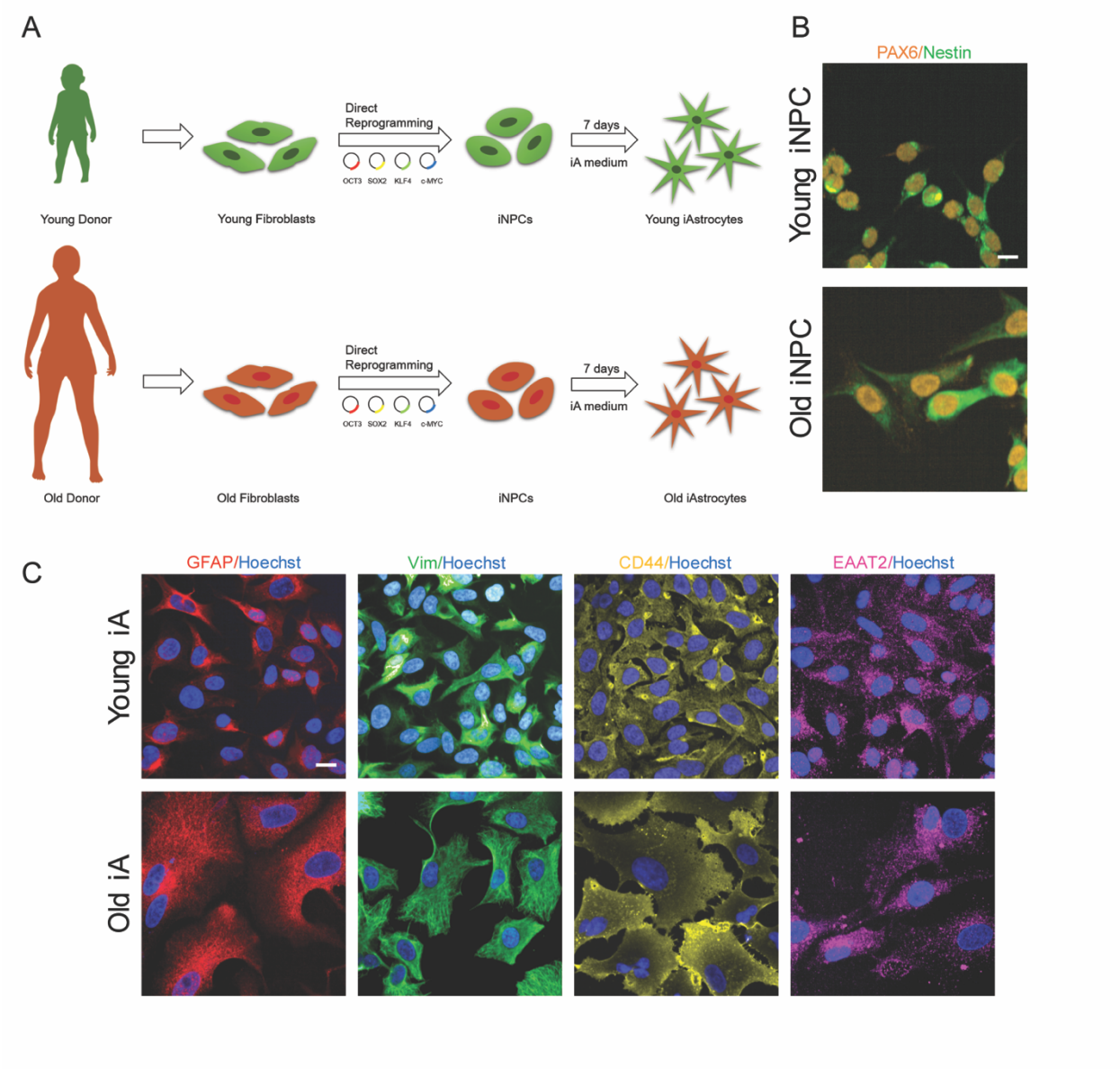

Figure 1. Characterization of iAstrocytes from old versus young donors

(A) Schematic illustration of the differentiation protocol, from young and old donor fibroblasts to induced neuronal progenitor cell (iNPC) derived iAstrocytes.

(B) Representative images of PAX6/Nestin staining in young and old donor derived iNPCs. Scale bar (10μm).

(C) Representative images of astrocytic markers (GFAP, vimentin (VIM), CD44 and EAAT2) in young and old donor derived iAstrocytes, Scale bar (10μm). See also Figure S1.

Transcription profile discriminates iAstrocytes from young and old donors and segregates them according to age-related gene expression signatures

To interrogate the transcriptional features of fibroblast-derived iAstrocytes in relation to their ageing phenotype, we compared transcriptomic data from iAstrocytes obtained from old and young donors to *bona fide* human astrocytes laser captured from *post-mortem* (PM) brains (Simpson *et al.*, 2011; Waller *et al.*, 2012) and fetal primary astrocytes (Table S2). After signal normalization and harmonization of the 4 datasets, gene expression levels of 18,357 transcripts were imported into the bioinformatics software Qlucore. The data were then visualised using a principal component analysis (PCA) plot (Figure 2A), with application of stringent multi-group comparison statistics (p-value ≤ 1x10e-4). This analysis identified 16,284 differentially expressed transcripts that determined sample grouping on the PCA plot (Figure 2A). Using the same parameters, we also visualised the sample groups based on transcript levels in a hierarchical cluster heat-map (Figure 2B). Both data representation plots showed that iAstrocytes from the two different age groups have distinct transcription profiles, which group closely with their *bona fide* astrocyte counterpart. In fact, individuals in their 5th-6th decade of life (old donor) group closely with astrocytes taken at *post-mortem* from older individuals, while iAstrocytes from individuals in their 1st decade of life (young donor), although clearly separate from fetal astrocytes, group more closely to these samples. In order to determine whether the transcripts described age-related features, we downloaded a human dataset of 307 genes commonly altered during ageing, from the Human Genomic Resources (HAGR), GenAge database (https://genomics.senescence.info/genes/index.html). From this list of 307 genes, 285 genes were present in the list of 16,284 transcripts that determined the sample sub-grouping. Consistently, the PCA plot (Figure S2A) and the hierarchical clustering (Figure S2B) of the 4 groups in relation to these 285 age-related transcripts confirmed the separation between PM and fetal astrocytes and iAstrocytes in the two age groups (Figure S2). We also performed two-group comparison analysis (p-value ≤ 0.05, fold change > 1.5), between *bona fide* astrocytes from different age groups, PM and fetal astrocytes, as well as iAstrocytes from young and old donors. The first comparison (PM vs fetal astrocytes) reported 7,875 differentially expressed transcripts, while the second (young vs old iAstrocytes) reported 1,639. We then proceeded to interrogate how many of these differentially expressed transcripts were common to both

comparisons, and almost 80% of the transcriptional differences between young and old iAstrocytes matched the corresponding comparison between PM and fetal primary human astrocytes (Figure 2C). Pathway analysis of these 1,298 transcripts (Table S3) via Panther (http://www.pantherdb.org/) identified several physiological and pathological processes known to be associated with ageing (Table 1).

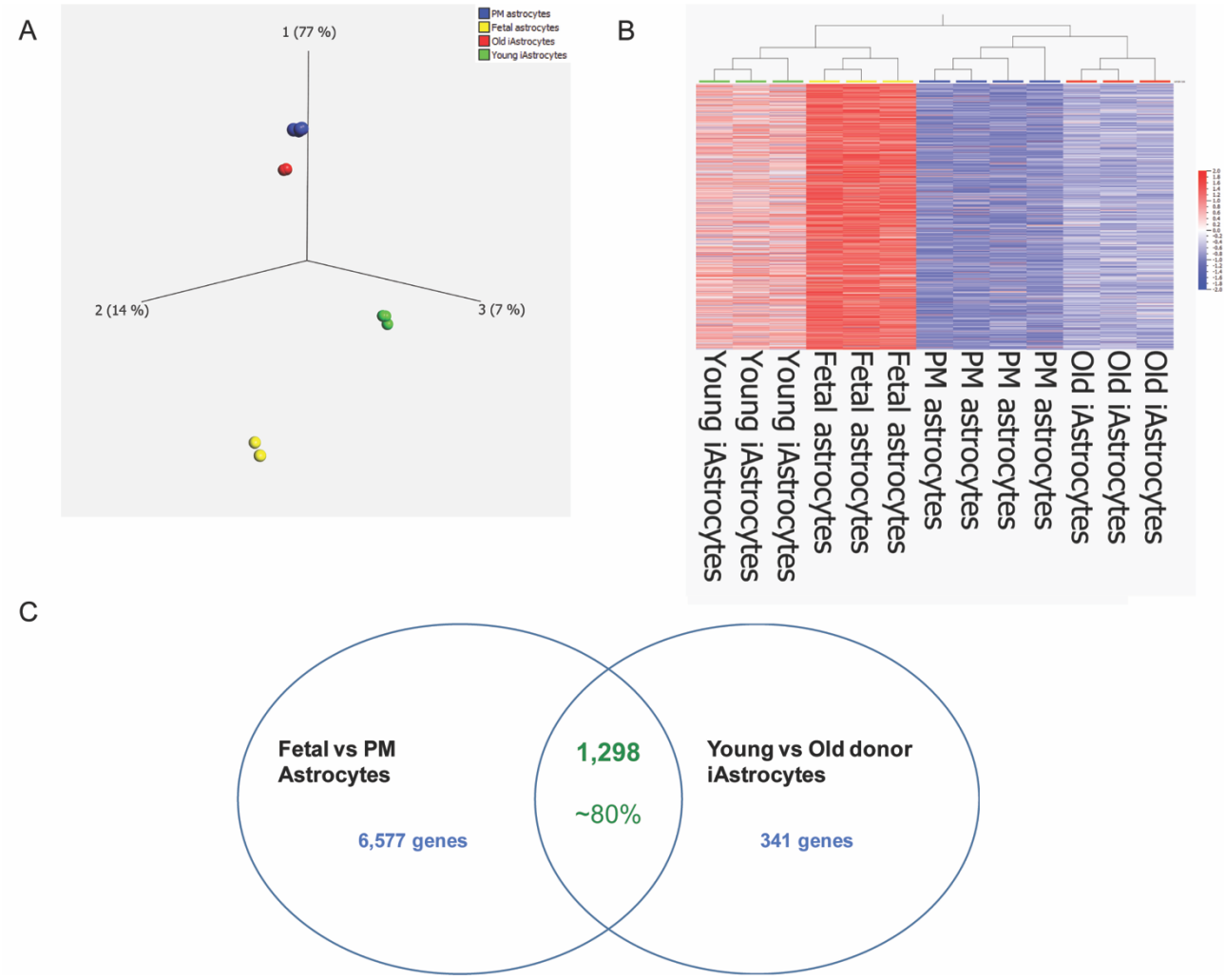

Figure 2. Old donor iAstrocytes and *post-mortem* (PM) astrocytes have distinctly different transcriptomes compared to fetal astrocytes and young donor iAstrocytes.

(A) Principal component analysis (PCA) plot of fetal astrocytes, PM astrocytes and old and young donor derived iAstrocytes. Multi-group comparison, p≤1x10e-4.

(B) Hierarchical cluster heat-map of fetal astrocytes, PM astrocytes and old and young donor iAstrocytes. Multi-group comparison, p≤1x10e-4.

(C) Venn diagram representing two-group comparison analysis (p-value ≤ 0.05; fold change > 1.5) between PM and fetal astrocytes as well as iAstrocytes from young and old donors. PM vs fetal astrocyte comparison reported 7,875 differentially expressed transcripts, while young and old donors iAstrocytes reported 1,639. 1,298 differentially expressed transcripts were common to both comparisons. Approximately 80% of the transcriptional differences between young and old iAstrocytes matched the corresponding comparison between PM and fetal primary human astrocytes. See also Figure S2 and Table S3.

Table 1 Table illustrating the pathways identified by the 1,298 transcripts intersecting the comparisons between PM vs fetal astrocytes as well as iAstrocytes from young vs old donors.

Pathway name	**% transcripts**
Integrin signalling pathway	4.50%
Wnt signaling pathway	4.20%
Huntington disease	3.40%
Inflammation mediated by chemokine and cytokine signalling pathway	3.40%
EGF receptor signalling pathway	3.20%
DNA damage signalling pathway	2.20%
Alzheimer disease-amyloid secretase and presenilin pathway	2%
Cytoskeletal regulation by Rho GTPase	1.90%
Parkinson disease	1.90%
p53 pathway	1.80%
Ubiquitin proteasome pathway	1.80%
TGF-beta signalling pathway	1.60%
Oxidative stress response	1.60%
Heterotrimeric G-protein signalling pathway-Gi alpha and Gs alpha mediated pathway	1.50%
Axon guidance mediated by semaphorins	1.40%
PI3 kinase pathway	1.30%
VEGF signalling pathway	1.30%
Glutamate receptor pathway	1%
Insulin/IGF pathway-mitogen activated protein kinase kinase/MAP kinase cascade	0.90%
Protein biosynthesis	0.70%
p38 MAPK pathway	0.60%

iAstrocytes from older donors recapitulate nuclear ageing features

In order to determine whether the expression of specific age-associated transcripts was preserved between iAstrocytes and their fibroblasts of origin, we interrogated the expression of 3 transcripts that have been previously identified as consistently decreasing with ageing in various tissues (Martínez *et al.*, 2014; Mertens *et al.*, 2015; Godin *et al.*, 2016). RAN binding protein 17 (*RANBP17*) and laminin subunit alpha 3A (*LAMA3A*) were identified by Mertens *et al* when comparing the transcriptomes of human fibroblasts and brain samples from a broad range of aged donors. Their change in expression was shown to be maintained between fibroblasts and derived directly reprogrammed neurons (iNeurons), but not iPSC-derived neurons. RANBP17 is a nuclear pore-associated transport receptor, a member of the importin-β family, involved in the transport of nuclear localisation signal (NLS)-containing cargo proteins through the nuclear pore complex (NuPC) (Koch et al., 2000; Lee, Zhou and Smas, 2010), while *LAMA3,* also reported to decrease with age in other *in vivo* studies (Godin et al., 2016), encodes an extracellular matrix protein. In addition, we also assessed the expression of telomeric repeat-binding factor 2 (TERF2), a component of shelterin that together with TERF1 is responsible for telomerase maintenance (Martínez et al., 2014). It is well known that telomerase activity is crucial in determining telomere length in ageing cells and that telomere length can be considered as a biomarker of chronological ageing (Rizvi, Raza and Mahdi, 2015; Fasching, 2018). In agreement with previous reports, our results show that *TERF2*, *RANBP17* and *LAMA3* mRNA levels decrease significantly with age in fibroblasts and we show here that iAstrocytes retain this decline in expression levels after reprogramming (Figures 3A, 3B and 3C).

In addition to assessment of transcriptional features, we interrogated cellular parameters that have previously been reported to change with age, including nuclear size and shape (Pienta, Getzenberg and Coffey, 1992; Haithcock *et al.*, 2005; Scaffidi and Misteli, 2006; Brandt, Krohne and Grohans, 2008), as well as histone methylation (Miller *et al.*, 2013).

DNA is contained in the nucleus and it is well documented how nuclear structure is affected during ageing (Haithcock *et al.*, 2005; Scaffidi, Gordon and Misteli, 2005). Heterochromatin organization and nuclear shape were assessed via immunostaining using the heterochromatin-associated trimethylated 'Lys-9' on histone H3 marker (H3K9me3) and the nuclear lamina marker lamin A/C. H3K9me3 is the hallmark of constitutive heterochromatin (Maleszewska, Mawer and Tessarz, 2016), whilst Lamin

A/C coded by the gene *LMNA*, is part of the lamin protein family, which form components of the nuclear lamina (Liu and Zhou, 2008).

Consistent with previous reports describing an overall decrease in H3K9me3 in cells and tissues (Miller *et al.*, 2013) iAstrocytes from older donors displayed a significant global reduction of H3K9me3 staining (Figures 3E and 3H). Immunostaining of lamin A/C also confirmed that iAstrocytes from older donors displayed significant nuclear morphology alterations, with increased nuclear folding and blebbing. Lamin staining is clearly localized in the nuclear membrane and defines nuclear shape in young iAstrocytes, while it displays fragmented and less spherical staining in iAstrocytes from older donors (Figures 3F and 3I). In addition, we report a significant increase in nuclear size assessed by Hoechst staining in old iAstrocytes (Figures 3D and 3G). Similar findings have been reported in *in vitro* and *in vivo* fibroblasts (Mitsui and Schneider, 1976; Mukherjee and Weinstein, 1986; Pienta, Getzenberg and Coffey, 1992).

Taken together, these results demonstrate that iAstrocytes reprogrammed from donors of different age groups retain some of the ageing features of their parental fibroblasts, and exhibit well described ageing morphological characteristics.

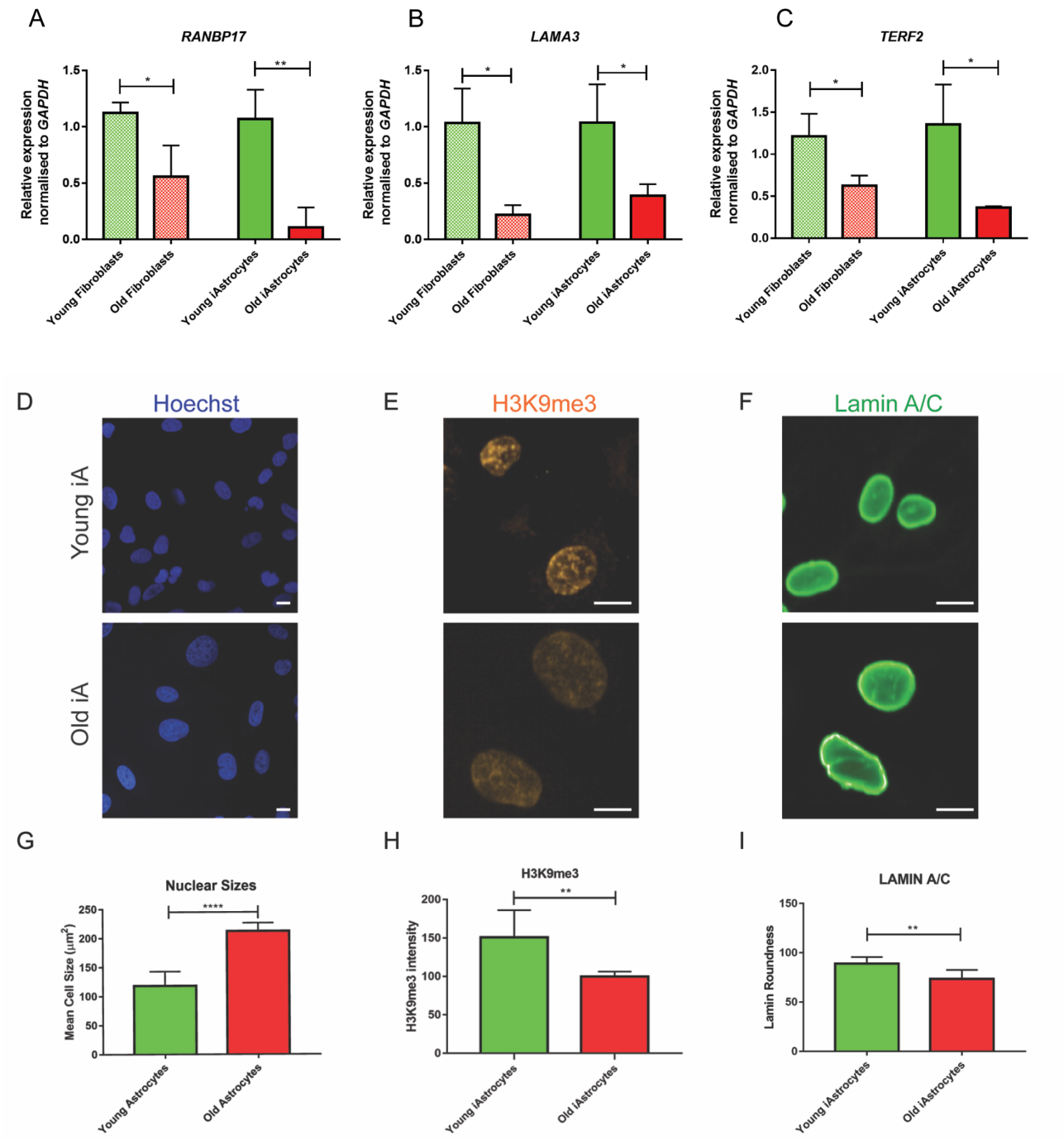

Figure 3. Young and old iAstrocytes retain the ageing phenotype of their fibroblasts of origin.

(A) Quantification of *RANBP17* mRNA levels in young and old donor fibroblasts and derived iAstrocytes. Results are expressed as the means ± SD. Unpaired t-test, *P<0.05, **P<0.01 (n=3).

(B) Quantification of *LAMA3A* mRNA levels in young and old donor fibroblasts and derived iAstrocytes. Results are expressed as the means ± SD. Unpaired t-test, *P<0.05 (n=3).

(C) Quantification of *TERF2* mRNA levels in young and old donor fibroblasts and derived iAstrocytes. Results are expressed as the means ± standard deviation (SD). Unpaired t-test, *P<0.05 (n=3).
(D) Representative images of Hoechst staining in young and old donor derived iAstrocytes. Scale bar (10µm).
(E) Representative images of H3K9me3 staining in young and old donor derived iAstrocytes. Scale bar (10µm).
(F) Representative images of Lamin A/C staining in young and old donor derived iAstrocytes. Scale bar (10µm).
(G) Quantitative image analysis of nuclear sizes in young vs old donor derived iAstrocytes. Nuclear size (μm^2) was assessed using Columbus Software. Results are expressed as the means ± SD. Unpaired t-test, ****P<0.0001 (n=3).
(H) Quantitative image analysis of H3K9me3 in young vs old donor derived iAstrocytes. H3K9me3 intensity was assessed using Columbus Software. Results are expressed as the means ± SD. Unpaired t-test, **P<0.01 (n=3).
(I) Quantitative image analysis of Lamin A/C in young vs old donor derived iAstrocytes. Lamin A/C roundness was assessed using Columbus Software. Results are expressed as the means ± SD. Unpaired t-test, **P<0.01 (n=3).

iAstrocytes reveal age-related nuclear permeability and nucleocytoplasmic transport defects

In order to examine further the nuclear envelope abnormalities detected via lamin A/C staining, we set out to interrogate the overall integrity of another nuclear component, the nuclear pore complex (NucPC). Seminal work (D'Angelo *et al.*, 2009) has previously revealed that the NucPC is highly affected by age in post-mitotic cells, leading to nuclear "leakiness". This phenomenon has also been recently highlighted as critically important also in age-related diseases, such as amyotrophic lateral sclerosis (ALS) and Alzheimer's disease (AD) (Kim and Taylor, 2017; Eftekharzadeh *et al.*, 2018).

In intact nuclei, molecules of up to 40-50 kDa can pass through the NucPC via passive diffusion, while molecules larger than 60 kDa are excluded from intact nuclei (Lénárt and Ellenberg, 2006). Thus, we analysed the overall nuclear permeability in young and old donor iAstrocytes, by isolating nuclei from both groups of iAstrocytes and incubating them with a 70 kDa fluorescently-labelled dextran (Figure 4A). Nuclei were then stained for Hoescht and imaged using a confocal microscope. We found that influx of the 70 kDa dextran was observed only in the old donor-derived iAstrocyte nuclei (Figure 4B), and not in young donor-derived iAstrocyte nuclei. This confirms that direct conversion of fibroblasts into iNPCs and subsequently iAstrocytes retains a key characteristic of ageing that is often associated with neurodegenerative conditions (D'Angelo *et al.*, 2009) and so far has been primarily associated with neuronal ageing.

Further, we assessed the levels of three proteins involved in active nucleocytoplasmic transport, i.e. Ran binding protein 17 (RANBP17), Importin 5 (IPO5) and Exportin 1 (XPO1). Importin 5 is a member of the importin-β family of nuclear transport receptors that mediates transport of proteins carrying a nuclear localisation signal (NLS), RANBP17 serves as nuclear import receptor, whilst Exportin 1 (XPO1) mediates the nuclear export of cellular proteins bearing a leucine-rich nuclear export signal (NES) and of some non-coding RNA molecules including snRNAs and rRNAs.

Consistent with reports that nucleocytoplasmic transport becomes impaired with age and in neurodegeneration (Ribezzo, Shiloh and Schumacher, 2016; Kim and Taylor, 2017; Ferreira, 2019; Hutten and Dormann, 2019), our results show that RANBP17, IPO5 and XPO1 protein levels are significantly decreased in older compared to young donor-derived iAstrocytes (Figures 4C- F).

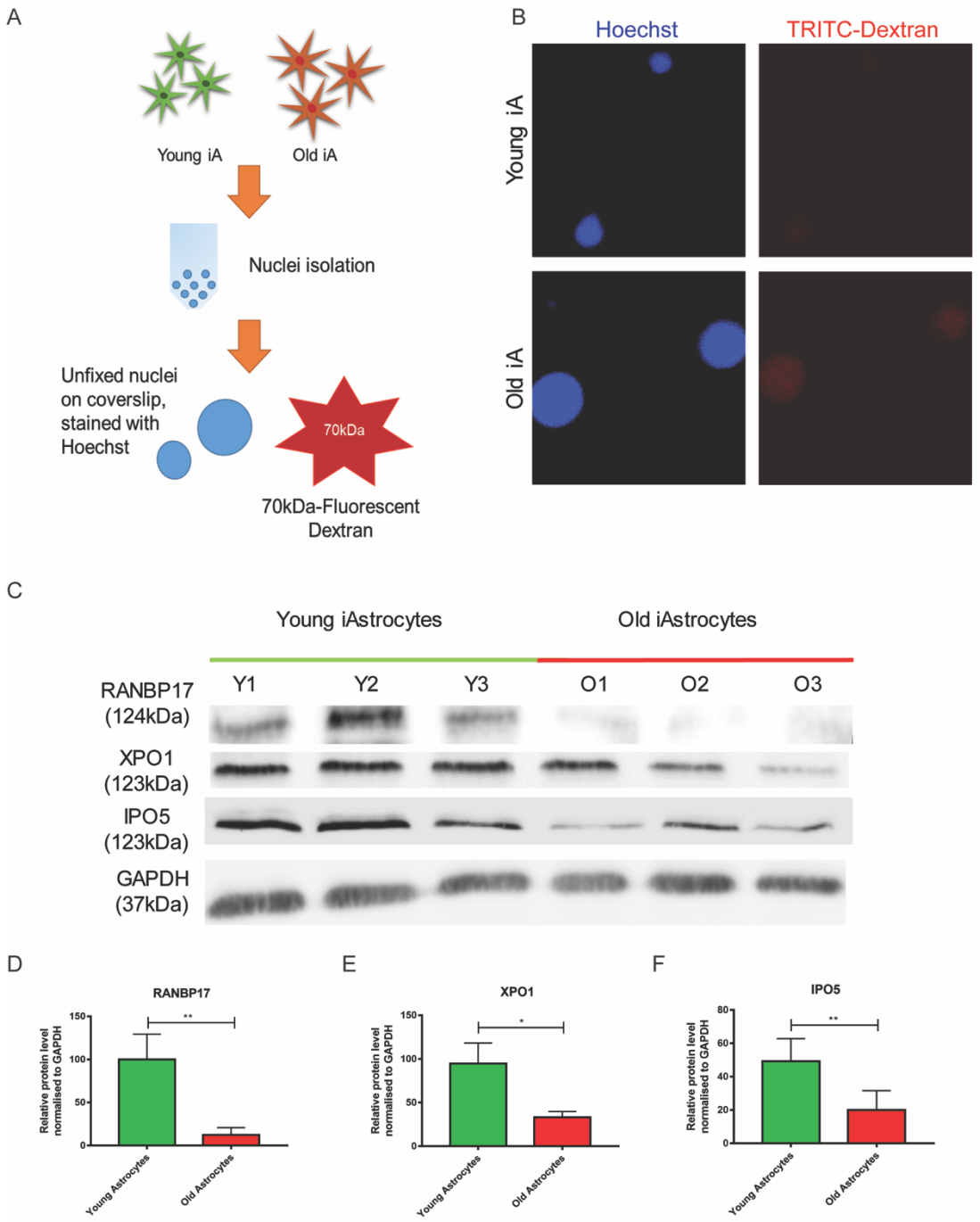

Figure 4. Old and young iAstrocytes show differential nuclear permeability and nucleocytoplasmic shuttling/export.

(A) Schematic illustration of the nuclear isolation protocol for dextran application

(B) Representative images of TRITC-labelled dextran influx in young vs old donor derived iAstrocytes.

(C) Representative images of western blot analysis of RANBP17, IPO5 and XPO1. Protein from young and old donor derived iAstrocytes was separated by sodium dodecyl sulfate-polyacrylamide gel electrophoresis followed by immunoblotting.

(D) Densitometric quantification of RANBP17 normalised to GAPDH. Values are expressed as means ± SD. Unpaired t-test, **P<0.01 (n=3).
(E) Densitometric quantification of XPO1 normalised to GAPDH. Values are expressed as means ± SD. Unpaired t-test, *P<0.05. (n=3).
(F) Densitometric quantification of IPO5 normalised to GAPDH. Values are expressed as means ± SD. Unpaired t-test, **P<0.01 (n=3).

Older donor-derived iAstrocytes display lower anti-oxidant defences

A key hallmark of ageing is rising levels of oxidative stress and accumulation of reactive oxygen species (ROS) that leads to nucleic acid, protein and lipid oxidation. Astrocytes are the principal cell type in the CNS responsible for counteracting the increase in oxidative stress through the anti-oxidant response and non-cell autonomous support of neurons (Bell *et al.*, 2011). To test the hypothesis that reprogrammed iAstrocytes from donors of different ages can model this central aspect of astrocyte function, we quantified the endogenous levels of ROS in iAstrocytes from naïve young and old donors, using the CellROX® Oxidative Stress Reagent, a fluorogenic probe designed to measure reactive oxygen species (ROS) in live cells. We found that ROS levels were significantly higher in old compared to young donor-derived iAstrocytes under basal conditions (Figures 5A and 5B). To test how iAstrocytes respond to stressors that increase oxidative stress over time, we also performed a time-course experiment. We measured intracellular levels of ROS in young and old donor iAstrocytes at baseline before subjecting the cells to 12h of serum starvation. After 12h we measured the levels of intracellular ROS in both groups of iAstrocytes, and then following a change to full iAstrocyte medium assessed how long it took the cells to return to baseline levels of ROS. Our measurements show that both young and old donor-derived iAstrocytes display an increase in intracellular ROS after serum starvation and recover after removing the stimulus, going back to baseline levels (Figure 5C). Remarkably, iAstrocytes from younger individuals recovered to their baseline levels after only 4 hours, while iAstrocytes from older individuals required a longer time-period of 6 hours (Figure 5C).

To understand what changes may underlie the increased levels of ROS seen in old iAstrocytes at baseline, and the delayed recovery from oxidative stress following serum starvation, we investigated the levels of NRF2, the master regulator of antioxidant defences, and superoxide dismutase 1 (SOD1), a major antioxidant enzyme responsible for the breakdown of superoxide radicals. Both *NRF2* and *SOD1* are present in the list of ageing genes that are down-regulated in both PM and old iAstrocytes versus fetal astrocytes and young iAstrocytes in our microarray analysis (Figure 2 and S2B). Consistent with *in vivo* data (Zhang, Davies and Forman, 2015; Paladino *et al.*, 2018) and our transcriptomic data, we found that NRF2 and SOD1 baseline levels are significantly lower in old as opposed to young donor-derived iAstrocytes (Figures 5D, 5E and 5F). The lowered antioxidant defences present in old

iAstrocytes may explain the increased levels of baseline ROS species observed (Figures 5A and 5B). Considering the ability of both young and old donor iAstrocytes to respond to the oxidative stress generated by serum starvation treatment (Figure 5C), we set out to evaluate the protein levels of NRF2 and SOD1 in response to this stressor. As suggested by our time-course experiments (Figure 5C), we observed a significant increase in NRF2 protein level in iAstrocytes from both age groups, thus showing that both groups can respond to acute oxidative stress insults. However, the total levels of NRF2 and SOD1 were still lower in old compared to young iAstrocytes in the serum starved conditions, giving a potential explanation for the decreased and slower response to counteract oxidative stress after the insult (Figures 5D, 5E and 5F).

Oxidative stress is known to affect cell function in many ways through protein, lipid and nucleic acid oxidation. In particular, DNA damage has been recognised as a causal factor in the ageing process and its markers are hallmarks of aged tissues, especially in the CNS, where cell turnover is limited (Lu *et al.*, 2004). The current hypothesis is that DNA damage accumulation with ageing causes loss of key cellular functions leading to degeneration (Ribezzo, Shiloh and Schumacher, 2016). In order to repair these lesions, in particular DNA double strand breaks (DSBs), the DNA damage response (DDR) starts at the damage site with the phosphorylation of the C-terminal of the core histone protein H2AX (γH2AX). Consistent with the increase in ROS and concomitant decrease in the anti-oxidant response, we detected an increase in γH2AX foci in old compared to young iAstrocytes (Figures 5G and 5H).

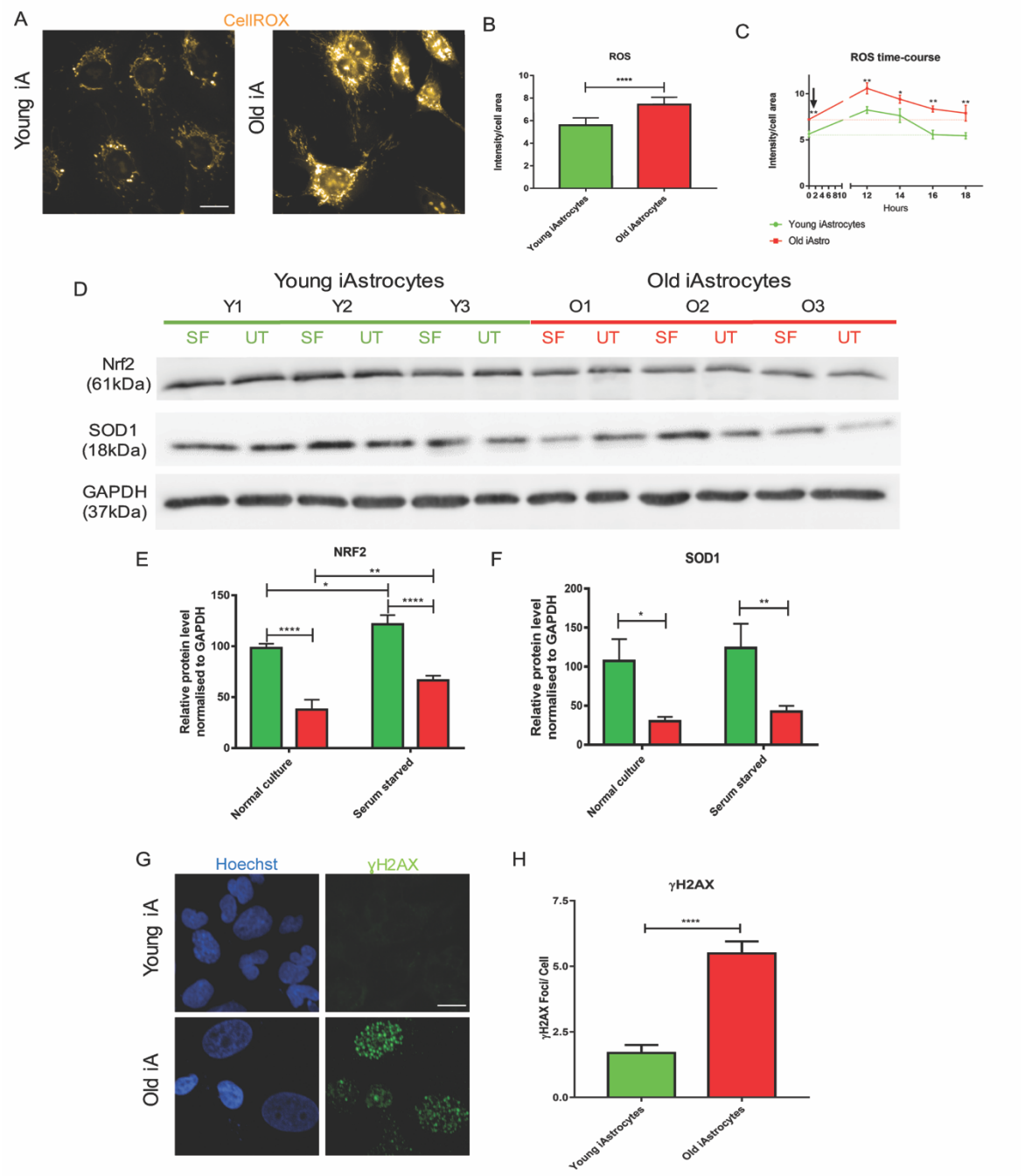

Figure 5. Altered oxidative stress capacities in old donor derived astrocytes.

(A) Representative immunofluorescence images of ROS in young and old donor derived iAstrocytes. Cellular ROS levels were assessed in iAstrocytes by CellROX® Reagent, Scale bar (10μm).

(B) Quantitative image analysis of ROS detected by CellROX® Reagent in young and old donor derived iAstrocytes. Fluorescence intensity was assessed using Columbus Software. Results are expressed as means ± SD. Unpaired t-test, ****P<0.0001 (n=3).

(C) Quantitative imaging analysis of ROS time course detected by CellROX® Reagent in young and old donor derived iAstrocytes. Fluorescence intensity was assessed

using Columbus Software. Results are expressed as means ± SD. Unpaired t-test between young and old iAstrocytes at each timepoint, **P<0.01, *P<0.05 (n=3).
(D) Representative images of western blot analysis of NRF2 and SOD1. Cells were incubated in serum-free media for 24h and harvested (UT=untreated, SF=Serum free media). Protein from young and old donor derived iAstrocytes was separated by sodium dodecyl sulfate-polyacrylamide gel electrophoresis followed by immunoblotting.
(E) Densitometric quantification of NRF2 protein levels, normalised to GAPDH. Values are expressed as means ± SD. Two-way ANOVA, ****P<0.0001, *P<0.05, **P<0.01 (n=3)
(F) Densitometric quantification of SOD1 protein levels, normalised to GAPDH. Values are expressed as means ± SD. Two-way ANOVA, *P<0.05 **P<0.01 (n=3).
(G) Representative images of yH2AX staining in young and old donor derived iAstrocytes, Scale bar (10μm).
(H) Quantitative imaging analysis of yH2AX Foci/cell in young vs old donor derived iAstrocytes. yH2AX foci were assessed using Columbus Software. Results are expressed as the means ± SD. Unpaired t-test, ****P<0.0001 (n=3).

Older donor-derived iAstrocytes are less supportive to MNs upon pro-inflammatory stress

So far, our results demonstrate that iAstrocytes derived from fibroblasts of donors from different age groups successfully recapitulate important transcriptional and functional age-related features. To probe the ageing astrocyte phenotype in more depth we wanted to assess one of the most important functions fulfilled by astrocytes *in vivo*, i.e. their ability to support neurons throughout the ageing process and under stressful conditions. In particular, recent studies have shown that, as astrocytes are exposed to microglia-secreted pro-inflammatory cytokines in the ageing brain (Liddelow *et al.*, 2017), they become less supportive to neurons. Therefore we tested the effect of IL-1β treatment, as this pro-inflammatory cytokine is released by microglia in the CNS during ageing (Clarke *et al.*, 2018) and after injury (Pineau and Lacroix, 2007).

To functionally test our cell model, both young and old donor-derived iAstrocytes were exposed to IL-1β for 6 hours, washed to remove any residual cytokine and were then co-cultured with human iPSC-derived motor neurons (Figures S3 and S4) to test their ability to support neurons when challenged with inflammatory stress.

Caspase-3, a master regulator of apoptosis, that catalyses the cleavage of many key cellular proteins, was used to assess neuronal health in co-culture. Immunostaining data showed that both young and old donor-derived iAstrocytes are equally able to support neuronal survival under basal conditions (Figures 6A and 6B). Treatment of iAstrocytes with IL-1β, however, led to a significant 3-fold increase of caspase-3 and apoptotic nuclear fragmentation in $MAP2^+$ cells cultured with old donor iAstrocytes (Figures 6A and 6B). In contrast, neurons cultured with young donor iAstrocytes did not show any difference between conditions, i.e. iAstrocytes untreated or pre-treated with IL-1β (Figures 6C and 6D). In order to understand the causes of this differential response, we assessed the effect of IL-1β treatment on iAstrocytes, with a particular focus on NFκB. NFκB is a transcription factor that regulates multiple aspects of innate and adaptive immune functions and represents a central mediator of inflammatory responses. Our results show that in IL-1β-stimulated old donor-derived iAstrocytes, nuclear activation of NFκB is four times higher than in young donor iAstrocytes (Figures 6D). Furthermore, old donor iAstrocytes become more reactive, displaying higher levels of GFAP and Vimentin, resulting in a significant increase in cell size (Figures 6 E-H).

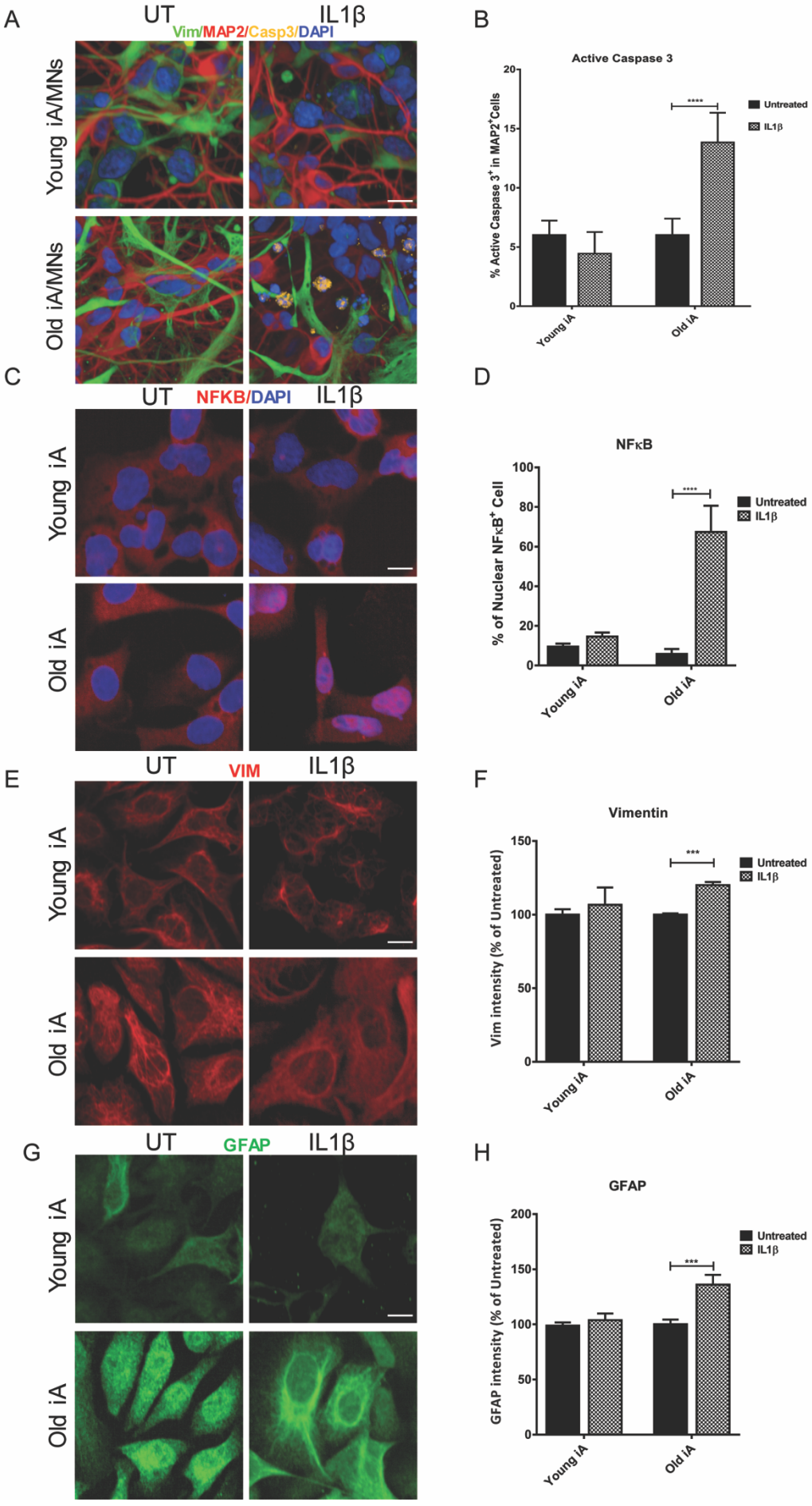
A
UT
IL1β
Vim/MAP2/Casp3/DAPI
Young iA/MNs
Old iA/MNs
B
Active Caspase 3
% Active Caspase 3+ in MAP2+Cells
Untreated
IL1β
Young iA
Old iA
C
UT
NFKB/DAPI
IL1β
Young iA
Old iA
D
NFκB
% of Nuclear NFκB+ Cell
E
UT
VIM
IL1β
F
Vimentin
Vim intensity (% of Untreated)
G
UT
GFAP
IL1β
H
GFAP
GFAP intensity (% of Untreated)

Figure 6. Old donor-derived iAstrocyte are less supportive to MNs after pro-inflammatory stress with IL-1β

(A) Representative images of human MN and young or old donor derived astrocytes co-culture. Scale bar (10μm).

(B) Quantitative imaging analysis of percentage of caspase-3 in MAP2+ cells. Results are expressed as the means ± SD. Two-way ANOVA, ****P<0.0001 (n=3).

(C) Representative images of NfκB staining in untreated and treated with IL-1β (20ng/mL) young and old donor derived iAstrocytes. Scale bar (10μm).

(D) Quantitative imaging analysis of NfκB nuclear activation. Results are expressed as the means ± SD. Two-way ANOVA, ****P<0.0001 (n=3).

(E) Representative images of Vimentin staining in untreated and treated with IL-1β (20ng/mL) young and old donor derived iAstrocytes. Scale bar (10μm).

(F) Quantitative imaging analysis of Vimentin intensity. Results are expressed as the means ± SD. Two-way ANOVA, ****P<0.001 (n=3).

(G) Representative images of GFAP staining in untreated and treated with IL-1β (20ng/mL) young and old donor derived iAstrocytes. Scale bar (10μm).

(H) Quantitative imaging analysis of GFAP intensity. Results are expressed as the means ± SD. Two-way ANOVA, ***P<0.001 (n=3).

Discussion

Astrocytes are the largest group of glial cells in the CNS and are responsible for vital homeostatic functions. Several studies have reported that glial cells are potentially more affected by the ageing process than neurons. In particular, astrocytes present dramatic transcriptional (Soreq *et al.*, 2017) and functional changes during ageing (Gemma *et al.*, 2007; Lynch *et al.*, 2010; Rea *et al.*, 2018) that hinder their ability to maintain homeostasis in the CNS and support neurons throughout their life-course.

Ageing is a leading risk factor for multiple neurodegenerative diseases, so it is fundamental to recapitulate age-related characteristics in cells that contribute to and are actively involved in diseases. It is well known that ageing and neurodegeneration share common mechanisms including increased oxidative stress, excitotoxicity and inflammation. Alzheimer's disease (AD), Parkinson's disease (PD) and amyotrophic lateral sclerosis (ALS) are three common adult-onset neurodegenerative diseases known to involve astrocyte dysfunction (Haidet-Phillips *et al.*, 2011; Meyer *et al.*, 2014; Booth, Hirst and Wade-Martins, 2017; González-Reyes *et al.*, 2017). As a consequence, lack of human *in vitro* models that mimic the functional features of astrocytes in young and old age is a limitation to studying mechanisms and potential therapies involved not only in maintaining brain health, but also in combatting neurodegenerative diseases and other neurological conditions.

In this study, we successfully derived iAstrocytes from young donors (5 months-3 years) and compared them to iAstrocytes derived from older donors (42 years-56 years). Comparative transcriptomic analysis demonstrated that the transcription profile of iAstrocytes from old donors recapitulates transcriptional features of laser-captured *post-mortem* (PM) astrocytes from adults of a similar age. Strikingly, the transcriptional differences between iAstrocytes from young and old donors display ~80% overlap with the differences discriminating between PM and fetal primary human astrocytes. This indicates that iAstrocytes derived from directly converted iNPCs retain astrocyte-relevant ageing transcriptomic features. When we specifically looked at the pathways described by these transcriptional changes, we identified multiple pathways involved in ageing and senescence, i.e. p53 signalling, oxidative stress, DNA damage and inflammatory response. Indeed, we confirmed these transcriptional changes at a functional level. We show here that direct conversion of fibroblasts to iNPCs and differentiation to iAstrocytes retains key age-related cellular characteristics. TERF2, an enzyme involved in telomere organization, decreases significantly with age in

fibroblasts and derived iAstrocytes recapitulate this decrease in expression level following reprogramming. Moreover, our model reproduces the global loss of the heterochromatin marker (H3K9me3) and nuclear organisation abnormalities reported in ageing and neurodegenerative conditions (Miller *et al.*, 2013; Tang *et al.*, 2017). Major Lamin A disruption occurs in Hutchinson-Gilford progeria syndrome (HGPS), as a consequence of mutations in the gene encoding for this protein, i.e. *LMNA*. HGPS is a rare genetic condition that leads to accelerated ageing and brain development abnormalities (Gonzalo, Kreienkamp and Askjaer, 2017), demonstrating the link between nuclear envelope integrity, ageing and neurodegeneration. At a cellular level, HGPS displays a number of characteristics typical of ageing cells including loss of heterochromatin, nuclear lobulation and increased DNA damage (Ghosh and Zhou, 2014). Expression of progerin, a truncated form of LMNA, is used to induce ageing in iPSC models (Miller *et al.*, 2013). Although this approach recapitulates some aspects of cellular ageing, it still carries the substantial limitation of introducing a pathogenic mutation to model a physiological process. In addition, this strategy might create confounding phenotypes when applied in the study of neurodegenerative conditions other than HGPS.

Without inserting any mutation, our data show that iAstrocytes derived from directly reprogrammed iNPCs from older individuals display decreased histone H3K9 trimethylation, accumulation of DNA damage and mild Lamin A/C disruption with associated loss of nuclear integrity, leading to nuclear “leakiness”. This phenotype has been reported in several ageing studies and is associated with loss of integrity of the nuclear pore complex (D’Angelo *et al.*, 2009; Lord *et al.*, 2015), thus favouring uncontrolled protein diffusion and loss of the normal compartmentalization between the nucleus and the cytoplasm.

In addition to this impairment, the present report reveals a significant decrease in three nucleocytoplasmic transporters, RANBP17, Importin 5 and Exportin 1, which play major roles in regulating nuclear import and export. Mertens et al (Mertens *et al.*, 2015) have previously reported that RANBP17 expression decreases in ageing cells and directly reprogrammed neurons from old donor fibroblasts, but not in iPSCs. Our data reveal that the age-related decrease in nucleocytoplasmic transport is bidirectional and is not limited to RANBP17. Nucleocytoplasmic transport has recently emerged as a key dysregulated pathway in neurodegenerative disorders. Several studies have shown how mutations in genes causing amyotrophic lateral sclerosis and

frontotemporal dementia (ALS/FTD) lead to aberrant nucleocytoplasmic partitioning of ALS-causing gene products and that this dysregulation includes both subcellular mis-localisation and cytoplasmic inclusions (Ferreira, 2019). For instance, it has been reported how mutations in *TARDBP* and *FUS* lead to accumulation of these proteins within the cytoplasm and mis-localisation from the nucleus, thus affecting nucleocytoplasmic transport (Neumann et al., 2006; Dormann et al., 2010; Mackenzie, Rademakers and Neumann, 2010). More recently, studies also revealed that the GGGGCC repeat expansion in C9orf72 compromises nucleocytoplasmic transport (Freibaum et al., 2015; Jovičić et al., 2015). Further evidence revealed that this pathway is also impaired in AD (Eftekharzadeh et al., 2018) and Huntington's disease (HD) (Gasset-Rosa et al., 2017; Grima et al., 2017). Specifically, exportin 1 (XPO1, also known as XPO1) has been identified as an important transporter for many proteins involved in neurodegenerative diseases (Chan et al., 2011a; Zhong et al., 2017; Ederle et al., 2018). XPO1 is an essential nuclear export receptor (Stade et al., 1997) which recognizes cargoes with the leucine-rich nuclear export sequence (NES) (Dong et al., 2009). Recently, a study in *C. elegans* showed that ALS-linked mutant SOD1, when misfolded, exposes a normally buried NES-like sequence, leading to XPO1-dependent nuclear export. This has been proposed as a potential protective mechanism against misfolded SOD1 proteotoxicity (Zhong et al., 2017), which, our data suggest, is likely to decrease with age, thus shifting the balance between accumulation of toxic proteins and neuroprotective cellular defences. A similar mechanism has also been reported for CAG repeat expansions associated with polyglutamine (polyQ) diseases, in which exportin 1 regulates the nucleocytoplasmic distribution of the expanded polyQ protein (Chan et al., 2011b). Decreased expression of XPO1 protein levels *in vivo* contributes to the accumulation of the expanded polyQ protein in the nucleus of symptomatic polyQ transgenic mice. This process drives the nuclear accumulation of the disease protein, thus the cell nucleus becomes an important site of pathology in polyQ diseases, where transcription is affected.

Additional stress that can significantly affect transcription, and also translation, is represented by accumulation of ROS that damage lipids, protein and nucleic acids, which are commonly detected as biochemical footprints in aged tissue (Brawek et al., 2010; Lukiw et al., 2012). Oxidative stress is caused by an imbalance in the redox state of the cell, by overproduction of ROS, or by impairment of the antioxidant defence system. In particular, the CNS is vulnerable to the effects of ROS due to its high

demand for oxygen, and its abundance of substrates highly susceptible to oxidative modification. Neurons are post-mitotic and have a very high energy demand, and thus are vulnerable to oxidative insults. Consistently, it has been shown that Nrf2 levels and activity are significantly higher in the longest-lived rodents compared to short-lived mice (Lewis et al., 2015). Surprisingly, however, neurons have weak endogenous antioxidant defences, as the main antioxidant pathways such as the Nrf2 pathway are silenced during development within neurons (Bell et al., 2015). Therefore, neurons rely heavily on non-cell autonomous antioxidant support from astrocytes. Antioxidant defences, however, have been shown to significantly decrease during ageing in astrocytes themselves, with consequent accumulation of ROS (Ishii et al., 2017). A recent study showed that Nrf2 overexpression in astrocytes protects against cerebral hypoperfusion, thus suggesting that Nrf2 overexpression specifically in astrocytes is protective, exerting beneficial effects through repression of inflammation (Sigfridsson *et al.*, 2018). In neurodegenerative diseases such as multiple sclerosis (MS), for example, astrocytes in active lesions display an increase of cytoplasmic accumulation of oxidized proteins and lipids (van Horssen et al., 2008) and nuclear accumulation of oxidized DNA (Haider et al., 2011). As the antioxidant defences of astrocytes decrease with age, they are unable to provide optimal support to neighbouring neurons, which start accumulating oxidative DNA damage, thus leading to an increased susceptibility to a number of age-related diseases and cognitive decline (Oksanen et al., 2019). Because of its crucial role in ageing and neurodegeneration, it is important that human *in vitro* models of astrocytes can recapitulate this age-dependent functional decline.

Strikingly, in the present report, we found that old iAstrocytes exhibited a higher baseline level of ROS and DNA damage compared to young iAstrocytes. Furthermore, when iAstrocytes were stressed by serum starvation, old iAstrocytes required more time to recover to baseline ROS levels, as the levels of both NRF2 and SOD1 were lower in old iAstrocytes compared to young iAstrocytes, both at baseline and following acute stress. Thus, our model recapitulates the age-related decrease in antioxidant defences reported from *in vivo* studies and, provides an explanation for the increased level of ROS seen in these cells.

It is well known that oxidative stress plays a central role in the pathophysiology of neurodegenerative diseases, such as ALS, AD, HD and PD (J. Li *et al.*, 2013; Niedzielska *et al.*, 2016) where the antioxidant response has been proposed as a potential therapeutic target (Barber, Mead and Shaw, 2006). Oxidative stress may

provoke cellular damage, dysregulation of DNA damage repair and mitochondrial dysfunction, all hallmarks of the ageing process as well as neurodegenerative disorders (Shibata and Kobayashi, 2008; Allen *et al.*, 2019).

Toxicity from free radicals also contributes to inflammation, another major component in neurodegeneration. In our study, we showed the age-related differential responses of iAstrocytes in their ability to support neurons in co-culture upon acute stimulation with the inflammatory cytokine interleukin-1 beta (IL-1β). Our data suggest that this is due to an exaggerated response of old donor-derived iAstrocytes to IL-1β stimulation, resulting in stronger nuclear activation of NFκB and higher levels of expression of GFAP and Vimentin. Although already at baseline old and young iAstrocytes differ in the activation of several stress defence mechanisms, we did not detect a significant difference in their ability to support neuronal survival, measured as caspase 3 activation. Other more subtle parameters, however, could be compromised in neurons cultured with older non stimulated astrocytes. Recent studies in *post-mortem* brains and *C. elegans*, in fact, have reported that dendrite restructuring, neuronal sprouting, and synaptic deteriorations are subtle changes commonly detected in physiological brain ageing, rather than neurodegeneration (Henstridge *et al.*, 2015; Hess *et al.*, 2019)

GFAP and vimentin are classical astrocytic markers that increase in expression as astrocytes become more reactive with age (Wu, Zhang and Yew, 2005; Boisvert *et al.*, 2018; Clarke *et al.*, 2018). Moreover, increased astrocyte reactivity has been reported in several neurodegenerative disorders. For example, studies in AD brain samples and mouse models detected amyloid plaques surrounded by reactive astrocytes, with higher expression of GFAP (Li *et al.*, 2011). Interestingly, the increased number of reactive astrocytes frequently correlates with the extent of cognitive decline (Kashon *et al.*, 2004). In patients with PD, astrocyte reactivity has been seen in the substantia nigra pars compacta (Hirsch and Hunot, 2009), whilst in ALS patients, it has been observed in susceptible regions and the degree of reactivity correlates with the severity of neurodegeneration (Haim *et al.*, 2015).

In conclusion, the present study demonstrates that direct conversion of fibroblasts to iNPCs and subsequent differentiation into iAstrocytes results in an *in vitro* model able to retain key hallmarks of the ageing process. Although not investigated in this study, it is likely that the iNPCs themselves and all cells derived from them would preserve ageing features through this reprogramming methodology, bypassing the epigenetic

landscape toward the pluripotent state of the IPSCs. This is of extreme importance, as this *in vitro* tool allows for more accurate and physiologically relevant modelling of ageing and disease, without the need to introduce age-inducing genetic mutations or insults.

In particular, the ability to model the behaviour of human astrocytes throughout the process of ageing as well as the cross-talk with age-matched neurons has the unique and unprecedented potential to answer important questions about the physiology and the pathophysiology of the CNS and to provide a powerful tool for novel therapeutic approaches for age-related neurodegenerative and neurological disorders.

Experimental procedures

Cell Culture

Human skin fibroblast samples were obtained from different sources (Table S1). Prof. Pamela Shaw (PJS) and Dr Daniel Blackburn (DB) provided the fibroblast samples from the University of Sheffield (Study number STH16573, Research Committee reference 12/YH/0330 and MODEL-AD research study number STH19080 Research and Ethics Committee number: 16/YH/0155 respectively). Human skin fibroblast samples from donors below the age of consent were from established tissue banks (Coriell Institute) as shown in Table S1. Informed consent was obtained from all subjects before sample collection.

The human induced pluripotent stem cells (iPSC) line used in this study named control MIFF1 (Desmarais JA et al., 2016) was kindly provided by Professor Peter Andrews and Dr. Ivana Barbaric (Centre for Stem Cell Biology, The University of Sheffield). iPSCs were maintained in complete mTeSR™-Plus™ Medium (StemCell Technologies) in Matrigel® growth factor reduced-coated plates (Corning®) according to the manufacturer's recommendations. Cultures were replenished with fresh medium every alternate day. The passage of cells was performed when the cells reached around 70% of confluence, every four to six days as clumps using ReLeSR™ an enzyme-free reagent for dissociation (StemCell Technologies) according to the manufacturer's recommendations. For all the experiments in this study, iPSCs were used between passage 20 and 28, all iPSCs were cultured in 5% O_2, 5% CO_2 at 37°C.

Direct Reprogramming of Skin Fibroblasts to iNPCs

Direct conversion was conducted with a modified version of the protocol described previously in Meyer et al., 2014. Fibroblasts were seeded in a well of a six-well plate and treated with retroviral vectors for *OCT3, SOX2*, *KLF4* and *c-MYC* (Meyer *et al.*, 2014). The medium was switched to NPC conversion medium, consisting of DMEM/F12, 1% N2, 1% B27, EGF (40ng/ml) and FGF (20 ng/mL). After 2-4 days the cells changed shape and created sphere-like structures or started growing into rosettes. These were collected or lifted using Accutase (StemPro® Accutase® Cell Dissociation Reagent, Gibco) and, depending on the density and their growth rate, they were expanded in multiple wells of a six-well plate or a 10cm dish coated with

human fibronectin (5 µg/mL; Millipore). Cells were then stained for Nestin and PAX6 to establish successful iNPC conversion.

Differentiation of iNPCs into iAstrocytes

To induce astrocyte differentiation, the iNPCs were plated in medium composed of DMEM, 10% fetal bovine serum (FBS) (Life Science Production), 1% penicillin-streptomycin (Lonza Biowhittaker), 0.2% N2-supplement (Gibco Life Tech) in a 10cm dish coated with human fibronectin (Millipore). Astrocytes were allowed to differentiate for 7 days.

Differentiation of iPSCs into motor neurons (MNs)

Motor neuron differentiation (Figure S3) of iPSCs was performed using the modified version dual SMAD inhibition protocol (Du *et al.*, 2015). To induce differentiation, iPSCs were transferred for matrigel-coated plate (Corning® Matrigel® Growth Factor Reduced). On the day after plating (day 1), after the cells had reached ~100% confluence, the cells were washed once with PBS and then the medium was replaced with neural medium (50% of KnockOut™ DMEM/F-12, 50 % of Neurobasal (ThermoFisher), 0.5× N2 supplement (ThermoFisher), 1x Gibco® GlutaMAX™ Supplement (ThermoFisher), 0.5x B-27 (ThermoFisher), 50 U ml^{-1} penicillin and 50 mg ml^{-1} streptomycin, supplemented with DMH-1 2 µM (Tocris), SB431542-10 µM (Tocris) and CHIR99021 3 µM (CHIR, Tocris). The medium was changed every day for 6 days. On day 7, the medium was replaced with neural medium supplemented with SB431542-10 µM, and CHIR 1 µM, DMH-1 2 µM, all-trans retinoic acid 0.1 µM (RA, StemCell Technologies), and purmorphamine 0.5 µM (PMN, Tocris). The medium was changed every day until day 12 when was possible to see a uniform neuroepithelial sheet. On day 12 the cells were split 1:6 with accutase (StemPro® Accutase® Cell Dissociation Reagent, Gibco), onto a matrigel-coated plate in the presence of 10 µM of rock inhibitor (Y-27632 dihydrochloride, Tocris), giving rise to a sheet of neural progenitor cells (NPC). After 24 hours of incubation, the medium was changed for neural medium supplemented with RA 0.5 µM and PMN 0.1 µM. The medium was changed every day until day 19 when the motor neuron progenitors (MNP) can be visualized. On day 20 MNP were split with accutase onto to matrigel-coated plates and the medium was replaced with neural medium supplemented with compound E 0.1 µM (Cpd E, Tocris), retinoic acid 0.5 µM, PMN

0.1 µM, BDNF 10ng/mL (ThermoFisher), CNTF 10ng/mL (ThermoFisher) and IGF 10ng/mL (ThermoFisher) - (this medium is named as neuronal medium). At this stage the cells were fed every other day with neuronal medium until day 40.

Co-culture of iAstrocytes and MNs

Motor neuron progenitors were plated onto matrigel-coated 96 well plates in the presence of 10 µM of rock inhibitor ($1x10^4$ cell/well) on day 20 of differentiation. The MNPs were differentiated into MN until day 40 when the astrocytes ($0.8x10^4$ cell/well) were added on the top of the motor neurons. The co-cultures were cultured for three days, and then the cells were fixed and processed for immunofluorescence staining (Figure S4).

Microarray analysis

Microarray analysis of human fetal astrocytes (purchased from Sciencell), *post-mortem* (PM) astrocytes laser-captured from brain and iAstrocytes reprogrammed from fibroblast donors was performed at SITraN, University of Sheffield (Table S2). Fetal astrocytes were run on GeneChip™ Human Gene 2.0 ST Array; while *post-mortem* astrocytes and iAstrocytes were run on GeneChip™ Human Genome U133 Plus 2.0 Array. All the included studies obtained relevant ethical approval. The quality of array data CEL files was assessed using the Affymetrix Expression Console software. Normalisation, with all the transcripts normalised by beta-tubulin and GAPDH, and harmonisation across Chip files was obtained using the Robust Multi-Array (RMA) algorithm. Differential gene expression between samples was determined using Qlucore Omics Explorer after normalisation. The software was used also for Principal Component Analysis (PCA) and hierarchical clustering. To access the functions of genes found in the meta-analysis, the Database for Annotation, Visualization and Integrated Discovery (DAVID, https://david.ncifcrf.gov/) and Panther (http://www.pantherdb.org/). The website Human Genomic Resources (HAGR, http://genomics.senescence.info/) was used to identify ageing-related genes.

RNA Isolation and quantitative real-time polymerase chain reaction (qPCR)

RNA was harvested using the RNAeasy Mini kit (Qiagen), and total RNA was reverse-transcribed with the High Capacity cDNA Reverse Kit (Applied Biosystem) according to the manufacturer's instructions.

Primers were designed using Primer-BLAST to assess transcriptional changes in a number of selected genes reported by microarray analysis identified through HAGR and validated ageing markers (Table S4). Samples were loaded at a concentration of 12.5 ng/µl per well. qPCR was performed using 2x SYBR Green/Rox PCR Master Mix (Bimake.com) and forward and reverse primers (final concentration 250nM), to a total volume of 20µL. After initial denaturation at 95°C for 10 minutes, templates were amplified by 40 cycles at 95°C for 15 seconds and 60°C for 1 minute, using the Stratagene MX300P machine. At the end, a dissociation curve was created to ensure amplification of a single product and the absence of primer dimers.

GAPDH was tested against other housekeeping genes, including B-actin, RLP13A and U1. GAPDH showed the most consistent and stable expression across samples of different ages as well as between fibroblasts and astrocytes. Hence, GAPDH was amplified on each plate to normalize expression levels of target genes between different samples using the ΔΔCt calculation (ABI) and to assess assay reproducibility.

iAstrocyte treatment for stress response assessment and cell collection

Serum starvation experiments were carried out by washing the cells with PBS twice and changing the culture medium to fresh media without FBS at day 6.

On day 7 iAstrocytes were washed twice with PBS to remove medium residuals and harvested by cell scraping. The cell pellets were stored at -80°C until processed for RNA or protein extraction.

IL-1β treatment to induce inflammation in iAstrocytes and CC

Astrocyte activation was stimulated by the addition of fresh medium containing IL-1β (20 ng/ml, R&D Systems) and incubated for 20 minutes for evaluation of NF-κB translocation, for 24 and 72 hours and for reactive gliosis.

For the co-culture experiments, young and old astrocytes were stimulated with IL-1β (20 ng/ml), for 6 hours and then gently washed X 3 with warm PBS to fully eliminate residual IL-1β in the culture. After that the astrocytes were seeded on the top of the MNs in the presence of neuronal medium. The co-cultures were maintained at 37°C

in a humidified atmosphere with 5% CO2 for 3 days when the analyses of cell death were performed. Young and old untreated astrocytes were used as controls.

Immunocytochemistry (ICC) iAstrocytes

10,000 iAstrocytes were plated per well in 96-well plates at day 6 of differentiation and fixed 24h after seeding with 4% paraformaldehyde (PFA) for 10 min. Cells were washed 3 times with phosphate-buffered saline (PBS) following which blocking (PBS,5% horse serum and 0.05% Triton X-100) was applied for 1 hour. All primary antibodies were diluted in blocking solution and their dilution and suppliers are listed in Table S5. Incubation of the primary antibody was performed overnight at 4°C. The next day, cells were washed 3 times in PBS before the secondary antibody (Table S6) in blocking solution was applied for 1 h at room temperature. Hoechst (Hoechst 33342, Trihydrochloride, Trihydrate, Life tech) diluted 1:6,000 was added for 5 minutes to visualise the nucleus. Cells were then washed twice with PBS and imaged using the Opera Phenix high-content imager (PerkinElmer).

Immunocytochemistry (ICC) MNs and CC

For immunostaining, after three days of co-culture (CC), cells were washed with PBS and fixed with 4% paraformaldehyde for 15 min at room temperature. After fixation samples were washed three times with PBS, incubated with 0.3% Triton X-100 in PBS (Sigma) for 5 min then blocked by incubation with PBS containing 5% donkey serum (DS) (Millipore) for 1 hour. After blocking, cell cultures were incubated with primary antibodies diluted in PBS containing 1% of DS overnight. Cells were washed with PBS three times. Then, secondary antibodies were added to cells and incubated for 1 hour. The samples were washed with PBS three more times and incubated with 1.0 mg/mL 4,6-diamidino-2-phenylindole (DAPI) for nuclear staining. The primary and secondary antibodies were used at the dilutions indicated in tables S5 and S6. All experiments included cultures where the primary antibodies were not added, and non-specific staining was not observed in these negative controls.

Oxidative-stress assay

7,000 iAstrocytes were plated per well in 96-well plates at day 5 of differentiation in complete astrocyte medium. On day 6, medium was replaced either with complete or with serum-free astrocyte medium for 12 hours. After 12h, medium was replaced in all

conditions with complete astrocyte medium and CellROX baseline measurements were collected, using the Opera Phenix Imaging System. A time-course experiment was also performed, in which CellROX measurements were collected every 2 hours for 6 hours. CellROX® Reagent (Life Technologies) was used at a final concentration of 2.5 μM as per manufacturer's instructions and incubated with cells for 30 minutes at 37°C. CellROX® Reagent was then removed, cells were washed three times with PBS before imaging.

Nuclear isolation and dextran influx assay

Two 10cm dishes of iAstrocytes (2 million cells) were used for isolation of nuclei. After two washes with PBS, accutase was added and the plates were incubated at 37°C for 3 minutes. Accutase was diluted with 3ml PBS and the cells were collected in a tube and spun at 1,000rpm for 4 minutes. The pellet was washed twice with PBS and then left to dry. 400μL of hypotonic lysis buffer (10mM HEPES, 1.5mM MgCl2, 10mM KCl, 0.5mM DTT, 20μL/mL PIC) was added to the pellet. The lysate was passed through a 19g needle 5 times, left for 10 minutes on ice and then spun down at 4,000rpm for 3 minutes at 4°C to separate the nuclear from the cytoplasmic fraction. The supernatant was discarded (cytoplasmic fraction), while 250μL of IP lysis buffer (150mM NaCl, 50mM HEPES, 1mM EDTA, 1mM DTT, 0.5% (v/v) Triton™ X-100, 20μL/mL PIC, pH 8.0) with 60μL of PMSF (phenylmethanesulfanyl) was added to the nuclear pellet. The lysate was passed through a 25g needle 5 times and then left for 30 minutes on ice. It was spun at 13,300rpm for 4 minutes at 4°C and the supernatant was kept as the nuclear fraction. Nuclei were stained with Hoechst (Hoechst 33342, Trihydrochloride, Trihydrate, Life tech) diluted 1:6,000 in PBS. Tetramethylrhodamine isothiocyanate-dextran was added to the nuclear fraction. The nuclei were mounted with ProLong™ Gold Antifade Mountant (Invitrogen) on cover slips and imaged with the confocal microscope Leica TCS SP5 II.

Western Blot (WB) Analysis

iAstrocyte samples were lysed using lysis buffer (150mM NaCl, 50mM HEPES, 1mM EDTA, 1mM DTT, 0.5% (v/v) Triton™ X-100, PIC, pH 8.0). Samples were then centrifuged at 13,300 rpm for 5 min at 4°C and the supernatant was collected. Lysates were subjected to sodium dodecyl sulfate-polyacrylamide gel electrophoresis (SDS-

PAGE) on 12% polyacrylamide gels. Resolved proteins were transferred to nitrocellulose membranes and processed for immunoblot analysis.
Membranes were blocked for 1 hour in 5% milk/tris-buffered saline and tween 20 (TBS-T). Primary antibodies (Table S5) were diluted in 5% milk/TBS-T and incubated with the membrane overnight at 4°C. After primary antibody incubation, the membrane was washed for 3 × 5 minutes each in TBS-T buffer. Secondary horseradish peroxidase (HRP) antibodies (Table S6) were diluted in 5% milk/TBS-T and incubated with the membrane for 1 hour at room temperature. After secondary antibody incubation, the membrane was washed for 3 × 5 minutes each in TBS-T buffer. Protein bands were visualized using EZ-ECL reagent (Geneflow) and the G-Box imaging system (Syngene). Densitometric analysis of protein bands was carried out using GeneTools Software (Syngene).

Image and statistical analysis

Columbus Software was used in the image analysis setting to measure different parameters including nuclei numbers, nuclear size (μm^2) (mean per well), CellROX intensity/Cell area, Lamin A/C distribution and H3K9me3 intensity.
To investigate whether IL-1β interferes with the translocation of NF-κB, young and old astrocytes were stained for NF-κB, untreated cells were used as a control for each line. Reactive gliosis was determined by GFAP and Vim staining intensity, which was quantified using Harmony software (Perkin Elmer). After the treatment the cells were fixed and stained for NF-κB and vimentin was used as a marker that define the boundary of cells and DAPI for nuclear staining. Quantitative image analysis of the astrocytes was conducted through the Opera Phenix™ High Content Screening System at 40× magnification using the Columbus™ Image analysis system. The following morphological features were assessed for both treated and control astrocytes: cell area and the intensity of GFAP and vimentin staining per cell. At least 20 fields were randomly selected and scanned per well of a 96-well plate in triplicate. To identify and remove any false readings generated by the system, three random treated and untreated wells were selected and counted manually (blind to group).

All experiments were performed at least in triplicate with a minimum of 3 technical repeats in each independent experiment. Data were analysed using GraphPad Prism

Software (V7.02): one-way ANOVA with Tukey's multiple comparisons post-test or, two-way ANOVA with Tukey's multiple comparisons post-test. Two-tailed *t*-test was used to compare old donor samples to the young donor samples for qPCR and western blot.

ACKNOWLEDGEMENTS We express grateful thanks to the individuals who donated biosamples for research.

This study was supported by the NIHR Sheffield Biomedical Research Centre. NG is supported by the Moody Fund Scholarship; SMB is supported by a Wellcome 4ward North Academy Clinical Training Fellowship (216340/Z/19/Z), and ARUK Yorkshire Network Centre Small Grant (Ref: ARUK-PCRF2016A-1). KM is supported by the MDA Investigator award, HM is a Parkinson's UK Senior Research Fellow (Ref: F-1301); GMH is supported by the Medical Research Council (MRC) New Investigator research grant MR/R024162/1 and Biotechnology and Biological Sciences Research Council (BBSRC) grant BB/S005277/1. MA acknowledges grants from Alzheimer's Research UK (ARUK-PG2018B-005), European Research Council (ERC Advanced Award 294745) and MRC DPFS (129016). PJS is supported as an NIHR Senior Investigator (Ref: NF-SI-0617-10077), by the MND Association (AMBROSIA Ref: MNDA 972-797) and by the Medical Research Council (COEN award Ref: MR/S004920/1). LF acknowledges grants from the Academy of Medical Sciences (Ref: SBF002/1142), MND Association (Ref: Apr16/848-7910) and Parkinson's UK (Ref: K-1506)

DECLARATION OF INTEREST: The authors declare no competing interests

AUTHOR CONTRIBUTION

Conceptualisation LF; Methodology LF, NG, CDS, EK; Validation AS, SMB; Investigation NG, CDS, SMB, AS, MAM, SP, LC, NMM; Resources LF and PJS; Data curation LF, NG, PRH; Writing Original draft NG, NMM, LF; Writing Review and editing NG, KM, HM, MA, GMH, NMM, PJS and LF; Supervision LF and PJS; Funding acquisition LF and PJS.

Supplementary material

Table S1. *Summary of the information on the astrocytes and fibroblast lines used in this study*

ID	Cell line	Age	Gender	Biobank
Young 1(Y1)	GM08680	5 months	Male	Coriell
Young 2 (Y2)	GM00498	3 years	Male	Coriell
Young 3 (Y3)	GM03813	3 years	Male	Coriell
Old 1 (O1)	MAD14	56 years	Male	Blackburn
Old 2 (O2)	3050	55 years	Male	Shaw
Old 3 (O3)	155	42 years	Male	Shaw

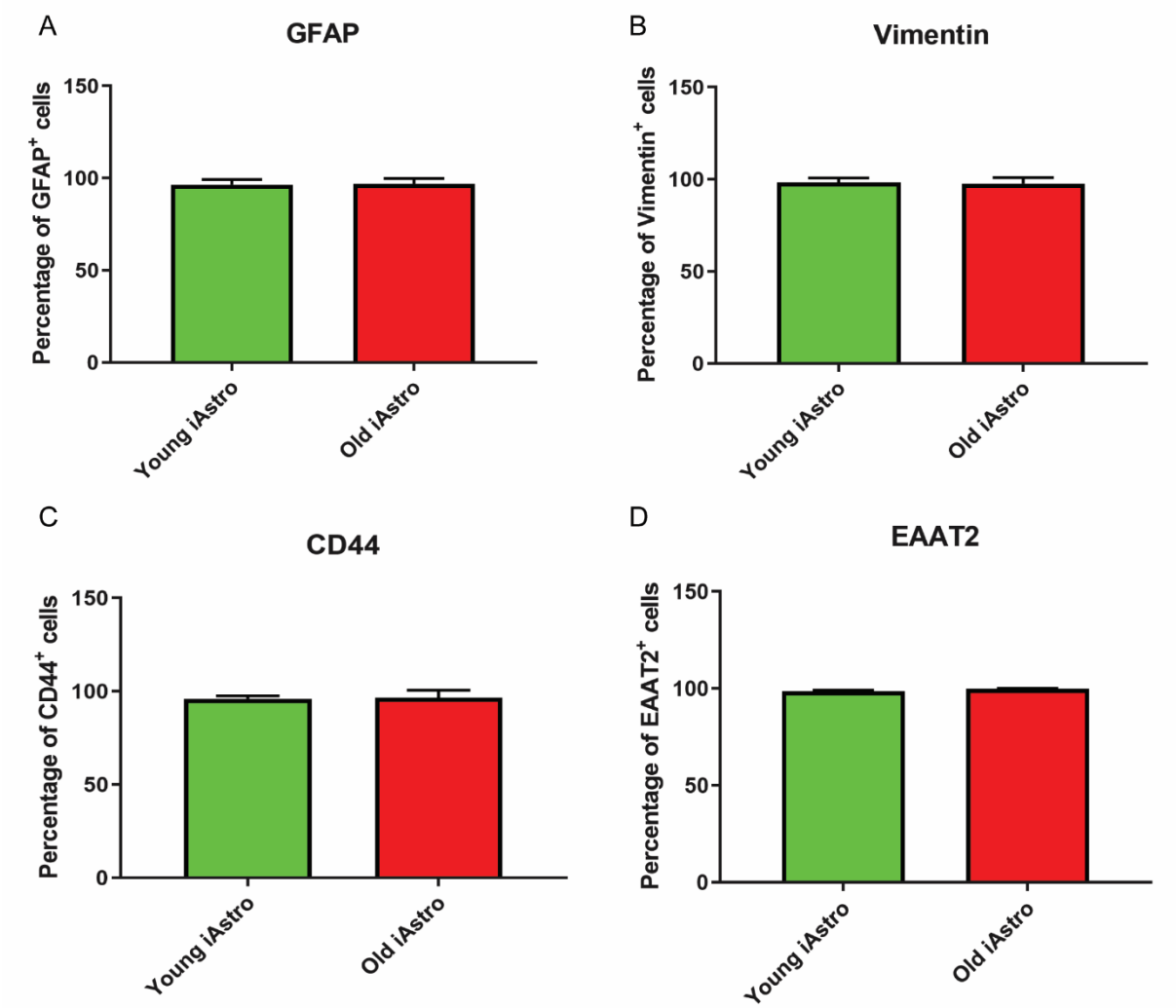

Figure S1 related to Figure 1 Characterization of iAstrocytes from old versus young donors

(A) Quantitative imaging analysis of astrocytic markers (GFAP, Vimentin (VIM), CD44 and EAAT2) in young and old donor derived iAstrocytes (n=3).

Table S2. *Summary of the information on microarray data used in this study*

ID	**Origin**	**Age**	**Gender**	**GEO accession number**
Fetal_1	Sciencell	-	M/F	pending
Fetal_2	Sciencell	-	M/F	pending
Fetal_3	Sciencell	-	M/F	pending
PM_1	Laser-captured from brain	72 years	F	GSE83670
PM_2	Laser-captured from brain	75 years	M	GSE83670
PM_3	Laser-captured from brain	78 years	F	GSE83670
PM_4	Laser-captured from brain	78 years	F	GSE83670
Old iA_1	Direct reprogramming from skin fibroblasts	55 years	F	GSE87385
Old iA_2	Direct reprogramming from skin fibroblasts	69 years	F	GSE87385
Old iA_3	Direct reprogramming from skin fibroblasts	47 years	M	GSE87385
Young iA_1	Direct reprogramming from skin fibroblasts	3 years	F	pending
Young iA_2	Direct reprogramming from skin fibroblasts	8 years	F	pending
Young iA_3	Direct reprogramming from skin fibroblasts	5 months	M	pending

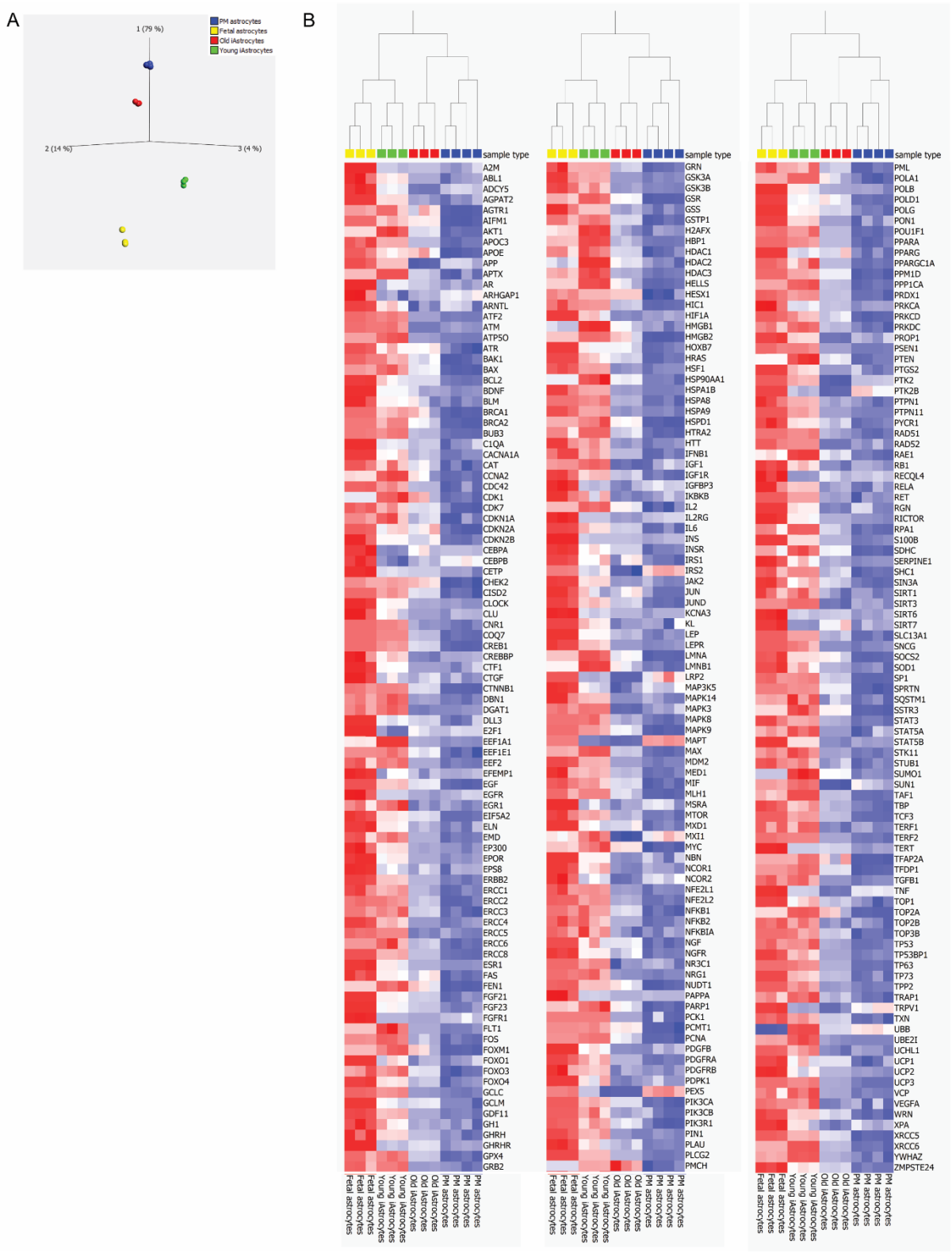

Figure S2 related to Figure 2 Old donor iAstrocytes and *post-mortem* (PM) astrocytes have distinctly different transcriptomes to fetal astrocytes and young donor iAstrocytes.

(A) Principal component analysis (PCA) plot of fetal astrocytes, PM astrocytes and old and young donor derived iAstrocytes. Multi-group comparison, p≤1x10e-4.

(B) Hierarchical cluster heat-map of fetal astrocytes, PM astrocytes and old and young donor iAstrocytes. Multi-group comparison, p≤1x10e-4.

Table S3 *Related to Figure 2 Genes in the intersection between the two comparisons (csv excel file Table S1 intersection)*

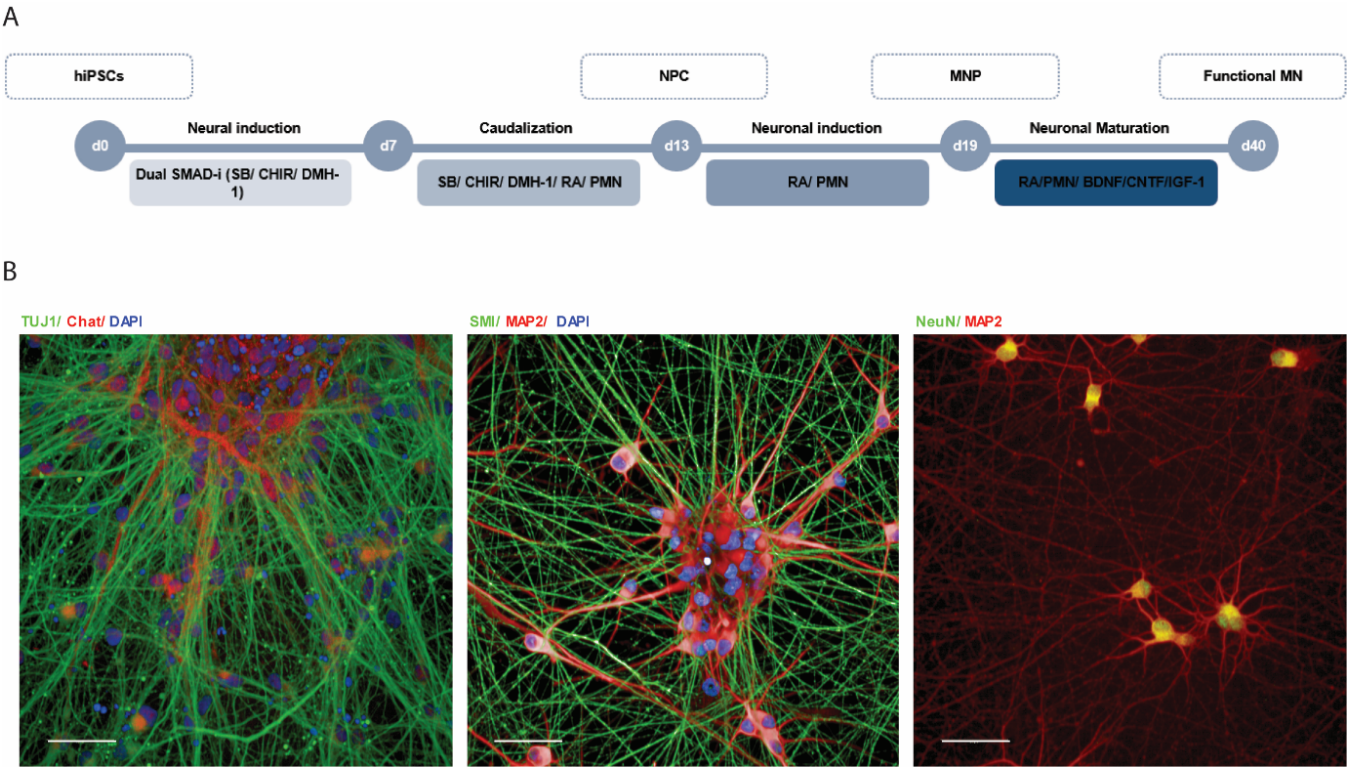

Figure S3. MN differentiation.

(A) Schematic illustration of the differentiation protocol for human MN derived from hiPSCs.

(B) Representative images of characterisation of MN with cell-specific markers Tuj1, Chat, SMI32, MAP2 and NeuN.

A

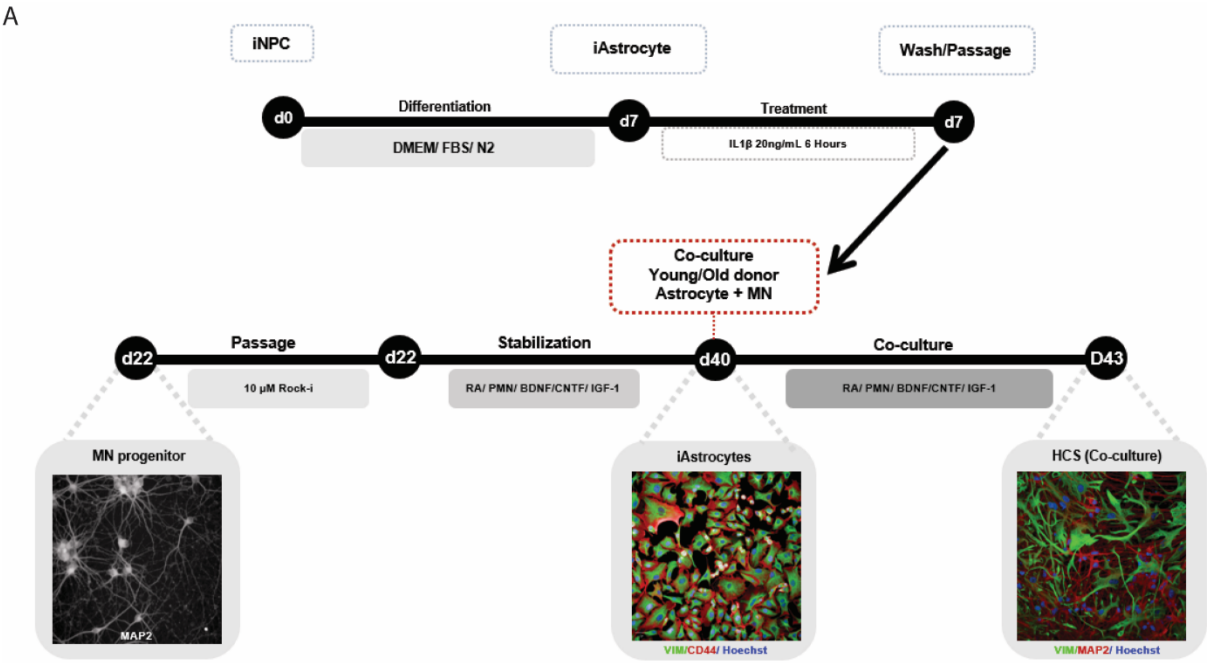

Figure S4 Human co-culture system workflow.

(A) Schematic illustration of the co-culture representing the differentiation of human astrocytes derived from iNPCs from young and old donors. After the differentiation, astrocytes were exposed to human IL-1β (20ng/mL) for 6 hours. After this treatment, the cells were washed and then seeded on to MNs. MN progenitors were seeded and on day 40 astrocytes were added on the MNs. The co-culture was kept for 72 hours.

***Table S4**. Primer sequences used for qPCR, Forward (Fw) and Reverse (Rv)*

Primer	**Sequence (5'-3')**
B-Actin_Fw	TCCCCCAACTTGAGATGTATGAAG
B-Actin_Rv	AACTGGTCTCAAGTCAGTGTACAGG
RLP13A_Fw	CAAGCGGATGAACACCAACC
RLP13A_Rv	TTTTGTGGGGCAGCATACCT
U1_Fw	CCATGATCACGAAGGTGGTT
U1_Rv	ATGCAGTCGAGTTTCCCACA
GAPDH_Fw	CAACTTTGGTATCGTGGAAGGAC
GAPDH_Rv	ACAGTCTTCTGGATGGCAGTG
TERF2_Fw	TTATTCGAGAAAAGAACTTGGCCC
TERF2_Rv	TGAGGAGGTAGGGCTCGG
RANBP17_Fw	CACTTCGATGCAGAGAGGCTA
RANBP17_Rv	CACTGGTTCCGACAGTCTTC
LAMA3_Fw	TGTTTAAACTGCAGCCTCCCA
LAMA3_Rv	ACACATTTCAAGTTCCCGGC

***Table S5** Primary antibodies used in this study*

Primary Antibody	**Source**	**Species**	**Assay (WB or ICC)**	**Dilution used**
GAPDH	Cell Signalling	Rabbit	WB	1:2,000
NRF2	Abcam	Rabbit	WB	1:1,000
SOD1	Cell Signalling	Rabbit	WB	1:1,000
XPO1	Abcam	Rabbit	WB	1:2,000
RANBP17	Abcam	Rabbit	WB	1:2,000
VIMENTIN	Millipore	Chicken	ICC	1:1,000
GFAP	Dako	Rabbit	ICC	1:1,000
CD44	Abcam	Rabbit	ICC	1:200
EAAT2	SantaCruz	Goat	ICC	1:100
Histone H3 (tri methyl K9)	Abcam	Rabbit	ICC	1:800

Lamin A/C	Abcam	Mouse	ICC	1:800
Nestin	Abcam	Mouse	ICC	1:200
Nestin	Biolegend	Rabbit	ICC	1:500
PAX6	Abcam	Rabbit	ICC	1:1,000
PAX6	Millipore	Mouse	ICC	1:200
Beta III Tubulin	Millipore	Chicken	ICC	1:1,000
Beta III Tubulin	Biolegend	Mouse	ICC	1:1,000
NeuN	Biolegend	Mouse	ICC	1:1,000
CHAT	Millipore	Goat	ICC	1:100
SMI32	Biolegend	Mouse	ICC	1:500
MAP2	*Synaptic systems*	*Guinea pig*	ICC	1:1,000
Caspase 3	*Millipore*	*Rabbit*	ICC	*1:200*
γH2AX clone JBW301	*Millipore*	*Mouse*	ICC	*1:500*

***Table S6**. Secondary antibodies used in this study*

Secondary antibody	Source	Assay	Dilution used
Alexa Fluor 488 donkey α-mouse IgG(H+L)	Invitrogen,ThermoFisher	ICC	1:400
Alexa Fluor 488 donkey α-rabbit IgG(H+L)	Invitrogen,ThermoFisher	ICC	1:400
Alexa Fluor 488 goat α-chicken IgG(H+L)	Invitrogen,ThermoFisher	ICC	1:1,000
Alexa Fluor 488 goat α-rabbit IgG(H+L)	Invitrogen,ThermoFisher	ICC	1:1,000
Alexa Fluor 555 donkey α-goat IgG(H+L)	Invitrogen,ThermoFisher	ICC	1:400/1000
Alexa Fluor 568 donkey α-mouse IgG(H+L)	Invitrogen,ThermoFisher	ICC	1:400/1000
Alexa Fluor 568 donkey α-rabbit IgG(H+L)	Invitrogen,ThermoFisher	ICC	1:400

Alexa Fluor 586 goat α-rabbit IgG(H+L)	Invitrogen,ThermoFisher	ICC	1:1,000
Alexa Fluor 594 donkey α-mouse IgG(H+L)	Invitrogen,ThermoFisher	ICC	1:400
Alexa Fluor 647 goat α-guinea pig IgG(H+L)	Invitrogen,ThermoFisher	ICC	1:400
α-Rabbit IgG (H+L), HRP Conjugate	Promega	WB	1:5,000
α-mouse IgG (H+L), HRP Conjugate	Promega	WB	1:5,000
α-chicken IgGY (H+L), HRP Conjugate	Invitrogen,ThermoFisher	WB	1:5,000

4. Results

SOD1 aberrantly accumulates in the nucleus due to altered interaction with nucleocytoplasmic transporters in ALS derived astrocytes

4.1 Introduction

In chapter 3, I showed that directly induced astrocytes retain functional age-related features, such as altered nuclear compartmentalization, nucleocytoplasmic shuttling properties, oxidative stress response and DNA damage response. Remarkably, nucleocytoplasmic transport emerged as a pathway commonly altered in ALS with subsequent protein mis-localisation and aggregation.

Nucleocytoplasmic defects have been brought to light and explored with interest due to the identification of mutations in *TARDBP* and C9orf72, where aberrant transport of proteins and RNA between nucleus and cytoplasm seem to play a pivotal role in disease pathophysiology.

The presence of TDP-43 proteinopathy in >97% of ALS cases is one of the strongest indications of the central role played by nucleocytoplasmic dysregulation in the disease. Beyond the disruption in RNA processing caused by TDP-43 nuclear loss and cytoplasmic aggregation described in section 1.1.2.6., recent elegant studies have highlighted how TDP-43 pathology can disrupt nuclear pore complexes and nucleocytoplasmic transport. Using a proximity-dependent biotin identification system termed BioID, Chou and colleagues interrogated the interactome of detergent-insoluble cytoplasmic TDP-43 aggregates, identifying components of the nuclear pore complex (NuPC) and nucleocytoplasmic transport machinery as a major group of proteins present in pathological TDP-43 aggregates (Chou et al., 2018). Interestingly, in this study, aggregated and disease-linked mutant TDP-43 caused the sequestration and/or mis-localisation of nucleoporins and transport factors and impaired the nuclear membrane and NuPC, affecting nuclear protein import and RNA export in mouse primary cortical neurons, human fibroblasts and iPSC–derived neurons (Chou et al., 2018). Next, it has been demonstrated how transient stress induces long-lasting separation of cytoplasmic TDP-43 in multiple cell types. Remarkably, the phase-separated TDP-43 compromises nuclear transport by de-mixing importin-α and Nup62 and inducing mis-localisation of RanGap1, Ran, and Nup107, and leads to clearance of nuclear TDP-43 and eventually, cell death (Gasset-Rosa *et al.*, 2019). These findings indicate that TDP-43-mediated nucleocytoplasmic transport disruption is a common disease mechanism.

Similarly, C9orf72 repeat expansions as well as mutant PFN1 are also able to affect the nuclear pore (Giampetruzzi *et al.*, 2019). In 2015 a *Drosophila* transgenic fly, able

to express 8, 28 or 58 G4C2 repeat-containing transcripts that do not have a translation start site (AUG) but contain an open-reading frame for green fluorescent protein (GFP) to detect repeat-associated non-AUG (RAN) translation, was generated. This model was used for a genetic screen that identified 18 genetic modifiers that encode components of the NuPC as well as the machinery implicated in the export of nuclear RNA and in the import of nuclear proteins (Freibaum *et al.*, 2015). Consistently, morphological changes in the architecture of the nuclear envelope in cells expressing expanded G4C2 repeats were found *in vitro* and *in vivo*. Furthermore, alterations in RNA export resulting in retention of RNA in the nucleus were observed in Drosophila cells expressing expanded G4C2 repeats and also in aged iPSC-derived neurons from C9orf72 patients (Freibaum *et al.*, 2015). This and further studies (Fallini *et al.*, 2020) have demonstrated that the disruption of nucleocytoplasmic transport through the nuclear pore is a primary consequence of G4C2 repeat expansion. Importantly, depletion of the nuclear export adaptor SRSF1 prevents neurodegeneration and locomotor deficits in a *Drosophila* model of C9orf72-related disease (Hautbergue *et al.*, 2017), suggesting the importance of nucleocytoplasmic transport in regulating pathology. Furthermore, nuclear pore pathology is present also in brain tissue from sporadic ALS patients (Fallini *et al.*, 2020), thus indicating that dysregulation of nucleocytoplasmic shuttling and disruption of the nuclear membrane and NuPCs may be a common mechanism in both sALS and fALS cases displaying TDP-43 proteinopathy.

SOD1 and nucleocytoplasmic transport

Mutations in SOD1 were first identified in 1993 (Rosen *et al.*, 1993) and a few years later, it was determined that mutant SOD1-linked ALS was related to a toxic gain of function (Wong *et al.*, 1995). Nearly 30 years later, we still do not fully understand the mechanisms related to this gain of toxicity and, for some aspects, we are still investigating the role of wild-type SOD1 beyond its anti-oxidant function. Several pieces of evidence indicate that misfolded wild-type SOD1 may be pathogenic in ALS through various processes summarised in section 1.3.2. Moreover, there is evidence indicating that SOD1 could function as a transcription factor, responding to oxidative stress and probably being regulated by endogenous ROS (Tsang *et al.*, 2014).

Since the other potential roles of wild-type SOD1 have been thoroughly investigated in ALS, the focus of this chapter is to interrogate SOD1 nuclear localisation and its

potential role. This still under-investigated localisation and physiological role of SOD1 might lead to a better understanding of ALS pathology and the link between SOD1 and the other major genes associated to ALS and involved in DNA or RNA binding, i.e. C9orf72, TARDBP and FUS.

Following on from the hypothesis of SOD1 as a transcription factor or potentially as a transcription regulator, SOD1 nuclear localisation has been reported in the literature (Chang *et al.*, 1988; Crapo *et al.*, 1992; Sau *et al.*, 2007). Furthermore, human SOD1 nuclear localisation was confirmed in transgenic mice expressing mutated forms of hSOD1 (Sau *et al.*, 2007; Gertz, Wong and Martin, 2012). Thus, the nuclear presence of SOD1 posed the question of how it enters into the nucleus and its subcellular function in this location. Inside the cell, movement of small proteins happens via passive diffusion through the nuclear pore complex (NuPC), while proteins bigger than ~40 kDa normally require specific transporters (Terry, Shows and Wente, 2007). The size of the native SOD1 dimer is 32 kDa, and it should be capable of moving spontaneously between the nuclear and the cytosolic compartments, via nuclear pores. Additionally, also misfolded SOD1 was detected in the nucleus of motoneurons and glial cells in spinal cord tissue from ALS patients, highlighting the nucleus as a potential site of SOD1 toxicity (Forsberg *et al.*, 2010, 2011, 2019).

It has been shown that misfolded mutant SOD1 and wtSOD1 expose a normally buried NES-like sequence that is then recognised by the nuclear export carrier protein XPO1 which binds the NES sequence and exports misfolded SOD1 to the cytoplasm. Removal of this NES-like domain leads to nuclear accumulation of mutant SOD1 in cell models and *C. elegans*, thus resulting respectively in cell death and locomotor defects. This study shows that SOD1 is removed from the nucleus by XPO1 as a defence mechanism against toxicity of nuclear misfolded SOD1 (Zhong *et al.*, 2017). A year later, Israelson et al., revealed that macrophage inhibitory factor (MIF), a multifunctional protein with cytokine/chemokine activity and cytosolic chaperone-like properties inhibits mutant SOD1 nuclear clearance when overexpressed in motor neuron-like NSC-34 cells and reduces the toxicity of misfolded SOD1 by directly interacting with it (Shvil *et al.*, 2018). MIF was shown to act as a chaperone for misfolded SOD1 *in vivo*, in fact eliminating MIF in a mutant SOD1 mouse model increased the accumulation of misfolded SOD1, accelerated disease onset and late disease progression, and shortened the lifespan of mice expressing mutant SOD1 (Leyton-Jaimes *et al.*, 2016).

These findings indicate that MIF might exert its beneficial effect by correctly folding SOD1, therefore restoring SOD1 physiological role into the nucleus. These findings indicate how nucleocytoplasmic transport could have an important role also in SOD1-linked ALS. Consistent with the literature reporting that nucleocytoplasmic shuttling becomes disrupted with physiological ageing and in neurodegenerative disorders (Ribezzo, Shiloh and Schumacher, 2016; Kim and Taylor, 2017; Ferreira, 2019; Hutten and Dormann, 2019), in the previous chapter I showed that several transporters such as RANBP17, IPO5 and XPO1 decrease with age. This decline in transporter proteins with age might account for the late onset of ALS symptoms, when neuroprotective cellular mechanisms fail to compensate for pathological events.
This evidence led to the formulation of the hypothesis that in all forms of fALS, caused by mutations in *SOD1* or other genes, as well as in sALS, misfolded SOD1 accumulates in the nucleus of astrocytes and contributes to toxicity.

Therefore, the aims of this chapter are:

1. To determine mutant and wild-type SOD1 localisation within induced astrocytes;

2. To confirm the direct interaction between SOD1 and XPO1;

3. To determine the mechanisms involved in SOD1 accumulation in the nucleus in sALS and fALS cases and the role of XPO1 in this process.

4.2 ALS patient derived astrocytes recapitulate typical pathological features observed in ALS

In the previous chapter, we demonstrated how directly reprogrammed astrocytes retain the ageing features of the donor fibroblasts. As in this chapter I set out to interrogate pathological mechanisms occurring in ALS, my first step was to determine whether iNPC-derived astrocytes retain known ALS pathological features. With the same procedure described in sections 2.2.1 and 2.2.2, iNPC were differentiated into iAstrocytes, and immunostaining was used to validate the successful cell differentiation using CD44, glial fibrillary acid protein (GFAP), EAAT2 and vimentin antibodies, identifying typical glial markers (Figure 4.1 A). Hoechst was used to stain the nuclei in all immunocytochemistry experiments. CD44 identifies astrocyte-restricted precursors (Schnitzer, Franke and Schachner, 1981) and is a cell-surface glycoprotein involved in cell-cell interactions, cell adhesion and migration. GFAP and vimentin are both intermediate neurofilaments. Vimentin is not astrocyte specific, but within the neural lineage, is a marker of astrocytes (Ribezzo, Shiloh and Schumacher, 2016; Kim and Taylor, 2017; Ferreira, 2019; Hutten and Dormann, 2019). EAAT2 is an astrocyte specific glutamate transporter and, with GFAP, is a marker of mature astrocyte identity. Hence, co-staining of all these markers confirms both successful differentiation and maturity of the reprogrammed astrocytes.

A

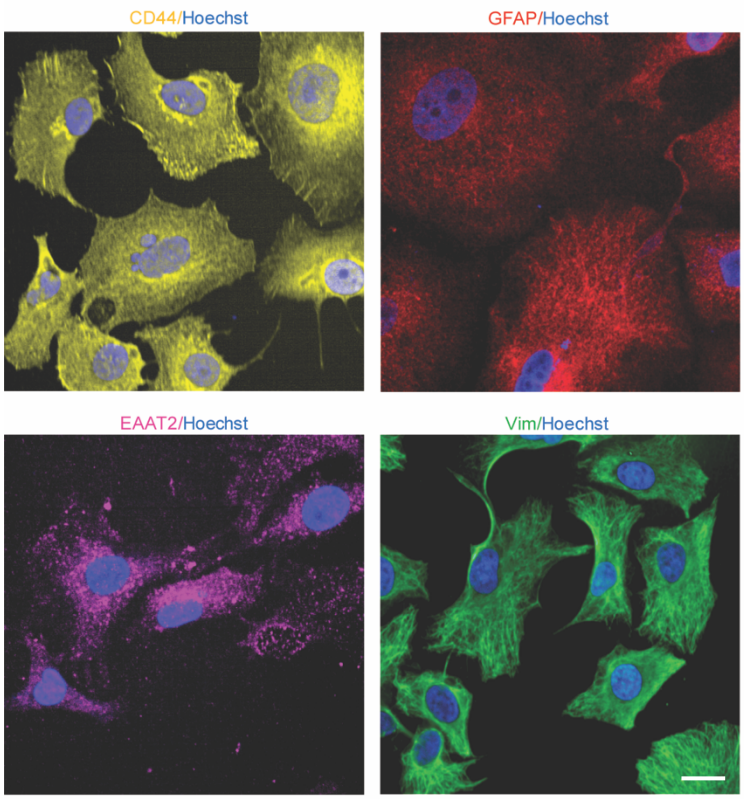

Figure 4.1 *Representative images of astrocytic markers*

A CD44, GFAP, EAAT2 and Vimentin (VIM) in derived iAstrocytes, Scale bar (10μm).

Subsequently, I focused on the characterisation of the disease phenotype in ALS iAstrocytes.

TDP43 (43kDa) proteinopathy is a hallmark of ALS. The TDP-43 protein was identified as a major component of the ubiquitinated neuronal cytoplasmic inclusions both in FTD and in spinal motor neurons in ALS (Liu *et al.*, 2004) as well as in glia cells (Nishihira *et al.*, 2008; Zhang *et al.*, 2008). TDP-43-positive inclusions are common in 97% of ALS cases. The main exceptions are cases caused by mutations in SOD1 or FUS (Neumann *et al.*, 2006).

TDP-43 protein levels were evaluated through western blot in our iAstrocytes, using a C-terminal TDP43 antibody. Although TDP-43 total levels show a certain degree of variability between different cell lines (Figure 4.2 B) grouped analysis reveals that sALS and SOD1 patients display significantly lower protein levels compared to healthy controls (Figure 4.2 D). The reduction in TDP-43 found in SOD1 patients could be representative of alteration in TDP-43 turnover. In addition, it was possible to observe a second band of 35kDa, which is a cleavage product of TDP-43, only present in sALS and C9orf72 patients (Figure 4.2 A,C). It has been demonstrated that this C-terminal cleavage fragment of 35kDa is prone to aggregate, forming cytoplasmic inclusions. Moreover, TDP-35 is able to sequester TDP-43 from nuclear localisation into cytoplasmic inclusions, that leads to alterations of RNA processing (Mackenzie, Rademakers and Neumann, 2010). Indeed, it was possible to observe the TDP-43 cytoplasmic inclusions also in iAstrocytes (Figure 4.2 E). Then the expression of p62 was analyses, as marker of protein homeostasis, using western blotting in order to evaluate the protein level of inclusions (

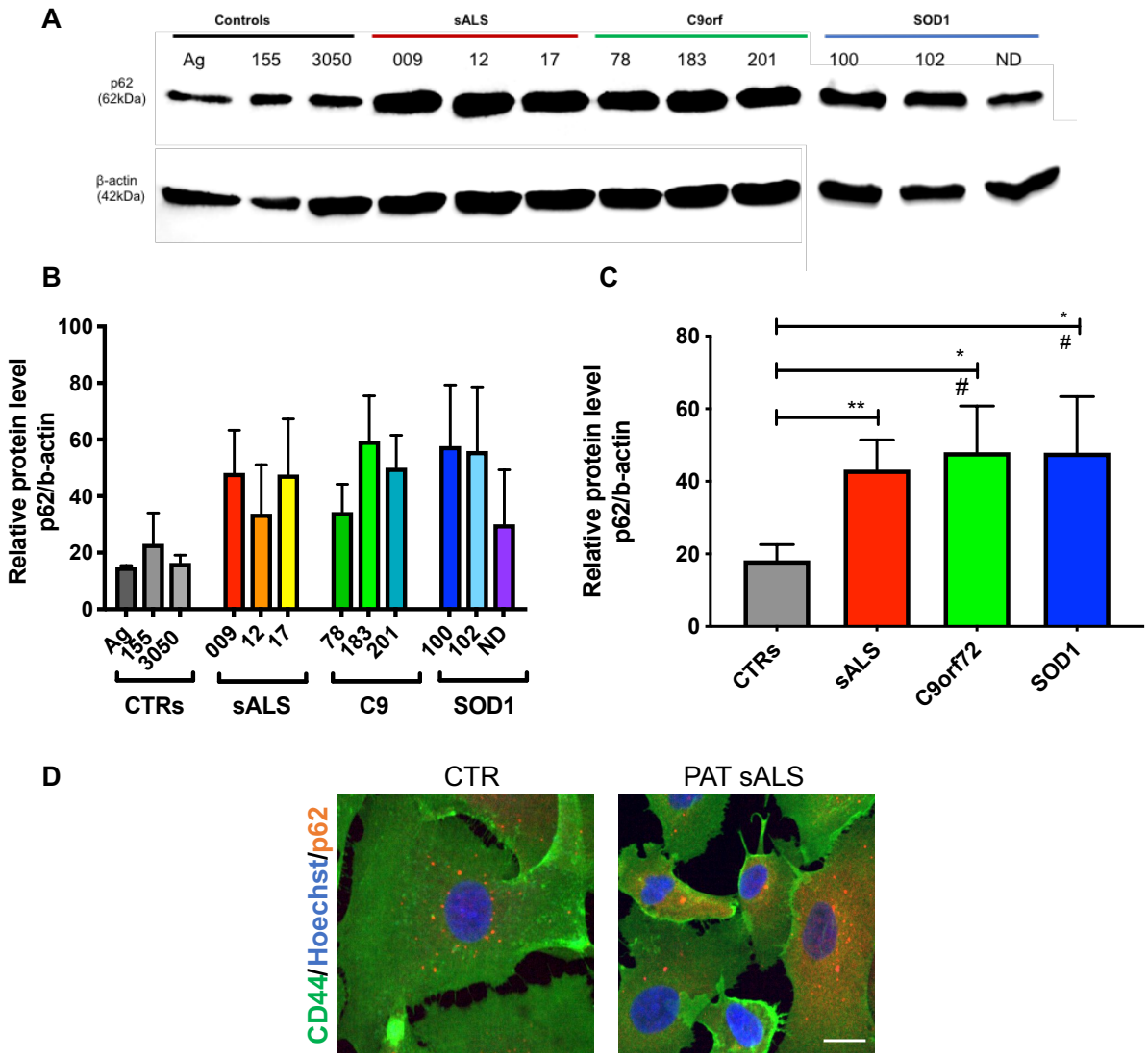

Figure 4.3 A). As expected due to its role in autophagy, as well as proteasomal protein degradation, and the reported impairment of these pathways in SOD1 and C9orf72 cases (Che *et al.*, 2011) p62 western blot showed a higher level of expression of this protein in patients compared to controls (Figure 4.3 B,C). Moreover, with immunostaining, it was possible to observe the typical p62-punctate pattern of staining in the perinuclear region of derived astrocytes (Figure 4.3 D).

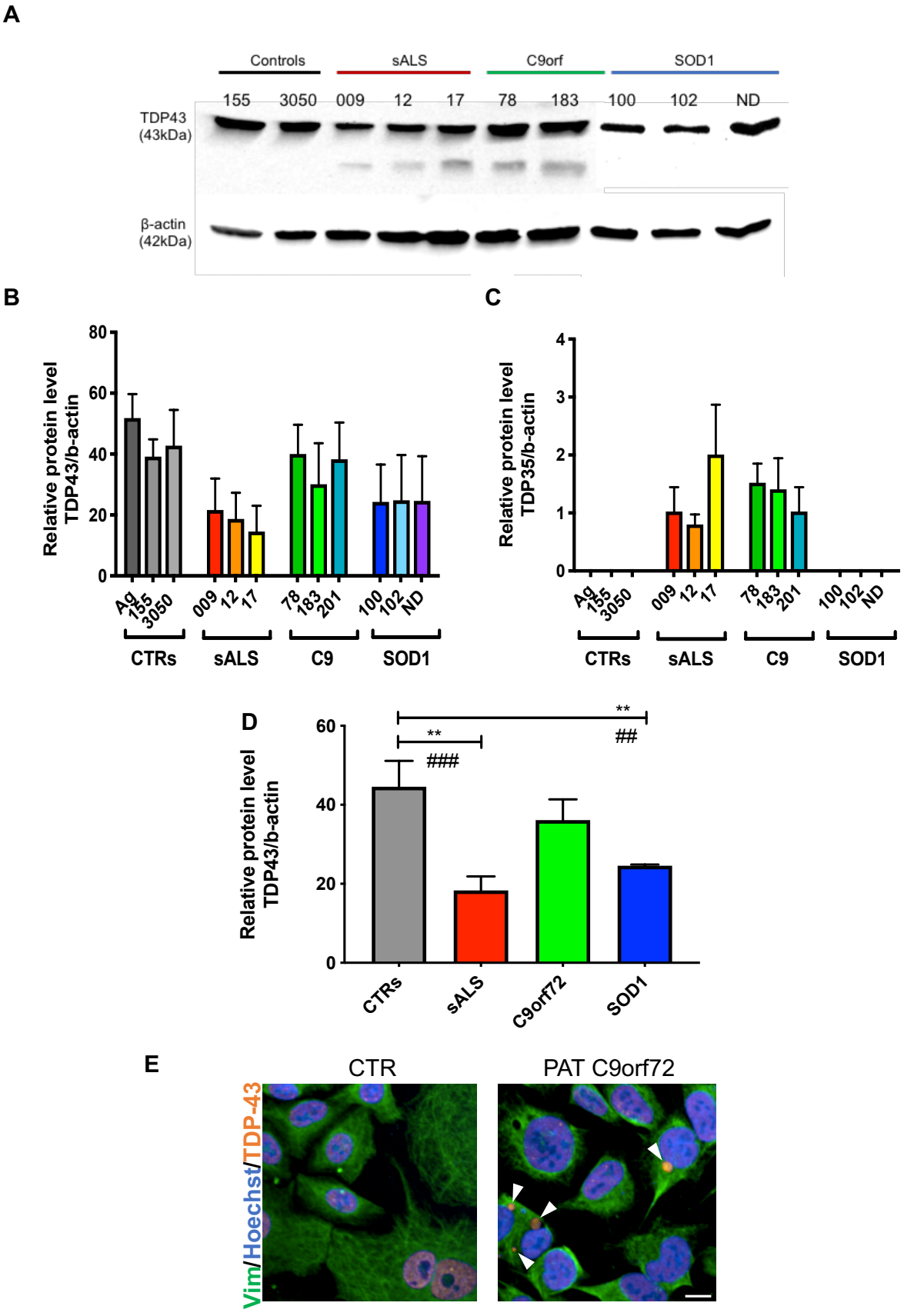
A
Controls
sALS
C9orf
SOD1
155
3050
009
12
17
78
183
100
102
ND
TDP43
(43kDa)
β-actin
(42kDa)
B
Relative protein level
TDP43/b-actin
80
60
40
20
0
Ag
155
3050
009
12
17
78
183
201
100
102
ND
CTRs
sALS
C9
SOD1
C
Relative protein level
TDP35/b-actin
4
3
2
1
0
D
Relative protein level
TDP43/b-actin
60
40
20
0
**
**
###
##
CTRs
sALS
C9orf72
SOD1
E
CTR
PAT C9orf72
Vim/Hoechst/TDP-43

Figure 4.2 *TDP-43 proteinopathy in iAstrocytes*

A Representative images of TDP-43 and β-actin western blot. **B** Western blot TDP-43 quantification graph (n≥3 per line). **C** Western blot TDP-35 quantification graph (n≥3 per line). **D** Quantification graph (n=3) of TDP-43 in ALS patient subgroups. Unpaired t-test CTR vs PAT subgroup, **P<0.01; One-way ANOVA, multiple comparisons ## P<0.01, ### P<0.001 (n=3). Results are expressed as the means ± SD. **E** Representative images of TDP-43 (rabbit antibody) cytoplasmic inclusions (indicated by white arrows) in iAstrocytes derived from a C9orf72 patient (PAT C9orf72) compared to control (CTR). Co-stained with Vimentin (chicken antibody) to discriminate the cytoplasm. Scale bar (10μm).

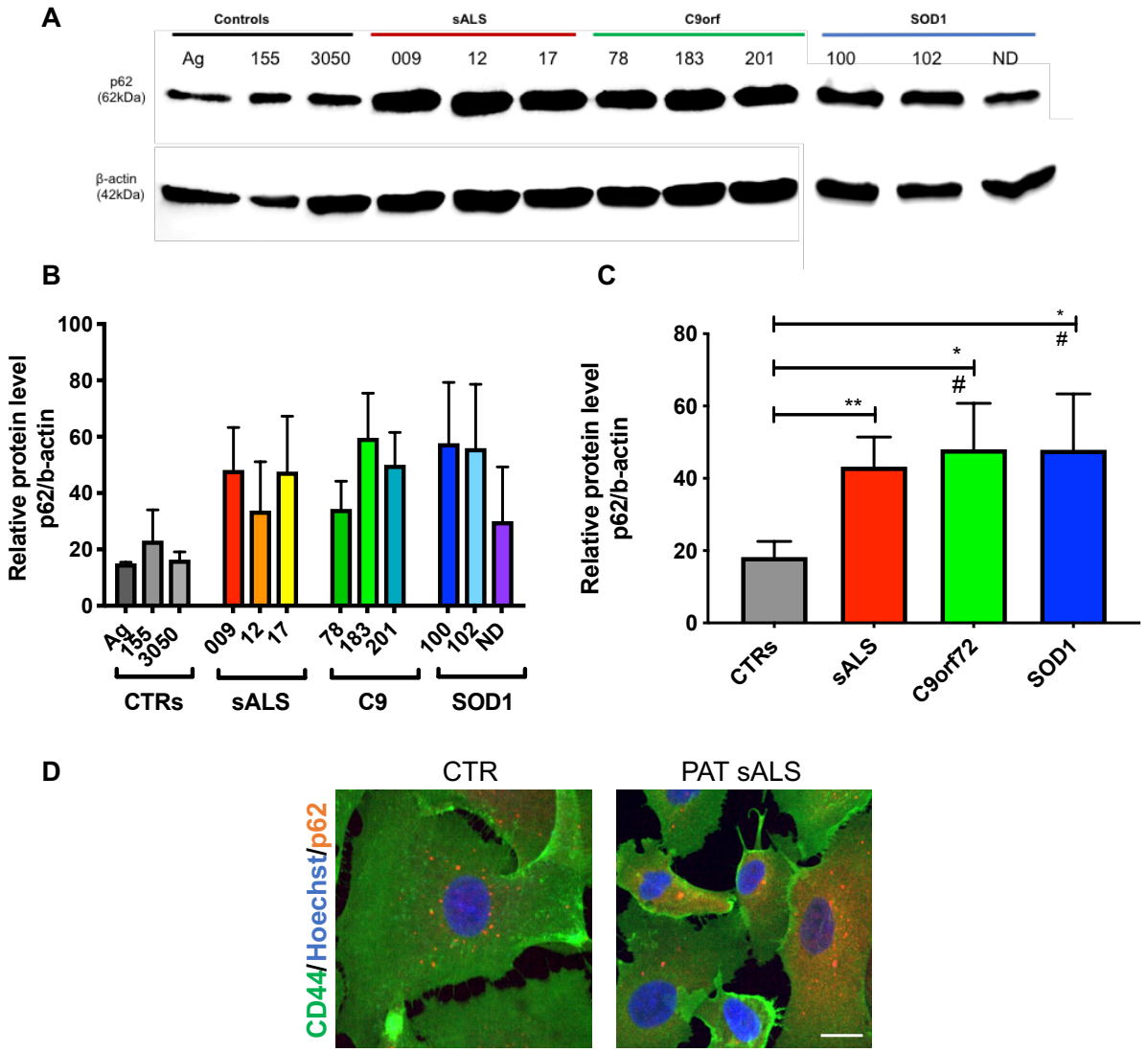

Figure 4.3 *p62 as a marker of ALS pathology*

A Representative images of p62 and β-actin blot. **B** Quantification graph with each single cell line (n≥3). **C** Quantification graph with patient subgroups. Unpaired t-test CTR vs PAT subgroup, *P<0.05, **P<0.01; One-way ANOVA, multiple comparisons # P<0.05 (n=3). Results are expressed as the means ± SD. **D** Representative image of p62-puncta (mouse antibody) in iAstrocytes derived from a sALS patient (PAT sALS) compared to control (CTR). Co-stained with CD44 (rabbit antibody) to discriminate the cytoplasm. Scale bar (10μm).

4.3 SOD1 localisation and quantification in derived iAstrocytes

After confirming that the direct reprogramming method used for this study is able to recapitulate some aspects of the disease phenotype observed in ALS *post-mortem* tissue, I focused on assessing the expression levels and distribution of the wild-type and misfolded SOD1 protein. Initially, a staining for wild-type and misfolded SOD1 was performed. Staining for total wild-type SOD1 showed that SOD1 is abundantly present in iAstrocytes, also with nuclear localisation (Figure 4.4 A). Several manuscripts have identified misfolded SOD1 as another pathological marker, usually located in protein inclusions in *post-mortem* samples from SOD1 familial cases, as well as other genetic and sporadic forms (Gal *et al.*, 2009; W. J. Liu *et al.*, 2016; Webster *et al.*, 2018). To identify misfolded SOD1 localisation via immunostaining, the B8H10 antibody was used, which was raised in the SOD1 G93A mouse model and that recognises misfolded forms of mutant human SOD1 protein (Gros-Louis *et al.*, 2010). The staining revealed misfolded SOD1 protein in the nucleus of patient derived astrocytes, and also misfolded SOD1 cytoplasmic aggregation in SOD1 patient astrocytes (Figure 4.4 B). Due to the qualitative nature of immunostaining, western blotting was used to quantify the total levels of SOD1 protein without discrimination between the misfolded and wild-type form. In order to demonstrate that the antibody (Cell Signalling #2770) used specifically recognises SOD1, the protein was knocked-down through an adenovirus expressing an shRNA against SOD1 (Figure 4.4 C). SOD1 (~16kDa) levels decrease with age, as reported in Chapter 3 (Figure 5, Chapter 3) and display some degree of variability within each patient and control cell line, however, without showing any further expression change in any patient subgroup (Figure 4.4 D-F). Remarkably, in ND, a patient with SOD1 D90A mutation, another band was detected below 16kDa that has been reported before in the literature and might represent a subunit truncated in the N-terminal region (Jacobsson, 2001).

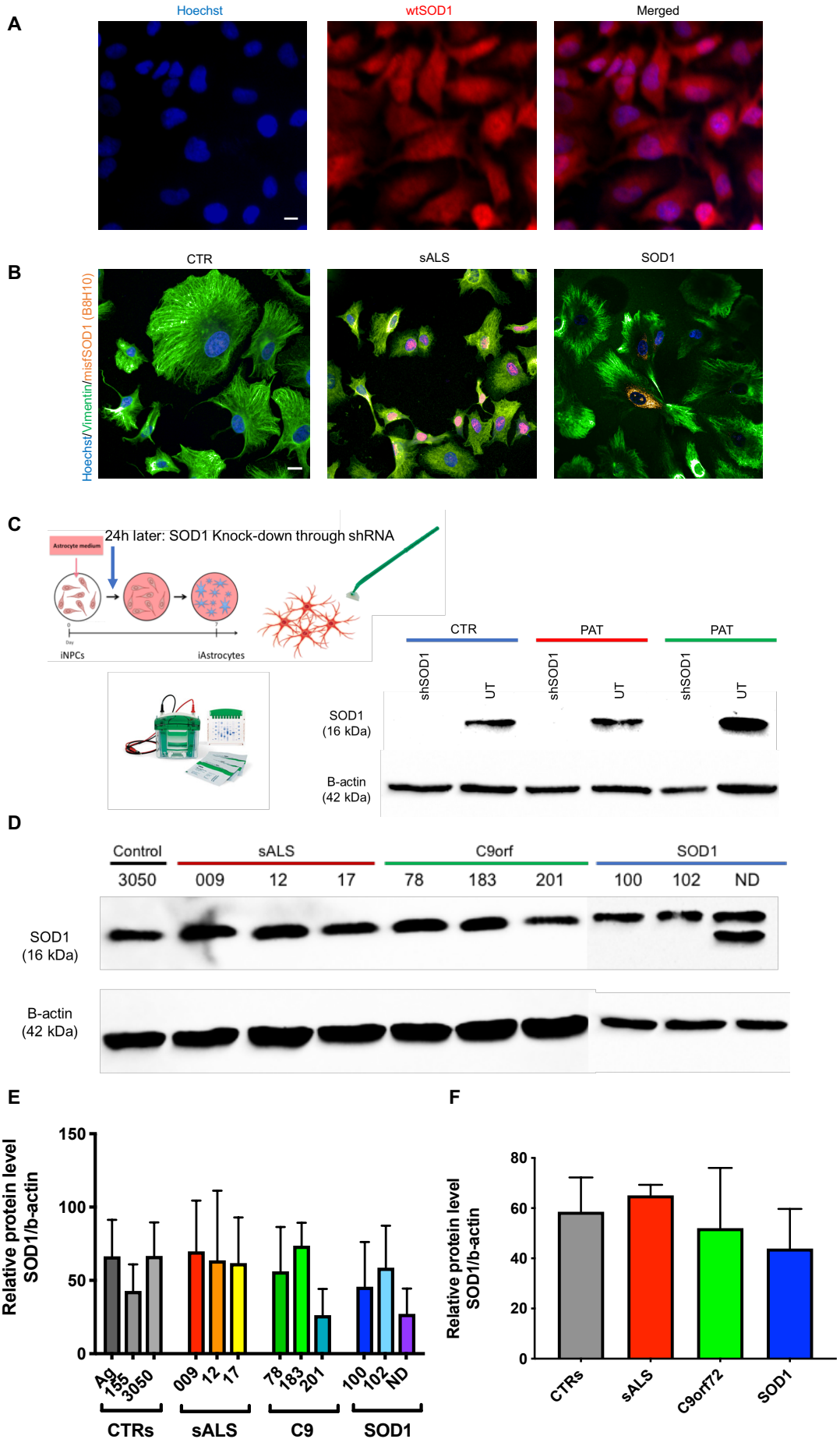
A
Hoechst
wtSOD1
Merged
B
CTR
sALS
SOD1
Hoechst/Vimentin/misfSOD1 (B8H10)
C
24h later: SOD1 Knock-down through shRNA
Astrocyte medium
iNPCs
iAstrocytes
CTR
PAT
PAT
shSOD1
UT
shSOD1
UT
shSOD1
UT
SOD1
(16 kDa)
B-actin
(42 kDa)
D
Control
sALS
C9orf
SOD1
3050
009
12
17
78
183
201
100
102
ND
SOD1
(16 kDa)
B-actin
(42 kDa)
E
Relative protein level
SOD1/b-actin
150
100
50
0
Ag
155
3050
009
12
17
78
183
201
100
102
ND
CTRs
sALS
C9
SOD1
F
Relative protein level
SOD1/b-actin
80
60
40
20
0
CTRs
sALS
C9orf72
SOD1

Figure 4.4 *SOD1 levels are variable in derived astrocytes*

A Representative images of wild-type SOD1 (Cell Signalling #2770) in iAstrocytes, Scale bar (10µm), . **B** Representative images of misfolded SOD1 (B8H10 antibody) in iAstrocytes, Scale bar (10µm). **C** Representative images of complete knock-down through adenovirus expressing a shRNA against SOD1. **D** Representative images of SOD1 and β-actin blot. **E** Quantification graph with each single cell line (n≥3). **F** Quantification graph with patient subgroups (n=3). Unpaired t-test CTR vs PAT subgroup; One-way ANOVA, multiple comparisons, no significance. Results are expressed as the means ± SD.

4.4 Nuclear and cytoplasmic fractionation revealed higher SOD1 nuclear levels in sALS and C9orf72 astrocytes

Due to the qualitative data obtained with the B8H10 antibody, showing the presence of misfolded SOD1 predominantly in sALS, the amount of SOD1 that was localised in the nucleus was assessed. As indicated in the materials and methods section, the fractionation protocol had to be optimised specifically for human iAstrocytes (2.2.13 Nuclear and Cytoplasmic Fractionation). β-tubulin was used as a cytoplasmic marker, even though there are reports of its localisation in the nuclear compartment (Walss-Bass *et al.*, 2002; Akoumianaki *et al.*, 2009). In the experimental conditions, β-tubulin was overall a good cytoplasmic marker with low level of nuclear contamination. SSRP1 (Structure Specific Recognition Protein 1) was used as nuclear marker. To confirm that there is no contamination between cell compartments after fractionation, the presence of β-tubulin and SSRP was examined in all compartments. Thereafter SOD1 was quantified by using the cell compartment-specific loading control. This protocol (Figure 4.5 A) was applied to the iAstrocytes (Figure 4.5 B) (ND was excluded because it was not confluent enough to perform fractionation) and the graphs were produced (Figure 4.5 C). The resulting western blots confirmed the presence of SOD1 in the nucleus, as well as in the cytoplasm, where it is more abundant. Interestingly, sALS and C9orf72 displayed significantly higher nuclear levels of SOD1, while SOD1 lines did not, although this was tested only in two SOD1 samples (Figure 4.5 C). The results of the nuclear and cytoplasmic fractionation experiments are in line with the finding that SOD1 might act as a transcription factor (Tsang *et al.*, 2014).

A

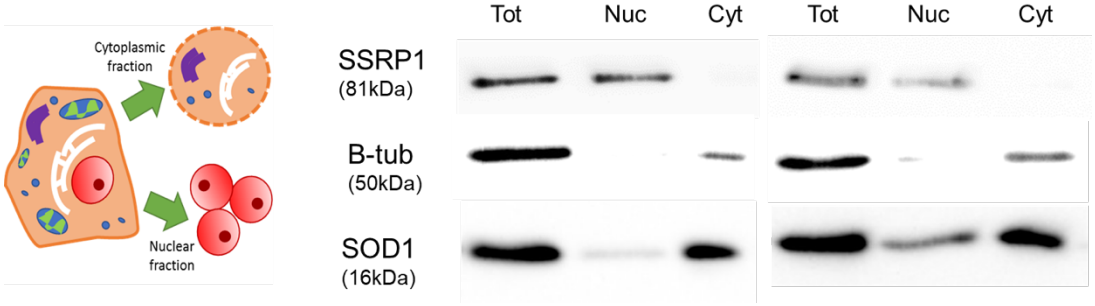
Cytoplasmic fraction
Nuclear fraction
CTR
PAT
Tot
Nuc
Cyt
Tot
Nuc
Cyt
SSRP1 (81kDa)
B-tub (50kDa)
SOD1 (16kDa)

B

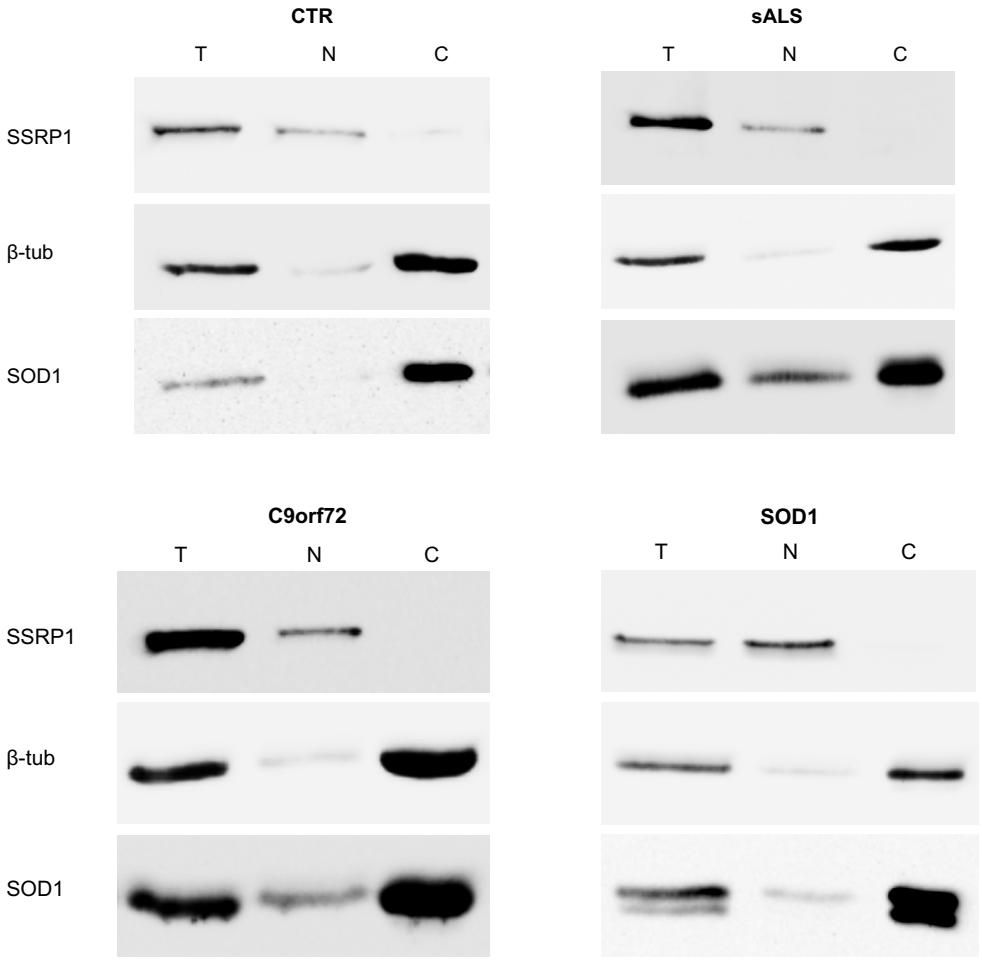
CTR
T
N
C
sALS
T
N
C
SSRP1
β-tub
SOD1
C9orf72
T
N
C
SOD1
T
N
C
SSRP1
β-tub
SOD1

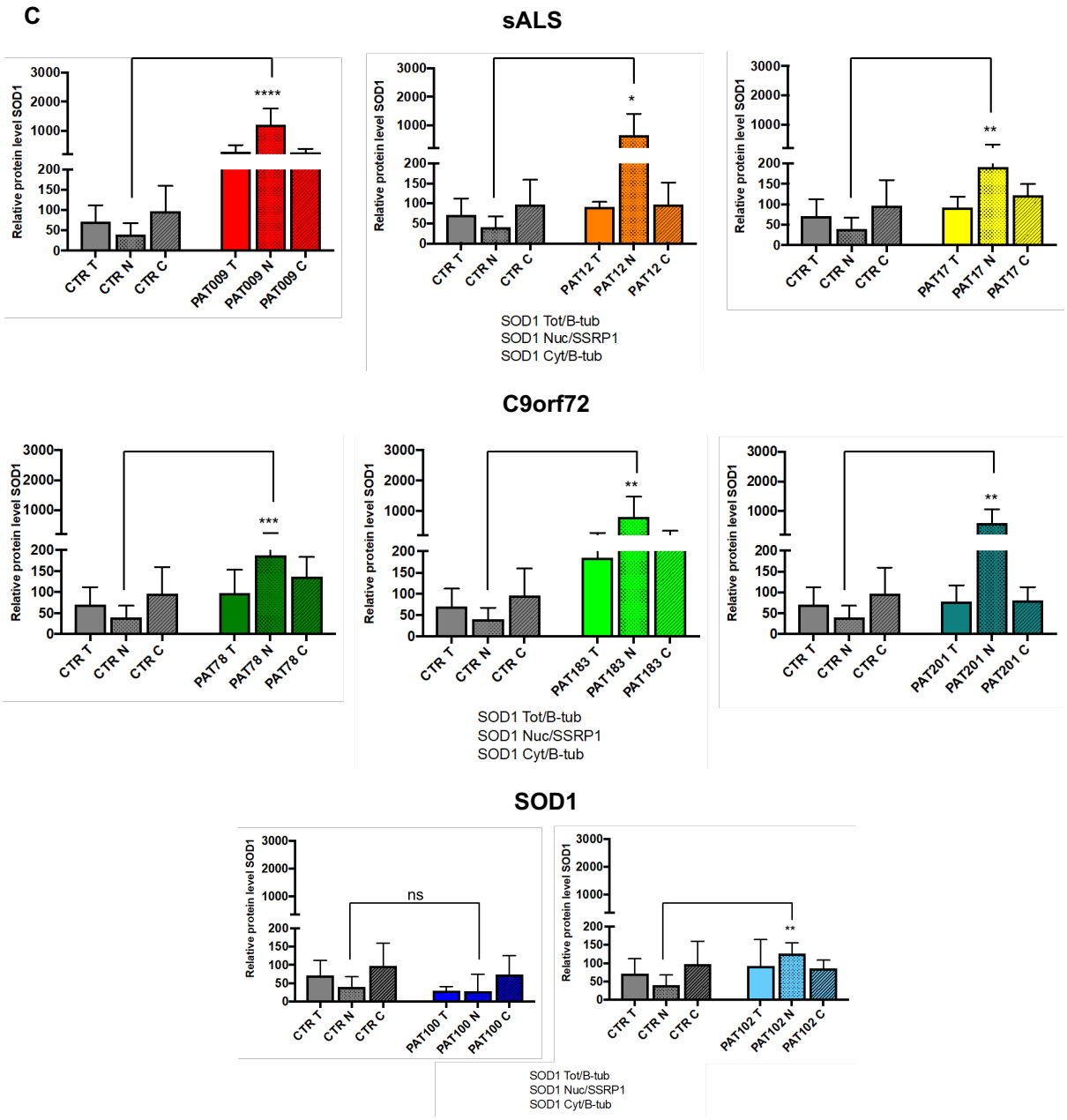

Figure 4.5 *Fractionation showed higher SOD1 nuclear levels in sALS and C9orf72 astrocytes*

A Schematic illustration of fractionation protocol: SSRP1 (Structure Specific Recognition Protein 1) was used as nuclear marker, while β-tubulin was used as cytoplasmic marker. **B** Representative image of fractionation in most of the lines. **C** Quantification of SOD1 in the cellular fractions in sALS, C9orf72 and SOD1 iAstrocytes. Unpaired t-test, CTR Nuclear vs PAT Nuclear, * P<0.05, ** P<0.01, **** P<0.0001. Results are expressed as the means ± SD.

4.5 SOD1 does not directly bind RNA in iAstrocytes

In order to determine the role of SOD1 in the nucleus, the hypothesis that SOD1 might act as an RNA-binding protein, like several other mutant proteins causing ALS, was investigated. To answer this question RNA pull-down was performed using an antibody against oxidised RNA (8-OHG, Abcam) and poly dT beads to pull down total polyadenylated RNA. A crosslinking step by UV was performed to strengthen the protein interaction with RNA in order to be able to detect them via western blotting. Since the oxidised RNA pull down relied on an antibody that gave high variability, the protocol for the total RNA pull-down was optimised. This experiment was repeated three times in a SOD1 patient cell line with a control, and once in C9orf72 patient with a control. In none of these experiments I was able to detect SOD1 in the output (Figure 4.6 A), thus indicating that SOD1 does not bind RNA. TDP-43, on the contrary, was consistently detected in the output. Interestingly, the ratio between the 35kDa and 43kDa changed within different patients depending as to whether they carried a SOD1 or C9orf72 mutation. In fact, although preliminary, my results show the TDP-35/43 ratio is half of the control level in the SOD1 patients, while it is 4 times higher in the C9orf72 patient (Figure 4.6 B, C), consistent with the literature, indicating an alteration in RNA metabolism in C9orf72 patients, while SOD1 patients are not affected by the same TDP-43 proteinopathy (Robertson et al., 2007; Turner et al., 2008). Interestingly, in the no UV cross-linked samples (-) it is possible to see the 35kDa fragment of TDP-43, indicating that this fragment can bind RNA in a non-specific manner (Figure 4.6 B, C).

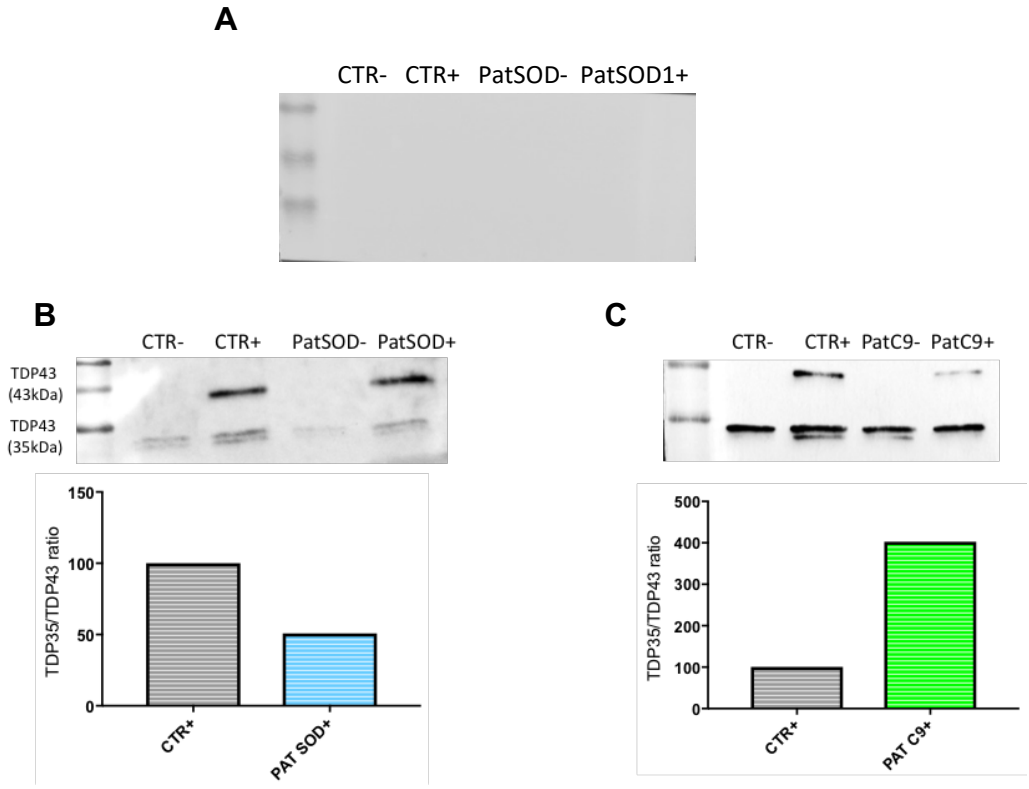

Figure 4.6 *SOD1 does not bind directly RNA*

A Poly-A RNA pull down output with control and SOD1 patient, blotted for SOD1. **B** Poly-A RNA pull down output with control and SOD1 patient, blotted for TDP-43 and the relative TDP-35/TDP-43 ratio. **C** Poly-A RNA pull down output with control and C9orf72 patient, blotted for TDP and the relative TDP-35/TDP-43 ratio. (-) No UV cross-linked (+) UV Cross-linked.

4.6 XPO1 levels decrease in sALS patient derived astrocytes

After discarding the hypothesis that SOD1 might bind RNA, I proceeded with a series of experiments to determine the mechanisms leading to SOD1 accumulation in the nucleus of sporadic and C9orf72 patients. I started with evaluating the expression of XPO1 through western blotting (Figure 4.7 A), since a recent paper (Zhong *et al.*, 2017) showed that this carrier protein is responsible for misfolded and mutant SOD1 export from the nucleus to the cytoplasm as a defence mechanism to avoid accumulation of misfolded SOD1 in the nucleus. It is reported that this nucleocytoplasmic transporter recognises a nuclear export signal (NES)-like sequence in SOD1 that is only accessible when the protein is misfolded (Zhong et al., 2017). Relevant in this context, my data showed that XPO1 levels decrease with age in iAstrocytes (Figure 4, Chapter 3), suggesting a potential role of ageing in affecting the balance between accumulation of toxic proteins and neuroprotective cellular defences. Interestingly, the resulting western blot showed a significant lower level of XPO1 in sALS iAstrocytes, but not in the other patient subgroups, compared to age-matched controls (Figure 4.7 B,C), indicating that this transporter is even more affected in sALS which might explain the higher level of SOD1 in the nucleus in this ALS patient group.

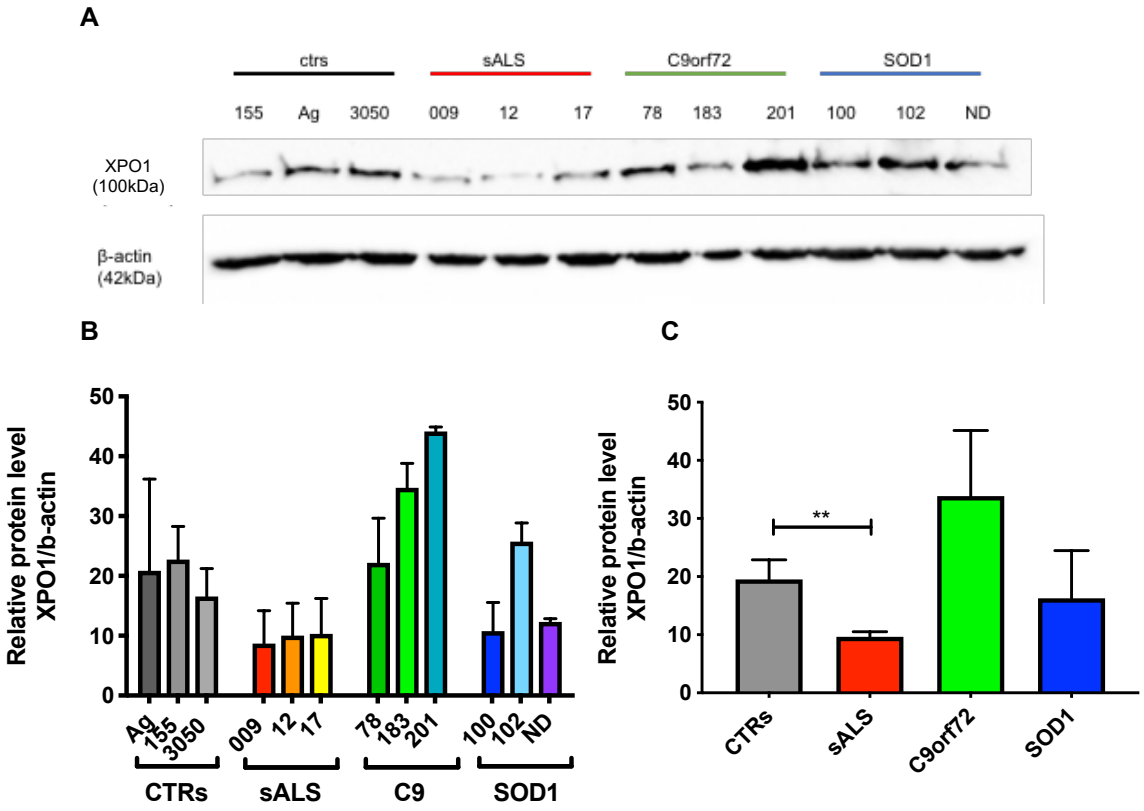

Figure 4.7 *XPO1 decreases in sALS patient derived astrocytes*

A Representative images of XPO1 and β-actin blot. **B** Quantification graph of XPO1/b-actin with each single cell line shown separately (n≥3). **C** Quantification graph with patients pooled together by genetic subgroup. Unpaired t-test CTR vs PAT subgroup **P<0.01; One-way ANOVA, multiple comparisons, no significance (n=3). Results are expressed as the means ± SD.

4.7 XPO1 displays differential interaction with misfolded or mutant SOD1

Next, I wanted to confirm whether there is a direct interaction between SOD1 and XPO1. To achieve this goal, immunoprecipitation technique was used to demonstrate the interaction between both misfolded SOD1 (B8H10 antibody) and wild-type SOD1 (Cell Signalling #2770) with XPO1 (Figure 4.8 A). SOD1 was knocked down through shRNA as a control in this experiment.

The obtained results showed in both cases a direct interaction. This procedure was repeated in one control line, one sALS and one SOD1 line (Figure 4.8 B, C). This experiment represents a proof of concept, demonstrating the interaction of XPO1 with both forms of SOD1 and not with misfolded SOD1 only as previously reported (Zhong *et al.*, 2017).

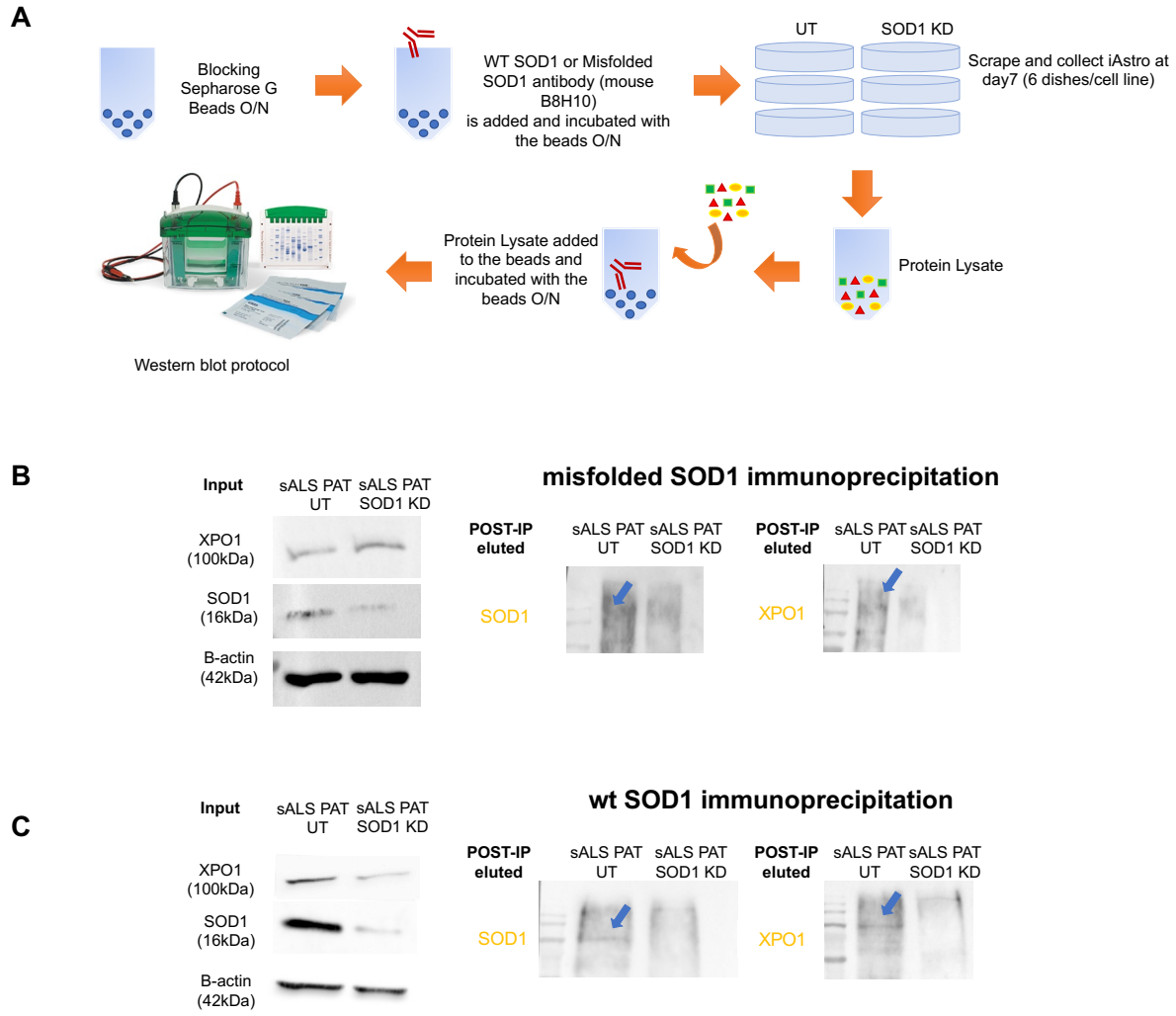

Figure 4.8 *Immunoprecipitation confirms the interaction between XPO1 with misfolded and wild-type SOD1*

A Schematic illustration describing the immunoprecipitation protocol. **B** Representative images of WB blot showing the direct interaction between XPO1 and misfolded SOD1; input on the left shows the protein levels loaded before the immunoprecipitation procedure. SOD1 KD=SOD1 knock-down through shRNA as a control, no binding with XPO1; POST-IP eluted on the right shows the output of the immunoprecipitation, after the final step of elution. **C** Representative images of WB blot showing the direct interaction between XPO1 and wild type SOD1, input on the left shows the protein levels loaded before the immunoprecipitation procedure. SOD1 KD=SOD1 knock-down through shRNA as a control no binding with XPO1; POST-IP eluted on the right shows the output of the immunoprecipitation, after the final step of elution.

Considering the qualitative nature of the immunoprecipitation assay, I next wanted to assess the level of interaction and the affinity of misfolded SOD1 and wild-type SOD1 for XPO1. To assess these parameters, a proximity ligation assay (PLA) was performed in the astrocyte lines. This assay allows detection of protein interaction in fixed cells and consists of a pair of PLA probes (one PLUS and one MINUS) with hosts corresponding to those of the primary antibodies, in this case mouse and rabbit, detection reagents and wash buffers. The two primary antibodies from different species that recognise two target epitopes were selected before the assay and validated in immunocytochemistry. In this assay, it was included as positive control, a separate sample with known protein interaction, p62-LC3, previously reported in the literature (Pankiv et al., 2007), while as negative control, one of the two primary antibodies by itself or no antibodies at all (Figure 4.9 A). Then, the nuclear interaction between XPO1 and both forms of SOD1 was evaluated, quantifying the nuclear spots per number of cells (Figure 4.9 B, D), and the misfolded SOD1-XPO1 interaction as a percentage of the total wtSOD1-XPO1 interaction (Figure 4.9 C, E), observing a reduction in the sALS and C9orf72 patients. This suggests that XPO1, further decreased in sALS cases (Figure 4.7) might not recognise the misfolded form of SOD1 that accumulates in the nucleus in this patient subgroup.

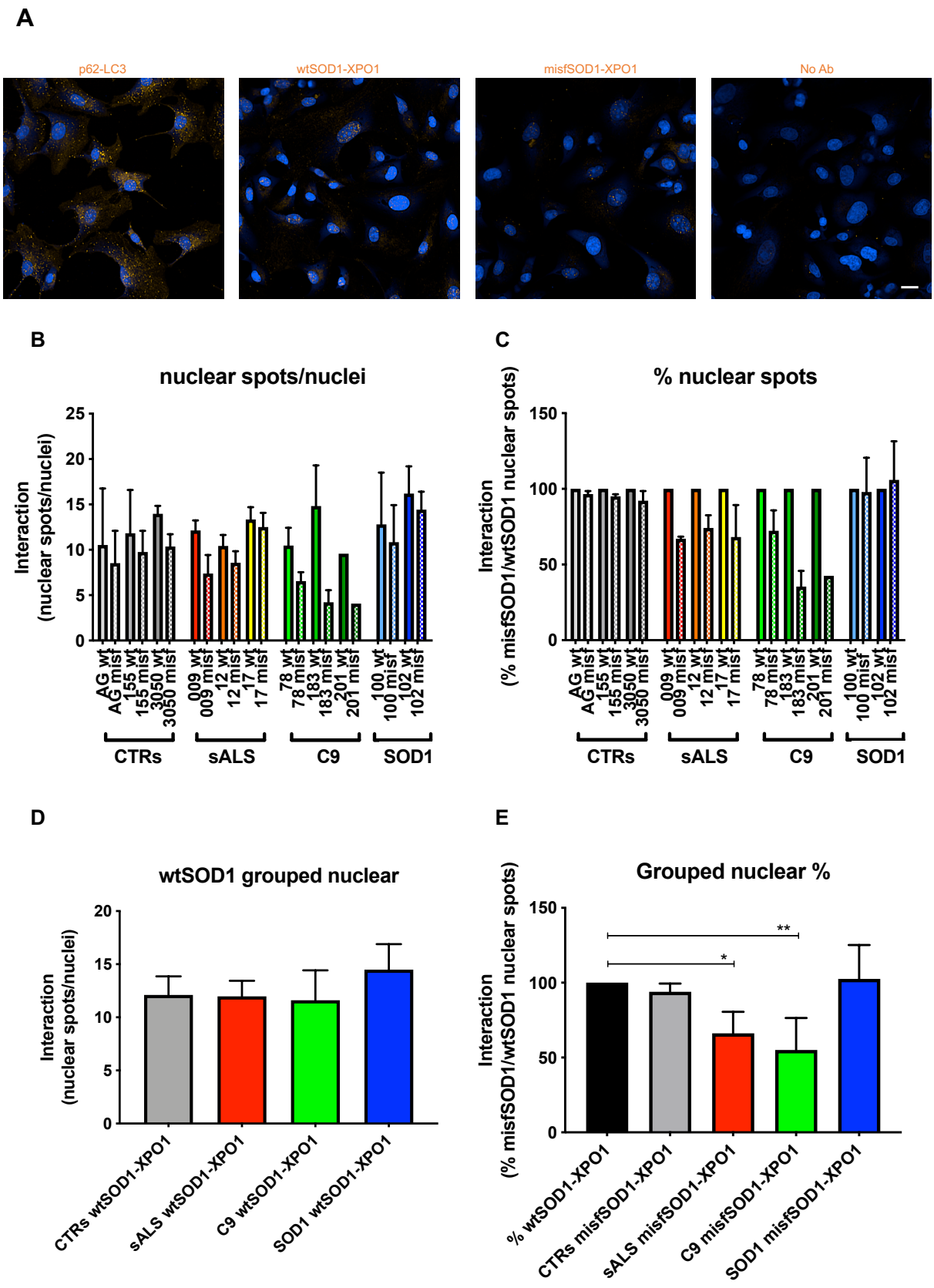

Figure 4.9 *Proximity ligation assay (PLA) results show a reduction in the interaction between misfolded SOD1 and XPO1 in sALS and C9orf72 derived astrocytes*

A Representative images of the positive control p62-LC3 interaction, SOD1-XPO1 interaction, misfolded SOD-XPO1 interaction, negative control (No Ab). **B** Quantification of nuclear spots normalised by number of cells to evaluate the interaction between wtSOD1 and XPO1, and misfolded SOD1 and XPO1 (n=2-3, n=1 for 201). **C** Quantification of nuclear interaction as percentage of wtSOD1 (100%), between misfolded SOD1 and XPO1 per cell line (n=2-3, n=1 for 201). **D** Quantification of nuclear spots normalised by number of cells to evaluate the interaction between wtSOD1 and XPO1 (n=3, 2 SOD1 patients). **E** Quantification of nuclear interaction as percentage of wtSOD1, between misfolded SOD1 and XPO1 per patient subgroups, One-way ANOVA, multiple comparisons *P<0.05, **P<0.01 (n=3, 2 SOD1 patients). Results are expressed as the means ± SD.

4.8 Discussion: SOD1 aberrantly accumulates in the nucleus due to altered interaction with nucleocytoplasmic transporters in ALS derived astrocytes

Mutations in the SOD1 gene were first identified in 1993 (Rosen *et al.*, 1993). Since then, several other ALS-causing mutations have been identified in more than 30 genes (Al Sultan *et al.*, 2016). Unfortunately, however, little progress has been made on the aetiology of the vast majority (90%) of sALS cases. Interestingly, several pieces of evidence indicate that misfolded wild-type SOD1 may also be pathogenic in sALS, through different processes, such as post-translational modifications, misfolding, aggregation and prion-like pathogenic behaviour. Moreover, there is evidence indicating that SOD1 could function as a transcription factor or potentially as a transcription regulator responding to oxidative stress and probably being regulated by endogenous ROS (Tsang *et al.*, 2014).

Mutant SOD1 exerts its neurotoxic effects via multiple mechanisms. It has been shown that age or environmental-dependent post-translational alterations lead to conformational rearrangements in the configuration of wild-type SOD1, that mimic the alterations observed in mutant SOD1 in fALS (Ezzi, Urushitani and Julien, 2007). In *in vitro* models, oxidized wild-type SOD1 forms protein aggregates that cause cell death (Kabashi *et al.*, 2009). Wild-type SOD1, depleted of zinc, induces death and metal-deficient SOD1 forms, like mutated SOD1, an unstable and aggregation-prone structure (Banci *et al.*, 2008). Furthermore, the use of specific antibodies has led to the detection of uncommon wild-type SOD1 species in a subgroup of sALS (Rakhit *et al.*, 2007; Bosco, Morfini, *et al.*, 2010). *In vitro*, these mutated SOD1-specific antibodies also have recognised the oxidized form of recombinant wild-type SOD1, suggesting that the wild-type SOD1 detected in sALS patients may also be oxidized (Bosco, Morfini, *et al.*, 2010). Therefore, it is possible that, in a cellular environment with chronic high levels of oxidative stress as in ALS cells, oxidised wild-type SOD1 might develop toxic properties, thus identifying a common SOD1-dependent mechanism linking mutant SOD1 fALS and a subgroup of sporadic ALS cases.

In agreement with this hypothesis, misfolded SOD1 has been reported in *post-mortem* CNS tissues of sporadic ALS patients (Rakhit *et al.*, 2007; Bosco, Morfini, *et al.*, 2010) and recent evidence showed misfolded SOD1 inclusions in patients with mutations in C9orf72 and other ALS/FTD-associated genes (Forsberg *et al.*, 2019). In addition, *in vitro* data using astrocytes from *post-mortem* spinal cords from sporadic ALS patients

showed that reducing the expression levels of wtSOD1 was a successful strategy to dampen astrocyte toxicity (Haidet-Phillips *et al.*, 2011). Similar data were obtained using oligodendrocytes reprogrammed from sporadic ALS patients (Ferraiuolo *et al.*, 2016), where reducing the levels of SOD1 improved oligodendrocyte function in SOD1 and sALS cases, but not in C9orf72 samples. This indicates that SOD1 misfolding might not be the main contributor to C9orf72 pathology in this cell type.

Since the pathogenicity of mutant SOD1 can be dampened by decreasing its expression levels, silencing SOD1 may also be relevant to sALS cases. Recently, different strategies to silence gene expression have been developed, such as anti-sense oligonucleotides (ASO) and RNA interference (RNAi) that enhance degradation of RNA or small inhibitory RNA (siRNA), short hairpin RNA (shRNA) and microRNA (miRNA) that are capable of permeating the central nervous system (CNS) and silencing genes (van Zundert and Brown, 2017). Indeed, a single injection of an adeno-associated virus serotype 9 (AAV9) encoding an shRNA decreases the production of ALS-causing human SOD1 mutants, penetrating the blood brain barrier and successfully transducing motor neurons and astrocytes (Foust *et al.*, 2013). This results in a slowdown of disease onset and of disease progression in SOD1 G93A and G37R models. This intravenous administration of AAV9-SOD1-shRNA is safe and tolerated in wild-type mice, with no adverse effects. This approach was successful in non-human primates as well. The authors determined that infusion directly into the CSF at the lumbar level in a non-human primate produces extensive SOD1 reduction, targeting MN and non-neuronal cells (Foust *et al.*, 2013). Another study, using ASO ISIS 333611 delivered to the CSF reduced SOD1 levels in spinal cord tissue of SOD1 G93A rat ALS model and prolonged survival. Moreover, its safety, tolerability an pharmacokinetics after intrathecal administration was assessed in patients with SOD1 fALS, showing no serious adverse events (Miller *et al.*, 2013). In conclusion, reducing the production of the aberrant misfolded protein could be a strategic therapy, as it can attenuate its toxicity and its aggregation, and also, the downstream intracellular and extracellular pathophysiological pathways.

In this context and motivated by the availability of therapeutic approaches aimed at targeting wild-type as well as mutant SOD1, we set out to interrogate the role of SOD1 in our patient-derived *in vitro* model. Firstly, astrocytes derived from patients and controls were characterised phenotypically for disease hallmarks. Patient-derived

astrocytes, in fact, showed TDP-43 proteinopathy as reported in the literature, and higher levels of p62. Furthermore, other members of the group are looking at other ALS characteristics within these cells, such as DNA damage accumulation, abnormal glutamate uptake and motor neuron survival in co-culture of astrocytes and motor neurons.

We then focused on SOD1 expression to determine whether the levels of this protein, which decrease with age, are further affected in ALS. However, we did not observe significant changes between the patient subgroups. Remarkably, in one patient with SOD1 D90A mutation another band was detected below 16kDa, that has been reported before in literature (Jacobsson, 2001). This might be due to an additional truncation mutation affecting even further SOD1 function. This specific cell line was acquired through Coriell and was not genotyped in house, therefore the presence of additional mutations cannot be excluded. Sanger sequencing of the SOD1 exons could exclude an additional second variant causing the truncated protein. The behaviour of this cell line in all assays, however, was comparable to the behaviour of the other two mutant SOD1 lines analysed.

Subsequently, misfolded SOD1 was evaluated through staining in control and patient cell lines. Interestingly, this experiment showed presence of misfolded SOD1 in the nucleus of sALS patient. In this regard, it has been demonstrated by Tsang et al., that in response to elevated endogenous and exogenous reactive oxygen species (ROS), in yeast cells, SOD1 relocates into the nucleus and could function as a transcription factor, elucidating the regulatory mechanism for its localisation.

The presence of SOD1 was confirmed in the nucleus of human iAstrocytes through cellular fractionation. A complete screen of all the lines confirmed accumulation of higher levels of nuclear SOD1 in sALS and C9orf72, but not SOD1 derived astrocytes.

Since all the major genes associated with ALS encode for proteins involved in RNA binding and transport, we also tested our own hypothesis that SOD1, like most ALS-associated proteins, might bind RNA. However, in our pull-down experiments on total or oxidised RNA, I was unable to detect SOD1 in the RNA-bound fraction, leading to the conclusion that SOD1 does not bind RNA.

Remarkably, total RNA pull-down preliminary data showed a different TDP-35 fragment/TDP-43 full-length protein ratio in SOD1 and C9orf72 patient cell lines. The ratio between TDP-35 and TDP-43 was 4 times higher than the control in C9orf72

samples, while in the SOD1 patient the ratio was the half the level of the control. These findings confirm that the TDP-35 fragment could bind RNA and lead to alteration in RNA metabolism in C9orf72 patients, while SOD1 patients do not display and are not affected by TDP-43 proteinopathy (Robertson et al., 2007; Turner et al., 2008).
Due to technical challenges with chromatin immunoprecipitation, however, I was unable in the timescale of the PhD programme to test the possibility that SOD1 could bind DNA, as suggested by previous studies (Tsang *et al.*, 2014).
In this regard, Barbosa et al. evaluated DNA damage, p53 activity and apoptosis in SH-SY5Y human neuroblastoma cells transfected with wild-type or mutant G93A SOD1. Their experiments, using different techniques, such as Western blot, FACS and confocal microscopy analysis, showed that mutant SOD1 is present in the nucleus in association with DNA. Additionally, G93A SOD1 present in the nucleus has identical superoxide dismutase activity but shows increased peroxidase activity, compared to wild-type SOD1. The authors hypothesised that SOD1 association with DNA might induce DNA damage and trigger the apoptotic response by activating the p53 pathway (Barbosa *et al.*, 2010).
The presence of SOD1 in the nucleus was demonstrated in *in vivo* models as well. Transgenic mice expressing hSOD1-G93A, hSOD1-G37R, and hSOD1-wild-type were used to investigate a new subcellular pathology involving mutant hSOD1 protein localizing to the nuclear compartment. Consistently, Gertz et al., reported a prominent nuclear accumulation of hSOD1-G93A, -G37R and -wild-type in transgenic mice. These data suggest new mechanisms involving hSOD1 accumulation in the cell nucleus and mutant hSOD1-specific perturbations in survival motor neuron protein (SMN) localisation, with disruption of the nuclear SMN complex in the ALS model mice (Gertz, Wong and Martin, 2012). Hence, further investigation should address the role of SOD1 in the nucleus and its link with DNA damage.

Due to our interest in WT misfolded SOD1, I focused on the abnormal and previously unreported accumulation of WT SOD1 in the nucleus of sALS and C9orf72 patients. SOD1 lacks a nuclear localisation sequence, however it might enter the nucleus through co-transport or passive diffusion. Data from my own research (Chapter 3) and the literature show nuclear lamina disruption and nuclear pore degradation occurring with age, indicating that passive protein transport is facilitated with age.

Hence, multiple age-related and pathology-driven mechanisms might be responsible for increased SOD1 nuclear localisation. However, only sALS and C9orf72 iAstrocytes, which do not carry SOD1 mutations, but are affected by the disease, display abnormal protein accumulation. A possible explanation for high levels of nuclear SOD1 in sALS and C9orf72 could be the accumulation of DNA damage or oxidative stress, as we observed in iAstrocytes derived from old donors (Chapter 3). Indeed, a body of evidence reported increased DNA damage and oxidative stress in C9orf72 cases (Lopez-Gonzalez *et al.*, 2016; Farg *et al.*, 2017; Walker *et al.*, 2017; Konopka and Atkin, 2018). Elevated levels of DNA/RNA hybrids (R-loops) and double-strand breaks (DSBs) have been observed in rodent neurons, human cells, and in C9orf72-ALS patient spinal cord tissues. Moreover, high levels of DNA damage are associated with impairment of ATM-mediated DNA repair signalling and accumulation of protein-linked DNA breaks (Walker *et al.*, 2017). This suggests that genomic instability partially drives C9orf72-linked neurodegeneration. Additionally to increased DNA damage, a study reported increased levels of oxidative stress by poly-GR in C9orf72 iPSC derived-neurons in an age-dependent manner (Lopez-Gonzalez *et al.*, 2016). Thus, poly-GR preferentially binding to mitochondrial ribosomal proteins and disrupting mitochondrial function, leading to increased oxidative stress in neurons, represents another pathogenic mechanism in C9orf72-associated ALS.

As regards the sALS cases, various studies have indicated increased oxidative damage and DNA damage (Ferrante *et al.*, 2002; Murata, Ohtsuka and Terayama, 2008; Riancho *et al.*, 2020). However, based on unpublished data from my laboratory, iAstrocytes derived from sALS cases have similar levels of DNA damage and oxidative stress as samples from patients with SOD1 mutations, so higher SOD1 nuclear levels might be not related to an increase increased oxidative damage and DNA damage.

Recently, it has been reported that Chromosomal Maintenance 1 (CRM1) or Exportin 1 (XPO1) recognizes a NES-like sequence that is usually hidden in wild-type SOD1 (Zhong *et al.*, 2017). When SOD1 is misfolded, however, the authors reported that this NES-like domain is revealed and can bind XPO1 for protein export to the cytoplasm. So, disruption of the NES consensus sequence or downregulation of XPO1 would lead to misfolded and mutant SOD1 accumulation to the nucleus (Zhong *et al.*, 2017). Consistently, our data showed that iAstrocytes also express XPO1 and, interestingly,

its level is lower in sALS patient- derived cells compared to controls and the other ALS genotypes assessed in this study. This downregulation of XPO1 could explain the SOD1 accumulation observed in the nucleus of sALS iAstrocytes, as opposed to controls, SOD1 and C9orf72 cases, which all express similar XPO1 levels. Nevertheless, C9orf72, like sALS, iAstrocytes displayed high levels of nuclear SOD1, but not lower levels of XPO1.

Another potential explanation for SOD1 nuclear accumulation could be lack of exposure of the NES-like domain that is recognised by XPO1. To confirm the interaction between SOD1 and XPO1, immunoprecipitation was performed with both wild-type SOD1 and misfolded SOD1 in our astrocytes. In both cases co-immunoprecipitation was observed. To further investigate this interaction, a proximity ligation assay (PLA) was performed, which enabled me to detect the interaction between both wild-type and misfolded SOD1 and XPO1. Interestingly, there was a reduction in the interaction between misfolded SOD1 and XPO1 in sALS and C9orf72 cases, in agreement with the higher SOD1 nuclear levels in these patient subgroups. This decreased interaction observed between wild-type misfolded SOD1 and mutant misfolded SOD1 could be due to a different misfolding/conformation of SOD1 in the presence or absence of mutations.

In conclusion, further studies are required in order to investigate the physiological and pathological relevance of SOD1 nuclear localisation. Importantly, SOD1 misfolding in the nucleus could have important pathological implications and it is still unclear what signals lead to SOD1 nuclear localisation and what functions this protein performs in this cell compartment.

Finally, my results show that wild-type SOD1 and mutant SOD1 are expressed at similar levels in controls and patients, however, they localise in different cellular compartments in ALS patients, with wild-type SOD1 accumulating in the nucleus in sALS and C9orf72 cases, while mutant SOD1 remains mainly cytoplasmic in SOD1 cases. This different localisation might be due to different misfolding conformations that might reduce wild-type SOD1 interaction with XPO1 compared to mutant SOD1, as opposed to what has been shown in overexpressing and stress-driven systems (Zhong *et al.*, 2017). Additionally, XPO1 levels are lower in sALS cases, thus

suggesting another mechanism for misfolded SOD1 accumulation in the nucleus of sALS patients and confirming the important role of nucleocytoplasmic dysregulation in sALS disease in the context of SOD1 misfolding.

5. Discussion

Astrocytes are the largest group of glial cells in the brain, having vital roles in the pathogenesis of ageing and neurodegenerative diseases. Indeed, they are involved in several functions of the brain, such as regulation of synapse formation and pruning, being part of the tripartite synapse, as well as the regulation of neuroinflammation together with microglia. Moreover, astrocytes provide metabolic support to neurons, play a crucial role in the antioxidant response of the CNS and maintain the integrity of the blood brain barrier (Oksanen *et al.*, 2019).

Remarkably, various studies have reported that glial cells, including microglia and astrocytes, are potentially more affected by the ageing process than neurons. In particular, astrocytes present dramatic transcriptional (Soreq *et al.*, 2017) and functional changes during ageing (Gemma *et al.*, 2007; Lynch *et al.*, 2010; Rea *et al.*, 2018), thus affecting their ability to maintain homeostasis in the CNS.

It is well known that ageing is a risk factor for several neurodegenerative diseases, so it is crucial to recapitulate age-related characteristics in human cells that contribute to and are actively involved in diseases. In fact, Alzheimer's disease (AD), Parkinson's disease (PD) and amyotrophic lateral sclerosis (ALS) are three common adult-onset neurodegenerative diseases which demonstrate astrocyte dysfunction (Haidet-Phillips *et al.*, 2011; Meyer *et al.*, 2014; Booth, Hirst and Wade-Martins, 2017; González-Reyes *et al.*, 2017). Moreover, it has been observed that human astrocytes are more complex than their rodents counterparts, thus creating the need for a human astrocytic model (Oberheim *et al.*, 2009).

In this context, human iPSCs are an invaluable model to study the pathogenic mechanisms occurring in neurodegenerative diseases while maintaining physiological expression levels of pathogenic proteins (Ziff and Patani, 2019; Chang *et al.*, 2020). However, they fail in retaining ageing features from the fibroblasts donor.

In this study, this limitation was overcome by performing direct conversion of skin fibroblasts into induced neural progenitor cells, which then allows for the generation of human astrocytes that recapitulate many aspects of ageing that have great relevance

in the context of ALS (Meyer *et al.*, 2014). For example, working with a cell model that reproduces the functional changes characteristic of ageing is likely to have a massive impact on the ability of the model to recapitulate pathological hallmarks related to protein homeostasis, oxidative stress and other pathways affected by age. As a matter of fact, iPSC-derived neurons and astrocytes from ALS patients display a milder pathological phenotype compared to the iAstrocyte model used in this study when assessing TDP-43 proteinopathy and p62 accumulation without the addition of stressors (Seminary, Sison and Ebert, 2018).

In addition, iAstrocytes from older cases exhibited a higher baseline level of ROS and DNA damage compared to young iAstrocytes. Furthermore, when exposed to serum starvation, old iAstrocytes required more time to return to baseline ROS levels. This is likely to be due to the lower levels of both NRF2 and SOD1 in old iAstrocytes compared to young iAstrocytes, both at baseline and following acute stress. Thus, the model used in this study recapitulates the age-related decrease in antioxidant defences reported from *in vivo* studies and, provides an explanation for the increased level of ROS seen in these cells. These low levels of SOD1 in iAstrocytes from older donors are a consistent feature in the age-matched iAstrocytes from ALS patients, where we did not observe any further significant decrease or increase. Interestingly, it is has been widely reported that both fALS and sALS cases display high levels of oxidative stress (Ferrante *et al.*, 2002; Lopez-Gonzalez *et al.*, 2016) and our own unpublished data have confirmed this observation in the ALS iAstrocytes used in this study. Increased levels of ROS would lead to an increase in the anti-oxidant response, hence SOD1, as it was shown in aged healthy iAstrocytes. However, the steady levels of SOD1 in ALS iAstrocytes indicate that patient cells might be unable to upregulate the anti-oxidant response, thus exacerbating this pathophysiological process. On the contrary, rejuvenated ALS models, like iPSCs, might fail to demonstrate an increase in oxidative stress. In fact, a recent study showed oxidative stress and astrocyte toxicity, only after ageing the cells *in vitro* for 80 days (Birger *et al.*, 2019).
Further, it is known that increased oxidative stress, such as toxicity of ROS, contributes to neuroinflammation. In my study, neuronal survival in co-culture decreases in the presence of old Astrocytes after IL-1β treatment. It is known that astrocytes are strictly involved in neuroinflammation, and play a major role in ALS pathogenesis. Our data indicate that inflammation might be one of the factors that, in

association with old age, can lead to neuronal death. Of relevance in this context, it has been seen that partial loss of function of TBK1, a major genetic cause for ALS and FTD, leads to age-dependent neurodegeneration (Xu *et al.*, 2018). TBK1 is a suppressor of RIPK1, that plays a crucial role in mediating neuroinflammation by promoting the activation of microglia and apoptosis (Geng *et al.*, 2017; Xu *et al.*, 2018). Normally, in the ageing human brain RIPK1 is inhibited by phosphorylation by TAK1, that decreases its expression with age. In *Tbk1 +/- mice*, reducing the expression of TAK1 induced all the key features of ALS, including neuroinflammation. Ageing then facilitates RIPK1 activation by reducing TAK1 expression, cooperating with genetic risk factors to promote the disease onset (Xu *et al.*, 2018). This suggests a strong link between ageing and neuroinflammation, leading to the conclusion that is important to preserve this aspect when modelling astrocytes pathophysiology.

Indeed oxidative stress, inflammation and DNA damage all are potential factors leading to SOD1 translocation into the nucleus. Although, as discussed in Chapter 4, further studies are needed in order to determine how specifically SOD1 enters into the nucleus, there is clear evidence that SOD1 has a physiological role in this cellular compartment. A study in peripheral blood mononuclear cells (PBMCs) of sALS and SH-SY5Y cells, in fact, has demonstrated that during oxidative stress SOD1 is phosphorylated by Chk2, guiding its translocation in the nucleus, where SOD1 protects DNA from oxidative damage (Bordoni *et al.*, 2019). However, the function of SOD1 in this compartment also still requires clarification and validation in a more physiological system, where protein levels are physiological.

Another aspect captured from the iAstrocytes is the dysfunction in nucleocytoplasmic transport, an emerging theme in physiological ageing and other related neurodegenerative diseases (Kim and Taylor, 2017). Of relevance in this context, a decrease in the expression of nucleocytoplasmic transporters occurred with age in iAstrocytes. In contrast to the levels of SOD1, where it was not observed any further expression change driven by disease, a significant down-regulation of XPO1 was observed only in sALS derived astrocytes. This might suggest that XPO1 is actually affected at transcriptional or post-transcriptional levels in some sALS cases. So, it would be ideal to test whether reducing or overexpressing XPO1 leads to the same accumulation of SOD1 in the nucleus of sporadic ALS cases.

Moreover, the downregulation of pathways related to protein homeostasis might impact on SOD1 misfolding. So, it would be interesting to test various antibodies against different conformations of misfolded SOD1 and determine if SOD1 misfolds in different ways in different ALS patient genotypes. In particular, it will be important to evaluate SOD1 misfolding in the nuclear compartment, potentially performing fractionation on a native gel. Evidence has demonstrated that protein homeostasis is subject to age-related decline (Koga, Kaushik and Cuervo, 2011; Hipp, Kasturi and Hartl, 2019). Alterations in proteostasis lead to protein misfolding and aggregation, strongly associated with neurodegeneration (Douglas and Dillin, 2010). In the case of SOD1, for example it has been seen how MIF, an ATP-independent protein folding chaperone, inhibits mutant SOD1 misfolding (Israelson *et al.*, 2015). Another important chaperone is Copper Chaperone for SOD1 (CCS). It transiently interacts with SOD1 and promotes its correct maturation by transferring copper and catalysing disulfide bond formation (Luchinat, Barbieri and Banci, 2017). Therefore, an aspect that must be studied in depth is how ageing affects components of proteostasis in old donor derived astrocytes and in ALS astrocytes.

This study presented some limitations, such as the sex ratios of the samples used in the ageing study, but also the number of samples in the patient subgroups, for example in the SOD1 group. Moreover, the use of additional antibodies for SOD1 in Chapter 4 would be beneficial to support our hypothesis and also it will be important to measure the amount of misfolded SOD1 in the nucleus of patient derived astrocytes.

In conclusion, the novelty of my study consists firstly, in the retention of ageing features in a human *in vitro* model of astrocytes. Indeed no study has assessed this aspect yet. Using a rejuvenated model might mask alteration of a lot of these pathways. Hence, iPSCs could be more relevant for the early phases of the disease, rather than the later ones. It was shown the nuclear function of SOD1 can have an important role in disease pathogenesis. In ALS research it is still controversial whether in a human non-overexpressing model wtSOD1 misfolds without adding any additional stressor. Thus, some evidence was added that wtSOD1 does misfold in human iAstrocytes and accumulates in the nucleus of ALS patients that do not carry a *SOD1* mutation. This implies that if SOD1 is misfolded it may not function correctly, may propagate between cells and it may represent a potential therapeutic target.

6. Bibliography

Aasen, T. *et al.* (2008) 'Efficient and rapid generation of induced pluripotent stem cells from human keratinocytes', *Nature Biotechnology*. doi: 10.1038/nbt.1503.

Ajami, B. *et al.* (2011) 'Infiltrating monocytes trigger EAE progression, but do not contribute to the resident microglia pool', *Nature Neuroscience*. doi: 10.1038/nn.2887.

Akoumianaki, T. *et al.* (2009) 'Nucleocytoplasmic shuttling of soluble tubulin in mammalian cells', *Journal of Cell Science*. doi: 10.1242/jcs.043034.

Al-Chalabi, A. (1998) 'Recessive amyotrophic lateral sclerosis families with the D90A SOD1 mutation share a common founder: evidence for a linked protective factor', *Human Molecular Genetics*, 7(13), pp. 2045–2050. doi: 10.1093/hmg/7.13.2045.

Al-Chalabi, A. *et al.* (1999) 'Deletions of the heavy neurofilament subunit tail in amyotrophic lateral sclerosis', *Human Molecular Genetics*. doi: 10.1093/hmg/8.2.157.

Al-Chalabi, A. *et al.* (2012) 'The genetics and neuropathology of amyotrophic lateral sclerosis', *Acta Neuropathologica*. doi: 10.1007/s00401-012-1022-4.

Al-Chalabi, A. *et al.* (2014) 'Analysis of amyotrophic lateral sclerosis as a multistep process: A population-based modelling study', *The Lancet Neurology*. doi: 10.1016/S1474-4422(14)70219-4.

Al-Chalabi, A. and Leigh, P. N. (2005) 'Trouble on the pitch: Are professional football players at increased risk of developing amyotrophic lateral sclerosis?', *Brain*. doi: 10.1093/brain/awh426.

Al-Saif, A., Al-Mohanna, F. and Bohlega, S. (2011) 'A mutation in sigma-1 receptor causes juvenile amyotrophic lateral sclerosis', *Annals of Neurology*. doi: 10.1002/ana.22534.

Alexander, G. M. *et al.* (2004) 'Effect of transgene copy number on survival in the G93A SOD1 transgenic mouse model of ALS', *Molecular Brain Research*. doi: 10.1016/j.molbrainres.2004.07.002.

Alexianu, M. E. *et al.* (2000) 'Ultrastructural evidence of calcium involvement in experimental autoimmune gray matter disease', *Journal of Neuroscience Research*. doi: 10.1002/(SICI)1097-4547(20000401)60:1<98::AID-JNR10>3.0.CO;2-B.

Alexianu, M. E., Kozovska, M. and Appel, S. H. (2001) 'Immune reactivity in a mouse model of familial ALS correlates with disease progression', *Neurology*. doi: 10.1212/WNL.57.7.1282.

Allen, S. P. *et al.* (2019) 'C9orf72 expansion within astrocytes reduces metabolic flexibility in amyotrophic lateral sclerosis', *Brain : a journal of neurology*. NLM (Medline), 142(12), pp. 3771–3790. doi: 10.1093/brain/awz302.

Almad, A. and Maragakis, N. J. (2018) 'A stocked toolbox for understanding the role of astrocytes in disease', *Nature Reviews Neurology*. Nature Publishing Group, pp. 351–362. doi: 10.1038/s41582-018-0010-2.

Alonso, A. *et al.* (2009) 'Incidence and lifetime risk of motor neuron disease in the United Kingdom: A population-based study', *European Journal of Neurology*. doi: 10.1111/j.1468-1331.2009.02586.x.

Andersen, P. M. *et al.* (1996) 'Autosomal recessive adult-onset amyohophic lateral sclerosis associated with homozygosity for Asp90A1a CuZn-superoxide dismutase mutation A clinical and genealogical study of 36 patients', *Brain*. doi: 10.1093/brain/119.4.1153.

Andersen, P. M. and Al-Chalabi, A. (2011) 'Clinical genetics of amyotrophic lateral sclerosis: What do we really know?', *Nature Reviews Neurology*. doi: 10.1038/nrneurol.2011.150.

Antonyuk, S. *et al.* (2005) 'Structural consequences of the familial amyotrophic lateral sclerosis SOD1 mutant His46Arg', *Protein Science*. doi: 10.1110/ps.041256705.

Appel, S. H., Beers, D. R. and Henkel, J. S. (2010) 'T cell-microglial dialogue in Parkinson's disease and amyotrophic lateral sclerosis: are we listening?', *Trends in Immunology*. doi: 10.1016/j.it.2009.09.003.

Arai, T. *et al.* (2006) 'TDP-43 is a component of ubiquitin-positive tau-negative inclusions in frontotemporal lobar degeneration and amyotrophic lateral sclerosis', *Biochemical and Biophysical Research Communications*. doi: 10.1016/j.bbrc.2006.10.093.

Ash, P. E. A. *et al.* (2013) 'Unconventional Translation of C9ORF72 GGGGCC Expansion Generates Insoluble Polypeptides Specific to c9FTD/ALS', *Neuron*. doi: 10.1016/j.neuron.2013.02.004.

Ayala, Y. M. *et al.* (2008) 'Structural determinants of the cellular localization and shuttling of TDP-43', *Journal of Cell Science*. doi: 10.1242/jcs.038950.

Ayers, J. I. *et al.* (2014) 'Experimental transmissibility of mutant SOD1 motor neuron disease', *Acta Neuropathologica*. doi: 10.1007/s00401-014-1342-7.

Ayers, J. I. *et al.* (2016) 'Distinct conformers of transmissible misfolded SOD1 distinguish human SOD1-FALS from other forms of familial and sporadic ALS', *Acta*

Neuropathologica. doi: 10.1007/s00401-016-1623-4.

Banati, R. B. *et al.* (1993) 'Cytotoxicity of microglia', *Glia*. doi: 10.1002/glia.440070117.

Banci, L. *et al.* (2008) 'SOD1 and amyotrophic lateral sclerosis: Mutations and oligomerization', *PLoS ONE*. doi: 10.1371/journal.pone.0001677.

Baradaran-Heravi, Y., Van Broeckhoven, C. and van der Zee, J. (2020) 'Stress granule mediated protein aggregation and underlying gene defects in the FTD-ALS spectrum', *Neurobiology of Disease*. Elsevier, 134(January 2019), p. 104639. doi: 10.1016/j.nbd.2019.104639.

Barber, S. C., Mead, R. J. and Shaw, P. J. (2006) 'Oxidative stress in ALS: A mechanism of neurodegeneration and a therapeutic target', *Biochimica et Biophysica Acta - Molecular Basis of Disease*, pp. 1051–1067. doi: 10.1016/j.bbadis.2006.03.008.

Barber, S. C. and Shaw, P. J. (2010) 'Oxidative stress in ALS: Key role in motor neuron injury and therapeutic target', *Free Radical Biology and Medicine*. doi: 10.1016/j.freeradbiomed.2009.11.018.

Barbosa, L. F. *et al.* (2010) 'Increased SOD1 association with chromatin, DNA damage, p53 activation, and apoptosis in a cellular model of SOD1-linked ALS', *Biochimica et Biophysica Acta - Molecular Basis of Disease*. doi: 10.1016/j.bbadis.2010.01.011.

Barker, H. V. *et al.* (2017) 'RNA misprocessing in C9orf72-linked neurodegeneration', *Frontiers in Cellular Neuroscience*. doi: 10.3389/fncel.2017.00195.

Beers, D. R. *et al.* (2001) 'Parvalbumin overexpression alters immune-mediated increases in intracellular calcium, and delays disease onset in a transgenic model of familial amyotrophic lateral sclerosis', *Journal of Neurochemistry*. doi: 10.1046/j.1471-4159.2001.00582.x.

Beers, D. R. *et al.* (2006) 'Wild-type microglia extend survival in PU.1 knockout mice with familial amyotrophic lateral sclerosis', *Proceedings of the National Academy of Sciences of the United States of America*. doi: 10.1073/pnas.0607423103.

Beers, D. R. *et al.* (2011) 'Endogenous regulatory T lymphocytes ameliorate amyotrophic lateral sclerosis in mice and correlate with disease progression in patients with amyotrophic lateral sclerosis', *Brain*. doi: 10.1093/brain/awr074.

Beghi, E. *et al.* (2011) 'The epidemiology and treatment of ALS: Focus on the heterogeneity of the disease and critical appraisal of therapeutic trials', *Amyotrophic Lateral Sclerosis*. doi: 10.3109/17482968.2010.502940.

Beghi, E. and Morrison, K. E. (2005) 'ALS and military service', *Neurology*. doi:

10.1212/01.WNL.0000150535.90358.2D.

Bell, K. F. *et al.* (2011) 'Mild oxidative stress activates Nrf2 in astrocytes, which contributes to neuroprotective ischemic preconditioning', *Proceedings of the National Academy of Sciences*. Proceedings of the National Academy of Sciences, 108(1), pp. E1–E2. doi: 10.1073/pnas.1015229108.

Bell, K. F. S. *et al.* (2015) 'Neuronal development is promoted by weakened intrinsic antioxidant defences due to epigenetic repression of Nrf2', *Nature Communications*. doi: 10.1038/ncomms8066.

Bellaver, B. *et al.* (2017) 'Hippocampal Astrocyte Cultures from Adult and Aged Rats Reproduce Changes in Glial Functionality Observed in the Aging Brain', *Molecular Neurobiology*. Springer US, 54(4), pp. 2969–2985. doi: 10.1007/s12035-016-9880-8.

Belli, S. and Vanacore, N. (2005) 'Proportionate mortality of Italian soccer players: Is amyotrophic lateral sclerosis an occupational disease?', *European Journal of Epidemiology*. doi: 10.1007/s10654-004-6879-7.

Bellingham, M. C. (2011) 'A Review of the Neural Mechanisms of Action and Clinical Efficiency of Riluzole in Treating Amyotrophic Lateral Sclerosis: What have we Learned in the Last Decade?', *CNS Neuroscience and Therapeutics*. doi: 10.1111/j.1755-5949.2009.00116.x.

Benatar, M. (2007) 'Lost in translation: Treatment trials in the SOD1 mouse and in human ALS', *Neurobiology of Disease*. doi: 10.1016/j.nbd.2006.12.015.

Bendotti, C. *et al.* (2004) 'Activated p38MAPK Is a Novel Component of the Intracellular Inclusions Found in Human Amyotrophic Lateral Sclerosis and Mutant SOD1 Transgenic Mice', *Journal of Neuropathology and Experimental Neurology*. doi: 10.1093/jnen/63.2.113.

Bilican, B. *et al.* (2012) 'Mutant induced pluripotent stem cell lines recapitulate aspects of TDP-43 proteinopathies and reveal cell-specific vulnerability', *Proceedings of the National Academy of Sciences of the United States of America*. doi: 10.1073/pnas.1202922109.

Birger, A. *et al.* (2019) 'Human iPSC-derived astrocytes from ALS patients with mutated C9ORF72 show increased oxidative stress and neurotoxicity', *EBioMedicine*. doi: 10.1016/j.ebiom.2019.11.026.

Blasko, I. *et al.* (2000) 'Costimulatory effects of interferon-β and interleukin-1β or tumor necrosis factor α on the synthesis of Aβ1-40 and Aβ1-42 by human astrocytes', *Neurobiology of Disease*. doi: 10.1006/nbdi.2000.0321.

Blitterswijk, M. Van and Landers, J. E. (2010) 'RNA processing pathways in amyotrophic lateral sclerosis', *Neurogenetics*. doi: 10.1007/s10048-010-0239-4.

Boczonadi, V. *et al.* (2018) 'Mutations in glycyl-tRNA synthetase impair mitochondrial metabolism in neurons.', *Human molecular genetics*, 27(12), pp. 2187–2204. doi: 10.1093/hmg/ddy127.

Boeynaems, S. *et al.* (2016) 'Drosophila screen connects nuclear transport genes to DPR pathology in c9ALS/FTD', *Scientific Reports*. doi: 10.1038/srep20877.

Boillée, S. *et al.* (2006) 'Onset and progression in inherited ALS determined by motor neurons and microglia', *Science*. doi: 10.1126/science.1123511.

Boillée, S., Vande Velde, C. and Cleveland, D. W. W. (2006) 'ALS: A Disease of Motor Neurons and Their Nonneuronal Neighbors', *Neuron*. doi: 10.1016/j.neuron.2006.09.018.

Boisvert, M. M. *et al.* (2018) 'The Aging Astrocyte Transcriptome from Multiple Regions of the Mouse Brain', *Cell Reports*. doi: 10.1016/j.celrep.2017.12.039.

Booth, H. D. E., Hirst, W. D. and Wade-Martins, R. (2017) 'The Role of Astrocyte Dysfunction in Parkinson's Disease Pathogenesis.', *Trends in neurosciences*. Elsevier, 40(6), pp. 358–370. doi: 10.1016/j.tins.2017.04.001.

Borchelt, D. R. *et al.* (1998) 'Axonal transport of mutant superoxide dismutase 1 and focal axonal abnormalities in the proximal axons of transgenic mice', *Neurobiology of Disease*. doi: 10.1006/nbdi.1998.0178.

Bordoni, M. *et al.* (2019) 'Nuclear Phospho-SOD1 Protects DNA from Oxidative Stress Damage in Amyotrophic Lateral Sclerosis', *Journal of Clinical Medicine*. doi: 10.3390/jcm8050729.

Borthwick, G. M. *et al.* (1999) 'Mitochondrial enzyme activity in amyotrophic lateral sclerosis: Implications for the role of mitochondria in neuronal cell death', *Annals of Neurology*. doi: 10.1002/1531-8249(199911)46:5<787::AID-ANA17>3.0.CO;2-8.

Bosco, D. A., Lemay, N., *et al.* (2010) 'Mutant FUS proteins that cause amyotrophic lateral sclerosis incorporate into stress granules', *Human Molecular Genetics*. doi: 10.1093/hmg/ddq335.

Bosco, D. A., Morfini, G., *et al.* (2010) 'Wild-type and mutant SOD1 share an aberrant conformation and a common pathogenic pathway in ALS', *Nature Neuroscience*. doi: 10.1038/nn.2660.

Boylan, K. *et al.* (2009) 'Immunoreactivity of the phosphorylated axonal neurofilament H subunit (pNF-H) in blood of ALS model rodents and ALS patients: Evaluation of

blood pNF-H as a potential ALS biomarker', *Journal of Neurochemistry*. doi: 10.1111/j.1471-4159.2009.06386.x.

Boylan, K. (2015) 'Familial Amyotrophic Lateral Sclerosis', *Neurologic Clinics*. doi: 10.1016/j.ncl.2015.07.001.

Brandes, N. *et al.* (2013) 'Time line of redox events in aging postmitotic cells', *eLife*. doi: 10.7554/eLife.00306.

Brandt, A., Krohne, G. and Grohans, J. (2008) 'The farnesylated nuclear proteins KUGELKERN and LAMIN B promote aging-like phenotypes in *Drosophila* flies', *Aging Cell*, 7(4), pp. 541–551. doi: 10.1111/j.1474-9726.2008.00406.x.

Brawek, B. *et al.* (2010) 'Reactive oxygen species (ROS) in the human neocortex: Role of aging and cognition', *Brain Research Bulletin*. Elsevier, 81(4–5), pp. 484–490. doi: 10.1016/J.BRAINRESBULL.2009.10.011.

Brotherton, T. E., Li, Y. and Glass, J. D. (2013) 'Cellular toxicity of mutant SOD1 protein is linked to an easily soluble, non-aggregated form in vitro', *Neurobiology of Disease*. doi: 10.1016/j.nbd.2012.08.010.

Bruijn, L. I. *et al.* (1997) 'ALS-linked SOD1 mutant G85R mediates damage to astrocytes and promotes rapidly progressive disease with SOD1-containing inclusions', *Neuron*. doi: 10.1016/S0896-6273(00)80272-X.

Bruijn, L. I., Miller, T. M. and Cleveland, D. W. (2004) 'UNRAVELING THE MECHANISMS INVOLVED IN MOTOR NEURON DEGENERATION IN ALS', *Annual Review of Neuroscience*. doi: 10.1146/annurev.neuro.27.070203.144244.

Burda, J. E. and Sofroniew, M. V. (2014) 'Reactive gliosis and the multicellular response to CNS damage and disease', *Neuron*, pp. 229–248. doi: 10.1016/j.neuron.2013.12.034.

Canals, I. *et al.* (2018) 'Rapid and efficient induction of functional astrocytes from human pluripotent stem cells', *Nature Methods*, 16(1), pp. 134–134. doi: 10.1038/s41592-018-0264-z.

Carrì, M. T., Grignaschi, G. and Bendotti, C. (2006) 'Targets in ALS: designing multidrug therapies', *Trends in Pharmacological Sciences*. doi: 10.1016/j.tips.2006.03.009.

Carter, C. D. *et al.* (2005) 'Loss of SOD1 and LYS7 Sensitizes Saccharomyces cerevisiae to Hydroxyurea and DNA Damage Agents and Downregulates MEC1 Pathway Effectors', *Molecular and Cellular Biology*. doi: 10.1128/mcb.25.23.10273-10285.2005.

Casoni, F. *et al.* (2005) 'Protein Nitration in a Mouse Model of Familial Amyotrophic Lateral Sclerosis', *Journal of Biological Chemistry*. doi: 10.1074/jbc.m413111200.

Cautain, B. *et al.* (2015) 'Components and regulation of nuclear transport processes', *FEBS Journal*. doi: 10.1111/febs.13163.

Chai, M. and Kohyama, J. (2019) 'Non-Cell-Autonomous Neurotoxicity in Parkinson's Disease Mediated by Astroglial α-Synuclein', *Stem Cell Reports*, 12(2), pp. 183–185. doi: 10.1016/j.stemcr.2019.01.011.

Chan, W. M. *et al.* (2011a) 'Expanded polyglutamine domain possesses nuclear export activity which modulates subcellular localization and toxicity of polyQ disease protein via exportin-1', *Human Molecular Genetics*. doi: 10.1093/hmg/ddr049.

Chan, W. M. *et al.* (2011b) 'Expanded polyglutamine domain possesses nuclear export activity which modulates subcellular localization and toxicity of polyQ disease protein via exportin-1', *Human Molecular Genetics*, 20(9), pp. 1738–1750. doi: 10.1093/hmg/ddr049.

Chang, C. Y. *et al.* (2020) 'Induced pluripotent stem cell (iPSC)-based neurodegenerative disease models for phenotype recapitulation and drug screening', *Molecules*. MDPI AG. doi: 10.3390/molecules25082000.

Chang, L. Y. *et al.* (1988) 'Molecular immunocytochemistry of the CuZn superoxide dismutase in rat hepatocytes', *Journal of Cell Biology*. The Rockefeller University Press, 107(6 I), pp. 2169–2179. doi: 10.1083/jcb.107.6.2169.

Che, M. X. *et al.* (2011) 'Aggregation of the 35-kDa fragment of TDP-43 causes formation of cytoplasmic inclusions and alteration of RNA processing', *FASEB Journal*. doi: 10.1096/fj.10-174482.

Chen, H.-J. *et al.* (2010) 'Characterisation of the properties of a novel mutation in VAPB in familial ALS', *The Journal of biological chemistry*.

Chen, H. *et al.* (2014) 'Modeling ALS with iPSCs reveals that mutant SOD1 misregulates neurofilament balance in motor neurons', *Cell Stem Cell*. doi: 10.1016/j.stem.2014.02.004.

Chen, S. *et al.* (2013) 'Genetics of amyotrophic lateral sclerosis: An update', *Molecular Neurodegeneration*. doi: 10.1186/1750-1326-8-28.

Chen, Y. and Cohen, T. J. (2019) 'Aggregation of the nucleic acid– binding protein TDP-43 occurs via distinct routes that are coordinated with stress granule formation', *Journal of Biological Chemistry*. doi: 10.1074/jbc.RA118.006351.

Cheroni, C. *et al.* (2005) 'Accumulation of human SOD1 and ubiquitinated deposits in

the spinal cord of SOD1G93A mice during motor neuron disease progression correlates with a decrease of proteasome', *Neurobiology of Disease*. doi: 10.1016/j.nbd.2004.12.007.

Cheroni, C. *et al.* (2009) 'Functional alterations of the ubiquitin-proteasome system in motor neurons of a mouse model of familial amyotrophic lateral sclerosis', *Human Molecular Genetics*. doi: 10.1093/hmg/ddn319.

Chia, R. *et al.* (2010) 'Superoxide dismutase 1 and tgSOD1G93A mouse spinal cord seed fibrils, suggesting a propagative cell death mechanism in amyotrophic lateral sclerosis', *PLoS ONE*. doi: 10.1371/journal.pone.0010627.

Chiò, A. *et al.* (2005) 'Severely increased risk of amyotrophic lateral sclerosis among Italian professional football players', *Brain*. doi: 10.1093/brain/awh373.

Chiò, A. *et al.* (2008) 'Prevalence of SOD1 mutations in the Italian ALS population', *Neurology*. doi: 10.1212/01.wnl.0000299187.90432.3f.

Chiò, A. *et al.* (2009) 'Prognostic factors in ALS: A critical review', *Amyotrophic Lateral Sclerosis*. doi: 10.3109/17482960802566824.

Chiò, A. *et al.* (2013) 'Global epidemiology of amyotrophic lateral sclerosis: A systematic review of the published literature', *Neuroepidemiology*. doi: 10.1159/000351153.

Choi, J. *et al.* (2005) 'Oxidative modifications and aggregation of Cu,Zn-superoxide dismutase associated with alzheimer and Parkinson diseases', *Journal of Biological Chemistry*. doi: 10.1074/jbc.M414327200.

Chou, C.-C. *et al.* (2018) 'TDP-43 pathology disrupts nuclear pore complexes and nucleocytoplasmic transport in ALS/FTD', *Nature Neuroscience*, 21(2), pp. 228–239. doi: 10.1038/s41593-017-0047-3.

Chow, C. Y. *et al.* (2009) 'Deleterious Variants of FIG4, a Phosphoinositide Phosphatase, in Patients with ALS', *American Journal of Human Genetics*. doi: 10.1016/j.ajhg.2008.12.010.

Clarke, L. E. *et al.* (2018) 'Normal aging induces A1-like astrocyte reactivity.', *Proceedings of the National Academy of Sciences of the United States of America*. National Academy of Sciences, 115(8), pp. E1896–E1905. doi: 10.1073/pnas.1800165115.

Cleveland, D. W. and Liu, J. (2000) 'Oxidation versus aggregation - How do SOD1 mutants cause ALS?', *Nature Medicine*. doi: 10.1038/82122.

Colombo, M., Raposo, G. and Théry, C. (2014) 'Biogenesis, secretion, and

intercellular interactions of exosomes and other extracellular vesicles', *Annual review of cell and developmental biology*. doi: 10.1146/annurev-cellbio-101512-122326.
Corcia, P. *et al.* (2002) 'Abnormal SMN1 gene copy number is a susceptibility factor for amyotrophic lateral sclerosis', *Annals of Neurology*. doi: 10.1002/ana.10104.
Corcia, P. *et al.* (2012) 'Molecular Imaging of Microglial Activation in Amyotrophic Lateral Sclerosis', *PLoS ONE*. doi: 10.1371/journal.pone.0052941.
Couillard-Després, S. *et al.* (1998) 'Protective effect of neurofilament heavy gene overexpression in motor neuron disease induced by mutant superoxide dismutase', *Proceedings of the National Academy of Sciences of the United States of America*. doi: 10.1073/pnas.95.16.9626.
Cox, L. E. *et al.* (2010) 'Mutations in CHMP2B in lower motor neuron predominant amyotrophic lateral sclerosis (ALS)', *PLoS ONE*. doi: 10.1371/journal.pone.0009872.
Crapo, J. D. *et al.* (1992) 'Copper,zinc superoxide dismutase is primarily a cytosolic protein in human cells', *Proceedings of the National Academy of Sciences of the United States of America*. doi: 10.1073/pnas.89.21.10405.
Crosio, C. *et al.* (2011) 'Astroglial inhibition of NF-κb does not ameliorate disease onset and progression in a mouse model for amyotrophic lateral sclerosis (ALS)', *PLoS ONE*. doi: 10.1371/journal.pone.0017187.
Crow, J. P. *et al.* (2002) 'Superoxide Dismutase Catalyzes Nitration of Tyrosines by Peroxynitrite in the Rod and Head Domains of Neurofilament-L', *Journal of Neurochemistry*. doi: 10.1046/j.1471-4159.1997.69051945.x.
Cudkowicz, M., Qureshi, M. and Shefner, J. (2004) 'Measures and Markers in Amyotrophic Lateral Sclerosis', *NeuroRx*, 1(2), pp. 273–283. doi: 10.1602/neurorx.1.2.273.
D'Angelo, M. A. *et al.* (2009) 'Age-Dependent Deterioration of Nuclear Pore Complexes Causes a Loss of Nuclear Integrity in Postmitotic Cells', *Cell*, 136(2), pp. 284–295. doi: 10.1016/j.cell.2008.11.037.
Dal Canto, M. C. and Gurney, M. E. (1994) 'Development of central nervous system pathology in a murine transgenic model of human amyotrophic lateral sclerosis', *American Journal of Pathology*.
Van Damme, P., Robberecht, W. and Van Den Bosch, L. (2017) 'Modelling amyotrophic lateral sclerosis: Progress and possibilities', *DMM Disease Models and Mechanisms*. Company of Biologists Ltd, pp. 537–549. doi: 10.1242/dmm.029058.
Daoud, H. *et al.* (2012) 'Exome sequencing reveals SPG11 mutations causing juvenile

ALS', *Neurobiology of Aging*. Elsevier Inc., 33(4), pp. 839.e5-839.e9. doi: 10.1016/j.neurobiolaging.2011.11.012.

DeJesus-Hernandez, M. *et al.* (2011) 'Expanded GGGGCC Hexanucleotide Repeat in Noncoding Region of C9ORF72 Causes Chromosome 9p-Linked FTD and ALS', *Neuron*. doi: 10.1016/j.neuron.2011.09.011.

Deng, H. X. *et al.* (1993) 'Amyotrophic lateral sclerosis and structural defects in Cu,Zn superoxide dismutase', *Science*. doi: 10.1126/science.8351519.

Deng, H. X. *et al.* (2011) 'Mutations in UBQLN2 cause dominant X-linked juvenile and adult-onset ALS and ALS/dementia', *Nature*. doi: 10.1038/nature10353.

Dimos, J. T. *et al.* (2008) 'Induced pluripotent stem cells generated from patients with ALS can be differentiated into motor neurons', *Science*. doi: 10.1126/science.1158799.

Dobrowolny, G. *et al.* (2008) 'Skeletal Muscle Is a Primary Target of SOD1G93A-Mediated Toxicity', *Cell Metabolism*. doi: 10.1016/j.cmet.2008.09.002.

di Domenico, A. *et al.* (2019) 'Patient-Specific iPSC-Derived Astrocytes Contribute to Non-Cell-Autonomous Neurodegeneration in Parkinson's Disease', *Stem Cell Reports*, 12(2), pp. 213–229. doi: 10.1016/j.stemcr.2018.12.011.

Dong, X. *et al.* (2009) 'Structural basis for leucine-rich nuclear export signal recognition by CRM1', *Nature*. doi: 10.1038/nature07975.

Dormann, D. *et al.* (2010) 'ALS-associated fused in sarcoma (FUS) mutations disrupt transportin-mediated nuclear import', *EMBO Journal*. doi: 10.1038/emboj.2010.143.

Douglas, P. M. and Dillin, A. (2010) 'Protein homeostasis and aging in neurodegeneration', *Journal of Cell Biology*. doi: 10.1083/jcb.201005144.

Du, Z. W. *et al.* (2015) 'Generation and expansion of highly pure motor neuron progenitors from human pluripotent stem cells', *Nature Communications*. doi: 10.1038/ncomms7626.

Duan, W. *et al.* (2009) 'Nrf2 activity is lost in the spinal cord and its astrocytes of aged mice.', *In vitro cellular & developmental biology. Animal*, 45(7), pp. 388–397. doi: 10.1007/s11626-009-9194-5.

Durafourt, B. A. *et al.* (2012) 'Comparison of polarization properties of human adult microglia and blood-derived macrophages', *GLIA*. doi: 10.1002/glia.22298.

Ederle, H. *et al.* (2018) 'Nuclear egress of TDP-43 and FUS occurs independently of Exportin-1/CRM1', *Scientific Reports*, 8(1), pp. 1–18. doi: 10.1038/s41598-018-25007-5.

Eftekharzadeh, B. *et al.* (2018) 'Tau Protein Disrupts Nucleocytoplasmic Transport in Alzheimer's Disease.', *Neuron*. NIH Public Access, 99(5), pp. 925-940.e7. doi: 10.1016/j.neuron.2018.07.039.

Egawa, N. *et al.* (2012) 'Drug screening for ALS using patient-specific induced pluripotent stem cells', *Science Translational Medicine*. doi: 10.1126/scitranslmed.3004052.

Eisen, A. *et al.* (1993) 'Duration of amyotrophic lateral sclerosis is age dependent', *Muscle & Nerve*, 16(1), pp. 27–32. doi: 10.1002/mus.880160107.

Elden, A. C. *et al.* (2010) 'Ataxin-2 intermediate-length polyglutamine expansions are associated with increased risk for ALS', *Nature*. doi: 10.1038/nature09320.

Endo, F., Komine, O. and Yamanaka, K. (2016) 'Neuroinflammation in motor neuron disease', *Clinical and Experimental Neuroimmunology*. doi: 10.1111/cen3.12309.

Eun, J. Y. *et al.* (2009) 'Intracellular amyloid beta interacts with SOD1 and impairs the enzymatic activity of SOD1: Implications for the pathogenesis of amyotrophic lateral sclerosis', *Experimental and Molecular Medicine*. doi: 10.3858/emm.2009.41.9.067.

Ezzi, S. A., Urushitani, M. and Julien, J. P. (2007) 'Wild-type superoxide dismutase acquires binding and toxic properties of ALS-linked mutant forms through oxidation', *Journal of Neurochemistry*. doi: 10.1111/j.1471-4159.2007.04531.x.

Fallini, C. *et al.* (2020) 'Traffic jam at the nuclear pore: All roads lead to nucleocytoplasmic transport defects in ALS/FTD', *Neurobiology of Disease*. Academic Press Inc., p. 104835. doi: 10.1016/j.nbd.2020.104835.

Farg, M. A. *et al.* (2014) 'C9ORF72, implicated in amytrophic lateral sclerosis and frontotemporal dementia, regulates endosomal trafficking', *Human Molecular Genetics*. doi: 10.1093/hmg/ddu068.

Farg, M. A. *et al.* (2017) 'The DNA damage response (DDR) is induced by the C9orf72 repeat expansion in amyotrophic lateral sclerosis', *Human Molecular Genetics*. doi: 10.1093/hmg/ddx170.

Fasching, C. L. (2018) 'Telomere length measurement as a clinical biomarker of aging and disease', *Critical Reviews in Clinical Laboratory Sciences*, 55(7), pp. 443–465. doi: 10.1080/10408363.2018.1504274.

Fecto, F. *et al.* (2011) 'SQSTM1 mutations in familial and sporadic amyotrophic lateral sclerosis', *Archives of Neurology*. doi: 10.1001/archneurol.2011.250.

Ferraiuolo, L. *et al.* (2007) 'Microarray analysis of the cellular pathways involved in the adaptation to and progression of motor neuron injury in the SOD1 G93A mouse model

of familial ALS', *Journal of Neuroscience*. J Neurosci, 27(34), pp. 9201–9219. doi: 10.1523/JNEUROSCI.1470-07.2007.

Ferraiuolo, L. *et al.* (2011) 'Molecular pathways of motor neuron injury in amyotrophic lateral sclerosis', *Nature Reviews Neurology*. doi: 10.1038/nrneurol.2011.152.

Ferraiuolo, L. *et al.* (2016) 'Oligodendrocytes contribute to motor neuron death in ALS via SOD1-dependent mechanism', *Proceedings of the National Academy of Sciences of the United States of America*. National Academy of Sciences, 113(42), pp. E6496–E6505. doi: 10.1073/pnas.1607496113.

Ferrante, R. J. *et al.* (2002) 'Evidence of Increased Oxidative Damage in Both Sporadic and Familial Amyotrophic Lateral Sclerosis', *Journal of Neurochemistry*. doi: 10.1046/j.1471-4159.1997.69052064.x.

Ferreira, P. A. (2019) 'The coming-of-age of nucleocytoplasmic transport in motor neuron disease and neurodegeneration', *Cellular and Molecular Life Sciences*. Springer International Publishing, 76(12), pp. 2247–2273. doi: 10.1007/s00018-019-03029-0.

Ferri, A. *et al.* (2006) 'Familial ALS-superoxide dismutases associate with mitochondria and shift their redox potentials', *Proceedings of the National Academy of Sciences of the United States of America*. doi: 10.1073/pnas.0605814103.

Figlewicz, D. A. *et al.* (1994) 'Variants of the heavy neurofilament subunit are associated with the development of amyotrophic lateral sclerosis', *Human Molecular Genetics*. doi: 10.1093/hmg/3.10.1757.

Forsberg, K. *et al.* (2010) 'Novel antibodies reveal inclusions containing non-native SOD1 in sporadic ALS patients', *PLoS ONE*. doi: 10.1371/journal.pone.0011552.

Forsberg, K. *et al.* (2011) 'Glial nuclear aggregates of superoxide dismutase-1 are regularly present in patients with amyotrophic lateral sclerosis', *Acta Neuropathologica*. Springer, 121(5), pp. 623–634. doi: 10.1007/s00401-011-0805-3.

Forsberg, K. *et al.* (2019) 'Misfolded SOD1 inclusions in patients with mutations in C9orf72 and other ALS/FTD-associated genes', *Journal of Neurology, Neurosurgery and Psychiatry*. BMJ Publishing Group. doi: 10.1136/jnnp-2018-319386.

Foust, K. D. *et al.* (2013) 'Therapeutic AAV9-mediated suppression of mutant SOD1 slows disease progression and extends survival in models of inherited ALS', *Molecular Therapy*. doi: 10.1038/mt.2013.211.

Frakes, A. E. *et al.* (2014) 'Microglia induce motor neuron death via the classical NF-κB pathway in amyotrophic lateral sclerosis', *Neuron*. doi:

10.1016/j.neuron.2014.01.013.
Freibaum, B. D. *et al.* (2015) 'GGGGCC repeat expansion in C9orf72 compromises nucleocytoplasmic transport', *Nature*. doi: 10.1038/nature14974.
Freischmidt, A. *et al.* (2015) 'Haploinsufficiency of TBK1 causes familial ALS and fronto-temporal dementia', *Nature Neuroscience*. doi: 10.1038/nn.4000.
Fujisawa, T. *et al.* (2012) 'A novel monoclonal antibody reveals a conformational alteration shared by amyotrophic lateral sclerosis-linked SOD1 mutants', *Annals of Neurology*. doi: 10.1002/ana.23668.
Furukawa, Y. and O'Halloran, T. V. (2005) 'Amyotrophic lateral sclerosis mutations have the greatest destabilizing effect on the apo- and reduced form of SOD1, leading to unfolding and oxidative aggregation', *Journal of Biological Chemistry*. doi: 10.1074/jbc.M500482200.
Gal, J. *et al.* (2009) 'Sequestosome 1/p62 links familial ALS mutant SOD1 to LC3 via an ubiquitin-independent mechanism', *Journal of Neurochemistry*. doi: 10.1111/j.1471-4159.2009.06388.x.
Gal, J. *et al.* (2011) 'Nuclear localization sequence of FUS and induction of stress granules by ALS mutants', *Neurobiology of Aging*. doi: 10.1016/j.neurobiolaging.2010.06.010.
Gasset-Rosa, F. *et al.* (2017) 'Polyglutamine-Expanded Huntingtin Exacerbates Age-Related Disruption of Nuclear Integrity and Nucleocytoplasmic Transport', *Neuron*. doi: 10.1016/j.neuron.2017.03.027.
Gasset-Rosa, F. *et al.* (2019) 'Cytoplasmic TDP-43 De-mixing Independent of Stress Granules Drives Inhibition of Nuclear Import, Loss of Nuclear TDP-43, and Cell Death', *Neuron*. doi: 10.1016/j.neuron.2019.02.038.
Gemma, C. *et al.* (2007) *Oxidative Stress and the Aging Brain: From Theory to Prevention*, *Brain Aging: Models, Methods, and Mechanisms*. Available at: http://www.ncbi.nlm.nih.gov/pubmed/21204345 (Accessed: 24 October 2019).
Gendron, T. F. *et al.* (2013) 'Antisense transcripts of the expanded C9ORF72 hexanucleotide repeat form nuclear RNA foci and undergo repeat-associated non-ATG translation in c9FTD/ALS', *Acta Neuropathologica*. doi: 10.1007/s00401-013-1192-8.
Geng, J. *et al.* (2017) 'Regulation of RIPK1 activation by TAK1-mediated phosphorylation dictates apoptosis and necroptosis', *Nature Communications*. doi: 10.1038/s41467-017-00406-w.

Gertz, B., Wong, M. and Martin, L. J. (2012) 'Nuclear localization of human SOD1 and mutant SOD1-specific disruption of survival motor neuron protein complex in transgenic amyotrophic lateral sclerosis mice', *Journal of Neuropathology and Experimental Neurology*. doi: 10.1097/NEN.0b013e318244b635.

Ghosh, S. and Zhou, Z. (2014) 'Genetics of aging, progeria and lamin disorders', *Current Opinion in Genetics and Development*. doi: 10.1016/j.gde.2014.05.003.

Giampetruzzi, A. *et al.* (2019) 'Modulation of actin polymerization affects nucleocytoplasmic transport in multiple forms of amyotrophic lateral sclerosis', *Nature Communications*. doi: 10.1038/s41467-019-11837-y.

Giordana, M. T. *et al.* (2010) 'TDP-43 redistribution is an early event in sporadic amyotrophic lateral sclerosis', *Brain Pathology*. doi: 10.1111/j.1750-3639.2009.00284.x.

Di Giorgio, F. P. *et al.* (2008) 'Human Embryonic Stem Cell-Derived Motor Neurons Are Sensitive to the Toxic Effect of Glial Cells Carrying an ALS-Causing Mutation', *Cell Stem Cell*. doi: 10.1016/j.stem.2008.09.017.

Gkogkas, C. *et al.* (2008) 'VAPB interacts with and modulates the activity of ATF6', *Human Molecular Genetics*. doi: 10.1093/hmg/ddn040.

Godin, L. M. *et al.* (2016) 'Decreased Laminin Expression by Human Lung Epithelial Cells and Fibroblasts Cultured in Acellular Lung Scaffolds from Aged Mice', *PLOS ONE*. Edited by S. Garantziotis. Public Library of Science, 11(3), p. e0150966. doi: 10.1371/journal.pone.0150966.

González-Reyes, R. E. *et al.* (2017) 'Involvement of Astrocytes in Alzheimer's Disease from a Neuroinflammatory and Oxidative Stress Perspective.', *Frontiers in Molecular Neuroscience*. Frontiers Media SA, 10, p. 427. doi: 10.3389/fnmol.2017.00427.

Gonzalo, S., Kreienkamp, R. and Askjaer, P. (2017) 'Hutchinson-Gilford Progeria Syndrome: A premature aging disease caused by LMNA gene mutations', *Ageing Research Reviews*. doi: 10.1016/j.arr.2016.06.007.

Gordon, S. (2003) 'Alternative activation of macrophages', *Nature Reviews Immunology*. doi: 10.1038/nri978.

Görlich, D. *et al.* (1997) 'A novel class of RanGTP binding proteins', *Journal of Cell Biology*. doi: 10.1083/jcb.138.1.65.

Gowing, G. *et al.* (2008) 'Ablation of proliferating microglia does not affect motor neuron degeneration in amyotrophic lateral sclerosis caused by mutant superoxide dismutase', *Journal of Neuroscience*. doi: 10.1523/JNEUROSCI.3494-08.2008.

Grad, L. I. *et al.* (2011) 'Intermolecular transmission of superoxide dismutase 1 misfolding in living cells', *Proceedings of the National Academy of Sciences of the United States of America*. doi: 10.1073/pnas.1102645108.

Grad, L. I. *et al.* (2014) 'Intercellular propagated misfolding of wild-type Cu/Zn superoxide dismutase occurs via exosome-dependent and -independent mechanisms', *Proceedings of the National Academy of Sciences of the United States of America*. doi: 10.1073/pnas.1312245111.

Grad, L. I. and Cashman, N. R. (2014) 'Prion-like activity of Cu/Zn superoxide dismutase Implications for amyotrophic lateral sclerosis', *Prion*. doi: 10.4161/pri.27602.

Graffmo, K. S. *et al.* (2013) 'Expression of wild-type human superoxide dismutase-1 in mice causes amyotrophic lateral sclerosis', *Human Molecular Genetics*. doi: 10.1093/hmg/dds399.

Greenway, M. J. *et al.* (2006) 'ANG mutations segregate with familial and "sporadic" amyotrophic lateral sclerosis', *Nature Genetics*. doi: 10.1038/ng1742.

Grima, J. C. *et al.* (2017) 'Mutant Huntingtin Disrupts the Nuclear Pore Complex', *Neuron*. doi: 10.1016/j.neuron.2017.03.023.

Gromicho, M. *et al.* (2017) 'Young-onset rapidly progressive ALS associated with heterozygous FUS mutation', *Amyotrophic Lateral Sclerosis and Frontotemporal Degeneration*. doi: 10.1080/21678421.2017.1299762.

Gros-Louis, F. *et al.* (2004) 'A frameshift deletion in peripherin gene associated with amyotrophic lateral sclerosis', *Journal of Biological Chemistry*. doi: 10.1074/jbc.M408139200.

Gros-Louis, F. *et al.* (2010) 'Intracerebroventricular infusion of monoclonal antibody or its derived Fab fragment against misfolded forms of SOD1 mutant delays mortality in a mouse model of ALS', *Journal of Neurochemistry*. doi: 10.1111/j.1471-4159.2010.06683.x.

Guareschi, S. *et al.* (2012) 'An over-oxidized form of superoxide dismutase found in sporadic amyotrophic lateral sclerosis with bulbar onset shares a toxic mechanism with mutant SOD1', *Proceedings of the National Academy of Sciences of the United States of America*. doi: 10.1073/pnas.1115402109.

Guo, Z., Deshpande, R. and Paull, T. T. (2010) 'ATM activation in the presence of oxidative stress', *Cell Cycle*. doi: 10.4161/cc.9.24.14323.

Gurney, M. E. *et al.* (1994) 'Motor neuron degeneration in mice that express a human

Cu,Zn superoxide dismutase mutation', *Science*, 264(5166), pp. 1772–1775. doi: 10.1126/science.8209258.

Hadano, S. *et al.* (2010) 'Loss of ALS2/Alsin exacerbates motor dysfunction in a SOD1H46R-expressing mouse ALS model by disturbing endolysosomal trafficking', *PLoS ONE*. doi: 10.1371/journal.pone.0009805.

Haider, L. *et al.* (2011) 'Oxidative damage in multiple sclerosis lesions', *Brain*, 134(7), pp. 1914–1924. doi: 10.1093/brain/awr128.

Haidet-Phillips, A. M. *et al.* (2011) 'Astrocytes from familial and sporadic ALS patients are toxic to motor neurons', *Nature Biotechnology*, 29(9), pp. 824–828. doi: 10.1038/nbt.1957.

Haim, L. Ben *et al.* (2015) 'Elusive roles for reactive astrocytes in neurodegenerative diseases', *Frontiers in Cellular Neuroscience*. Frontiers Media S.A. doi: 10.3389/fncel.2015.00278.

Haithcock, E. *et al.* (2005) *Age-related changes of nuclear architecture in Caenorhabditis elegans*. Available at: www.pnas.orgcgidoi10.1073pnas.0506955102 (Accessed: 13 July 2019).

Hand, C. K. *et al.* (2002) 'A novel locus for familial amyotrophic lateral sclerosis, on chromosome 18q', *American Journal of Human Genetics*. doi: 10.1086/337945.

Hardiman, O. and van den Berg, L. H. (2017) 'Edaravone: a new treatment for ALS on the horizon?', *The Lancet Neurology*. Lancet Publishing Group, pp. 490–491. doi: 10.1016/S1474-4422(17)30163-1.

Harraz, M. M. *et al.* (2008) 'SOD1 mutations disrupt redox-sensitive Rac regulation of NADPH oxidase in a familial ALS model', *Journal of Clinical Investigation*. doi: 10.1172/JCI34060.

Harwood, C. A. *et al.* (2016) 'Long-term physical activity: an exogenous risk factor for sporadic amyotrophic lateral sclerosis?', *Amyotrophic Lateral Sclerosis and Frontotemporal Degeneration*. Taylor and Francis Ltd, 17(5–6), pp. 377–384. doi: 10.3109/21678421.2016.1154575.

Hautbergue, G. M. *et al.* (2017) 'SRSF1-dependent nuclear export inhibition of C9ORF72 repeat transcripts prevents neurodegeneration and associated motor deficits', *Nature Communications*. doi: 10.1038/ncomms16063.

Hayashi, Y., Homma, K. and Ichijo, H. (2016) 'SOD1 in neurotoxicity and its controversial roles in SOD1 mutation-negative ALS', *Advances in Biological Regulation*. doi: 10.1016/j.jbior.2015.10.006.

Hayward, L. J. *et al.* (2002) 'Decreased metallation and activity in subsets of mutant superoxide dismutases associated with familial amyotrophic lateral sclerosis', *Journal of Biological Chemistry*. doi: 10.1074/jbc.M112087200.

Heiman-Patterson, T. D. *et al.* (2005) 'Background and gender effects on survival in the TgN(SOD1-G93A)1Gur mouse model of ALS', *Journal of the Neurological Sciences*. doi: 10.1016/j.jns.2005.02.006.

Henkel, J. S. *et al.* (2004) 'Presence of Dendritic Cells, MCP-1, and Activated Microglia/Macrophages in Amyotrophic Lateral Sclerosis Spinal Cord Tissue', *Annals of Neurology*. doi: 10.1002/ana.10805.

Henkel, J. S. *et al.* (2009) 'Microglia in ALS: The good, the bad, and the resting', *Journal of Neuroimmune Pharmacology*. doi: 10.1007/s11481-009-9171-5.

Henstridge, C. M. *et al.* (2015) 'Post-mortem brain analyses of the Lothian Birth Cohort 1936: extending lifetime cognitive and brain phenotyping to the level of the synapse', *Acta Neuropathologica Communications*. doi: 10.1186/s40478-015-0232-0.

Hess, M. *et al.* (2019) 'In-vivo quantitative image analysis of age-related morphological changes of C. elegans neurons reveals a correlation between neurite bending and novel neurite outgrowths', *eNeuro*. doi: 10.1523/ENEURO.0014-19.2019.

Higgins, C. M. J., Jung, C. and Xu, Z. (2003) 'ALS-associated mutant SODIG93A causes mitochondrial vacuolation by expansion of the intermembrane space by involvement of SODI aggregation and peroxisomes', *BMC Neuroscience*. doi: 10.1186/1471-2202-4-16.

Hipp, M. S., Kasturi, P. and Hartl, F. U. (2019) 'The proteostasis network and its decline in ageing', *Nature Reviews Molecular Cell Biology*. Nature Publishing Group, pp. 421–435. doi: 10.1038/s41580-019-0101-y.

Hirano, A. *et al.* (1984) 'Fine structural study of neurofibrillary changes in a family with amyotrophic lateral sclerosis', *Journal of Neuropathology and Experimental Neurology*. doi: 10.1097/00005072-198409000-00002.

Hirsch, E. C. and Hunot, S. (2009) 'Neuroinflammation in Parkinson's disease: a target for neuroprotection?', *The Lancet Neurology*, pp. 382–397. doi: 10.1016/S1474-4422(09)70062-6.

Hishikawa, N. *et al.* (2003) 'Dorfin localizes to the ubiquitylated inclusions in Parkinson's disease, dementia with Lewy bodies, multiple system atrophy, and amyotrophic lateral sclerosis', *American Journal of Pathology*. doi: 10.1016/S0002-9440(10)63688-7.

Ho, Y. *et al.* (2002) 'Systematic identification of protein complexes in Saccharomyces cerevisiae by mass spectrometry', *Nature*. doi: 10.1038/415180a.

Hong, K. *et al.* (2012) 'Full-length TDP-43 and its C-terminal fragments activate mitophagy in NSC34 cell line', *Neuroscience Letters*. doi: 10.1016/j.neulet.2012.10.003.

Hooten, K. G. *et al.* (2015) 'Protective and Toxic Neuroinflammation in Amyotrophic Lateral Sclerosis', *Neurotherapeutics*. Springer New York LLC, pp. 364–375. doi: 10.1007/s13311-014-0329-3.

van Horssen, J. *et al.* (2008) 'Severe oxidative damage in multiple sclerosis lesions coincides with enhanced antioxidant enzyme expression', *Free Radical Biology and Medicine*. Pergamon, 45(12), pp. 1729–1737. doi: 10.1016/J.FREERADBIOMED.2008.09.023.

Hübers, A. *et al.* (2015) 'De novo FUS mutations are the most frequent genetic cause in early-onset German ALS patients', *Neurobiology of Aging*. doi: 10.1016/j.neurobiolaging.2015.08.005.

Huh, C. J. *et al.* (2016) 'Maintenance of age in human neurons generated by microRNA-based neuronal conversion of fibroblasts', *eLife*, 5. doi: 10.7554/eLife.18648.

Hutten, S. and Dormann, D. (2019) 'Nucleocytoplasmic transport defects in neurodegeneration — Cause or consequence?', *Seminars in Cell & Developmental Biology*. Academic Press. doi: 10.1016/J.SEMCDB.2019.05.020.

Ince, P. G. *et al.* (1996) 'Familial amyotrophic lateral sclerosis with a mutation in exon 4 of the Cu/Zn superoxide dismutase gene: Pathological and immunocytochemical changes', *Acta Neuropathologica*. doi: 10.1007/s004010050535.

Inoue, E. *et al.* (2010) 'SOD1 Is Essential for the Viability of DT40 Cells and Nuclear SOD1 Functions as a Guardian of Genomic DNA', *Journal of Nucleic Acids*. Hindawi Limited, 2010. doi: 10.4061/2010/795946.

Irvin, C. W., Kim, R. B. and Mitchell, C. S. (2015) 'Seeking homeostasis: Temporal trends in respiration, oxidation, and calcium in SOD1 G93A amyotrophic lateral sclerosis mice', *Frontiers in Cellular Neuroscience*. doi: 10.3389/fncel.2015.00248.

Ishigaki, S. and Sobue, G. (2018) 'Importance of functional loss of FUS in FTLD/ALS', *Frontiers in Molecular Biosciences*. doi: 10.3389/fmolb.2018.00044.

Ishii, T. *et al.* (2017) 'Endogenous reactive oxygen species cause astrocyte defects and neuronal dysfunctions in the hippocampus: a new model for aging brain', *Aging*

Cell. Wiley/Blackwell (10.1111), 16(1), pp. 39–51. doi: 10.1111/acel.12523.

Islam, M. T. (2017) 'Oxidative stress and mitochondrial dysfunction-linked neurodegenerative disorders', *Neurological Research*. doi: 10.1080/01616412.2016.1251711.

Israelson, A. *et al.* (2015) 'Macrophage migration inhibitory factor as a chaperone inhibiting accumulation of misfolded SOD1', *Neuron*. doi: 10.1016/j.neuron.2015.02.034.

Jacobsson, J. (2001) 'Superoxide dismutase in CSF from amyotrophic lateral sclerosis patients with and without CuZn-superoxide dismutase mutations', *Brain*. doi: 10.1093/brain/124.7.1461.

Jaiswal, M. K. (2013) 'Calcium, mitochondria, and the pathogenesis of ALS: The good, the bad, and the ugly', *Frontiers in Cellular Neuroscience*. doi: 10.3389/fncel.2013.00199.

Janowitz, D. *et al.* (2019) 'Inflammatory markers and imaging patterns of advanced brain aging in the general population', *Brain Imaging and Behavior*. doi: 10.1007/s11682-019-00058-y.

Johnson, J. O. *et al.* (2010) 'Exome Sequencing Reveals VCP Mutations as a Cause of Familial ALS', *Neuron*. doi: 10.1016/j.neuron.2010.11.036.

Johnson, J. O., Glynn, S. M., *et al.* (2014) 'Mutations in the CHCHD10 gene are a common cause of familial amyotrophic lateral sclerosis', *Brain*. doi: 10.1093/brain/awu265.

Johnson, J. O., Pioro, E. P., *et al.* (2014) 'Mutations in the Matrin 3 gene cause familial amyotrophic lateral sclerosis', *Nature Neuroscience*. doi: 10.1038/nn.3688.

Jovičić, A. *et al.* (2015) 'Modifiers of C9orf72 dipeptide repeat toxicity connect nucleocytoplasmic transport defects to FTD/ALS', *Nature Neuroscience*. Nature Publishing Group, 18(9), pp. 1226–1229. doi: 10.1038/nn.4085.

Kabashi, E. *et al.* (2008) 'TARDBP mutations in individuals with sporadic and familial amyotrophic lateral sclerosis', *Nature Genetics*. doi: 10.1038/ng.132.

Kabashi, E. *et al.* (2009) 'Gain and loss of function of ALS-related mutations of TARDBP (TDP-43) cause motor deficits in vivo', *Human Molecular Genetics*. doi: 10.1093/hmg/ddp534.

Kalra, S. *et al.* (1998) 'Recovery of N-acetylaspartate in corticomotor neurons of patients with ALS after riluzole therapy', *NeuroReport*. Lippincott Williams and Wilkins, 9(8), pp. 1757–1761. doi: 10.1097/00001756-199806010-00016.

Kaneb, H. M. *et al.* (2015) 'Deleterious mutations in the essential mRNA metabolism factor, hGle1, in amyotrophic lateral sclerosis', *Human Molecular Genetics*. doi: 10.1093/hmg/ddu545.

Kashon, M. L. *et al.* (2004) 'Associations of cortical astrogliosis with cognitive performance and dementia status', *Journal of Alzheimer's Disease*. IOS Press, 6(6), pp. 595–604. doi: 10.3233/jad-2004-6604.

Kato, S. (1999) 'Recent advances in research on neuropathological aspects of familial amyotrophic lateral sclerosis with superoxide dismutase 1 gene mutations: Neuronal Lewy body-like hyaline inclusions and astrocytic hyaline inclusions', *Histology and Histopathology*. doi: 10.14670/HH-14.973.

Kaur, S. J., McKeown, S. R. and Rashid, S. (2016) 'Mutant SOD1 mediated pathogenesis of Amyotrophic Lateral Sclerosis', *Gene*. doi: 10.1016/j.gene.2015.11.049.

Kawamata, T. *et al.* (1992) 'Immunologic reactions in amyotrophic lateral sclerosis brain and spinal cord tissue', *American Journal of Pathology*.

Kerman, A. *et al.* (2010) 'Amyotrophic lateral sclerosis is a non-amyloid disease in which extensive misfolding of SOD1 is unique to the familial form', *Acta Neuropathologica*. doi: 10.1007/s00401-010-0646-5.

Khan, S. S., Singer, B. D. and Vaughan, D. E. (2017) 'Molecular and physiological manifestations and measurement of aging in humans', *Aging Cell*. doi: 10.1111/acel.12601.

Kiernan, M. C. *et al.* (2011) 'Amyotrophic lateral sclerosis', in *The Lancet*, pp. 942–955. doi: 10.1016/S0140-6736(10)61156-7.

Kim, H. J. *et al.* (2013) 'Mutations in prion-like domains in hnRNPA2B1 and hnRNPA1 cause multisystem proteinopathy and ALS', *Nature*. doi: 10.1038/nature11922.

Kim, H. J. and Taylor, J. P. (2017) 'Lost in Transportation: Nucleocytoplasmic Transport Defects in ALS and Other Neurodegenerative Diseases.', *Neuron*. NIH Public Access, 96(2), pp. 285–297. doi: 10.1016/j.neuron.2017.07.029.

King, A. E. *et al.* (2012) 'Degeneration of axons in spinal white matter in G93A mSOD1 mouse characterized by NFL and alpha-internexin immunoreactivity', *Brain Research*. doi: 10.1016/j.brainres.2012.05.018.

Kiskinis, E. *et al.* (2014) 'Pathways disrupted in human ALS motor neurons identified through genetic correction of mutant SOD1', *Cell Stem Cell*. doi: 10.1016/j.stem.2014.03.004.

Knott, A. B. *et al.* (2008) 'Mitochondrial fragmentation in neurodegeneration', *Nature Reviews Neuroscience*. doi: 10.1038/nrn2417.

Koch, P. *et al.* (2000) 'Identification of a novel putative Ran-binding protein and its close homologue', *Biochemical and Biophysical Research Communications*. doi: 10.1006/bbrc.2000.3788.

Koga, H., Kaushik, S. and Cuervo, A. M. (2011) 'Protein homeostasis and aging: The importance of exquisite quality control', *Ageing Research Reviews*. doi: 10.1016/j.arr.2010.02.001.

Kondo, T. *et al.* (1997) 'Reduction of CuZn-superoxide dismutase activity exacerbates neuronal cell injury and edema formation after transient focal cerebral ischemia', *Journal of Neuroscience*. doi: 10.1523/jneurosci.17-11-04180.1997.

Konopka, A. and Atkin, J. D. (2018) 'The emerging role of DNA damage in the pathogenesis of the C9Orf72 repeat expansion in amyotrophic lateral sclerosis', *International Journal of Molecular Sciences*. doi: 10.3390/ijms19103137.

Koppers, M. *et al.* (2015) 'C9orf72 ablation in mice does not cause motor neuron degeneration or motor deficits', *Annals of Neurology*. doi: 10.1002/ana.24453.

Kwiatkowski, T. J. *et al.* (2009) 'Mutations in the FUS/TLS gene on chromosome 16 cause familial amyotrophic lateral sclerosis', *Science*. doi: 10.1126/science.1166066.

Kwon, M. J. *et al.* (2012) 'Screening of the SOD1, FUS, TARDBP, ANG, and OPTN mutations in Korean patients with familial and sporadic ALS', *Neurobiology of Aging*. doi: 10.1016/j.neurobiolaging.2011.12.003.

Lagier-Tourenne, C. *et al.* (2013) 'Targeted degradation of sense and antisense C9orf72 RNA foci as therapy for ALS and frontotemporal degeneration', *Proceedings of the National Academy of Sciences of the United States of America*. doi: 10.1073/pnas.1318835110.

Lagier-Tourenne, C., Polymenidou, M. and Cleveland, D. W. (2010) 'TDP-43 and FUS/TLS: Emerging roles in RNA processing and neurodegeneration', *Human Molecular Genetics*. doi: 10.1093/hmg/ddq137.

Lambrechts, D. *et al.* (2003) 'VEGF is a modifier of amyotrophic lateral sclerosis in mice and humans and protects motoneurons against ischemic death', *Nature Genetics*. doi: 10.1038/ng1211.

Lapasset, L. *et al.* (2011) 'Rejuvenating senescent and centenarian human cells by reprogramming through the pluripotent state.', *Genes & Development*. Cold Spring Harbor Laboratory Press, 25(21), pp. 2248–53. doi: 10.1101/gad.173922.111.

Lattante, S., Rouleau, G. A. and Kabashi, E. (2013) 'TARDBP and FUS Mutations Associated with Amyotrophic Lateral Sclerosis: Summary and Update', *Human Mutation*. doi: 10.1002/humu.22319.

Lee, J. *et al.* (2016) 'Astrocytes and Microglia as Non-cell Autonomous Players in the Pathogenesis of ALS', *Experimental Neurobiology*, 25(5), p. 233. doi: 10.5607/en.2016.25.5.233.

Lee, J. B. *et al.* (2012) 'Homozygous SMN2 deletion is a major risk factor among twenty-five Korean sporadic amyotrophic lateral sclerosis patients', *Yonsei Medical Journal*. Yonsei University College of Medicine, 53(1), pp. 53–57. doi: 10.3349/ymj.2012.53.1.53.

Lee, J. H., Zhou, S. and Smas, C. M. (2010) 'Identification of RANBP16 and RANBP17 as novel interaction partners for the bHLH transcription factor E12', *Journal of Cellular Biochemistry*. doi: 10.1002/jcb.22689.

Lee, Y. B. *et al.* (2013) 'Hexanucleotide repeats in ALS/FTD form length-dependent RNA Foci, sequester RNA binding proteins, and are neurotoxic', *Cell Reports*. doi: 10.1016/j.celrep.2013.10.049.

Léger, B. *et al.* (2006) 'Human skeletal muscle atrophy in amyotrophic lateral sclerosis reveals a reduction in Akt and an increase in atrogin-1', *FASEB Journal*. doi: 10.1096/fj.05-5249fje.

Lehman, E. J. *et al.* (2012) 'Neurodegenerative causes of death among retired national football league players', *Neurology*. doi: 10.1212/WNL.0b013e31826daf50.

Lénárt, P. and Ellenberg, J. (2006) 'Monitoring the permeability of the nuclear envelope during the cell cycle', *Methods*. doi: 10.1016/j.ymeth.2005.07.010.

Lepore, A. C. *et al.* (2008) 'Focal transplantation-based astrocyte replacement is neuroprotective in a model of motor neuron disease', *Nature Neuroscience*. doi: 10.1038/nn.2210.

Leung, C. L. *et al.* (2006) 'A Pathogenic Peripherin Gene Mutation in a Patient with Amyotrophic Lateral Sclerosis', *Brain Pathology*. doi: 10.1111/j.1750-3639.2004.tb00066.x.

Levine, J. B. *et al.* (1999) 'Astrocytes interact intimately with degenerating motor neurons in mouse amyotrophic lateral sclerosis (ALS)', *GLIA*. doi: 10.1002/(SICI)1098-1136(199912)28:3<215::AID-GLIA5>3.0.CO;2-C.

Lewis, K. N. *et al.* (2015) 'Regulation of Nrf2 signaling and longevity in naturally long-lived rodents', *Proceedings of the National Academy of Sciences of the United States*

of America. National Academy of Sciences, 112(12), pp. 3722–3727. doi: 10.1073/pnas.1417566112.

Leyton-Jaimes, M. F. *et al.* (2016) 'Endogenous macrophage migration inhibitory factor reduces the accumulation and toxicity of misfolded SOD1 in a mouse model of ALS', *Proceedings of the National Academy of Sciences of the United States of America*. doi: 10.1073/pnas.1604600113.

Li, C. *et al.* (2011) 'Astrocytes: Implications for Neuroinflammatory Pathogenesis of Alzheimers Disease', *Current Alzheimer Research*. Bentham Science Publishers Ltd., 8(1), pp. 67–80. doi: 10.2174/156720511794604543.

Li, C. C. Y. *et al.* (2013) 'Glioma microvesicles carry selectively packaged coding and noncoding RNAs which alter gene expression in recipient cells', *RNA Biology*. doi: 10.4161/rna.25281.

Li, J. *et al.* (2013) 'Oxidative Stress and Neurodegenerative Disorders', *International Journal of Molecular Sciences*, 14(12), pp. 24438–24475. doi: 10.3390/ijms141224438.

Li, J. M. and Shah, A. M. (2002) 'Intracellular localization and preassembly of the NADPH oxidase complex in cultured endothelial cells', *Journal of Biological Chemistry*. doi: 10.1074/jbc.M110073200.

Li, Q. *et al.* (2010) 'ALS-linked mutant superoxide dismutase 1 (SOD1) alters mitochondrial protein composition and decreases protein import', *Proceedings of the National Academy of Sciences of the United States of America*. doi: 10.1073/pnas.1014862107.

Liddelow, S. A. *et al.* (2017) 'Neurotoxic reactive astrocytes are induced by activated microglia', *Nature*. doi: 10.1038/nature21029.

Ligon, L. A. *et al.* (2005) 'Mutant superoxide dismutase disrupts cytoplasmic dynein in motor neurons', *NeuroReport*. doi: 10.1097/00001756-200504250-00002.

Lin, C. L. G. *et al.* (1998) 'Aberrant RNA processing in a neurodegenerative disease: The cause for absent EAAT2, a glutamate transporter, in amyotrophic lateral sclerosis', *Neuron*. doi: 10.1016/S0896-6273(00)80997-6.

Lindberg, M. J. *et al.* (2004) 'Folding of human superoxide dismutase: Disulfide reduction prevents dimerization and produces marginally stable monomers', *Proceedings of the National Academy of Sciences of the United States of America*. doi: 10.1073/pnas.0403979101.

Lindberg, M. J., Tibell, L. and Oliveberg, M. (2002) 'Common denominator of Cu/Zn

superoxide dismutase mutants associated with amyotrophic lateral sclerosis: Decreased stability of the apo state', *Proceedings of the National Academy of Sciences of the United States of America*. doi: 10.1073/pnas.262527099.

Lindenau, J. *et al.* (2000) 'Cellular distribution of superoxide dismutases in the rat CNS', *GLIA*. doi: 10.1002/(SICI)1098-1136(20000101)29:1<25::AID-GLIA3>3.0.CO;2-G.

Ling, S. C., Polymenidou, M. and Cleveland, D. W. (2013) 'Converging mechanisms in als and FTD: Disrupted RNA and protein homeostasis', *Neuron*. doi: 10.1016/j.neuron.2013.07.033.

Liu-Yesucevitz, L. *et al.* (2010) 'Tar DNA binding protein-43 (TDP-43) associates with stress granules: Analysis of cultured cells and pathological brain tissue', *PLoS ONE*, 5(10). doi: 10.1371/journal.pone.0013250.

Liu, B. and Zhou, Z. (2008) 'Lamin A/C, laminopathies and premature ageing.', *Histology and Histopathology*, 23(6), pp. 747–63. doi: 10.14670/HH-23.747.

Liu, Q. *et al.* (2016) 'Whole-exome sequencing identifies a missense mutation in hnRNPA1 in a family with flail arm ALS', *Neurology*. doi: 10.1212/WNL.0000000000003256.

Liu, W. J. *et al.* (2016) 'p62 links the autophagy pathway and the ubiqutin-proteasome system upon ubiquitinated protein degradation', *Cellular and Molecular Biology Letters*. BioMed Central Ltd., p. 29. doi: 10.1186/s11658-016-0031-z.

Liu, Y. *et al.* (2004) 'CD44 expression identifies astrocyte-restricted precursor cells', *Developmental Biology*. Academic Press Inc., 276(1), pp. 31–46. doi: 10.1016/j.ydbio.2004.08.018.

Lobsiger, C. S. and Cleveland, D. W. (2007) 'Glial cells as intrinsic components of non-cell-autonomous neurodegenerative disease.', *Nature Neuroscience*. NIH Public Access, 10(11), pp. 1355–60. doi: 10.1038/nn1988.

Lopez-Gonzalez, R. *et al.* (2016) 'Poly(GR) in C9ORF72-Related ALS/FTD Compromises Mitochondrial Function and Increases Oxidative Stress and DNA Damage in iPSC-Derived Motor Neurons', *Neuron*. doi: 10.1016/j.neuron.2016.09.015.

López-Otín, C. *et al.* (2013) 'The hallmarks of aging.', *Cell*. Europe PMC Funders, 153(6), pp. 1194–217. doi: 10.1016/j.cell.2013.05.039.

Lord, C. L. *et al.* (2015) 'Altering nuclear pore complex function impacts longevity and mitochondrial function in S. cerevisiae', *Journal of Cell Biology*. doi:

10.1083/jcb.201412024.
Lu, C. H. *et al.* (2012) 'Plasma neurofilament heavy chain levels correlate to markers of late stage disease progression and treatment response in SOD1G93A mice that model ALS', *PLoS ONE*. doi: 10.1371/journal.pone.0040998.
Lu, T. *et al.* (2004) 'Gene regulation and DNA damage in the ageing human brain', *Nature*. doi: 10.1038/nature02661.
Luchinat, E., Barbieri, L. and Banci, L. (2017) 'A molecular chaperone activity of CCS restores the maturation of SOD1 fALS mutants', *Scientific Reports*. doi: 10.1038/s41598-017-17815-y.
Lukiw, W. J. *et al.* (2012) 'Generation of Reactive Oxygen Species (ROS) and Pro-Inflammatory Signaling in Human Brain Cells in Primary Culture.', *Journal of Alzheimer's disease & Parkinsonism*, Suppl 2(July 2011), p. 001. doi: 10.4172/2161-0460.S2-0011.
Luty, A. A. *et al.* (2010) 'Sigma nonopioid intracellular receptor 1 mutations cause frontotemporal lobar degeneration-motor neuron disease', *Annals of Neurology*. doi: 10.1002/ana.22274.
Lynch, A. M. *et al.* (2010) 'The impact of glial activation in the aging brain', *Aging and Disease*. International Society on Aging and Disease, pp. 262–278.
Lynch, M. A. (2010) 'Age-related neuroinflammatory changes negatively impact on neuronal function', *Frontiers in Aging Neuroscience*. Frontiers Media SA, 1. doi: 10.3389/neuro.24.006.2009.
Mackenzie, I. R. A. *et al.* (2007) 'Pathological TDP-43 distinguishes sporadic amyotrophic lateral sclerosis from amyotrophic lateral sclerosis with SOD1 mutations', *Annals of Neurology*. doi: 10.1002/ana.21147.
Mackenzie, I. R. A., Rademakers, R. and Neumann, M. (2010) 'TDP-43 and FUS in amyotrophic lateral sclerosis and frontotemporal dementia', *The Lancet Neurology*, pp. 995–1007. doi: 10.1016/S1474-4422(10)70195-2.
Madji Hounoum, B. *et al.* (2017) 'Wildtype motoneurons, ALS-Linked SOD1 mutation and glutamate profoundly modify astrocyte metabolism and lactate shuttling', *GLIA*. doi: 10.1002/glia.23114.
Magrané, J. *et al.* (2014) 'Abnormal mitochondrial transport and morphology are common pathological denominators in SOD1 and TDP43 ALS mouse models', *Human Molecular Genetics*. doi: 10.1093/hmg/ddt528.
Magrané, J. and Manfredi, G. (2009) 'Mitochondrial function, morphology, and axonal

transport in amyotrophic lateral sclerosis', *Antioxidants and Redox Signaling*. doi: 10.1089/ars.2009.2604.

Majounie, E. *et al.* (2012) 'Frequency of the C9orf72 hexanucleotide repeat expansion in patients with amyotrophic lateral sclerosis and frontotemporal dementia: A cross-sectional study', *The Lancet Neurology*. doi: 10.1016/S1474-4422(12)70043-1.

Maleszewska, M., Mawer, J. S. P. and Tessarz, P. (2016) 'Histone Modifications in Ageing and Lifespan Regulation', *Current Molecular Biology Reports*. Springer Science and Business Media LLC, 2(1), pp. 26–35. doi: 10.1007/s40610-016-0031-9.

Mancuso, R. *et al.* (2012) 'Effect of genetic background on onset and disease progression in the SOD1-G93A model of amyotrophic lateral sclerosis', *Amyotrophic Lateral Sclerosis*. doi: 10.3109/17482968.2012.662688.

Manjaly, Z. R. *et al.* (2010) 'The sex ratio in amyotrophic lateral sclerosis: A population based study', *Amyotrophic Lateral Sclerosis*. doi: 10.3109/17482961003610853.

Mann, D. M. *et al.* (2013) 'Dipeptide repeat proteins are present in the p62 positive inclusions in patients with frontotemporal lobar degeneration and motor neurone disease associated with expansions in C9ORF72', *Acta Neuropathologica Communications*. doi: 10.1186/2051-5960-1-68.

Maragakis, N. J. and Rothstein, J. D. (2006) 'Mechanisms of Disease: Astrocytes in neurodegenerative disease', *Nature Clinical Practice Neurology*. doi: 10.1038/ncpneuro0355.

Martínez, P. *et al.* (2014) 'Essential role for the TRF2 telomere protein in adult skin homeostasis', *Aging Cell*, 13(4), pp. 656–668. doi: 10.1111/acel.12221.

Maruyama, H. *et al.* (2010) 'Mutations of optineurin in amyotrophic lateral sclerosis', *Nature*. doi: 10.1038/nature08971.

Matias, I., Morgado, J. and Gomes, F. C. A. (2019) 'Astrocyte Heterogeneity: Impact to Brain Aging and Disease', *Frontiers in Aging Neuroscience*. Frontiers, 11, p. 59. doi: 10.3389/fnagi.2019.00059.

Mattiazzi, M. *et al.* (2002) 'Mutated human SOD1 causes dysfunction of oxidative phosphorylation in mitochondria of transgenic mice', *Journal of Biological Chemistry*. doi: 10.1074/jbc.M203065200.

Matus, S., Medinas, D. B. and Hetz, C. (2014) 'Common ground: Stem cell approaches find shared pathways underlying ALS', *Cell Stem Cell*. doi: 10.1016/j.stem.2014.05.001.

Meier, J. *et al.* (1999) 'Extra neurofilament NF-L subunits rescue motor neuron disease

caused by overexpression of the human NF-H gene in mice', *Journal of Neuropathology and Experimental Neurology*. doi: 10.1097/00005072-199910000-00009.

Mertens, J. *et al.* (2015) 'Directly Reprogrammed Human Neurons Retain Aging-Associated Transcriptomic Signatures and Reveal Age-Related Nucleocytoplasmic Defects', *Cell Stem Cell*. Cell Press, 17(6), pp. 705–718. doi: 10.1016/J.STEM.2015.09.001.

Mertens, J. *et al.* (2018) 'Aging in a Dish: iPSC-Derived and Directly Induced Neurons for Studying Brain Aging and Age-Related Neurodegenerative Diseases', *Annual Review of Genetics*, 52(1). doi: 10.1146/annurev-genet-120417-031534.

Meyer, K. *et al.* (2014) 'Direct conversion of patient fibroblasts demonstrates non-cell autonomous toxicity of astrocytes to motor neurons in familial and sporadic ALS.', *Proceedings of the National Academy of Sciences*. doi: 10.1073/pnas.1314085111.

Migheli, A. *et al.* (1990) 'Ubiquitinated filamentous inclusions in spinal cord of patients with motor neuron disease', *Neuroscience Letters*. doi: 10.1016/0304-3940(90)90419-A.

Milanese, M. *et al.* (2011) 'Abnormal exocytotic release of glutamate in a mouse model of amyotrophic lateral sclerosis', *Journal of Neurochemistry*. doi: 10.1111/j.1471-4159.2010.07155.x.

Miller *et al.* (2013) 'Human iPSC-Based Modeling of Late-Onset Disease via Progerin-Induced Aging', *Cell Stem Cell*. Cell Press, 13(6), pp. 691–705. doi: 10.1016/J.STEM.2013.11.006.

Miller, R. *et al.* (2002) 'Riluzole for amyotrophic lateral sclerosis (ALS)/motor neuron disease (MND)', in *Cochrane Database of Systematic Reviews*. doi: 10.1002/14651858.cd001447.

Miller, R. G., Mitchell, J. D. and Moore, D. H. (2012) 'Riluzole for amyotrophic lateral sclerosis (ALS)/motor neuron disease (MND)', *Cochrane Database of Systematic Reviews*. Wiley. doi: 10.1002/14651858.cd001447.pub3.

Miller, T. M. *et al.* (2006) 'Gene transfer demonstrates that muscle is not a primary target for non-cell-autonomous toxicity in familial amyotrophic lateral sclerosis', *Proceedings of the National Academy of Sciences of the United States of America*. doi: 10.1073/pnas.0609411103.

Miller, T. M. *et al.* (2013) 'An antisense oligonucleotide against SOD1 delivered intrathecally for patients with SOD1 familial amyotrophic lateral sclerosis: A phase 1,

randomised, first-in-man study', *The Lancet Neurology*. doi: 10.1016/S1474-4422(13)70061-9.

Mitsui, Y. and Schneider, E. L. (1976) 'Increased nuclear sizes in senescent human diploid fibroblast cultures', *Experimental Cell Research*. doi: 10.1016/0014-4827(76)90336-0.

Mitsumoto, H., Brooks, B. R. and Silani, V. (2014) 'Clinical trials in amyotrophic lateral sclerosis: Why so many negative trials and how can trials be improved?', *The Lancet Neurology*. doi: 10.1016/S1474-4422(14)70129-2.

Mori, K., Arzberger, T., *et al.* (2013) 'Bidirectional transcripts of the expanded C9orf72 hexanucleotide repeat are translated into aggregating dipeptide repeat proteins', *Acta Neuropathologica*. doi: 10.1007/s00401-013-1189-3.

Mori, K., Weng, S. M., *et al.* (2013) 'The C9orf72 GGGGCC repeat is translated into aggregating dipeptide-repeat proteins in FTLD/ALS', *Science*. doi: 10.1126/science.1232927.

Mórotz, G. M. *et al.* (2012) 'Amyotrophic lateral sclerosis-associated mutant VAPBP56s perturbs calcium homeostasis to disrupt axonal transport of mitochondria', *Human Molecular Genetics*. doi: 10.1093/hmg/dds011.

Mukherjee, A. B. and Weinstein, M. E. (1986) 'Culture media variation as related to in vitro aging of human fibroblasts: I. Effects on population doubling, nuclear volume and nuclear morphology', *Mechanisms of Ageing and Development*. doi: 10.1016/0047-6374(86)90118-1.

Münch, C. and Bertolotti, A. (2010) 'Exposure of hydrophobic surfaces initiates aggregation of diverse ALS-causing superoxide dismutase-1 mutants', *Journal of Molecular Biology*. doi: 10.1016/j.jmb.2010.04.019.

Münch, C., O'Brien, J. and Bertolotti, A. (2011) 'Prion-like propagation of mutant superoxide dismutase-1 misfolding in neuronal cells', *Proceedings of the National Academy of Sciences of the United States of America*. doi: 10.1073/pnas.1017275108.

Murata, T., Ohtsuka, C. and Terayama, Y. (2008) 'Increased mitochondrial oxidative damage and oxidative DNA damage contributes to the neurodegenerative process in sporadic amyotrophic lateral sclerosis', *Free Radical Research*. doi: 10.1080/10715760701877262.

Myszczynska, M. and Ferraiuolo, L. (2016) 'New in vitro models to study amyotrophic lateral sclerosis', in *Brain Pathology*. Blackwell Publishing Ltd, pp. 258–265. doi:

10.1111/bpa.12353.
Nagai, M. *et al.* (2007) 'Astrocytes expressing ALS-linked mutated SOD1 release factors selectively toxic to motor neurons', *Nature Neuroscience*. doi: 10.1038/nn1876.
Nardo, G. *et al.* (2009) 'Nitroproteomics of peripheral blood mononuclear cells from patients and a rat model of ALS', *Antioxidants and Redox Signaling*. doi: 10.1089/ars.2009.2548.
Nardo, G. *et al.* (2013) 'Transcriptomic indices of fast and slow disease progression in two mouse models of amyotrophic lateral sclerosis', *Brain*. doi: 10.1093/brain/awt250.
Nassif, M., Woehlbier, U. and Manque, P. A. (2017) 'The enigmatic role of C9ORF72 in autophagy', *Frontiers in Neuroscience*. doi: 10.3389/fnins.2017.00442.
Neumann, M. *et al.* (2006) 'Ubiquitinated TDP-43 in frontotemporal lobar degeneration and amyotrophic lateral sclerosis', *Science*, 314(5796), pp. 130–133. doi: 10.1126/science.1134108.
Niccoli, T., Partridge, L. and Isaacs, A. M. (2017) 'Ageing as a risk factor for ALS/FTD', *Human Molecular Genetics*, 26(R2), pp. R105–R113. doi: 10.1093/hmg/ddx247.
Niedzielska, E. *et al.* (2016) 'Oxidative Stress in Neurodegenerative Diseases', *Molecular Neurobiology*. Humana Press Inc., pp. 4094–4125. doi: 10.1007/s12035-015-9337-5.
Nishihira, Y. *et al.* (2008) 'Sporadic amyotrophic lateral sclerosis: Two pathological patterns shown by analysis of distribution of TDP-43-immunoreactive neuronal and glial cytoplasmic inclusions', *Acta Neuropathologica*. doi: 10.1007/s00401-008-0385-z.
Nishimura, A. L. *et al.* (2004) 'A mutation in the vesicle-trafficking protein VAPB causes late-onset spinal muscular atrophy and amyotrophic lateral sclerosis', *American Journal of Human Genetics*. doi: 10.1086/425287.
Nousiainen, H. O. *et al.* (2008) 'Mutations in mRNA export mediator GLE1 result in a fetal motoneuron disease', *Nature Genetics*. doi: 10.1038/ng.2007.65.
Oberheim, N. A. *et al.* (2009) 'Uniquely Hominid Features of Adult Human Astrocytes'. doi: 10.1523/Jneurosci.4707-08.2009.
Okado-Matsumoto, A. and Fridovich, I. (2002) 'Amyotrophic lateral sclerosis: A proposed mechanism', *Proceedings of the National Academy of Sciences of the United States of America*. doi: 10.1073/pnas.132260399.
Oksanen, M. *et al.* (2019) 'Astrocyte alterations in neurodegenerative pathologies and their modeling in human induced pluripotent stem cell platforms', *Cellular and*

Molecular Life Sciences. Birkhauser Verlag AG, pp. 2739–2760. doi: 10.1007/s00018-019-03111-7.

Oliveira, A. S. B. and Pereira, R. D. B. (2009) 'Amyotrophic lateral sclerosis (ALS): Three letters that change the people's life. For ever', *Arquivos de Neuro-Psiquiatria*. doi: 10.1590/S0004-282X2009000400040.

Ortmann, D. and Vallier, L. (2017) 'Variability of human pluripotent stem cell lines', *Current Opinion in Genetics and Development*. Elsevier Ltd, pp. 179–185. doi: 10.1016/j.gde.2017.07.004.

Osorio, F. G. *et al.* (2016) 'NF-κB signaling as a driver of ageing', in *International Review of Cell and Molecular Biology*. Elsevier Inc., pp. 133–174. doi: 10.1016/bs.ircmb.2016.04.003.

Paladino, S. *et al.* (2018) 'Nrf2 Pathway in Age-Related Neurological Disorders: Insights into MicroRNAs', *Cellular Physiology and Biochemistry*. Karger Publishers, 47(5), pp. 1951–1976. doi: 10.1159/000491465.

Pankiv, S. *et al.* (2007) 'p62/SQSTM1 binds directly to Atg8/LC3 to facilitate degradation of ubiquitinated protein aggregates by autophagy*[S]', *Journal of Biological Chemistry*. doi: 10.1074/jbc.M702824200.

Pant, S., Hilton, H. and Burczynski, M. E. (2012) 'The multifaceted exosome: Biogenesis, role in normal and aberrant cellular function, and frontiers for pharmacological and biomarker opportunities', *Biochemical Pharmacology*. doi: 10.1016/j.bcp.2011.12.037.

Papadeas, S. T. *et al.* (2011) 'Astrocytes carrying the superoxide dismutase 1 (SOD1 G93A) mutation induce wild-type motor neuron degeneration in vivo', *Proceedings of the National Academy of Sciences of the United States of America*. doi: 10.1073/pnas.1103141108.

Pardo, C. A. *et al.* (1995) 'Superoxide dismutase is an abundant component in cell bodies, dendrites, and axons of motor neurons and in a subset of other neurons', *Proceedings of the National Academy of Sciences of the United States of America*. doi: 10.1073/pnas.92.4.954.

Paré, B. *et al.* (2018) 'Misfolded SOD1 pathology in sporadic Amyotrophic Lateral Sclerosis', *Scientific Reports*. doi: 10.1038/s41598-018-31773-z.

Parone, P. A. *et al.* (2013) 'Enhancing mitochondrial calcium buffering capacity reduces aggregation of misfolded SOD1 and motor neuron cell death without extending survival in mouse models of inherited amyotrophic lateral sclerosis', *Journal*

of Neuroscience. doi: 10.1523/JNEUROSCI.1119-12.2013.

Parpura, V. *et al.* (2012) 'Glial cells in (patho)physiology.', *Journal of neurochemistry*. NIH Public Access, 121(1), pp. 4–27. doi: 10.1111/j.1471-4159.2012.07664.x.

Pasinelli, P. *et al.* (2004) 'Amyotrophic lateral sclerosis-associated SOD1 mutant proteins bind and aggregate with Bcl-2 in spinal cord mitochondria', *Neuron*. doi: 10.1016/j.neuron.2004.06.021.

Pasinelli, P. and Brown, R. H. (2006) 'Molecular biology of amyotrophic lateral sclerosis: Insights from genetics', *Nature Reviews Neuroscience*. doi: 10.1038/nrn1971.

Patterson, M. *et al.* (2012) 'Defining the nature of human pluripotent stem cell progeny', *Cell Research*. Nature Publishing Group, 22(1), pp. 178–193. doi: 10.1038/cr.2011.133.

Pegtel, D. M. *et al*. (2010) 'Functional delivery of viral miRNAs via exosomes', *Proceedings of the National Academy of Sciences of the United States of America*. doi: 10.1073/pnas.0914843107.

Perlson, E. *et al.* (2009) 'A switch in retrograde signaling from survival to stress in rapid-onset neurodegeneration', *Journal of Neuroscience*. doi: 10.1523/JNEUROSCI.0813-09.2009.

Petrov, D. *et al.* (2017) 'ALS clinical trials review: 20 years of failure. Are we any closer to registering a new treatment?', *Frontiers in Aging Neuroscience*. Frontiers Research Foundation. doi: 10.3389/fnagi.2017.00068.

Philips, T. and Rothstein, J. D. (2014) 'Glial cells in amyotrophic lateral sclerosis', *Experimental Neurology*. doi: 10.1016/j.expneurol.2014.05.015.

Pickles, S. *et al.* (2013) 'Mitochondrial damage revealed by immunoselection for ALS-linked misfolded SOD1', *Human Molecular Genetics*. doi: 10.1093/hmg/ddt249.

Pickles, S. *et al.* (2016) 'ALS-linked misfolded SOD1 species have divergent impacts on mitochondria', *Acta Neuropathologica Communications*. doi: 10.1186/s40478-016-0313-8.

Pienta, K. J., Getzenberg, R. H. and Coffey, D. S. (1992) 'Characterization of nuclear morphology and nuclear matrices in ageing human fibroblasts', *Mechanisms of Ageing and Development*. Elsevier, 62(1), pp. 13–24. doi: 10.1016/0047-6374(92)90140-9.

Pineau, I. and Lacroix, S. (2007) 'Proinflammatory cytokine synthesis in the injured mouse spinal cord: Multiphasic expression pattern and identification of the cell types involved', *The Journal of Comparative Neurology*. John Wiley & Sons, Ltd, 500(2), pp.

267–285. doi: 10.1002/cne.21149.
Poesen, K. and Van Damme, P. (2019) ‘Diagnostic and prognostic performance of neurofilaments in ALS’, *Frontiers in Neurology*. doi: 10.3389/fneur.2018.01167.
Praline, J. *et al.* (2011) ‘APOE ε4 allele is associated with an increased risk of bulbar-onset amyotrophic lateral sclerosis in men’, *European Journal of Neurology*. doi: 10.1111/j.1468-1331.2010.03330.x.
Prasad, A. *et al.* (2019) ‘Molecular mechanisms of TDP-43 misfolding and pathology in amyotrophic lateral sclerosis’, *Frontiers in Molecular Neuroscience*. doi: 10.3389/fnmol.2019.00025.
Prudencio, M. *et al.* (2009) ‘Variation in aggregation propensities among ALS-associated variants of SOD1: Correlation to human disease’, *Human Molecular Genetics*. doi: 10.1093/hmg/ddp260.
Rakhit, R. *et al.* (2002) ‘Oxidation-induced misfolding and aggregation of superoxide dismutase and its implications for amyotrophic lateral sclerosis’, *Journal of Biological Chemistry*. doi: 10.1074/jbc.M207356200.
Rakhit, R. *et al.* (2004) ‘Monomeric Cu,Zn-superoxide Dismutase Is a Common Misfolding Intermediate in the Oxidation Models of Sporadic and Familial Amyotrophic Lateral Sclerosis’, *Journal of Biological Chemistry*. doi: 10.1074/jbc.M313295200.
Rakhit, R. *et al.* (2007) ‘An immunological epitope selective for pathological monomer-misfolded SOD1 in ALS’, *Nature Medicine*. doi: 10.1038/nm1559.
Rao, S. D., Yin, H. Z. and Weiss, J. H. (2003) ‘Disruption of glial glutamate transport by reactive oxygen species produced in motor neurons’, *Journal of Neuroscience*. doi: 10.1523/jneurosci.23-07-02627.2003.
Raposo, G. and Stoorvogel, W. (2013) ‘Extracellular vesicles: Exosomes, microvesicles, and friends’, *Journal of Cell Biology*. doi: 10.1083/jcb.201211138.
Rattray, M. and Bendotti, C. (2006) ‘Does excitotoxic cell death of motor neurons in ALS arise from glutamate transporter and glutamate receptor abnormalities?’, *Experimental Neurology*. doi: 10.1016/j.expneurol.2006.05.001.
Re, D. B. *et al.* (2014) ‘Necroptosis drives motor neuron death in models of both sporadic and familial ALS’, *Neuron*. Cell Press, 81(5), pp. 1001–1008. doi: 10.1016/j.neuron.2014.01.011.
Rea, I. M. *et al.* (2018) ‘Age and age-related diseases: Role of inflammation triggers and cytokines’, *Frontiers in Immunology*. Frontiers Media S.A. doi: 10.3389/fimmu.2018.00586.

Renton, A. E. *et al.* (2011) ‘A hexanucleotide repeat expansion in C9ORF72 is the cause of chromosome 9p21-linked ALS-FTD’, *Neuron*. doi: 10.1016/j.neuron.2011.09.010.

Renton, A. E., Chiò, A. and Traynor, B. J. (2014) ‘State of play in amyotrophic lateral sclerosis genetics’, *Nature Neuroscience*. doi: 10.1038/nn.3584.

Riancho, J. *et al.* (2020) ‘ALS-derived fibroblasts exhibit reduced proliferation rate, cytoplasmic TDP-43 aggregation and a higher susceptibility to DNA damage’, *Journal of Neurology*. doi: 10.1007/s00415-020-09704-8.

Ribezzo, F., Shiloh, Y. and Schumacher, B. (2016) ‘Systemic DNA damage responses in aging and diseases.’, *Seminars in Cancer Biology*. Europe PMC Funders, 37–38, pp. 26–35. doi: 10.1016/j.semcancer.2015.12.005.

Rizvi, S., Raza, S. T. and Mahdi, F. (2015) ‘Telomere Length Variations in Aging and Age-Related Diseases’, *Current Aging Science*, 7(3), pp. 161–167. doi: 10.2174/1874609808666150122153151.

Robertson, J. *et al.* (2007) ‘Lack of TDP-43 abnormalities in mutant SOD1 transgenic mice shows disparity with ALS’, *Neuroscience Letters*. doi: 10.1016/j.neulet.2007.03.066.

Rojas, F. *et al.* (2014) ‘Astrocytes expressing mutant SOD1 and TDP43 trigger motoneuron death that is mediated via sodium channels and nitroxidative stress’, *Frontiers in Cellular Neuroscience*. doi: 10.3389/fncel.2014.00024.

Rosen, D. R. *et al.* (1993) ‘Mutations in Cu/Zn superoxide dismutase gene are associated with familial amyotrophic lateral sclerosis’, *Nature*. doi: 10.1038/362059a0.

Rothstein, J. D. *et al.* (1991) ‘Excitatory amino acids in amyotrophic lateral sclerosis: An update’, *Annals of Neurology*. doi: 10.1002/ana.410300223.

Rothstein, J. D. *et al.* (1996) ‘Knockout of glutamate transporters reveals a major role for astroglial transport in excitotoxicity and clearance of glutamate’, *Neuron*. doi: 10.1016/S0896-6273(00)80086-0.

Rothstein, J. D. *et al.* (2005) ‘β-Lactam antibiotics offer neuroprotection by increasing glutamate transporter expression’, *Nature*. doi: 10.1038/nature03180.

Rothstein, J. D., Martin, L. J. and Kuncl, R. W. (1992) ‘Decreased Glutamate Transport by the Brain and Spinal Cord in Amyotrophic Lateral Sclerosis’, *New England Journal of Medicine*. doi: 10.1056/NEJM199205283262204.

Rowland, L. P. and Shneider, N. A. (2001) ‘Amyotrophic lateral sclerosis’, *New England Journal of Medicine*, 344(22), pp. 1688–1700. doi:

10.1056/NEJM200105313442207.
Rutherford, N. J. *et al.* (2008) 'Novel mutations in TARDBP(TDP-43) in patients with familial amyotrophic lateral sclerosis', *PLoS Genetics*. doi: 10.1371/journal.pgen.1000193.
Saccon, R. A. *et al.* (2013) 'Is SOD1 loss of function involved in amyotrophic lateral sclerosis?', *Brain*. doi: 10.1093/brain/awt097.
Sama, R. R. K. *et al.* (2013) 'FUS/TLS assembles into stress granules and is a prosurvival factor during hyperosmolar stress', *Journal of Cellular Physiology*. doi: 10.1002/jcp.24395.
Sanelli, T. *et al.* (2007) 'Evidence that TDP-43 is not the major ubiquitinated target within the pathological inclusions of amyotrophic lateral sclerosis', *Journal of Neuropathology and Experimental Neurology*. doi: 10.1097/nen.0b013e31815c5edd.
Sapp, P. C. *et al.* (2003) 'Identification of two novel loci for dominantly inherited familial amyotrophic lateral sclerosis', *American Journal of Human Genetics*. doi: 10.1086/377158.
Sareen, D. *et al.* (2013) 'Targeting RNA foci in iPSC-derived motor neurons from ALS patients with a C9ORF72 repeat expansion', *Science Translational Medicine*. doi: 10.1126/scitranslmed.3007529.
Sasaki, S., Horie, Y. and Iwata, M. (2007) 'Mitochondrial alterations in dorsal root ganglion cells in sporadic amyotrophic lateral sclerosis', *Acta Neuropathologica*. doi: 10.1007/s00401-007-0299-1.
Sau, D. *et al.* (2007) 'Mutation of SOD1 in ALS: A gain of a loss of function', *Human Molecular Genetics*. doi: 10.1093/hmg/ddm110.
Sawada, H. (2017) 'Clinical efficacy of edaravone for the treatment of amyotrophic lateral sclerosis', *Expert Opinion on Pharmacotherapy*. Taylor and Francis Ltd, 18(7), pp. 735–738. doi: 10.1080/14656566.2017.1319937.
Saxena, S., Cabuy, E. and Caroni, P. (2009) 'A role for motoneuron subtype-selective ER stress in disease manifestations of FALS mice', *Nature Neuroscience*. doi: 10.1038/nn.2297.
Scaffidi, P., Gordon, L. and Misteli, T. (2005) 'The cell nucleus and aging: tantalizing clues and hopeful promises.', *PLoS Biology*. Public Library of Science, 3(11), p. e395. doi: 10.1371/journal.pbio.0030395.
Scaffidi, P. and Misteli, T. (2006) 'Lamin A-dependent nuclear defects in human aging.', *Science (New York, N.Y.)*. American Association for the Advancement of

Science, 312(5776), pp. 1059–63. doi: 10.1126/science.1127168.
Schiffer, D. *et al.* (1996) 'Reactive astrogliosis of the spinal cord in amyotrophic lateral sclerosis', in *Journal of the Neurological Sciences*. doi: 10.1016/0022-510X(96)00073-1.
Schipper, L. J. *et al.* (2016) 'Prevalence of brain and spinal cord inclusions, including dipeptide repeat proteins, in patients with the C9ORF72 hexanucleotide repeat expansion: a systematic neuropathological review', *Neuropathology and Applied Neurobiology*, 42(6), pp. 547–560. doi: 10.1111/nan.12284.
Schmidt, H. B. and Görlich, D. (2016) 'Transport Selectivity of Nuclear Pores, Phase Separation, and Membraneless Organelles', *Trends in Biochemical Sciences*. doi: 10.1016/j.tibs.2015.11.001.
Schnitzer, J., Franke, W. W. and Schachner, M. (1981) 'Immunocytochemical demonstration of vimentin in astrocytes and ependymal cells of developing and adult mouse nervous system', *Journal of Cell Biology*, 90(2), pp. 435–447. doi: 10.1083/jcb.90.2.435.
Schymick, J. C., Talbot, K. and Traynor, B. J. (2007) 'Genetics of sporadic amyotrophic lateral sclerosis', *Human Molecular Genetics*. doi: 10.1093/hmg/ddm215.
Seminary, E. R., Sison, S. L. and Ebert, A. D. (2018) 'Modeling protein aggregation and the heat shock response in ALS iPSC-derived motor neurons', *Frontiers in Neuroscience*. doi: 10.3389/fnins.2018.00086.
Shan, X., Vocadlo, D. and Krieger, C. (2009) 'Mislocalization of TDP-43 in the G93A mutant SOD1 transgenic mouse model of ALS', *Neuroscience Letters*. doi: 10.1016/j.neulet.2009.04.031.
Shaw, P. J. *et al.* (1995) 'CSF and plasma amino acid levels in motor neuron disease: Elevation of CSF glutamate in a subset of patients', *Neurodegeneration*. doi: 10.1006/neur.1995.0026.
Shechter, R. and Schwartz, M. (2013) 'Harnessing monocyte-derived macrophages to control central nervous system pathologies: No longer if' but how'', *Journal of Pathology*. doi: 10.1002/path.4106.
Shefner, J. M. *et al.* (1999) 'Mice lacking cytosolic copper/zinc superoxide dismutase display a distinctive motor axonopathy', *Neurology*. doi: 10.1212/wnl.53.6.1239.
Shi, K. Y. *et al.* (2017) 'Toxic PRn poly-dipeptides encoded by the C9orf72 repeat expansion block nuclear import and export', *Proceedings of the National Academy of Sciences of the United States of America*. doi: 10.1073/pnas.1620293114.

Shi, P. *et al.* (2010) 'Effects of ALS-related SOD1 mutants on dynein- and KIF5-mediated retrograde and anterograde axonal transport', *Biochimica et Biophysica Acta - Molecular Basis of Disease*. doi: 10.1016/j.bbadis.2010.05.008.

Shi, Y. *et al.* (2018) 'Haploinsufficiency leads to neurodegeneration in C9ORF72 ALS/FTD human induced motor neurons', *Nature Medicine*. doi: 10.1038/nm.4490.

Shibata, N. *et al.* (2001) 'Morphological evidence for lipid peroxidation and protein glycoxidation in spinal cords from sporadic amyotrophic lateral sclerosis patients', *Brain Research*. doi: 10.1016/S0006-8993(01)02926-2.

Shibata, N. and Kobayashi, M. (2008) 'The role for oxidative stress in neurodegenerative diseases', *Brain and Nerve*, pp. 157–170. doi: 10.5607/en.2015.24.4.325.

Shvil, N. *et al.* (2018) 'MIF inhibits the formation and toxicity of misfolded SOD1 amyloid aggregates: Implications for familial ALS article', *Cell Death and Disease*. doi: 10.1038/s41419-017-0130-4.

Siddique, T. *et al.* (1991) 'Linkage of a Gene Causing Familial Amyotrophic Lateral Sclerosis to Chromosome 21 and Evidence of Genetic-Locus Heterogeneity', *New England Journal of Medicine*. doi: 10.1056/NEJM199105163242001.

Sigfridsson, E. *et al.* (2018) 'Astrocyte-specific overexpression of Nrf2 protects against optic tract damage and behavioural alterations in a mouse model of cerebral hypoperfusion', *Scientific Reports*. Nature Publishing Group, 8(1). doi: 10.1038/s41598-018-30675-4.

Silani, V. *et al.* (2011) 'The diagnosis of Amyotrophic Lateral Sclerosis', *Archives Italiennes de Biologie*, 149(1), pp. 5–27. doi: 10.4449/aib.v149i1.1260.

Silverman, J. M. *et al.* (2019) 'CNS-derived extracellular vesicles from superoxide dismutase 1 (SOD1)G93A ALS mice originate from astrocytes and neurons and carry misfolded SOD1', *Journal of Biological Chemistry*. doi: 10.1074/jbc.RA118.004825.

Simpson, J. E. *et al.* (2011) 'Microarray analysis of the astrocyte transcriptome in the aging brain: Relationship to Alzheimer's pathology and APOE genotype', *Neurobiology of Aging*, 32(10), pp. 1795–1807. doi: 10.1016/j.neurobiolaging.2011.04.013.

Smith, B. N. *et al.* (2014) 'Exome-wide rare variant analysis identifies TUBA4A mutations associated with familial ALS', *Neuron*. doi: 10.1016/j.neuron.2014.09.027.

Son, E. Y. *et al.* (2011) 'Conversion of mouse and human fibroblasts into functional spinal motor neurons', *Cell Stem Cell*. doi: 10.1016/j.stem.2011.07.014.

Soniat, M. and Chook, Y. M. (2015) ‘Nuclear localization signals for four distinct Karyopherin-β nuclear import systems’, *Biochemical Journal*. doi: 10.1042/BJ20150368.

Soreq, L. *et al.* (2017) ‘Major Shifts in Glial Regional Identity Are a Transcriptional Hallmark of Human Brain Aging’, *Cell Reports*. doi: 10.1016/j.celrep.2016.12.011.

Sreedharan, J. *et al.* (2008) ‘TDP-43 mutations in familial and sporadic amyotrophic lateral sclerosis’, *Science*. doi: 10.1126/science.1154584.

Stade, K. *et al.* (1997) ‘Exportin 1 (Crm1p) is an essential nuclear export factor’, *Cell*. doi: 10.1016/S0092-8674(00)80370-0.

Steele, J. C. and McGeer, P. L. (2008) ‘The ALS/PDC syndrome of Guam and the cycad hypothesis’, *Neurology*. Lippincott Williams and Wilkins, pp. 1984–1990. doi: 10.1212/01.wnl.0000312571.81091.26.

Stephens, B. *et al.* (2006) ‘Widespread loss of neuronal populations in the spinal ventral horn in sporadic motor neuron disease. A morphometric study’, *Journal of the Neurological Sciences*. doi: 10.1016/j.jns.2005.12.003.

Stieber, A., Gonatas, J. O. and Gonatas, N. K. (2000) ‘Aggregates of mutant protein appear progressively in dendrites, in periaxonal processes of oligodendrocytes, and in neuronal and astrocytic perikarya of mice expressing the SOD1(G93A) mutation of familial amyotrophic lateral sclerosis’, *Journal of the Neurological Sciences*. doi: 10.1016/S0022-510X(00)00351-8.

Strange, R. W. *et al.* (2003) ‘The structure of holo and metal-deficient wild-type human Cu, Zn superoxide dismutase and its relevance to familial amyotrophic lateral sclerosis’, *Journal of Molecular Biology*. doi: 10.1016/S0022-2836(03)00355-3.

Al Sultan, A. *et al.* (2016) ‘The genetics of amyotrophic lateral sclerosis: current insights’, *Degenerative Neurological and Neuromuscular Disease*, p. 49. doi: 10.2147/dnnd.s84956.

Sundaramoorthy, V. *et al.* (2013) ‘Extracellular wildtype and mutant SOD1 induces ER-Golgi pathology characteristic of amyotrophic lateral sclerosis in neuronal cells’, *Cellular and Molecular Life Sciences*. doi: 10.1007/s00018-013-1385-2.

Suraweera, A. *et al.* (2007) ‘Senataxin, defective in ataxia oculomotor apraxia type 2, is involved in the defense against oxidative DNA damage’, *Journal of Cell Biology*. doi: 10.1083/jcb.200701042.

Synofzik, M. *et al.* (2012) ‘Mutant superoxide dismutase-1 indistinguishable from wild-type causes ALS’, *Human Molecular Genetics*. doi: 10.1093/hmg/dds188.

Tadic, V. *et al.* (2014) 'The ER mitochondria calcium cycle and ER stress response as therapeutic targets in amyotrophic lateral sclerosis', *Frontiers in Cellular Neuroscience*. doi: 10.3389/fncel.2014.00147.

Tainer, J. A. *et al.* (1982) 'Determination and analysis of the 2 Å structure of copper, zinc superoxide dismutase', *Journal of Molecular Biology*. doi: 10.1016/0022-2836(82)90174-7.

Takahashi, K. *et al.* (2007) 'Induction of Pluripotent Stem Cells from Adult Human Fibroblasts by Defined Factors', *Cell*. Cell Press, 131(5), pp. 861–872. doi: 10.1016/J.CELL.2007.11.019.

Takahashi, Y. *et al.* (2013) 'Erbb4 mutations that disrupt the neuregulin-erbb4 pathway cause amyotrophic lateral sclerosis type 19', *American Journal of Human Genetics*. doi: 10.1016/j.ajhg.2013.09.008.

Takeuchi, R. *et al.* (2016) 'Heterogeneity of cerebral TDP-43 pathology in sporadic amyotrophic lateral sclerosis: Evidence for clinico-pathologic subtypes', *Acta Neuropathologica Communications*. doi: 10.1186/s40478-016-0335-2.

Tan, C. F. *et al.* (2007) 'TDP-43 immunoreactivity in neuronal inclusions in familial amyotrophic lateral sclerosis with or without SOD1 gene mutation', *Acta Neuropathologica*. doi: 10.1007/s00401-007-0206-9.

Tan, R. H. *et al.* (2017) 'ALS/FTLD: experimental models and reality', *Acta Neuropathologica*. doi: 10.1007/s00401-016-1666-6.

Tang, Y. *et al.* (2017) 'Direct Reprogramming Rather than iPSC-Based Reprogramming Maintains Aging Hallmarks in Human Motor Neurons', *Frontiers in Molecular Neuroscience*. Frontiers, 10, p. 359. doi: 10.3389/fnmol.2017.00359.

Taupin, V. *et al.* (1997) 'Increased severity of experimental autoimmune encephalomyelitis, chronic macrophage/microglial reactivity, and demyelination in transgenic mice producing tumor necrosis factor-α in the central nervous system', *European Journal of Immunology*, 27(4), pp. 905–913. doi: 10.1002/eji.1830270416.

Taura, D. *et al.* (2009) 'Adipogenic differentiation of human induced pluripotent stem cells: Comparison with that of human embryonic stem cells', *FEBS Letters*. doi: 10.1016/j.febslet.2009.02.031.

Tchieu, J. *et al.* (2019) 'NFIA is a gliogenic switch enabling rapid derivation of functional human astrocytes from pluripotent stem cells', *Nature Biotechnology*. Nature Publishing Group, pp. 267–275. doi: 10.1038/s41587-019-0035-0.

Terry, L. J., Shows, E. B. and Wente, S. R. (2007) 'Crossing the nuclear envelope:

Hierarchical regulation of nucleocytoplasmic transport', *Science*. Science, pp. 1412–1416. doi: 10.1126/science.1142204.

Ticozzi, N. *et al.* (2010) 'Paraoxonase gene mutations in amyotrophic lateral sclerosis', *Annals of Neurology*. doi: 10.1002/ana.21993.

Ticozzi, N. *et al.* (2011) 'Genetics of familial amyotrophic lateral sclerosis', *Archives Italiennes de Biologie*. doi: 10.5772/32498.

Tilstra, J. S. *et al.* (2011) 'NF-κB in aging and disease', *Aging and Disease*. International Society on Aging and Disease, pp. 449–465.

Tobisawa, S. *et al.* (2003) 'Mutant SOD1 linked to familial amyotrophic lateral sclerosis, but not wild-type SOD1, induces ER stress in COS7 cells and transgenic mice', *Biochemical and Biophysical Research Communications*. doi: 10.1016/S0006-291X(03)00353-X.

Tokuda, E. *et al.* (2019) 'Wild-type Cu/Zn-superoxide dismutase is misfolded in cerebrospinal fluid of sporadic amyotrophic lateral sclerosis', *Molecular Neurodegeneration*. BioMed Central Ltd., 14(1). doi: 10.1186/s13024-019-0341-5.

Tomkins, J. *et al.* (1998) 'Novel insertion in the KSP region of the neurofilament heavy gene in amyotrophic lateral sclerosis (ALS)', *NeuroReport*. doi: 10.1097/00001756-199812010-00036.

Tortelli, R. *et al.* (2012) 'Elevated cerebrospinal fluid neurofilament light levels in patients with amyotrophic lateral sclerosis: A possible marker of disease severity and progression', *European Journal of Neurology*. doi: 10.1111/j.1468-1331.2012.03777.x.

Trist, B. G. *et al.* (2017) 'Amyotrophic lateral sclerosis-like superoxide dismutase 1 proteinopathy is associated with neuronal loss in Parkinson's disease brain', *Acta Neuropathologica*. doi: 10.1007/s00401-017-1726-6.

Troost, D. *et al.* (1989) 'Lymphocytic infiltration in the spinal cord of patients with amyotrophic lateral sclerosis', *Clinical Neuropathology*.

Troost, D., van den Oord, J. J. and Jong, J. M. B. V. de (1990) 'Immunohistochemical characterization of the inflammatory infiltrate in amyotrophic lateral sclerosis', *Neuropathology and Applied Neurobiology*. doi: 10.1111/j.1365-2990.1990.tb01276.x.

Trotti, D. *et al.* (1999) 'SOD1 mutants linked to amyotrophic lateral sclerosis selectively inactivate a glial glutamate transporter', *Nature Neuroscience*. doi: 10.1038/8091.

Tsang, C. K. wa. *et al.* (2014) 'Superoxide dismutase 1 acts as a nuclear transcription factor to regulate oxidative stress resistance', *Nature Communications*. doi:

10.1038/ncomms4446.

Turner, B. J. *et al.* (2008) 'TDP-43 expression in mouse models of amyotrophic lateral sclerosis and spinal muscular atrophy', *BMC Neuroscience*. doi: 10.1186/1471-2202-9-104.

Turner, M. R. *et al.* (2004) 'Evidence of widespread cerebral microglial activation in amyotrophic lateral sclerosis: An [11C](R)-PK11195 positron emission tomography study', *Neurobiology of Disease*. doi: 10.1016/j.nbd.2003.12.012.

Urushitani, M. *et al.* (2006) 'Chromogranin-mediated secretion of mutant superoxide dismutase proteins linked to amyotrophic lateral sclerosis', *Nature Neuroscience*. doi: 10.1038/nn1603.

Valadi, H. *et al.* (2007) 'Exosome-mediated transfer of mRNAs and microRNAs is a novel mechanism of genetic exchange between cells', *Nature Cell Biology*. doi: 10.1038/ncb1596.

Valentine, J. S., Doucette, P. A. and Zittin Potter, S. (2005) 'COPPER-ZINC SUPEROXIDE DISMUTASE AND AMYOTROPHIC LATERAL SCLEROSIS', *Annual Review of Biochemistry*. doi: 10.1146/annurev.biochem.72.121801.161647.

Vance, C. *et al.* (2009) 'Mutations in FUS, an RNA processing protein, cause familial amyotrophic lateral sclerosis type 6', *Science*. doi: 10.1126/science.1165942.

Varcianna, A. *et al.* (2019) 'Micro-RNAs secreted through astrocyte-derived extracellular vesicles cause neuronal network degeneration in C9orf72 ALS', *EBioMedicine*. doi: 10.1016/j.ebiom.2018.11.067.

Vande Velde, C. *et al.* (2011) 'Misfolded SOD1 associated with motor neuron mitochondria alters mitochondrial shape and distribution prior to clinical onset', *PLoS ONE*. doi: 10.1371/journal.pone.0022031.

Veldink, J. H. *et al.* (2005) 'SMN genotypes producing less SMN protein increase susceptibility to and severity of sporadic ALS', *Neurology*. doi: 10.1212/01.wnl.0000174472.03292.dd.

Verkhratsky, A. and Nedergaard, M. (2016) 'The homeostatic astroglia emerges from evolutionary specialization of neural cells', *Philosophical Transactions of the Royal Society B: Biological Sciences*. doi: 10.1098/rstb.2015.0428.

Victor, M. B. *et al.* (2018) 'Striatal neurons directly converted from Huntington's disease patient fibroblasts recapitulate age-associated disease phenotypes', *Nature Neuroscience*. doi: 10.1038/s41593-018-0075-7.

Vijayvergiya, C. *et al.* (2005) 'Mutant superoxide dismutase 1 forms aggregates in the

brain mitochondrial matrix of amyotrophic lateral sclerosis mice', *Journal of Neuroscience*. doi: 10.1523/JNEUROSCI.4385-04.2005.

De vos, K. J. *et al.* (2007) 'Familial amyotrophic lateral sclerosis-linked SOD1 mutants perturb fast axonal transport to reduce axonal mitochondria content', *Human Molecular Genetics*. doi: 10.1093/hmg/ddm226.

Vyas, K. J. and Weiss, J. H. (2009) 'BMAA – an unusual cyanobacterial neurotoxin', *Amyotrophic Lateral Sclerosis*, 10(sup2), pp. 50–55. doi: 10.3109/17482960903268742.

Waite, A. J. *et al.* (2014) 'Reduced C9orf72 protein levels in frontal cortex of amyotrophic lateral sclerosis and frontotemporal degeneration brain with the C9ORF72 hexanucleotide repeat expansion', *Neurobiology of Aging*. doi: 10.1016/j.neurobiolaging.2014.01.016.

Walker, A. K. *et al.* (2013) 'ALS-associated TDP-43 induces endoplasmic reticulum stress, which drives cytoplasmic TDP-43 accumulation and stress granule formation', *PLoS ONE*. doi: 10.1371/journal.pone.0081170.

Walker, C. *et al.* (2017) 'C9orf72 expansion disrupts ATM-mediated chromosomal break repair', *Nature Neuroscience*. doi: 10.1038/nn.4604.

Waller, R. *et al.* (2012) 'Isolation of enriched glial populations from post-mortem human CNS material by immuno-laser capture microdissection', *Journal of Neuroscience Methods*. doi: 10.1016/j.jneumeth.2012.04.014.

Walss-Bass, C. *et al.* (2002) 'Occurrence of nuclear βII-tubulin in cultured cells', *Cell and Tissue Research*. doi: 10.1007/s00441-002-0539-6.

Wang, L. *et al.* (2008) 'Restricted expression of mutant SOD1 in spinal motor neurons and interneurons induces motor neuron pathology', *Neurobiology of Disease*. doi: 10.1016/j.nbd.2007.10.004.

Wang, L., Popko, B. and Roos, R. P. (2011) 'The unfolded protein response in familial amyotrophic lateral sclerosis', *Human Molecular Genetics*. doi: 10.1093/hmg/ddq546.

Wang, Q. *et al.* (2008) 'Protein aggregation and protein instability govern familial amyotrophic lateral sclerosis patient survival', *PLoS Biology*. doi: 10.1371/journal.pbio.0060170.

Wang, W. *et al.* (2013) 'The ALS disease-associated mutant TDP-43 impairs mitochondrial dynamics and function in motor neurons', *Human Molecular Genetics*. doi: 10.1093/hmg/ddt319.

Wang, W. *et al.* (2016) 'The inhibition of TDP-43 mitochondrial localization blocks its

neuronal toxicity', *Nature Medicine*. doi: 10.1038/nm.4130.
Watanabe, M. *et al.* (2001) 'Histological evidence of protein aggregation in mutant SOD1 transgenic mice and in amyotrophic lateral sclerosis neural tissues', *Neurobiology of Disease*. doi: 10.1006/nbdi.2001.0443.
Webster, C. P. *et al.* (2016) 'The C9orf72 protein interacts with Rab1a and the ULK1 complex to regulate initiation of autophagy.', *The EMBO Journal*, 35(15), pp. 1656–76. doi: 10.15252/embj.201694401.
Webster, C. P. *et al.* (2018) 'C9orf72 plays a central role in Rab GTPase-dependent regulation of autophagy', *Small GTPases*. doi: 10.1080/21541248.2016.1240495.
Wicks, P. (2012) 'Hypothesis: Higher prenatal testosterone predisposes ALS patients to improved athletic performance and manual professions', *Amyotrophic Lateral Sclerosis*. doi: 10.3109/17482968.2011.634009.
Wiedemann, F. R. *et al.* (2002) 'Mitochondrial DNA and respiratory chain function in spinal cords of ALS patients', *Journal of Neurochemistry*. doi: 10.1046/j.0022-3042.2001.00731.x.
Williamson, T. L. *et al.* (1998) 'Absence of neurofilaments reduces the selective vulnerability of motor neurons and slows disease caused by a familial amyotrophic lateral sclerosis-linked superoxide dismutase 1 mutant', *Proceedings of the National Academy of Sciences of the United States of America*. doi: 10.1073/pnas.95.16.9631.
Woerner, A. C. *et al.* (2016) 'Cytoplasmic protein aggregates interfere with nucleocytoplasmic transport of protein and RNA', *Science*. doi: 10.1126/science.aad2033.
Wong, P. C. *et al.* (1995) 'An adverse property of a familial ALS-linked SOD1 mutation causes motor neuron disease characterized by vacuolar degeneration of mitochondria', *Neuron*. doi: 10.1016/0896-6273(95)90259-7.
Wu, C. H. *et al.* (2012) 'Mutations in the profilin 1 gene cause familial amyotrophic lateral sclerosis', *Nature*. doi: 10.1038/nature11280.
Wu, Y., Zhang, A.-Q. and Yew, D. T. (2005) 'Age related changes of various markers of astrocytes in senescence-accelerated mice hippocampus', *Neurochemistry International*. Pergamon, 46(7), pp. 565–574. doi: 10.1016/J.NEUINT.2005.01.002.
Xu, D. *et al.* (2018) 'TBK1 Suppresses RIPK1-Driven Apoptosis and Inflammation during Development and in Aging', *Cell*. doi: 10.1016/j.cell.2018.07.041.
Yamanaka, K. *et al.* (2008) 'Astrocytes as determinants of disease progression in inherited amyotrophic lateral sclerosis', *Nature Neuroscience*. doi: 10.1038/nn2047.

Yin, F. *et al.* (2012) 'Alterations of signaling pathways in muscle tissues of patients with amyotrophic lateral sclerosis', *Muscle and Nerve*. doi: 10.1002/mus.23411.
Yokoseki, A. *et al.* (2008) 'TDP-43 mutation in familial amyotrophic lateral sclerosis', *Annals of Neurology*. doi: 10.1002/ana.21392.
Zhang, H. *et al.* (2008) 'TDP-43-immunoreactive neuronal and glial inclusions in the neostriatum in amyotrophic lateral sclerosis with and without dementia', *Acta Neuropathologica*. doi: 10.1007/s00401-007-0285-7.
Zhang, H., Davies, K. J. A. and Forman, H. J. (2015) 'Oxidative stress response and Nrf2 signaling in aging', *Free Radical Biology and Medicine*. Elsevier Inc., pp. 314–336. doi: 10.1016/j.freeradbiomed.2015.05.036.
Zhang, K., Donnelly, C. J., Haeusler, A. R., Grima, J. C., Machamer, J. B., Steinwald, P., Daley, E. L., Miller, S. J., Cunningham, K. M., Vidensky, S., Gupta, S., Thomas, M. A., Hong, I., Chiu, S.-L., *et al.* (2015) 'The C9orf72 repeat expansion disrupts nucleocytoplasmic transport', *Nature*, 525(7567), pp. 56–61. doi: 10.1038/nature14973.
Zhang, K., Donnelly, C. J., Haeusler, A. R., Grima, J. C., Machamer, J. B., Steinwald, P., Daley, E. L., Miller, S. J., Cunningham, K. M., Vidensky, S., Gupta, S., Thomas, M. A., Hong, I., Chiu, S. L., *et al.* (2015) 'The C9orf72 repeat expansion disrupts nucleocytoplasmic transport', *Nature*. doi: 10.1038/nature14973.
Zhao, X. and Rothstein, R. (2002) 'The Dun1 checkpoint kinase phosphorylates and regulates the ribonucleotide reductase inhibitor Sml1', *Proceedings of the National Academy of Sciences of the United States of America*. doi: 10.1073/pnas.062502299.
Zhong, Y. *et al.* (2017) 'Nuclear export of misfolded SOD1 mediated by a normally buried NES-like sequence reduces proteotoxicity in the nucleus', *eLife*. doi: 10.7554/eLife.23759.
Zhou, Z. and Elledge, S. J. (1993) 'DUN1 encodes a protein kinase that controls the DNA damage response in yeast', *Cell*. doi: 10.1016/0092-8674(93)90321-G.
Ziff, O. J. and Patani, R. (2019) 'Harnessing cellular aging in human stem cell models of amyotrophic lateral sclerosis', *Aging Cell*. Blackwell Publishing Ltd. doi: 10.1111/acel.12862.
Zinszner, H. *et al.* (1997) 'TLS (FUS) binds RNA in vivo and engages in nucleo-cytoplasmic shuttling', *Journal of Cell Science*.
Zou, Z. Y. *et al.* (2017) 'Genetic epidemiology of amyotrophic lateral sclerosis: A systematic review and meta-analysis', *Journal of Neurology, Neurosurgery and*

Psychiatry. doi: 10.1136/jnnp-2016-315018.
Zu, T. *et al.* (2013) 'RAN proteins and RNA foci from antisense transcripts in C9ORF72 ALS and frontotemporal dementia', *Proceedings of the National Academy of Sciences of the United States of America*. doi: 10.1073/pnas.1315438110.
van Zundert, B. and Brown, R. H. (2017) 'Silencing strategies for therapy of SOD1-mediated ALS', *Neuroscience Letters*. doi: 10.1016/j.neulet.2016.07.059.

7. Outputs from my PhD work: Awards, communications and publications

7.1 Awards

Guarantors of Brain travel grant April, 2019

2nd place for Sheffield Neuroscience Imaging Twitter Competition November, 2017

7.2 Communications at national and international scientific meetings

Poster presentation: *"Direct conversion of human fibroblasts to induced neural progenitor cells (iNPCs) retains ageing hallmarks in derived astrocytes"* University of Sheffield, Faculty of Science Symposium, Multidisciplinary Perspectives on Ageing, 17th June 2019

Platform presentation European ALS meeting (ENCALS) 2019*: "Using patient-derived astrocytes to unravel the nuclear role of SOD1 and its link with nucleus/cytoplasm shuttling"* Tours, France, May 2019

Platform presentation *"Direct conversion of human fibroblasts to induced NPCs retains ageing hallmarks in derived astrocytes"* Sheffield Glia Symposium 2019

Platform presentation ENCALS 2018, "*Using patient-derived astrocytes to unravel the role of misfolded SOD1 in sALS cases"* University of Oxford, June 2018

Poster presentation ENCODS 2018 *"The role of wild type SOD1 in sporadic ALS"* European Neuroscience Conference by Doctoral Students, Berlin, July 2018

Selected for Research snapshot: *"Using patient-derived astrocytes to unravel the role of misfolded SOD1 in MND"* Sheffield Glia Symposium, 2017

Poster presentation: *"The role of wild type SOD1 in sporadic ALS"* Sheffield Neuroscience conference, 2017

Poster presentation: *"The role of wild type SOD1 in sporadic ALS"* University of Sheffield Medical School Research Meeting, 2017

7.3 Publications

1. Under revision in Aging Cell: **Gatto** et al*., Directly converted astrocytes retain the ageing features of the donor fibroblasts and elucidate the astrocytic contribution to human CNS health and disease*

2. *C9orf72 expansion within astrocytes reduces metabolic flexibility in amyotrophic lateral sclerosis* Scott P Allen, Benjamin Hall, Ryan Woof, Laura Francis, **Noemi Gatto**, Allan C Shaw, Monika Myszczynska, Jordan Hemingway, Ian Coldicott, Amelia Willcock, Lucy Job, Rachel M Hughes, Camilla Boschian, Nadhim Bayatti, Paul R Heath, Oliver Bandmann, Heather Mortiboys, Laura Ferraiuolo, Pamela J Shaw

8. Appendix

Table S3 *Related to Figure 2 Genes in the intersection between the two comparisons*

Gene Symbol	p-value
AAAS	3,07E-05
AAMDC	0,0003726
ABCA1	0,001535125
ABI1	1,07E-05
ACAA2	7,64E-06
ACAT1	3,67E-05
ACLY	6,94E-07
ACOX1	2,83E-06
ACP1	5,39E-06
ACSL4	1,39E-05
ACTA1	4,38E-08
ACTG1	0,000307765
ACTN4	0,000134117
ACTR2	4,61E-06
ACTR3	1,92E-06
ADAM22	2,44E-05
ADAM23	0,017339494
ADGRL2	0,001406916
AES	1,93E-07
AGAP4	7,74E-05
AGFG1	0,000110766
AGK	4,73E-05
AGO2	0,001079036
AHCYL1	1,06E-07
AHR	0,001732575
AKAP12	0,000516723
AKAP8L	7,01E-06

AKIRIN1	1,18E-06
ALCAM	0,002380606
ALDH1L2	0,01277142
AMD1	5,32E-06
ANAPC11	0,000528467
ANAPC7	2,53E-05
ANGEL2	1,22E-05
ANGPT1	0,003217141
ANKMY1	2,20E-08
ANKRD36	0,000510121
ANKRD52	8,61E-09
ANPEP	0,00075944
ANTXR1	0,00200466
ANXA1	8,57E-05
ANXA2	1,44E-06
AP2B1	1,37E-05
AP4E1	9,09E-05
APH1A	6,90E-06
APLP2	8,84E-05
APOBEC3C	0,000771163
APP	3,73E-06
ARF1	0,000258148
ARF4	0,000841142
ARF6	3,95E-05
ARFGEF2	7,99E-05
ARHGAP18	0,001196748
ARHGAP35	5,28E-05
ARHGAP42	1,32E-07
ARHGDIA	2,41E-05
ARHGEF12	1,54E-05
ARHGEF7	6,86E-07
ARID2	6,04E-05

ARID5B	0,000292019
ARIH1	1,75E-05
ARMC8	6,16E-05
ARNT	5,24E-05
ARPC5	0,000115547
ARRB2	1,24E-05
ARSB	3,10E-06
ASPH	6,96E-06
ASS1	0,00089176
ASTN2	6,17E-07
ATF2	4,71E-06
ATF6B	0,000218554
ATF7IP	1,81E-07
ATG3	2,19E-05
ATL3	1,64E-06
ATM	4,74E-05
ATP2A2	4,05E-06
ATP2B4	0,00014027
ATP2C1	0,002011325
ATP5A1	9,11E-06
ATP5B	6,46E-06
ATP5G2	8,09E-06
ATP5H	0,000133528
ATP5J2	0,000414776
ATP5O	7,25E-06
ATP5SL	1,56E-07
ATP6AP2	5,15E-05
ATP6V0A1	0,005861696
ATP6V0A2	7,16E-06
ATP6V0C	0,002614981
ATP6V0E1	7,17E-05
ATP6V1H	1,93E-05

ATRAID	0,000259208
ATRN	0,000260366
ATXN1	2,77E-05
ATXN10	3,44E-05
ATXN2L	0,000820857
AVL9	6,39E-06
AXL	2,90E-08
B2M	0,000541542
B4GALT2	1,90E-07
BANF1	0,000285112
BBS9	7,68E-08
BBX	4,59E-11
BCAP31	1,02E-05
BCL10	2,54E-05
BCL2L13	2,80E-09
BECN1	3,77E-09
BEND7	3,99E-05
BGN	0,000329381
BHLHA15	4,61E-05
BLID	0,000207538
BLZF1	3,29E-05
BMP2K	0,001593381
BMPR1A	0,000150158
BNIP3	1,72E-06
BNIP3L	9,17E-05
BRD3	3,04E-09
BRE	0,000474729
BRIX1	0,000148843
BRK1	0,00021254
BSG	3,34E-05
BTBD2	2,18E-06
BTRC	1,24E-07

BUB3	3,97E-05
C10orf76	6,39E-05
C11orf1	0,000317515
C11orf54	2,68E-06
C11orf58	2,94E-05
C12orf49	8,85E-05
C14orf1	0,001925703
C16orf62	1,22E-05
C16orf70	5,80E-05
C17orf89	0,000259163
C18orf21	0,000513548
C1orf123	1,90E-05
C1orf43	6,39E-05
C4orf27	3,18E-05
C5AR1	2,04E-05
C6orf89	3,16E-06
C7orf49	4,37E-05
C9orf3	5,81E-05
CA5B	0,031221765
CACUL1	0,000179693
CALCOCO2	4,01E-07
CALR	6,71E-06
CALU	6,50E-05
CAMK2D	0,015833852
CAMKK2	7,81E-09
CAMKMT	0,004027158
CAND1	5,85E-06
CANX	0,000144405
CAPNS1	3,08E-06
CAPRIN1	2,08E-05
CAPZA2	6,80E-07
CARF	6,84E-06

CASC4	3,40E-05
CASP16P	1,43E-08
CASP4	0,005085804
CASP8	2,08E-06
CBLB	0,000286062
CBR4	0,000277967
CBWD2	9,64E-05
CBX3	0,001173945
CBY1	2,73E-07
CCAR2	5,81E-08
CCDC122	1,62E-05
CCDC124	0,000415692
CCDC14	0,000395244
CCDC183	8,03E-05
CCDC34	2,78E-05
CCDC47	3,34E-05
CCDC6	0,000386404
CCDC82	6,78E-06
CCDC88A	0,000316643
CCDC90B	0,002239962
CCDC91	0,000474068
CCNA2	0,008822375
CCND2	0,033253855
CCNG2	0,000114695
CCNI	5,83E-05
CCNK	1,15E-05
CCNT1	1,54E-05
CCNY	1,48E-05
CCSER2	4,44E-05
CCT3	4,31E-07
CD151	0,00400436
CD55	0,00087778

CD59	0,010414141
CDC123	0,000113881
CDC42	0,000241779
CDC42BPB	1,20E-06
CDC42EP1	5,36E-05
CDK17	0,000790571
CDK19	0,000757551
CDKAL1	2,07E-07
CDKN2AIPNL	3,65E-08
CDON	0,000374995
CDR1	0,036162455
CDV3	0,000228985
CENPF	7,74E-05
CEP95	1,45E-06
CEPT1	3,93E-06
CFAP97	1,93E-08
CFLAR	0,000636061
CGGBP1	0,00105565
CHD3	5,86E-05
CHD6	4,84E-08
CHM	7,12E-05
CHML	1,36E-07
CHMP1B	0,000534986
CITED2	0,011252769
CKAP2	3,15E-07
CLDN11	0,001057743
CLEC2B	0,0048632
CLN6	4,12E-09
CLTA	0,000115388
CMPK1	7,08E-07
CMTM3	1,30E-05
CMTM6	3,84E-05

CMTM7	6,05E-05
CNKSR3	2,19E-05
CNOT1	1,67E-06
CNOT6L	5,80E-11
CNOT7	3,81E-05
CNTNAP3	0,005763783
COA1	2,42E-05
COG3	6,65E-07
COL1A2	0,017663554
COL6A1	0,001721466
COL8A1	0,011649949
COLGALT1	0,00021785
COPA	4,48E-07
COPS3	6,30E-05
COQ10B	5,59E-05
COTL1	0,000197953
COX1	5,42E-05
COX17	3,43E-05
COX2	4,96E-07
COX20	0,000107915
COX8A	0,000558713
CPPED1	3,06E-05
CRKL	1,90E-06
CRNDE	0,001860954
CRTAP	0,000131318
CSDE1	1,20E-07
CSF1	0,009674138
CSNK1A1	8,73E-06
CSNK2A2	0,000242359
CTNNA1	0,003075046
CTNNB1	2,59E-06
CTSA	7,05E-05

CTSC	2,15E-05
CTSZ	0,009407338
CTTN	2,62E-05
CUL3	0,000260906
CYB5R1	1,34E-05
CYB5R3	0,000152287
CYBRD1	0,000528905
CYHR1	1,10E-05
CYS1	3,86E-05
CYYR1	0,005867621
DAB2	1,46E-05
DAD1	0,000169281
DCAF13	8,32E-06
DCAF5	0,000309049
DCAKD	0,009521252
DCBLD2	0,002834703
DCTN5	2,61E-05
DDR2	0,002036466
DDX10	1,67E-07
DDX17	4,93E-05
DDX19A	3,95E-06
DDX19B	2,33E-05
DDX3X	1,32E-05
DDX42	3,77E-11
DDX50	0,000419401
DDX52	7,11E-05
DDX6	0,000236922
DEK	0,000425755
DESI2	0,00036109
DHX30	3,18E-06
DHX36	0,000780826
DHX8	5,42E-05

DIAPH1	4,34E-09
DIAPH3	1,18E-05
DIP2B	1,05E-05
DMTF1	0,000157227
DNAJC13	1,80E-05
DNAJC2	0,000105007
DNAJC4	4,33E-09
DNAJC7	2,12E-05
DOCK10	0,002707755
DOCK5	0,006689282
DPY19L1	7,35E-05
DPY19L4	0,000136336
DPYD	0,000824645
DR1	4,30E-06
DSE	3,31E-05
DST	0,000108967
DTD1	3,57E-07
DTWD1	0,000174021
DVL2	1,32E-05
DVL3	1,76E-06
DYM	2,71E-05
DYNC1H1	0,000143298
DYNC2H1	9,26E-05
DYNLRB1	6,31E-05
E2F4	5,89E-05
ECH1	0,000642061
EDNRA	0,015881254
EEF1A1	3,06E-08
EEF1G	5,33E-07
EEF2	1,28E-05
EFEMP2	0,00334949
EFNA5	0,000395781

EFTUD2	1,42E-06
EGFL7	0,000344088
EGR1	0,000852326
EHD2	7,83E-06
EHD4	0,000312045
EIF1	2,71E-05
EIF2AK1	1,92E-06
EIF2AK2	1,04E-05
EIF2S2	0,000115531
EIF2S3	4,82E-07
EIF3K	0,000151821
EIF4A1	4,88E-06
EIF4B	1,52E-05
EIF4EBP2	5,70E-06
EIF4G2	1,04E-05
EIF4G3	1,61E-05
EIF5	5,74E-05
ELAC2	2,49E-06
ELK4	6,87E-06
ELL2	0,00333085
ELOVL5	5,84E-06
ELP3	1,65E-05
EMC10	1,80E-05
EMC3	9,21E-06
EMD	9,69E-05
EML2-AS1	2,24E-05
EML4	2,15E-06
EMP1	8,47E-07
EMP2	0,00253193
EMSY	0,000403532
ENAH	0,001616579
ENG	0,000248319

ENPP1	0,002637033
EPB41L2	0,005798544
EPHA7	0,014730959
ERGIC3	1,72E-06
ERO1A	5,97E-05
ERP44	0,000654947
ERRFI1	0,006846282
ESYT2	6,09E-05
EXOSC1	3,59E-05
EXOSC10	1,17E-05
EZR	0,004807015
F2RL2	0,006615736
F2RL3	1,35E-07
FADS2	0,001458405
FAF2	0,0006083
FAM117B	0,000508662
FAM120A	2,30E-05
FAM120AOS	0,001352645
FAM160B1	5,97E-06
FAM49B	0,000252921
FAM98B	0,000985349
FAR2	0,011724668
FARP1	0,000730041
FARP2	2,24E-06
FARSB	7,42E-06
FASTKD2	5,15E-05
FBL	3,42E-05
FBXL14	0,000232374
FBXO18	0,001691953
FBXO22	4,21E-06
FBXO4	1,92E-05
FBXW2	4,21E-07

FCF1	8,41E-05
FCHSD2	0,001779789
FERMT2	4,47E-05
FFAR1	2,32E-06
FGD6	6,67E-05
FGF8	3,46E-06
FGFR1OP2	3,95E-05
FILIP1L	0,01328783
FIP1L1	7,55E-07
FKBP10	0,001123935
FKBP15	2,46E-07
FKBP4	2,03E-06
FKBP7	0,000210886
FKBP8	7,53E-05
FKBP9	0,000547876
FLT1	0,001195278
FN1	0,047182143
FNDC3B	1,14E-05
FNIP1	1,82E-06
FOS	0,000248335
FOXN2	0,000215987
FOXP1	0,001214978
FRRS1	4,54E-05
FSCN1	0,001059919
FTL	0,000334773
FUS	5,86E-07
FUT10	4,41E-09
FXR1	0,000680238
G3BP1	1,13E-05
G3BP2	6,24E-06
G6PC3	0,000533888
G6PD	3,60E-05

GAB1	0,000857676
GABARAP	0,000816617
GAL	0,00023883
GANAB	1,08E-05
GARS	0,003299642
GART	5,59E-06
GBF1	6,70E-06
GFI1	7,86E-09
GFM1	0,000177862
GGNBP2	9,94E-10
GHITM	1,22E-05
GIGYF2	0,000124048
GIT2	1,12E-06
GLG1	6,02E-05
GLI4	1,88E-05
GLRX3	0,000862385
GLS	0,000410609
GNA13	1,71E-05
GNB1	6,59E-07
GNB4	0,000219398
GNG12	0,000136477
GNS	1,56E-05
GOLGA8A	9,35E-06
GOLIM4	4,66E-10
GOLM1	4,80E-09
GOSR1	1,48E-08
GPBP1L1	2,04E-05
GPNMB	0,001066195
GPR157	3,08E-08
GPR89B	7,14E-07
GPRIN3	7,76E-05
GRIK2	2,64E-05

GRSF1	4,79E-05
GSK3B	0,002012045
GSTP1	1,14E-05
GTF2A1	3,85E-06
GTF2H1	0,000116505
GTF2H5	0,00015419
GTF2I	4,73E-06
GTF3C3	1,58E-05
GTPBP10	4,24E-07
GVQW2	3,06E-07
H2AFJ	1,17E-05
H2AFY	4,02E-06
HAT1	0,000374804
HBP1	1,43E-05
HEATR1	1,06E-05
HEATR5B	7,03E-05
HECTD1	8,43E-05
HERC2P3	2,85E-08
HERC4	1,44E-06
HERPUD1	0,000106023
HES1	0,0149001
HEXA	2,77E-06
HGSNAT	0,00032737
HINT1	0,000376959
HIPK1	8,14E-06
HIPK3	0,000229609
HIST1H1E	7,37E-05
HIST1H2AE	0,000795951
HIST1H2AL	9,08E-09
HIST1H2BG	0,000242074
HIST1H2BH	9,37E-05
HIST1H2BK	0,000201661

HIST1H2BM	2,20E-05
HIST1H3A	2,35E-05
HIST1H3F	1,54E-05
HIST1H3I	2,99E-09
HIST1H4C	0,003257339
HIST1H4D	2,53E-05
HIST1H4E	1,13E-06
HIST1H4H	0,000492837
HIST1H4J	1,23E-06
HIST1H4L	3,08E-05
HM13	8,79E-08
HMGA1	0,001444852
HNRNPC	4,17E-07
HNRNPDL	0,000346852
HNRNPF	0,000401397
HNRNPH3	6,93E-05
HNRNPK	1,53E-06
HNRNPM	1,60E-09
HNRNPR	2,41E-06
HNRNPUL1	2,39E-05
HNRNPUL2	1,99E-05
HOOK3	8,01E-05
HP1BP3	0,000674336
HPRT1	3,08E-06
HSD17B12	5,35E-05
HSD17B4	3,41E-07
HSDL2	6,41E-07
HSP90AB1	6,73E-06
HSP90B1	0,000970976
HSPA1B	1,16E-08
HSPA4	7,39E-05
HSPA5	1,13E-05

HSPA8	3,95E-05
HSPA9	4,86E-06
HSPB1	0,000390142
ICK	8,75E-05
IDH3G	4,69E-05
IER3	0,003319151
IFI16	0,000598898
IFI44	0,004259609
IFI44L	0,025343849
IFIH1	0,004748935
IFT122	0
IGF2BP3	2,10E-05
IGF2R	7,06E-05
IL6ST	0,000862788
ILF2	0,000111641
IMMP2L	2,97E-06
IMPAD1	0,000505403
INIP	3,46E-09
INTS10	1,14E-07
INTS4	1,21E-05
INTS6	0
IPO11	5,35E-06
IPO7	0,000246227
IPO9	0,000157437
IREB2	2,46E-07
IST1	6,03E-05
ITFG2	0,000150851
ITGB1	0,001576931
ITGBL1	0,001163866
ITM2B	0,000982523
ITM2C	0,000372353
ITSN1	0,00011373

IVD	4,39E-06
IWS1	1,08E-06
JRK	2,97E-07
KANSL3	6,78E-05
KAT6B	7,99E-06
KCNQ5	0,000153039
KDM1B	6,34E-09
KDM5B	9,82E-13
KDSR	4,37E-05
KHSRP	6,74E-07
KIAA0100	0,000142972
KIAA0513	5,62E-06
KIAA1109	9,08E-11
KIF13A	2,59E-06
KLF12	3,01E-06
KLF3	0,001495684
KLHDC3	2,76E-07
KMT2A	7,15E-05
KMT2C	0,000178731
KPNA4	1,55E-06
KRIT1	0,000192226
LAMC1	6,05E-05
LANCL1	0,000305662
LAPTM4A	2,23E-05
LARP1	3,46E-05
LATS1	0,000232988
LCORL	3,12E-07
LDB1	0,000149258
LGALS1	0,007019296
LGALS3	0,001574969
LIFR	0,000548809
LIMS1	1,02E-07

LINC00337	4,69E-07
LINC01521	7,84E-11
LLPH	8,83E-05
LMAN1	3,15E-05
LMAN2	8,62E-06
LMO7	0,000109636
LOX	0,004190145
LPP	0,000533279
LRCH3	1,80E-05
LRIG3	0,002610927
LRP1	9,10E-05
LRPPRC	0,00025137
LRRC16A	5,53E-05
LRRC59	9,19E-08
LSAMP	0,000952706
LSG1	0,000121963
LSM12	0,000165538
LTBR	4,36E-06
LUC7L	7,76E-06
LY6E	0,001282538
LYST	0,000192725
M6PR	4,36E-06
MACF1	0,001309394
MACROD1	2,59E-06
MAF	0,000240031
MAGEA8	1,01E-07
MAGT1	1,45E-05
MAN1A2	0,001158233
MANEA	4,41E-06
MAP3K11	4,18E-06
MAP3K2	4,14E-06
MAPK1	2,41E-05

MAPK1IP1L	0,000841234
MAPKAP1	1,13E-05
MAPKAPK5	2,40E-06
MAPRE1	2,66E-07
MARCKS	0,000250088
MATR3	0,000613776
MAX	4,76E-07
MBNL1	7,99E-05
MBNL2	0,000444172
MBTD1	4,18E-05
MBTPS2	1,33E-05
MCCC2	7,61E-06
MCFD2	9,11E-05
MCL1	1,90E-05
MCM9	1,26E-05
MDFIC	0,009698921
MDM2	1,58E-07
MDM4	0,000287496
MECOM	9,89E-05
MED14	1,06E-09
MEN1	7,06E-05
METAP1D	0,00017255
METTL15	2,79E-05
METTL2B	7,38E-05
METTL5	0,000359112
MEX3C	0,0001424
MFAP3	2,27E-05
MFGE8	8,20E-05
MFN2	1,29E-05
MGA	1,90E-09
MGST1	0,002380026
MINA	0,010669636

MIR99AHG	2,40E-06
MKLN1	8,59E-05
MKRN2	1,61E-07
MKX	4,11E-05
MLF2	0,003780194
MLLT1	0,000881243
MLLT3	1,28E-06
MOCS1	4,11E-05
MORN1	9,57E-09
MPDU1	1,73E-07
MRC2	0,000214708
MRPS18A	6,94E-05
MRPS2	0,000139042
MRPS21	0,000230365
MRPS27	3,77E-10
MTA1	2,01E-05
MTA2	4,53E-08
MTCH2	8,93E-05
MTDH	9,91E-05
MTHFD1L	4,36E-06
MTHFSD	1,59E-06
MTMR10	0,000343137
MYEOV2	0,005095489
MYL12A	3,35E-05
MYL9	0,000259406
MYNN	4,66E-05
MYSM1	0,000123051
mar-06	7,59E-05
mar-07	6,84E-07
N4BP1	5,26E-05
N4BP2L2	2,37E-05
NAA35	2,26E-05

NAALADL2	1,56E-05
NABP1	0,002227939
NACA2	0,002346033
NADSYN1	1,92E-07
NBR1	1,86E-08
NCBP1	5,63E-08
NCLN	2,59E-10
NCOA2	1,12E-08
NCOA3	9,60E-10
NCOA7	6,90E-05
ND6	0,00013798
NDUFA2	0,000526343
NDUFA6	0,001123259
NDUFA7	0,000276175
NDUFAF5	0,000106489
NDUFB6	8,39E-05
NDUFS4	5,37E-05
NEK1	9,34E-06
NF2	0,00015984
NFATC3	1,57E-05
NFE2L2	1,68E-05
NFIA	0,007824577
NFIX	0,00052036
NFKBIZ	0,001623063
NFYC	0,000216061
NID1	0,001540191
NIFK	0,0001219
NIN	2,97E-05
NKTR	8,76E-06
NLN	6,33E-06
NOB1	1,16E-07
NOMO3	2,62E-06

NOP10	0,000396168
NOP56	3,52E-05
NR2C2	0,000143604
NRAS	0,000130112
NREP	0,00285635
NRG1	0,001249443
NRP1	0,001624211
NSF	0,000253998
NSL1	3,28E-06
NSMAF	0,00083506
NSUN4	9,92E-06
NT5DC2	6,69E-05
NT5E	0,032188202
NUB1	0,000459363
NUCB1	2,52E-06
NUDT14	3,25E-08
NUDT21	0,000833342
NUDT3	7,82E-07
NUMA1	2,73E-06
NUMB	0,000208222
NUP153	5,68E-06
NUP54	3,13E-06
NUPR1	0,003987999
OSBP	2,38E-05
OSBPL1A	1,25E-05
OSMR	7,12E-05
OST4	0,002198127
OTUD4	0,000267355
OXSR1	0,000832966
P4HA2	0,000198762
P4HB	2,27E-05
PABPC1	0,00119381

PACS1	0,001198644
PAFAH1B1	0,000632354
PAFAH1B2	5,04E-05
PAICS	0,000126887
PAIP2	8,44E-06
PALLD	0,014187339
PAPD4	2,83E-05
PAPOLA	7,03E-07
PAPOLG	3,47E-05
PARP14	0,001874086
PARVA	2,13E-05
PCCB	8,25E-12
PCNX	9,67E-06
PCNXL4	0,000134835
PCOLCE	0,002820903
PCYOX1	0,000129917
PDCD4	2,79E-05
PDIA4	3,14E-05
PDIA6	0,000149287
PDK1	4,05E-06
PDLIM5	0,00013448
PDLIM7	0,000240616
PDS5B	2,50E-08
PDXDC1	5,62E-08
PEA15	0,000788255
PER3	0,000184695
PEX2	9,57E-08
PFDN4	0,00259628
PFDN6	8,15E-06
PFKL	0,000397264
PFN1	0,000261912
PGD	0,000162226

PGK1	1,16E-05
PGLS	6,21E-05
PGRMC1	0,00510746
PGRMC2	0,000213661
PHAX	0,004089741
PHC3	0,000801497
PHF14	0,000141895
PHF20	0,000811672
PHF20L1	3,10E-05
PHF3	2,69E-06
PHF6	0,000321228
PHKG2	1,59E-09
PHLPP1	3,85E-05
PIAS1	0,000275609
PICALM	0,000111701
PIGK	0,000373838
PIGT	0,000356187
PIK3C3	5,76E-05
PIKFYVE	3,70E-08
PITHD1	0,000243515
PKD1	0,000148315
PKM	6,62E-08
PKN2	2,30E-06
PLAA	0,001193323
PLD3	9,64E-05
PLK1	0,000261445
PLOD1	3,35E-05
PLOD2	0,008629701
PLP2	0,006665136
PLPP3	0,000684027
PLXDC2	0,045315209
PLXNA1	5,75E-05

PLXND1	8,78E-05
PMP22	0,000140697
PMPCB	4,59E-06
PMS1	7,00E-06
PNN	0,000116406
PNRC1	5,52E-05
POFUT1	3,62E-09
POLDIP3	1,50E-09
POLK	3,19E-06
POLR1E	0,000743278
POLR2B	2,21E-05
POLR2J3	2,28E-05
POLR2L	0,004460716
POLR3A	1,59E-05
POLR3B	1,30E-06
POLR3H	5,41E-09
POM121	0,000124816
POMK	3,02E-06
PPFIBP1	0,001419712
PPHLN1	4,75E-06
PPIB	1,58E-07
PPP1CA	1,38E-05
PPP1R11	1,38E-05
PPP1R7	0,00038389
PPP2CB	0,000829375
PPP2R2B	0,000345744
PPP2R3C	2,33E-06
PPP2R5A	1,68E-05
PPP2R5C	0,000128338
PPP4R3B	1,41E-05
PPP5C	7,20E-06
PRCP	2,66E-05

PRDX1	1,46E-05
PRDX2	1,73E-05
PRIM2	4,06E-05
PRKAA1	1,13E-06
PRKAG1	0,000147754
PRKAR1A	2,24E-05
PRKCI	0,000405738
PRKCSH	2,69E-05
PRKD3	0,000233059
PRMT1	3,14E-05
PRR14L	0,000110837
PRRX1	0,028361829
PRSS12	0,001856109
PSAP	0,000218242
PSEN1	5,20E-06
PSENEN	0,000840298
PSIP1	0,00030139
PSMC2	1,10E-06
PSMD11	2,29E-05
PSMD6	4,38E-05
PSMD8	9,92E-05
PSMF1	5,46E-05
PTBP1	0,001592908
PTBP3	2,05E-06
PTCH1	0,000101989
PTK2	6,92E-06
PTK7	2,89E-05
PTMS	2,34E-05
PTP4A1	0,00031864
PTPN11	6,47E-05
PTPRG	0,000510779
PTPRS	1,16E-06

PUM3	0,000196043
PWWP2A	2,31E-05
PXK	7,58E-05
QKI	0,000538395
QPRT	0,009441879
QSER1	0,001088556
QTRTD1	8,93E-08
RAB11B	1,79E-09
RAB1A	0,000464725
RAB5A	0,000330183
RAB5C	0,000311446
RAB6A	1,70E-07
RAB7A	0,0001297
RAB8A	1,66E-07
RAC1	6,40E-05
RAD23B	9,02E-05
RALGAPA1	4,85E-06
RAN	3,76E-06
RANBP1	1,23E-05
RAP1A	0,00025375
RAP2A	0,000104012
RAPH1	0,001257664
RARA	1,68E-07
RASAL2	9,81E-05
RASSF8	3,73E-05
RAVER2	2,72E-07
RBAK	6,55E-05
RBL1	2,37E-08
RBM17	6,56E-05
RBM18	4,94E-05
RBM26	0,002414929
RBM34	5,03E-07

RBM8A	3,39E-05
RBMS3	2,39E-05
RBMX	6,32E-05
RBSN	1,23E-06
RC3H1	1,46E-05
RCN1	1,13E-05
RDH11	0,001293247
RECK	1,11E-06
REPS1	5,63E-05
RERE	4,09E-07
REXO1	4,32E-06
RFTN1	3,31E-06
RHNO1	0,004636814
RHOA	0,001269402
RHOQ	5,15E-05
RIC1	4,66E-07
RIPK2	0,00025959
RMND5A	0,000367796
RNF130	0,001221887
RNF141	1,11E-05
RNF168	1,09E-06
RNF180	0,00082573
RNF216	1,85E-05
RNF5	2,32E-07
RNH1	1,80E-05
ROCK1	0,000368501
RP2	1,37E-07
RPARP-AS1	0,000139872
RPE	2,29E-10
RPL10	3,70E-06
RPL11	6,93E-06
RPL13	6,88E-05

RPL3L	4,07E-05
RPL4	9,49E-05
RPL5	2,02E-05
RPLP2	2,50E-05
RPN1	6,13E-07
RPN2	0,000406619
RPRD1A	3,35E-05
RPS11	1,39E-06
RPS13	0,000686298
RPS15	7,88E-05
RPS19	1,44E-07
RPS2	6,93E-05
RPS24	6,72E-05
RPS28	7,71E-06
RPS6KB2	9,01E-06
RPS9	1,52E-06
RQCD1	4,82E-05
RRM1	0,002226811
RSU1	3,87E-06
RUFY2	9,12E-06
RUNX1T1	5,29E-05
RUNX2	0,000654759
RUVBL2	3,44E-08
SAE1	7,60E-05
SAFB	0,000144638
SAMD4B	3,05E-05
SAMD5	0,00144421
SAMHD1	4,61E-05
SAP18	0,001003216
SAP30	1,44E-05
SART3	5,15E-09
SAXO2	3,74E-07

SBNO1	1,69E-05
SBNO2	7,14E-05
SCAF11	0,000367103
SCAF4	9,14E-06
SCML1	3,59E-05
SCPEP1	2,46E-06
SEC22B	0,000397909
SEC23B	0,000146054
SEC23IP	3,92E-07
SEC62	3,35E-05
SELT	0,000923499
SEMA3C	0,003391508
SEMA5A	0,003542697
SEMA6D	0,00218908
SERBP1	9,71E-07
SERINC3	6,45E-05
SERPINB6	0,000110375
SERPINE1	0,011419873
SESN3	3,52E-08
SF3A2	7,34E-06
SF3B6	3,25E-05
SFPQ	0,000834491
SHC1	0,000346115
SHISA3	1,21E-06
SIAE	2,04E-05
SIKE1	1,57E-08
SIRT5	2,28E-07
SKIV2L2	4,84E-05
SKP1	0,000327406
SLAIN2	0,000105959
SLC16A1	3,81E-07
SLC19A1	3,98E-05

SLC25A11	1,17E-05
SLC2A1	0,001116384
SLC30A5	2,09E-05
SLC30A9	0,000277249
SLC31A1	0,001294061
SLC35F5	0,000230343
SLC38A10	1,70E-06
SLC38A2	0,000126342
SLC39A14	0,001492749
SLC39A7	0,000455659
SLC39A9	6,47E-08
SLC3A2	2,19E-05
SLC4A7	0,001163787
SLC6A9	0,000224285
SLC7A1	0,001552372
SLK	6,56E-06
SMAD4	8,24E-05
SMAD5	2,62E-05
SMARCA1	1,33E-06
SMARCA4	5,16E-05
SMARCC2	0,000140421
SMARCD1	6,03E-06
SMC1A	3,02E-05
SMC3	2,02E-07
SMC4	0,003536256
SMCHD1	0,00025143
SMG1	0,000195344
SMIM14	8,71E-05
SMIM7	1,30E-05
SMYD2	5,14E-07
SNAI2	7,07E-05
SND1	6,15E-07

SNRK	1,53E-07
SNRPB2	2,60E-05
SNRPN	9,85E-05
SOCS4	5,02E-05
SORT1	0,006127788
SOS1	2,05E-06
SOX13	7,68E-05
SOX4	9,29E-06
SP1	1,96E-05
SPAG16	2,44E-05
SPAG9	5,39E-10
SPARC	3,14E-05
SPATS2	8,24E-07
SPATS2L	0,001430214
SPCS3	1,41E-05
SPDL1	0,000382169
SPG11	3,98E-05
SPICE1	1,03E-05
SPIN1	4,13E-05
SPTBN1	0,000160294
SRC	1,43E-08
SRD5A3	0,000643027
SREBF1	0,001021468
SREK1	0,000148942
SRGAP1	0,002825332
SRGAP2	5,31E-05
SRI	0,000249972
SRPR	2,64E-05
SRRM2	5,46E-05
SRSF1	5,75E-05
SRSF11	0,00113903
SRSF6	0,003558389

SSB	0,000236685
SSBP1	3,48E-05
SSBP2	0,004501609
SSH2	6,03E-07
SSR1	0,001272092
SSR2	9,43E-05
SSR3	0,000111963
ST7L	0,000530691
STAG2	1,22E-06
STAT1	0,002365171
STAU2	3,49E-06
STIM1	1,09E-05
STMN1	0,000162171
STOML2	3,29E-05
STRADA	4,92E-05
STRAP	0,000202237
STRN	4,35E-05
STT3A	4,31E-06
STT3B	0,000371964
STX8	0,000214917
STXBP3	0,000259384
SULF1	0,044210723
SUPT20H	2,25E-06
SUPT6H	1,42E-07
SUPT7L	0,003729721
SUZ12	5,81E-05
SVEP1	7,63E-06
SYF2	0,00097763
SYNCRIP	2,68E-05
SYNRG	2,10E-05
SYT11	0,000661055
SYTL2	0,001450259

set-07	3,16E-05
set-09	3,03E-06
TAB2	6,94E-05
TAB3	4,77E-07
TADA3	5,52E-06
TAF13	0,005877353
TAF15	7,05E-05
TAF8	9,08E-06
TAF9B	0,001637318
TAOK1	2,28E-05
TAPT1	4,66E-08
TBC1D1	1,74E-05
TBC1D7	7,33E-09
TBL2	4,25E-05
TCAIM	2,62E-05
TCEA1	1,46E-05
TEAD1	9,71E-05
TECR	2,20E-07
TENM3	7,98E-05
TERF2	2,33E-09
TEX10	4,97E-05
TFB2M	0,000161625
TFDP1	4,60E-05
TFPI2	0,004573959
TGFB1	0,000778286
TGFBR1	0,006983234
THADA	1,07E-07
THBS1	0,000921386
THRAP3	2,57E-06
TIA1	3,60E-05
TIMM17B	2,60E-05
TIMM23	7,05E-05

TIMM50	4,10E-06
TIMP1	0,002080945
TKTL1	1,05E-06
TM2D1	6,35E-05
TM9SF4	0,000120341
TMBIM4	3,61E-05
TMED4	0,000168265
TMED5	5,82E-07
TMEM109	0,001035154
TMEM126B	3,42E-05
TMEM135	0,001674461
TMEM138	5,78E-06
TMEM19	0,000172637
TMEM230	0,000590968
TMEM30A	0,00218319
TMEM50A	2,30E-05
TMEM59	2,70E-05
TMEM64	0,000174995
TMSB10	0,000117828
TMTC3	6,92E-05
TMTC4	0,000692106
TMX3	2,01E-05
TNFRSF10B	5,13E-05
TNPO1	1,99E-07
TNPO2	4,82E-06
TNRC6A	7,50E-06
TOP1MT	2,32E-06
TOR1A	6,33E-06
TOR1AIP1	3,18E-06
TOR1AIP2	8,10E-06
TP53	0,000398378
TPM1	0,020267013

TPM4	3,28E-06
TPMT	4,93E-05
TPP2	0,000136302
TPT1	5,03E-05
TRA2B	9,59E-05
TRAF3IP2	0,001807614
TRAM1	6,87E-05
TRAM2	0,000141472
TRAPPC1	4,02E-05
TRAPPC2	3,04E-06
TRIM16L	0,00043845
TRIM24	0,000160822
TRIM25	0,000232479
TRIM44	5,76E-06
TRIQK	5,93E-07
TROVE2	0,000112495
TSPAN3	2,65E-05
TSPYL1	2,07E-05
TTC3	3,93E-05
TTC37	6,00E-07
TTC9C	2,76E-06
TTF2	3,93E-05
TTLL5	9,01E-10
TUBA1B	2,84E-06
TUBB	0,000630172
TUBG1	1,09E-05
TUSC3	0,00027249
TXLNA	1,61E-07
TXN	0,000571264
TXNL4A	0,002103734
TXNRD1	9,44E-06
TYMS	0,004837732

U2AF2	3,65E-05
UACA	5,63E-05
UBA1	0,001014754
UBA3	6,82E-07
UBA52	8,88E-06
UBA6	0,000311258
UBAP2L	7,38E-07
UBE2H	0,000867514
UBE2I	2,41E-05
UBE2W	4,33E-08
UBE3C	1,45E-06
UBE4B	3,01E-05
UBIAD1	8,73E-05
UBQLN1	2,48E-05
UBR2	3,61E-05
UBR4	3,14E-05
UBXN4	8,13E-07
UCHL1	0,000584487
UCHL5	9,33E-06
UGGT1	5,25E-08
UGGT2	4,62E-05
UHMK1	0,000124113
UHRF1BP1L	0,000405436
UQCRC2	0,000116579
URI1	6,77E-08
USO1	0,000126419
USP10	4,92E-05
USP25	4,74E-05
USP36	2,53E-06
USP42	5,18E-05
USP48	1,34E-08
USP53	7,18E-05

USP9X	0,000939577
USPL1	1,05E-06
UTP15	0,003370513
VAPB	3,01E-05
VCL	1,62E-08
VCP	0,000125433
VDAC3	4,49E-06
VEGFC	0,002026642
VEZT	4,03E-07
VGLL3	0,010527075
VIM	2,03E-05
VKORC1	0,000236257
VPS13B	3,28E-11
VPS29	2,74E-05
VPS35	1,38E-06
VPS41	6,01E-06
VPS45	2,32E-05
VPS8	4,10E-05
VRK3	7,27E-09
VWA9	2,20E-08
WARS	0,000929962
WARS2	4,93E-05
WBSCR16	6,01E-07
WDR19	0,000480292
WDR3	3,32E-05
WDR33	3,21E-08
WDR43	9,20E-05
WHSC1L1	1,25E-06
WIPI2	4,46E-09
WNK1	7,57E-06
WNT9B	3,02E-06
WRNIP1	2,81E-06

WSB1	0,002103153
WTAP	2,21E-05
XPO4	2,24E-06
XRN1	2,38E-05
YBX1	2,35E-05
YIPF3	9,16E-05
YTHDF3	7,94E-06
YWHAE	4,52E-06
YWHAZ	8,40E-07
ZAK	0,000248382
ZBED6	9,20E-06
ZBTB1	8,32E-06
ZBTB33	1,88E-05
ZBTB38	2,38E-05
ZC2HC1A	0,000529013
ZC3HAV1L	4,38E-05
ZCCHC7	2,89E-05
ZDHHC2	9,82E-06
ZFC3H1	2,68E-06
ZFP36L2	6,55E-05
ZFYVE16	4,07E-07
ZGRF1	2,10E-09
ZKSCAN8	1,08E-07
ZMYND11	2,54E-05
ZMYND8	5,21E-05
ZNF100	0,00024536
ZNF134	1,92E-06
ZNF138	0
ZNF17	4,89E-06
ZNF207	5,41E-05
ZNF236	1,31E-05
ZNF24	3,56E-09

ZNF254	1,73E-05
ZNF264	2,40E-13
ZNF277	2,96E-05
ZNF283	9,02E-06
ZNF292	3,98E-07
ZNF33A	9,56E-10
ZNF362	1,69E-05
ZNF37A	0,001314646
ZNF407	0,001142262
ZNF417	1,39E-06
ZNF460	1,25E-09
ZNF461	7,82E-10
ZNF507	2,04E-06
ZNF605	5,12E-09
ZNF611	1,11E-05
ZNF639	0,000783434
ZNF664	0,000356571
ZNF674	0,000534431
ZNF740	0,000152483
ZNF780B	5,78E-08
ZNF808	2,66E-06
ZNF814	4,69E-06
ZNF880	3,77E-06